2016 Asia–Europe–Pacific School of High-Energy Physics
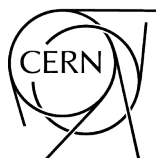
Beijing, China
12 – 25 October 2016

Editors: M. Mulders
C. Z. Yuan

This volume is indexed in: CERN Document Server (CDS), INSPIRE, Scopus.

This volume should be cited as:

Proceedings of the 2016 Asia–Europe–Pacific School of High-Energy Physics, Beijing, China, 2 – 25 October
2016, edited by M. Mulders and C. Z. Yuan, CERN Yellow Reports: School Proceedings, Vol. 2/2018,
CERN-2018-004-SP (CERN, Geneva, 2018), KEK Proceedings 2018-9,
https://doi.org/10.23730/CYRSP-2018-002

A contribution in this volume should be cited as:

[Author name(s)], in Proceedings of the 2016 Asia–Europe–Pacific School of High-Energy Physics, Beijing,
China, 2 – 25 October 2016, edited by M. Mulders and C. Z. Yuan, CERN Yellow Reports: School
Proceedings, Vol. 2/2018, CERN-2018-004-SP (CERN, Geneva, 2018), KEK Proceedings 2018-9, pp. [first
page]–[last page], https://doi.org/10.23730/CYRSP-2018-002.[first page]

Abstract

The Asia–Europe–Pacific School of High-Energy Physics is intended to give young physicists an introduction to the theoretical aspects of recent advances in elementary particle physics. These proceedings contain lecture notes on Higgs physics, the theory of quantum chromodynamics, quarkonium physics, and physics beyond the Standard Model.

Preface

The third event in the series of the Asia–Europe–Pacific School of High-Energy Physics took place in Beijing, China, from 12 to 25 October 2016. A strong team from IHEP and UCAS took care of the local organization, while CERN and KEK collaborated to provide administrative support in preparation for the School.

The staff and students were housed in comfortable accommodation in the International Conference Centre on the Yanqihu Campus, University of the Chinese Academy of Sciences that also provided the conference facilities. The students shared accommodation, mixing nationalities to foster cultural exchange between participants from different countries.

A total of 91 students of 22 different nationalities attended the school. About 74% of the students were from Asia-Pacific countries, most of the others coming from Europe. Almost 90% of the participants were working towards a PhD, while most of the others were advanced Masters students; the School was also open to postdocs. Over 80% of the students were experimentalists; the school was also open to phenomenologists.

A total of 35 lectures were complemented by daily discussion sessions led by five discussion leaders. The teachers (lecturers and discussion leaders) came from many different countries: Belgium, China, France, Germany, India, Japan, Korea, Russia, Switzerland, the UK and the USA.

The programme required the active participation of the students. In addition to the discussion sessions that addressed questions from the lecture courses, there was an evening session in which many students presented posters about their own research work to their colleagues and the teaching staff.

Collaborative student projects in which the students of each discussion group worked together on an in-depth study of a published experimental data analysis were an important activity. This required interacting, outside of the formal teaching sessions, with colleagues from different countries and different cultures. A student representative of each of the five groups presented a short summary of the conclusions of the group's work in a special evening session.

In addition to the academic side of the School, the participants had the occasion to experience many aspects of Chinese culture, including visits to the Great Wall and to central Beijing where they saw the Temple of Heaven and the Forbidden City. They also had ample opportunity to appreciate excellent Chinese food.

Our thanks go to the local-organization team and, in particular, to Jiangxi Lan, Yeliu Mo and Huan Xing under the chairmanship of Changzheng Yuan, for all their work and assistance in preparing the School, on both scientific and practical matters, and for their presence throughout the event.

Very great thanks are due to the lecturers and discussion leaders for their active participation in the School and for making the scientific programme so stimulating. The students, who in turn manifested their good spirits during two intense weeks, undoubtedly appreciated listening to and discussing with the teaching staff of world renown.

We would like to express our special appreciation to Professor Fabiola Gianotti, Director General of CERN, Professor Yifang Wang, Director General of IHEP, and Professor Masanori Yamauchi, Director General of KEK, for their lectures on the particle-physics programmes at CERN, in China and in Japan. We would also like to thank Professor Takaaki Kajita, winner of the 2015 Nobel Prize in Physics, for his special lecture about Super Kamiokande.

We are very grateful to Kate Ross from CERN and to Misa Miyai from KEK for their untiring efforts on administration for the School. We would also like to thank the members of the International Committees.

Nick Ellis
(On behalf of the Organizing Committee)

The 3rd Asia–Europe–Pacific School of High Energy Physics
12–25 October 2016, Beijing, China

The 3rd Asia–Europe–Pacific School of High Energy Physics
12–25 October 2016, Beijing, China

People in the photograph

1	Savannah Thais	38	Nick Ellis	75	Naoki Nagakura
2	Lydia Beresford	39	Inseok Yoon	76	Santosh Parajuli
3	Fahmi Maulida	40	Yuanfang Yue	77	Naoyuki Sumi
4	Priya Sajid	41	Karola Dette	78	Hiromitsu Goto
5	Qamar Ul Hassan	42	Young Joon Kwon	79	Kazunori Hanagaki
6	Abeeha Batool	43	Daniel Kerszberg	80	Jinyun Wu
7	Muhammad Waqas	44	Satoshi Higashino	81	Masanori Yamauchi
8	Jia Jia Qin	45	Binlong Wang	82	Ruobing Zhang
9	Qiyun Li	46	Peirong Li	83	Khuram Tariq
10	Giulio Mezzadri	47	Resmi PK	84	Seokhee Park
11	Elizaveta Nazarova	48	Pradiphat Muangha	85	Henrik Oppen
12	Eiasha Waheed	49	Kirill Grevtsov	86	Sarmad Masood Shaheen
13	Kazuki Yajima	50	Changzheng Yuan	87	Vivek Sharma
14	Chen Qian	51	Leonora Vesterbacka	88	Cen Zhang
15	Kaibao Chen	52	Jae Sung Kim	89	Rémy Le Breton
16	Jochen Jens Heinrich	53	Laurie McClymont	90	Kiyotomo Kawagoe
17	Dooyeon Gyun	54	Hitoshi Oshima	91	Muhammad Ahmad
18	Alexander Ermakov	55	Ryuichiro Kitano	92	Shuddha Shankar Dasgupta
19	Arthur Chomont	56	Rebin Karaparambil Rajan	93	Xian Xiong
20	Kunfeng Lyu	57	Ann-Kathrin Perrevoort	94	Kimiko Yamashita
21	Ke-Pan Xie	58	Adam Dendek	95	Huajie Cheng
22	Brian Le	59	Thorwald Klapdor-Kleingrothaus	96	Huan Xing
23	Anton Hawthorne	60	Maren Meinhard	97	Yifan Yang
24	Qing-Hong Cao	61	Takaaki Kajita	98	Sergii Raspopov
25	Andrey Seryakov	62	Benjamin Sowden	99	Yeliu Mo
26	Liupan An	63	Shohei Shirabe	100	Jun Hao Liu
27	James Kahn	64	Ye Chen	101	Yu Zhang
28	Ya Zhang	65	Suvankar Roy Chowdhury	102	Martijn Mulders
29	Yang Zhang	66	Muzamil Ahmad Bhat	103	Sebastien Descotes-Genon
30	Jing Chen	67	Govinda Adhikari	104	Muhammad Usman
31	Kate Ross	68	Yifang Wang	105	Wenjie Wu
32	Yinqiang Gong	69	Yosuke Maeda	106	Yan Jia Xiao
33	Yu Hu	70	Dharmesh Rathaud	107	Guo-yuan Huang
34	AKM Moinul Haque Meaze	71	Miao Jiang	108	Hua-Sheng Shao
35	Anthony Lionti	72	Tanmay Sarkar	109	Ingrid-Maria Gregor
36	Xing Wang	73	Yuta Sano	110	Kentarou Mawatori
37	Alexandr Korobov	74	On Kim	111	Jing-yu Zhu
				112	Hongrong Qi

Photographs (montage)

Contents

Topics in Higgs Physics

J. Ellis*

Theoretical Particle Physics & Cosmology Group, Department of Physics, King's College London,
United Kingdom

Abstract

These lecture notes review the theoretical background to the Higgs boson, provide an introduction to its phenomenology, and describe the experimental tests that lead us to think that "beyond any reasonable doubt, it is a Higgs boson". Motivations for expecting new physics beyond the Standard Model are recalled, and the Standard Model effective field theory is advocated as a tool to help search for it. The phenomenology of $N = 1$ and $N = 2$ supersymmetric Higgs bosons is reviewed, and the prospects for possible future Higgs factories are previewed.

1 Background to the Higgs Discovery

1.1 Historical introduction

The fundamental equations of physics have a high degree of symmetry - think the rotation and translation symmetry of Newton's equations, the gauge invariance of Maxwell's equations for electrodynamics, the boost symmetry of special relativity, or the the general coordinate invariance of general relativity - and these theories are generally considered to be very beautiful. However, the solutions to these equations often conceal these symmetries, and they appear asymmetric - people are not spherical, for example. Sometimes these asymmetric solutions may even appear more beautiful than symmetric solutions - the image of the Mona Lisa, for example, would not be so interesting if it were symmetric. Regardless of these aesthetic considerations, the rich variety of physical phenomena clearly requires the potential to break symmetries.

However, breaking a symmetry must be done with care - for example, the gauge invariance of electrodynamics guarantees the renormalisability of quantum electrodynamics (QED) and hence its calculability. The trick in formulating theories with 'broken' symmetry is often to hide the symmetry so that it is not manifest, while maintaining it at a fundamental level and thereby preserving its attractive features such as renormalizability. This can be done by postulating a lowest-energy ('vacuum') state of the symmetric equations that does not possess the full symmetry of the underlying equations - an idea known as spontaneously-broken or 'hidden' symmetry.

This idea originated in condensed-matter physics - an early example being the superfluidity that plays an essential rôle in the LHC magnet system. In this case, the spontaneously-broken symmetry is global, i.e., the symmetry transformations are independent of the spatial location within the superfluid. This type of hidden symmetry was introduced into particle physics by Yoichiro Nambu [1], who used it to understand the (relatively) low mass and the low-energy dynamics of the pion. According to his theory,

---

*Also Theoretical Physics Department, CERN, Geneva, Switzerland

Table 1: Particle content of the Standard Model. Each quark comes in 3 colours, and the electric charges of the fermions are listed in the Table.

Bosons	
Gauge bosons	**Higgs boson**
$\gamma, W^+, W^-, Z^0, g_{1\ldots 8}$	ϕ

Fermions	
Quarks	**Leptons**
$2/3:$ $\begin{pmatrix} u \\ d \end{pmatrix}, \begin{pmatrix} c \\ s \end{pmatrix}, \begin{pmatrix} t \\ b \end{pmatrix}$ $-1/3:$	$0:$ $\begin{pmatrix} \nu_e \\ e^- \end{pmatrix}, \begin{pmatrix} \nu_\mu \\ \mu^- \end{pmatrix}, \begin{pmatrix} \nu_\tau \\ \tau^- \end{pmatrix}$ $-1:$

the underlying symmetry (in this case chiral symmetry) is not manifest, but is reflected in the couplings of the pion, which would have no mass if the up and down quarks were strictly massless. Jeffrey Goldstone subsequently published a simple elementary field-theoretical model of this phenomenon [2] and he, Abdus Salam and Steven Weinberg [3] subsequently proved rigorously that in a relativistic theory every spontaneously-broken global symmetry would be reincarnated in a massless particle with specific couplings, called a Nambu-Goldstone boson.

All well and good, but there are interesting cases where the spontaneously-broken symmetry is local, as in a gauge theory - the prime example being the superconductivity that also plays an essential rôle in the LHC magnet system. The theory of spontaneous gauge symmetry breaking in this non-relativistic situation was first developed by Philip Anderson [4] and Nambu [5]. According to their theory, inside a superconductor the (externally massless) photon acquires a medium-dependent mass by 'eating' Cooper pairs of electrons in the lowest-energy ('vacuum') state inside the medium. Anderson also conjectured that a similar phenomenon might be possible in a relativistic theory, but did not develop this idea. Indeed, Walter Gilbert [6] argued that this would *not* be possible, because spontaneous symmetry breaking seemed to require the presence of a vector breaking Lorentz symmetry explicitly.

However, in 1964 this argument was circumvented in papers by François Englert and Robert Brout [7], and by Peter Higgs [8, 9]. The Englert-Brout paper was received by the journal where it was published on June 26th, 1964, and a first paper by Higgs was received on July 27th, 1964. Unaware of the paper by Englert and Brout, he pointed out a potential loophole in the Gilbert argument, and in a second paper he constructed an explicit example. Curiously, whereas the first paper was accepted quickly by the journal Physics Letters, that journal refused the second paper. It was subsequently accepted by Physical Review Letters after an anonymous referee (generally held to be Nambu) suggested to Higgs that he emphasise more the physical implications of his theory. Later in 1964, a more detailed description of this idea appeared in a paper by Gerald Guralnik, Carl Hagen and Tom Kibble [10]. Among all these 1964 papers, the only one to point out explicitly on the appearance in the theory of a massive scalar boson was Higgs, in his second paper [9], which is why it is generally referred to as the Higgs boson.

These authors considered the spontaneous breaking of an Abelian U(1) gauge theory. The analogous phenomenon in a non-Abelian theory was first studied by Sashas Migdal and Polyakov [11], who were unaware of the earlier papers. Publication of their paper was delayed because Soviet academicians could not believe that two young students, as they were then, could come up with such a ground-breaking theory. Partial breaking of a non-Abelian gauge symmetry was subsequently rediscovered by Kibble [12], and this is the form of spontaneous symmetry breaking that is central to the Standard Model.

1.2 Summary of the Standard Model

Table 1 summarizes the particle content of the Standard Model (SM) [13, 14]. The weak and electromagnetic interactions are described by a Lagrangian that is symmetric under gauge transformations in a $SU(2)_L \times U(1)_Y$ group, where the subscript L recalls that the weak SU(2) group acts only on left-handed

fermions, and Y is the hypercharge. We can write the $\text{SU}(2)_L \times \text{U}(1)_Y$ part of the SM Lagrangian as

$$
\begin{aligned}
\mathcal{L} &= -\frac{1}{4} F^a_{\mu\nu} F^{a\mu\nu} \\
&+ i\bar{\psi} \slashed{D} \psi + h.c. \\
&+ \psi_i y_{ij} \psi_j \phi + h.c. \\
&+ |D_\mu \phi|^2 - V(\phi) \,,
\end{aligned}
\tag{1}
$$

which is short enough to write on a T-shirt or a pullover!

The first line in (1) contains the kinetic terms for the gauge bosons of the electroweak theory, where the index a runs over the single $\text{U}(1)_Y$ gauge field, $\mathcal{A}_\mu$, and the three gauge fields $W^{1,2,3}_\mu$ associated with $\text{SU}(2)_L$. The U(1) field-strength tensor is the familiar

$$
f_{\mu\nu} = \partial_\nu \mathcal{A}_\mu - \partial_\mu \mathcal{A}_\nu \,,
\tag{2}
$$

and the $\text{SU}(2)_L$ field-strength tensor is

$$
F^a_{\mu\nu} = \partial_\nu W^a_\mu - \partial_\mu W^a_\nu + ig\epsilon_{abc} W^b_\mu W^c_\nu \quad \text{for } a = 1, 2, 3 \,.
\tag{3}
$$

where g in (3) is the gauge coupling of $\text{SU}(2)_L$ and the ϵ_{abc} are its structure constants. The last term in (3) arises from the non-Abelian nature of the SU(2) group. At first sight, all the gauge fields are massless, in conflict with the massive nature of the weak bosons $W^\pm$ and Z^0. As we see later, they acquire masses through the Englert-Brout-Higgs mechanism, whose physical manifestation is the Higgs boson.

The second line in (1) contains the interactions between the spin-1/2 matter fields ψ and the gauge fields via the covariant derivatives

$$
D_\mu = \partial_\mu + \frac{ig'}{2} A_\mu Y + \frac{ig}{2} \tau \cdot W_\mu \,,
\tag{4}
$$

where g' is the U(1) coupling constant, Y is the generator of the U(1) hypercharge, and $\tau \equiv (\tau_1, \tau_2, \tau_3)$ is the set of SU(2) Pauli matrices that represent the SU(2) algebra.

The third line in (1) describes the interactions between the matter fields and the Higgs field, ϕ, via the Yukawa couplings y_{ij}, which give fermions their masses when the Higgs field acquires a vacuum expectation value (vev) $\langle \phi \rangle \neq 0$. In the SM the Higgs field ϕ is a complex doublet of SU(2) with non-zero U(1) hypercharge Y, so this vev breaks electroweak symmetry.

The fourth and final line in (1) describes dynamics of the Higgs sector. The first term is the kinetic term for the Higgs field, which also includes a covariant derivative D_μ (4), and the second term in the final line of (1) is the Higgs potential $V(\phi)$:

$$
V(\phi) = -\mu^2 |\phi|^2 + \lambda |\phi|^4 \,.
\tag{5}
$$

The negative sign of the first, quadratic term in (5) destabilizes the symmetric case $\langle \phi \rangle = 0$, and the second, quartic term in (5) ensures that there is a stable minimum of the potential with

$$
\langle \phi \rangle \equiv \frac{v}{\sqrt{2}} = \frac{\mu}{\sqrt{2\lambda}} \neq 0 \,,
\tag{6}
$$

if $\lambda > 0$. The requirements that the coefficient of the quadratic term is negative and that of the quartic term is positive are both problematic in the SM, as we shall see later.

Many different experiments have confirmed with high precision theoretical predictions derived from the first two lines in the SM Lagrangian (1). However, until 2012 there was no experimental evidence for the last two lines, and there was considerable theoretical doubt whether it could be correct. However, during Run 1 of the LHC the ATLAS [15] and CMS [16] Collaborations discovered a particle

with properties resembling those of the Higgs boson in the SM, as discussed later in this Lecture, albeit with much less accuracy than, e.g., the precision electroweak tests based on properties of the $W^{\pm}$ and Z^0 boson. The major tasks for future experiments at the LHC and elsewhere will include probing whether the Higgs and other sectors of the SM Lagrangian in (1) hold up under more detailed scrutiny, whether there are additional interactions between SM particles, and whether there is any evidence for new physics beyond the SM, as discussed in the second Lecture.

1.3 Abelian (NG)AEBHGHKMP mechanism

As a warm-up exercise, we consider the simplest Abelian model for spontaneous gauge symmetry breaking, with just a U(1) gauge field A_μ and a single complex field ϕ described by the Lagrangian

$$\mathcal{L}(A, \phi) = -\frac{1}{4} f_{\mu\nu} f^{\mu\nu} + (D_\mu \phi^\dagger)(D^\mu \phi) - V(\phi), \tag{7}$$

where $f_{\mu\nu}$ is given by (2), $D_\mu \equiv \partial_\mu - ieA_\mu$ and $V(\phi)$ has the 'Mexican hat' form (5) illustrated in Fig. 1. The U(1) gauge invariance implies that the theory is invariant under the local transformations

$$\phi \to \phi' = e^{i\alpha(x)}\phi = e^{i\alpha(x)}e^{i\theta(x)}\eta(x),$$
$$A_\mu \to A'_\mu = A_\mu(x) + \frac{1}{e}\partial_\mu \alpha(x), \tag{8}$$

where $\eta(x)$ and $\theta(x)$ are the magnitude and phase of $\phi(x)$, respectively.
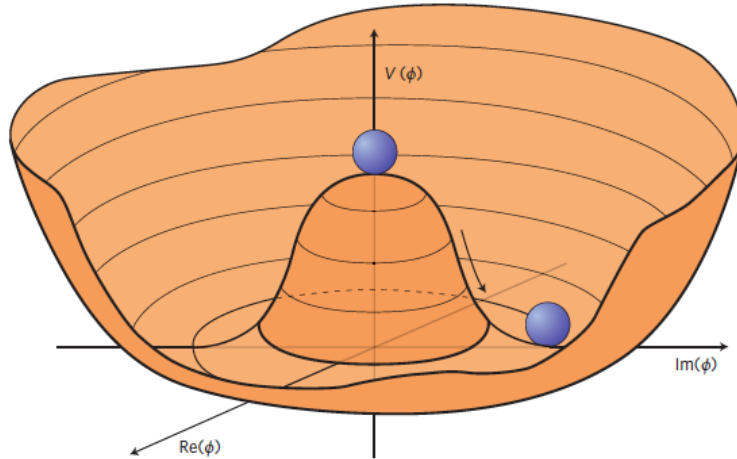
Fig. 1: The 'Mexican hat' potential (5). The lowest-energy state may be described by a random point around the base of the hat. In the case of a global symmetry, motion around the bottom of the hat corresponds to a massless spin-zero Nambu-Goldstone boson [1, 2]. In the case of a local (gauge) symmetry, this boson combines with a massless spin-one gauge boson to yield a massive spin-one particle with three polarization states. The Higgs boson [9] is a massive spin-zero particle corresponding to quantum fluctuations in the radial direction, up the side of the hat.

We can exploit this gauge invariance to choose $\alpha(x) = -\theta(x)$, in which case $\phi'(x) = \eta(x)$ and the Lagrangian (7) takes the form

$$\mathcal{L}(A'_\mu, \eta) = -\frac{1}{4} f'_{\mu\nu} f'^{\mu\nu} + |(\partial_\mu - ieA'_\mu)\eta|^2 - V(\eta), \tag{9}$$

The minimum of the potential $V(\eta)$ occurs at the following value of η:

$$\eta = \frac{v}{\sqrt{2}} \equiv \frac{\mu}{\sqrt{2\lambda}}. \tag{10}$$

We can then rewrite (9) writing $\eta = (v + H)/\sqrt{2}$ and simplifying the notation: $A'_\mu \to A_\mu$, to obtain

$$\mathcal{L}(A_\mu, H) = -\frac{1}{4} f_{\mu\nu} f^{\mu\nu} + |(\partial_\mu - ieA_\mu)(\frac{v+H}{\sqrt{2}})|^2 - V(\frac{v+H}{\sqrt{2}}). \tag{11}$$

Expanding (11) to quadratic order in A_μ and H, we find

$$\mathcal{L}(A_\mu, H) \ni -\frac{1}{4} f_{\mu\nu} f^{\mu\nu} + e^2 v^2 A_\mu A^\mu + \frac{1}{2}[(\partial_\mu H)^2 - m_H^2 H^2] + \dots, \tag{12}$$

where the gauge boson has acquired a mass $m_A = ev/2$ and $m_H = \sqrt{2}\mu = \sqrt{2\lambda}v$. The mass of the vector boson results from the spontaneous symmetry gauge breaking mechanism, with the phase degree of freedom θ of the complex scalar field ϕ, which is a Nambu-Goldstone boson, being 'eaten' by the previously massless gauge boson - which has two polarization degrees of freedom - to become the third polarization state needed for a massive gauge boson.

The simultaneous appearance of a massive scalar boson H is an inescapable feature of this mechanism, since it is related to the positivity of the curvature in the scalar potential around the minimum, which is needed to fix the vev v. This insight was made explicit in the second 1964 paper by Higgs [9], but was not mentioned in any of the other 1964 papers.

1.4 Spontaneous gauge symmetry breaking in the Standard Model

The principle of spontaneous gauge symmetry breaking can easily be extended to the case of a non-Abelian group, in particular the SU(2)$_L \times$U(1)$_Y$ of the Standard Model. In this case, using the expressions (2) and (3) for the gauge field strengths and the expression (4) for the covariant derivative of what is now an isospin doublet of Higgs fields ϕ, we can expand the first (kinetic) term in the bottom line of equation (1), $|D_\mu \phi|^2$, to obtain

$$\mathcal{L} \ni -\frac{g^2 v^2}{4} W_\mu^+ W^{\mu-} - \frac{g'^2 v^2}{8} B_\mu B^\mu + \frac{gg'}{4} B_\mu W^{\mu 3} - \frac{g^2 v^2}{8} W_\mu^3 W^{\mu 3} + \dots. \tag{13}$$

where v is the vev of the scalar field, which is determined in the same way as the previous Abelian example.

The first term in (13) yields masses for the charged vector bosons $W^\pm$:

$$m_W = g\frac{v}{2}. \tag{14}$$

The other three terms yield a mass matrix for the two neutral gauge fields (B, W^3), which can be diagonalized to yield

$$m_Z = \sqrt{g^2 + g'^2}\frac{v}{2} \quad : \quad Z \equiv \frac{gW^3 - g'B}{\sqrt{g^2 + g'^2}},$$
$$m_A = 0 \quad : \quad A \equiv \frac{g'W^3 + g'B}{\sqrt{g^2 + g'^2}}. \tag{15}$$

The first of these mass eigenstates is the massive Z studied in detail in experiments at the LEP accelerator, in particular, and the second, massless eigenstate is identified with the photon. It is useful to introduce the weak mixing angle θ_W:

$$\tan\theta_W \equiv \frac{g'}{g} \to m_Z = \frac{m_W}{\cos\theta_W}, \; Z = \cos\theta_W W^3 - \sin\theta_W B, \; A = \sin\theta_W W^3 + \cos\theta_W A. \tag{16}$$

Measuring θ_W in different ways with high precision has provided important consistency tests of the Standard Model, and provided a clue about the mass of the Higgs boson before its discovery, as we discuss later.

As in the previous Abelian case, there is again a massive scalar (Higgs) boson whose mass is related to the curvature of the potential $V(\phi)$ in the radial direction, and has the value

$$M_H = \sqrt{2}\mu. \tag{17}$$

The couplings of the Higgs boson to other Standard Model particles are predicted exactly. Expanding the first (kinetic) term in the bottom line of equation (1), $|D_\mu \phi|^2$, beyond quadratic order, we find trilinear couplings of the Higgs boson to the massive gauge bosons:

$$g_{HWW} = \frac{2m_W}{v}, \;\; g_{HZZ} == \frac{2m_Z^2}{v}, \tag{18}$$

and there are also important trilinear and quartic Higgs couplings. As was first pointed out be Weinberg [14], the third line in (1) links the Higgs-fermion couplings to their masses:

$$m_f = y_f v \leftrightarrow y_f = \frac{m_f}{v}. \tag{19}$$

The couplings (18, 19) lead to characteristic predictions for the partial decay rates of the Standard Model Higgs boson:

$$\Gamma(H \to f\bar{f}) = N_c \frac{G_F m_H}{4\pi\sqrt{2}} m_f^2, \tag{20}$$

where the number of colours $N_c = 3$ for quarks, 1 for leptons, and (for a sufficiently heavy Higgs boson) [18]

$$\Gamma(H \to W^+ W^-) = \frac{G_F m_H^3}{8\pi\sqrt{2}} F\left(\frac{m_W}{m_H}\right), \tag{21}$$

where $F(m_W/m_H)$ is a phase-space factor, and there is a corresponding formula for $\Gamma(H \to ZZ)$ with a prefactor $1/2$. Experimentally, $m_H < 2m_W$, so the Higgs boson cannot decay into pairs of on-shell gauge bosons, but the decays $H \to WW^*, ZZ^*$ are quite distinctive, and have been measured.

Measurements of the couplings of the boson discovered in 2012 and checking their consistency with the predictions (18, 19) have led to the general acceptance that it is indeed a Higgs boson, as we also discuss later. Future higher-precision measurements will see whether it is consistent with being the single Higgs boson of the Standard Model, or whether the couplings exhibit deviations characteristic of some scenario for new physics beyond the Standard Model.

1.5 Embarking on Higgs phenomenology

In 1975 Mary Gaillard, Dimitri Nanopoulos and I made the first attempt at a systematic survey of the possible phenomenological profile of the Higgs boson [17, 18]. At that time, the Standard Model was not established, idea of spontaneous gauge symmetry breaking was far from being generally accepted, there was general scepticism about scalar particles and, even if one bought all that, nobody had any idea how heavy a Higgs boson might be. For all these reasons, we were rather cautious in the final paragraph of our paper, writing "we do not want to encourage big experimental searches for the Higgs boson, but we do feel that people doing experiments vulnerable to the Higgs boson should know how it may turn up."

Subsequently, searches for the Higgs boson were placed on the experimental agendas of the LEP [19, 20] and LHC accelerators at CERN. For example, a review of the possibilities for new particle searches presented at the first workshop on prospective LHC physics in 1984 [21] discussed various ways of producing the Standard Model Higgs boson at the LHC. There were also studies of Higgs production at the ill-fated SSC [22], and the state of play was described extensively in [23]. However, in the 1980s there was still no indication what the Higgs mass might be.

The first clues about m_H emerged from the high-precision measurements at LEP and the SLC that started in 1989. These and other experiments found excellent overall agreement with the predictions of the Standard Model. However, this consistency depended on the existences if the top quark (which was discovered several years later) and the Higgs boson. The accuracy of the LEP *et al.* measurements pointed towards (what seemed at that time) a relatively heavy top quark [24] and a Higgs boson weighing $\lesssim 180$ GeV [26].

These indications came about through quantum (loop) corrections to electroweak observables, such as the $W^\pm$ and Z masses:

$$m_W^2 \sin^2 \theta_W \;=\; m_Z^2 \sin^2 \theta_W \cos^2 \theta_W \;=\; \frac{\pi\alpha}{\sqrt{2}G_F}\left(1 + \Delta r\right) , \tag{22}$$

where Δr is the leading one-loop radiative correction, which exhibits the following dependences on the top and Higgs masses:

$$\Delta r \;\ni\; \frac{3G_F}{8\pi^2\sqrt{2}}m_t^2 + \ldots , \; \frac{G_F}{16\pi^2}m_W^2\left(\frac{11}{3}\ln\frac{m_H^2}{m_W^2} + \ldots\right) , \tag{23}$$

where we have exhibited the leading dependences on m_t and m_H for large masses. These are relics of the divergences that would appear if either the top quark or the Higgs boson were absent from the Standard Model, which would render it non-renormalizable.

In the early 1990s, even before the top quark was discovered, the precision electroweak data were providing indications that the Higgs mass was probably well below the unitarity limit of 1 TeV [25], which were strengthened when the top quark mass was measured [26]. Back in 2011, just before the Higgs boson was discovered, the precision electroweak data suggested a range $m_H = 100 \pm 30$ GeV. In parallel, unsuccessful searches at LEP had implied that $m_H \geq 114$ GeV [27], and searches at the Fermilab Tevatron collider had excluded a range around $(160, 170)$ GeV [28]. Combining all the information available in 2011, the Gfitter Group obtained the χ^2 likelihood function shown in Fig. 2 [29], corresponding to the estimate

$$m_H \;=\; 125 \pm 10 \text{ GeV} . \tag{24}$$

The success of this prediction was a tremendous success for the Standard Model at the quantum level.

1.6 Higgs production at the LHC

Fig. 3 displays various leading-order diagrams contributing to Higgs production at a proton-proton collider: those for $gg \to H$, vector boson fusion and associated $V + H$ production are shown in the upper row, and diagrams for associated $\bar{t}t + H$ and some of those for single $t + H$ production are shown in the lower row. The left panel of Fig. 4 displays the most important Higgs production cross sections at the LHC at 13 TeV in the centre of mass, as functions of the Higgs mass [30]. The dominant cross section for $m_H \lesssim 1$ TeV is that for gluon fusion: $gg \to H$ via intermediate quark loops [31], the most important in the Standard Model being the top quark. The next most important processes at low masses $m_H \lesssim 100$ GeV are the associated-production mechanisms $q\bar{q} \to W + H, Z + H$ [32], whereas the vector-boson fusion processes $W^+W^-, ZZ \to H$ [33] are more important for $m_H \gtrsim 100$ GeV. Next in the hierarchy of cross sections are the associated-production processes $gg, q\bar{q} \to b\bar{b}H$ (which is difficult to distinguish) and $t\bar{t}H$ [34] (which is more distinctive). Lowest in the hierarchy for $m_H \lesssim 200$ GeV is the cross section for producing H in association with a single t or $\bar{t}$ [35]. The right panel of Fig. 4 displays is a zoom of the cross sections in a limited range of Higgs mass around 125 GeV [30]. The good news is that for $m_H \sim 125$ GeV most of these cross sections are potentially measurable at the LHC, and several of them have already been observed, as discussed later.

As can be seen in Fig. 4, the dominant $gg \to H$ cross section has a relatively large uncertainty. This is because it is a strong-interaction process, which has relatively large perturbative corrections, and
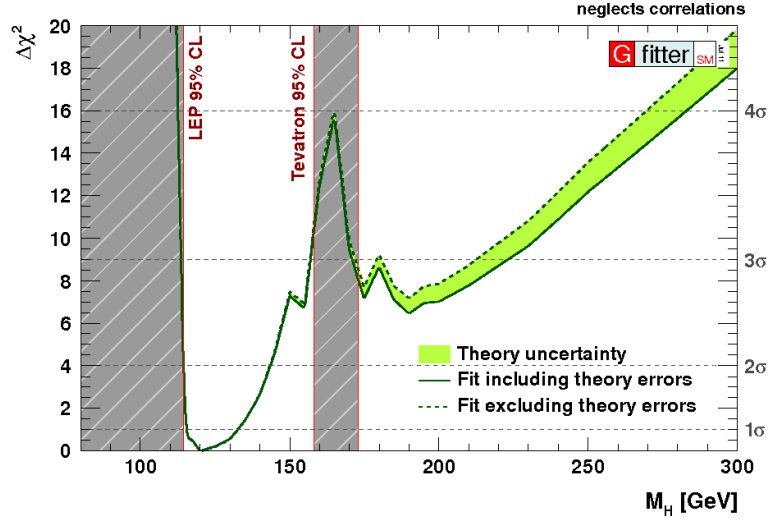
Fig. 2: The $\Delta\chi^2$ as a function of m_H for a complete fit to the data available in mid-2011 [29], including precision electroweak data and the negative results of searches at LEP [27] and the Fermilab Tevatron [29] (grey bands). The solid (dashed) lines represent results that include (omit) theoretical uncertainties.

$$gg \rightarrow H \qquad\qquad \text{Vector boson fusion} \qquad \text{Associated } V + H \text{ production}$$

$$\bar{t}t + H \text{ production} \qquad\qquad s\text{-channel diagrams for } t + H \text{ production}$$
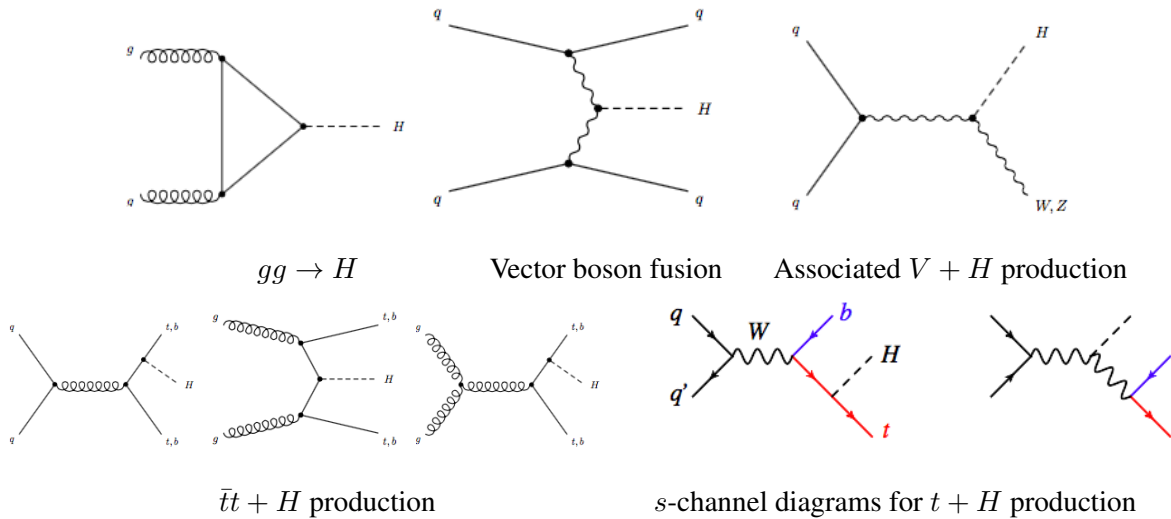
Fig. 3: Leading-order diagrams for Higgs production. Upper row: $gg \rightarrow H$, vector boson fusion and associated $V + H$ production. Lower row: $\bar{t}t + H$ production and s-channel diagrams for single $t + H$ production.

is induced at the loop level, implying that the calculation of these corrections is more arduous than for a tree-level process. Nevertheless, a complete calculation of the $gg \rightarrow H$ cross section at the next-to-next-to-leading order (NNLO) is available, as is a heroic N^{3}LO calculation in the limit of a heavy top quark [36]. The result of these efforts is the following estimate of the $gg \rightarrow H$ cross section [30]:

$$\sigma \;=\; 48.58 \, {}^{+2.22}_{-3.27} \, (\text{theory}) \; \pm 1.56 \, (\text{PDF}, \, \alpha_s) \, \text{pb} \,, \qquad (25)$$

corresponding to a total uncertainty of $< 10\%$. It is worth noting that the NLO correction more than doubled the cross section, that the the NNLO correction was about 20% of the final estimate (25). However, the N^{3}LO correction was only $\sim 3\%$, indicating that the perturbative QCD corrections are under

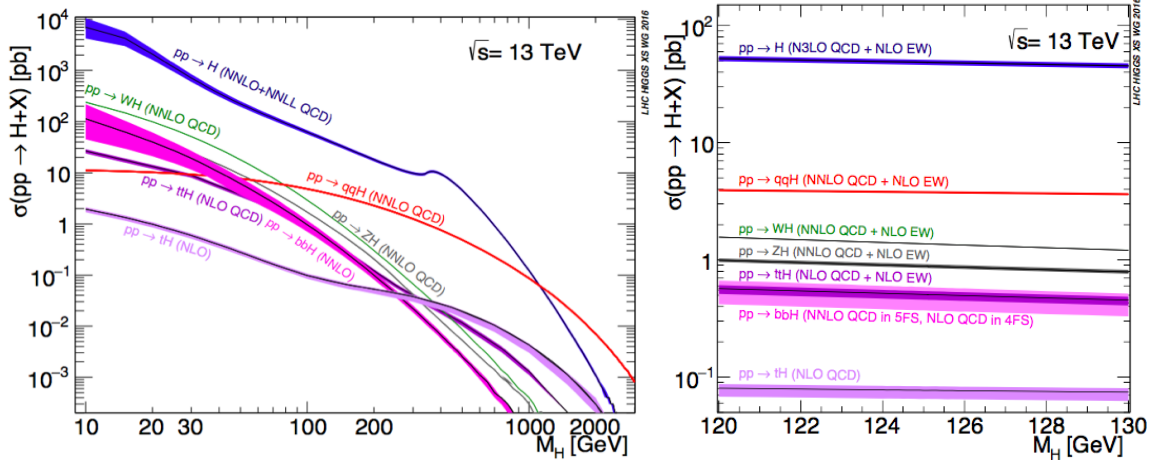**Fig. 4:** Calculations of the dominant production cross sections for a Standard Model Higgs boson, for a wide range of masses (left panel) and for with a $m_H \in [120, 130]$ GeV (right panel) [30]. The uncertainties are represented by the widths of the coloured bands for each production mechanism displayed.

Table 2: Breakdown of the theoretical uncertainties (in pb) in (25) that are associated with different approximations in the calculation of the $gg \to H$ cross section [30].

Scale	Truncation	PDFs (TH)	Electroweak	$m_{t,b,c}$	$1/m_t$
$^{+0.10}_{-1.15}$	± 0.18	± 0.56	± 0.49	± 0.40	± 0.49

control. Table 2 compiles the principal theoretical uncertainties in the calculation (25) of the $gg \to H$ cross section. The first is associated with the choice of scale in the perturbative QCD calculation, and the second is an estimate of the uncertainty due to the truncation of the perturbative expansion. The third is an estimate of the theoretical uncertainty in the use of the parton distribution functions (PDFs) and α_s, and the fourth is an estimate of the uncertainty in higher-order mixed electroweak and QCD perturbative corrections. The fifth is the parametric uncertainty in the values of $m_{t,b,c}$ to be used, and the sixth and last is an estimate of the uncertainty in the heavy-top approximation in the N^{3}LO calculation. We see that many uncertainties are comparable at the level of $\pm \mathcal{O}(0.5)$ pb, indicating that a struggle on many fronts will be needed to reduce substantially the theoretical error in (25).

Concerning the PDF uncertainties in (25), Fig. 5 shows that there is now good consistency between the gg collision luminosities estimated by different PDF fitting groups with the recommendation of the PDF4LHC Working Group [37]. The uncertainty from this source is currently estimated at $\sim 2\%$, which is comparable to the parametric uncertainty associated with α_s. These are currently the largest individual sources of uncertainty in the $gg \to H$ cross section.

There are smaller uncertainties in the cross sections for vector boson fusion (shown in the upper panels of Fig. 6) and H production in association with a $W^\pm$ or Z boson (lower left panel of Fig. 6), both of which have been calculated at NNLO including electroweak corrections at NLO [30]. In both cases, there is good convergence of the perturbation expansion, and there are also quite small uncertainties in the relevant quark parton PDFs. On the other hand, the uncertainties in the cross section for associated $t\bar{t} + H$ production (shown in the lower right panel of Fig. 6) are significantly greater. This is a strong interaction cross section that has been calculated only at NLO, so there are considerable uncertainties associated with the perturbation expansion. Also, there are greater uncertainties associated with the choices of quark, antiquark and gluon PDFs. The situation is similar for single t or $\bar{t} + H$ associated production.
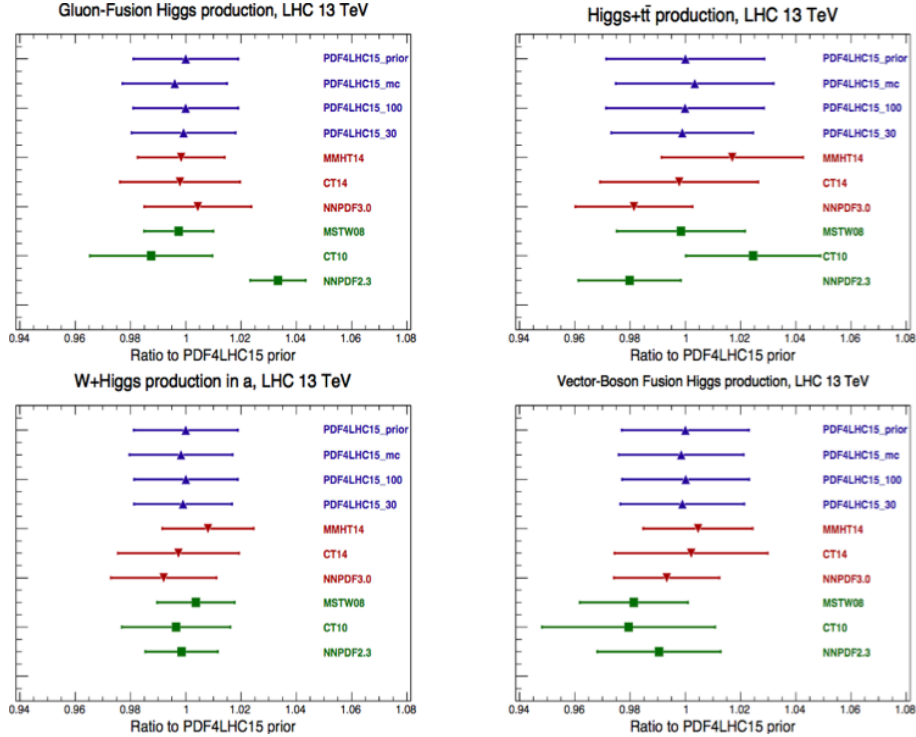
Fig. 5: Comparison between the parton-parton production luminosities calculated using different PDF sets [30], compared to the PDF4LHC recommendation [37].

1.7 Higgs decays

Since Higgs couplings to other particles are proportional to their masses, as seen in (18) and (19), it is expected to decay predominantly into the heaviest particles that are kinematically accessible [17]. This is apparent in the left panel of Fig. 7, which gives an overview of Higgs decay branching ratios for a wide range of Higgs masses. In the specific case of interest when $m_H \simeq 125$ GeV, as seen in the right panel of Fig. 7 [30], we see that $H \to b\bar{b}$ decays are expected to dominate, with $H \to c\bar{c}$ decays suppressed by $(m_c/m_b)^2$, and $H \to \tau^+\tau^-$ decays suppressed by a missing colour factor as well. Since $m_H < 2m_{W,Z}$, only the off-shell decays $H \to WW^*, ZZ^*$ followed by $W^*, Z^* \to f\bar{f}$ decays are possible. Nevertheless, because of the large vector-boson mass factors in (18), these three-body decays have branching ratios comparable to the leading $H \to f\bar{f}$ two-body decays, as seen in the right panel of Fig. 7.

Also comparable is the rate for $H \to gg$ decay, which is a loop-induced process: see Fig. 8. It is difficult to observe $H \to gg$ decay directly, but is related to the rate for the dominant $gg \to H$ fusion production process. The electroweak loop-induced decays $H \to \gamma\gamma$ and $Z\gamma$ occur with somewhat lower branching ratios. However, the $H \to \gamma\gamma$ mode is very clean, and was one of the discovery modes at the LHC. The amplitude for $H \to \gamma\gamma$ decay is generated by loops of massive charged particles [17] as shown in Fig. 8. The most important contributors in the Standard Model are the top quark and the $W^\pm$ boson. Their contributions may be written as follows:

$$\Gamma(H \to \gamma\gamma) = \frac{G_F \alpha^2 m_H^3}{128\pi^3\sqrt{2}} \left| \Sigma_f N_c Q_f^2 A_{1/2}(r_f) + A_1(r_W) \right|^2 , \qquad (26)$$

where $A_{1/2}$ and A_1 are known functions of $r_f \equiv m_f/m_H$ and $r_f \equiv m_W/m_H$ that have opposite signs, so that the top and $W^\pm$ contributions interfere destructively. In the Standard Model, the ggH amplitude receives contributions only from the top and (less important) lighter quarks.
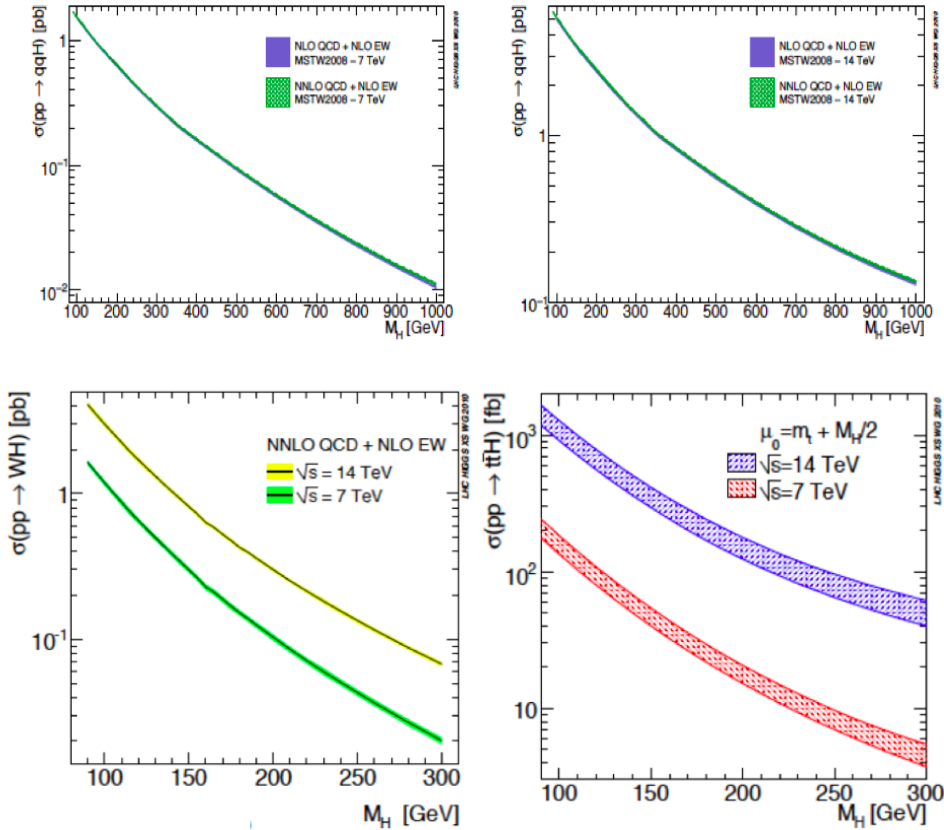
Fig. 6: The cross sections for vector boson fusion production of the Higgs boson with the LHC at 7 TeV (upper left panel), and at 14 TeV (upper right panel), for associated WH production at 7 and 14 TeV (lower left panel), and for $\bar{t}tH$ production at 7 and 14 TeV (lower right panel), all as functions of m_H [38].

The last decay mode shown in the right panel of Fig. 7 is $H \to \mu^+\mu^-$, which is suppressed relative to $H \to \tau^+\tau^-$ by a factor $(m_\mu/m_\tau)^2$. Nevertheless, it also has quite a clean experimental signature, and is expected to be the first decay of H into second-generation fermions to be probed.

There have been strong theoretical efforts to calculate perturbative corrections to H decays [30], leading to the relatively small uncertainties shown in Fig. 7. The largest relative uncertainties are in $H \to gg$ decay, because it is a loop-induced decay into strongly-interacting particles, and $H \to Z\gamma$ decay, where high-order calculations are complicated by the masses of the initial-state H and the final-state Z.

Echoing what was said earlier about Higgs production mechanisms, another piece of good news is that for $m_H \simeq 125$ GeV many Higgs decay modes ares measurable at the LHC. These happy chances provide many opportunities to measure distinctive properties of the Higgs boson. Also, it is an amusing irony that the largest H production mechanism, $gg \to H$, and one of the cleanest H decay channels, $H \to \gamma\gamma$, are both loop-induced processes. Thus, LHC data already give us access to quantum aspects of Higgs physics, including the possible existence of new heavy particles beyond the Standard Model.

If the Higgs boson had weighed 750 GeV (just saying) [39], gathering a lot of information about it would have been more difficult. In that case, observing other production modes besides $gg \to H$ and vector-boson fusion at the LHC would have been difficult, and observing any other decays besides $H \to W^+W^-$, ZZ and $t\bar{t}$ would probably have been impossible in the absence of any other new particles [40]. Obviously, we regret the passing of the late lamented $X(750)$ particle, which would have required new physics to explain its production and decay, but we should thank our lucky stars for the openness of the
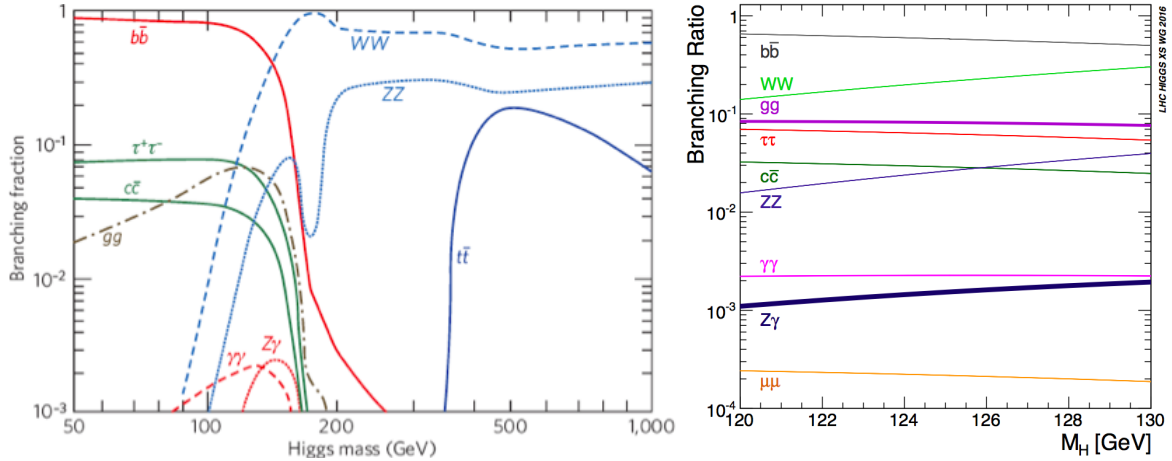
Fig. 7: Calculations of the dominant decay branching ratios for a Standard Model Higgs boson over a large range of masses (left panel) and with mass $m_H \in [120, 130]$ GeV (right panel) [30], where the uncertainties are represented by the widths of the coloured bands for each decay mode displayed.
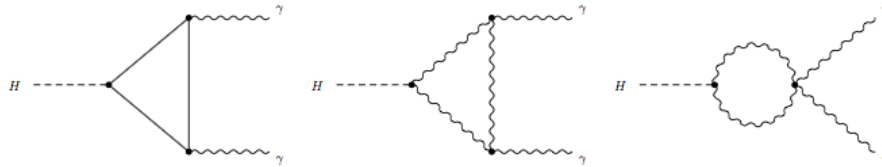

Fig. 8: Loop diagrams for H couplings to massless gauge bosons. In the Standard Model, the dominant fermion diagram (left) for $H \to gg$ and $\gamma\gamma$ involves the top quark. The $W^\pm$ diagrams (middle and right) contribute only to $H \to \gamma\gamma$. There are similar diagrams for $H \to Z\gamma$.

$H(125)$!

1.8 The stakes in the Higgs search

The stakes in the Higgs search were very high. How is gauge symmetry broken: spontaneously (elegantly) or explicitly (ugly and uncalculably)? Assuming that it is broken spontaneously, is it broken by an elementary scalar field, which would be a novelty that raises perhaps more questions than it answers, many of which are related to the hierarchy of mass scales in physics? The Higgs is very likely a portal towards many issues in physics beyond the Standard Model. It would have been associated with a phase transition in the Universe when it was about 10^{-12} seconds old, which maight have been when the baryon asymmetry of the Universe was generated. The Higgs or a related scalar field might have caused the Universe to expand (near-)exponentially in a bout of cosmological inflation when it was about 10^{-35} seconds old. And a Higgs field should contribute a factor $\sim 10^{60}$ too much to the dark energy measured in the Universe today. The stakes in the search for the Higgs boson were undoubtedly high!

1.9 The mass of the Higgs boson

The discovery of the Higgs boson in 2012 [15, 16] was primarily based on the observation of excesses of events in the $\gamma\gamma$ and $2\ell^+2\ell^-$ channels (where $\ell = \mu$ or e), interpreted as being due to $H \to ZZ^*$, together with a broad excess of $\ell^+\ell^-$ + missing transverse energy events, interpreted as being due to $H \to WW^*$.

Measurements of the $\gamma\gamma$ and $2\ell^+2\ell^-$ final states have enabled the mass of the Higgs boson to be determined with high precision. The final combined results from ATLAS and CMS LHC Run 1 data yield [41]

$$m_H = 125.09 \pm 0.21 \,(\text{statistical}) \pm 0.11 \,(\text{systematic}) \,\text{GeV} \,, \tag{27}$$

a measurement at the level of 2 *per mille* that is dominated by the statistical error and hence can be further reduced. An accurate measurement of m_H is a *sine qua non* for precision tests of the Standard Model, since it enters in the Higgs production cross section and decay branching ratios, as seen in the right panels of Figs. 4 and 7. Moreover, it is crucial for the discussion below of the stability of electroweak vacuum. As already mentioned, the measurement (27) is fully in line with previous indications from precision electroweak data and previous searches at LEP [27] and the Fermilab Tevatron collider [28], see Fig. 2. Fig. 9 shows a direct comparison between the ATLAS and CMS measurements of m_H and the χ^2 function from a global analysis of the precision electroweak data, omitting the LEP and Tevatron constraints [42]. We see that the measured value of m_H agrees with the indication from the electroweak data at the $\Delta\chi^2 \sim 1.5$ level.

This may seem like a disaster for the quest for physics beyond the Standard Model, but not so fast!
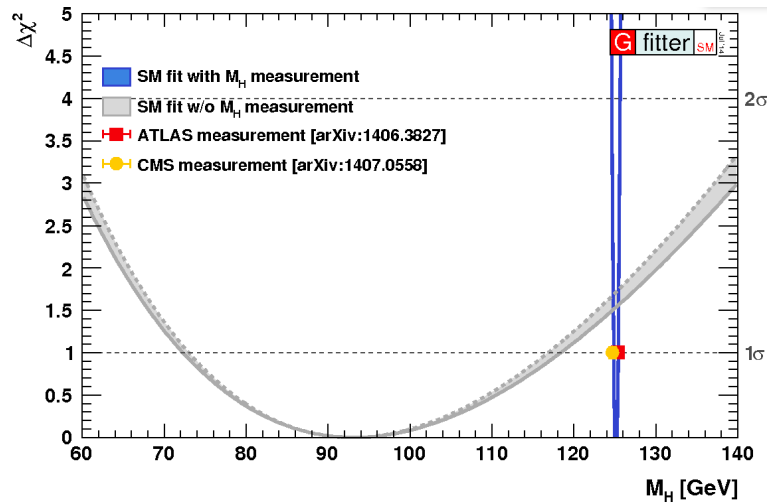
Fig. 9: The $\Delta\chi^2$ as a function of m_H for a fit to the precision electroweak data compared with the measurements of m_H by the ATLAS and CMS Collaborations [42].

1.10 The instability (?) of the electroweak vacuum

Let us consider the second, $\lambda\phi^4$, term in the Higgs potential (5) It is essential for the Mexican hat form of the potential seen in Fig. 1 and the existence of the non-zero vev (6) that $\lambda > 0$. However, like any other coupling in a quantum field theory, λ is subject to renormalization. In the Standard Model, there are two important sources of this renormalization at the one-loop level. One is that due to λ itself, which tends to *increase* λ as the renomalization scale Q increases:

$$\lambda(Q) \simeq \frac{\lambda(v)}{1 - \frac{3}{4\pi^2}\lambda(v)\ln\left(Q^2/v^2\right)} \,. \tag{28}$$

Left to itself, this self-renormalization would cause λ to blow up at some high renormalization scale Q. However, there is also importantant one-loop renormalization of λ due to loops of top quarks:

$$\lambda(Q) \simeq \lambda(v) - \frac{3m_t^4}{4\pi^2 v^2}\ln\left(Q^2/v^2\right) \,, \tag{29}$$

which tends to *decrease* λ as the renomalization scale Q increases, driving it towards negative values. If λ indeed turns negative, there soon appears a field value with lower energy than our electroweak vacuum, which becomes unstable or at least metastable.

The left panel of Fig. 10 illustrates how the negative renormalization by the top quark drives $\lambda < 0$ in the Standard Model [43, 44], though this is subject to uncertainties in m_t, in particular. As seen in the right panel of Fig. 10, the current world averages of m_t and m_H suggest that these parameters indeed lie within the region where the Standard Model electroweak vacuum is metastable. *In my view, this is a potential disaster (pun intended) that would require new physics to avert it.*
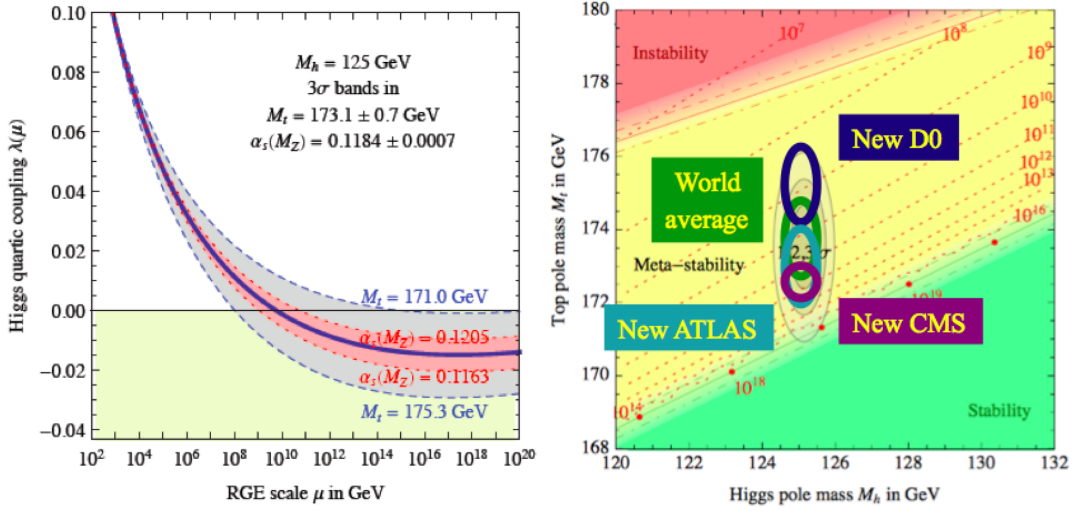

Fig. 10: Left panel: The negative renormalization of the Higgs self-coupling by the top quark within the Standard Model leads to an instability in the Higgs potential for field values $\sim 10^9$ GeV [43]. Right panel: Experimental measurements of m_t and m_H suggest that the electroweak vacuum of the Standard Model would be metastable, modulo uncertainties in m_t, in particular [44].

As seen in Fig. 10, the location and indeed existence of the instability scale Λ_I are particularly sensitive to m_t, and also to α_s as well as to m_H. One calculation including higher-order effects yields the following dependences on these parameters [44]:

$$\log_{10}\left(\frac{\Lambda_I}{\text{GeV}}\right) = 9.4 + 0.7\left(\frac{m_H}{\text{GeV}} - 125.15\right) - 1.0\left(\frac{m_t}{\text{GeV}} - 173.34\right) + 0.3\left(\frac{\alpha_s(m_Z) - 0.1184}{0.0007}\right). \tag{30}$$

Inserting the world average value (27) for m_H, $m_t = 173.3 \pm 1.0$ GeV and $\alpha_s(m_Z) = 0.1181 \pm 0.0011$, we estimate

$$\log_{10}\Lambda_I) = 9.4 \pm 1.1\,, \tag{31}$$

indicating that (in the immortal words of the Apollo 13 astronauts) we have a problem [45].

Several words of caution are in order. The first is that the experimental measurement of m_H (27) is already so accurate that it is the smallest source of uncertainty in (30). Concerning the larger uncertainty due to m_t, subsequent to the compilation of the world average value [46], several new measurements have been published, including by D0: $m_t = 174.98 \pm 0.76$ GeV [47], by ATLAS: $m_t = 172.99 \pm 0.91$ GeV [48] and by CMS: $m_t = 172.4 \pm 0.49$ GeV [49]. These scatter above and below the official world average, and a new compilation awaits better understanding of the discrepancies between them. However, all these measurements lie in the unstable region of m_t. A second comment concerns the interpretation of the value of m_t that the experiments measure. This is defined within a specific Monte Carlo event simulation code, and one issue concerns the relation between this and the pole mass. Present understanding is that the difference between these definitions $\sim \Lambda_{QCD} < 1$ GeV, so this correction seems

manageably small at the present time, though it will require more detailed analysis as the experimental precision improves. Another issue concerns the relation between the pole mass and the $\overline{MS}$ mass that is used in the loop calculations of vacuum stability. This relation has been calculated to $\mathcal{O}(\alpha_s^4)$ [50]:

$$
\begin{aligned}
\frac{m_t|_{\text{pole}} - m_t|_{\overline{\text{MS}}}}{m_t|_{\overline{\text{MS}}}} \equiv \frac{\delta m}{m_t|_{\overline{\text{MS}}}} \equiv \Delta = {}& 0.4244\,\alpha_s(m_t) + 0.8345\,\alpha_s(m_t) \\
& + 2.375\,\alpha_s(m_t)^3 + (8.49 \pm 0.25)\,\alpha_s(m_t)^4 + \dots, \quad (32)
\end{aligned}
$$

leading to the numerical result

$$
m_t|_{\text{pole}} = m_t|_{\overline{\text{MS}}} + 7.557 + 1.1617 + 0.501 + 0.195 + \dots, \quad (33)
$$

where the numbers are for the $\mathcal{O}(\alpha_s^n)$ corrections calculated for $n = 1, 2, 3, 4$ assuming $m_t|_{\overline{MS}} = 163.643$ GeV. These corrections decrease systematically in magnitude, so the QCD perturbation series seems to be well-behaved. The sum of the uncalculated higher-order terms has been estimated to be ~ 250 GeV, with uncertainty of ~ 70 GeV [51]. These effects are also below within the current experimental precision.

Another comment concerns the length of the lifetime of our (in principle) unstable electroweak vacuum, which may be much longer than the age of the Universe to date. This is certainly a necessary consistency condition for the existence of physicists capable of recognizing the problem, but also leads some of them to disregard it as unimportant. I disagree with this attitude for two reasons. One is because the present vacuum energy is very small and positive. Arguments have been proposed how this might come about if our vacuum is (one of) the lowest-energy state(s) in an extensive landscape, or one might imagine that some approximate symmetry could yield a small positive value. Personally, I would find the small value of the present vacuum energy much more difficult to understand if it is only a temporary state, and if our universe will eventually decay into an anti-De Sitter state with negative vacuum energy of much larger magnitude. The other reason for taking vacuum stability seriously as a requirement is that, if it were not, fluctuations in the Higgs field in the hot and dense early universe would have taken most of it into the anti-De Sitter "Big Crunch" phase, and the conventional expansion of the universe would never have occurred [52, 53]. On the other hand, one could argue anthr*p*c*lly that if even an infinitesimal part of the universe escaped the "Big Crunch", that would have been enough for sentient physicists to come into being.

My own take on the instability problem is that we should take it seriously, and that it motivates some form of new physics to stabilize the electroweak vacuum [1]. Clearly, any such physics should appear at some energy scale below $\Lambda_I \sim 10^9$ GeV, but might lie far beyond the reach of conceivable accelerators. However, in my view it is the best hint for some new physics beyond the Standard Model provided by Run 1 of the LHC.

What might this new physics look like? As we saw above, it is the negative sign of the top quark loop that destabilizes the effective Higgs potential. In order to counteract it, one should introduce a scalar ϕ, whose loop would have a positive sign, and which could in general have couplings of the forms [54]:

$$
\mathcal{L} \ni M^2|\phi|^2 + \frac{M_0^2}{v^2}|H|^2|\phi|^2, \quad (34)
$$

where M and M_0 are two mass parameters. Indeed, if one chooses $M \lesssim 10^5$ GeV, the effective Higgs potential can be stabilized. However, avoiding a blow-up in λ as well as a negative value typically requires some fine-tuning of M_0, i.e., the coupling of the new scalar ϕ to the Higgs field H, at the *per mille* level. The simplest way to stabilize the coupling is to postulate new fermions to counteract the $\phi-H$ coupling in (34). But now we have introduced scalar partners of the top and fermionic partners of the Higgs that make the theory reminiscent of supersymmetry [54]. So, why not postulate supersymmetry, as we discuss in the second Lecture?

---

[1] Assuming that we have not misunderstood the experimental measurements of m_t.

1.11 Higgs coupling measurements

The ATLAS and CMS Collaborations have published a joint analysis of their measurements of Higgs production and decay in various channels [55], as shown in Fig. 11. Several Higgs decay modes have been established with high significance, including $\gamma\gamma$, WW^*, ZZ^* and $\tau^+\tau^-$, and there are important constraints on other Higgs decay models. The $gg \to H$ and vector boson fusion production mechanisms have been established, and there are interesting constraints on H production in association with $W^\pm$, Z and $t\bar{t}$ pairs.
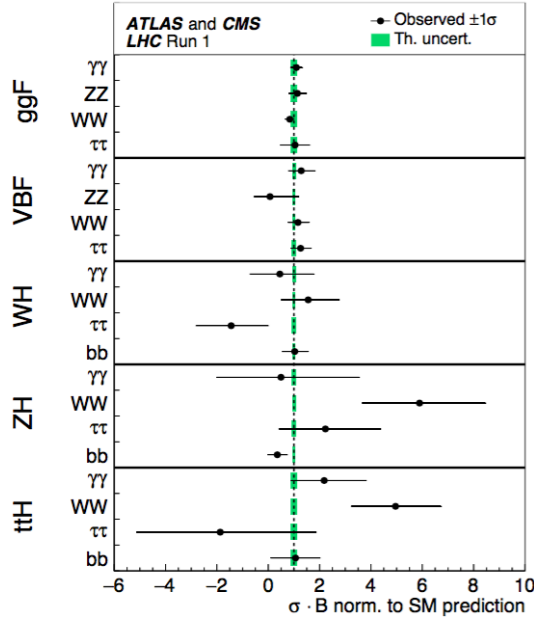

Fig. 11: The products of cross sections σ and branching ratios B measured by the ATLAS and CMS Collaborations in various channels, normalized to the Standard Model predictions [55].

However, many H couplings remain to be established. Most prominently, the $H \to b\bar{b}$ decay that is expected to dominate has been seen only at the 2.6-σ level at the LHC and the 2.8-σ level at the Tevatron [56]. Moreover, although there is indirect evidence for a $t\bar{t}H$ coupling from measurements of the induced ggH and $\gamma\gamma H$ couplings, there is no direct evidence in the absence of measurements of $t\bar{t}H$ (or single $t/\bar{t}H$) associated production. Also, there is as yet no evidence for $H \to \mu^+\mu^-$ decay, though upper limits on it already provide interesting information, as we see in the second Lecture.

The first analyses of Higgs data from Run 2 of the LHC have also been shown by ATLAS and CMS [57]. The distinctive $H \to \gamma\gamma$ and ZZ^* decays have been seen again with 10-σ significance, the Higgs production cross section at 13 TeV is in line with theoretical calculations, and the searches are on for $H \to \mu^+\mu^-$ and associated $t\bar{t}H$ and single $t/\bar{t}H$ production.

1.12 Not a big deal?

Shortly after the discovery of the Higgs boson, Peter Higgs was quoted in the Times of London as saying: "A discovery widely acclaimed as the most important scientific advance in a generation has been overhyped" [58]. I would very humbly and respectfully beg to disagree. Without the Higgs boson (or something to do its job), there would be no atoms because electrons would escape from nuclei at the speed of light, the weak interactions responsible for radioactivity would not be weak, and the universe would be totally unliveable. *It was a big deal.*

2   The Particle Physics Higgsaw Puzzle

2.1   Has the LHC found the missing piece?

The first piece of the particle physics jigsaw puzzle to be discovered was the electron in 1997, and it took 115 years until a candidate for the final missing piece of the Standard Model, the Higgs boson, was discovered in 2012 [15, 16]. In the first Lecture, I was jumping the gun, blithely assuming that the particle discovered in 2012 is indeed the Higgs boson. In this Lecture we first review the experimental and theoretical justifications for this assumption. In the language of jigsaw puzzles, is it the right shape, and does it have the right size, in the language of particle physics, does it have the right spin, parity and couplings? We then discuss what physics may lie behind and beyond it, and review how to probe these ideas with possible future accelerators.

2.2   What are its spin and parity?

Since the $H(125)$ particle decays into pairs of photons, Lorentz invariance assures us that it cannot have spin 1, but it might *a priori* have spin 0, 2 or higher and, in each case, it might have either positive or negative parity. Many tests of the $H(125)$ spin and parity have been proposed theoretically and carried out by the LHC experiments. Examples include the polar angle distribution in $H \to \gamma\gamma$ decays and final-state angular correlations in $H \to WW^* \to \ell + \ell^- +$ missing transverse energy decays and in $H \to ZZ^* \to 2\ell + 2\ell^-$ decays [59]. Also, the kinematics of $H(125)$ production mechanisms such as production in association with a W or Z boson would differ for different spin-parity assignments [60], which have been probed by the Fermilab Tevatron experiments [61].

One example of a spin-parity analysis of the $H(125)$ in the $X \to ZZ \to 2\ell^+ 2\ell^1$ final state is shown in Fig. 12 [62]. This and all the other published analyses are in excellent agreement with the $J^P = 0^+$ spin-parity assignment predicted for the Higgs boson, and all the alternative spin-parity assignments studied have been strongly excluded. These include the pseudoscalar 0^- possibility and various spin-2 possibilities. The $H(125)$ passed these first important experimental tests with flying colours.
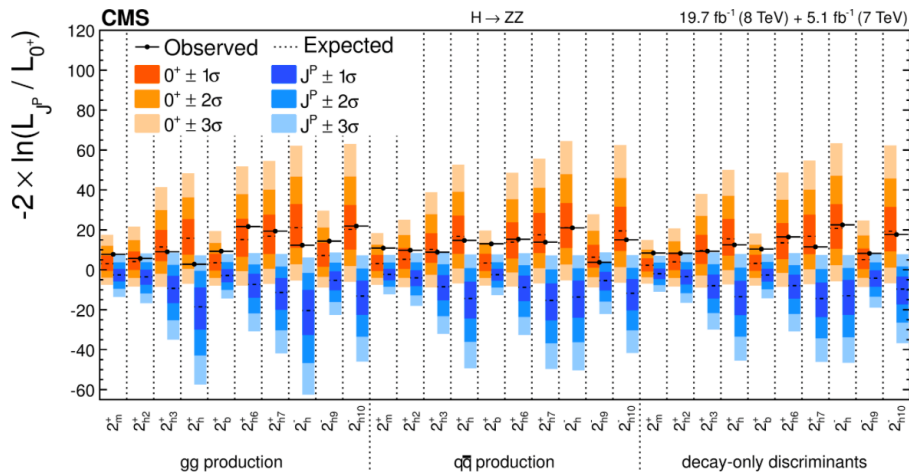
Fig. 12: Comparison between the Standard Model Higgs boson hypothesis in the $X \to ZZ \to 2\ell^+ 2\ell^-$ final state with various spin-two J^P hypotheses [62].

2.3   Does it couple to particle masses?

It is a fundamental property of the Higgs boson that, since the field vev gives masses to the other elementary particles, the H couplings to them should be proportional to their masses, see (18) and (19). One

way to test this is to analyze the $H(125)$ production and decay data assuming couplings to other particles that are proportional to some nonlinear power of their masses [63]:

$$y_f = \left(\frac{m_f}{M}\right)^{1+\epsilon}, \quad g_V = \left(\frac{m_V^{2(1+\epsilon)}}{M^{1+2\epsilon}}\right), \quad (35)$$

where the unknown power ϵ and mass scale M are to be fitted to the data, the Standard Model expectations being $\epsilon = 0$ and $M = v = 246$ GeV. The result of such an analysis performed jointly by the ATLAS and CMS Collaborations is shown in Fig. 13 [55], including the best fit and the 68 and 95% CL bands. The joint analysis yields

$$\epsilon = 0.023^{+0.029}_{-0.027}, \quad M = 233 \pm 13 \text{ GeV}, \quad (36)$$

which are highly compatible with the Standard Model predictions. In this way, the $H(125)$ passed another crucial experimental test. We can also see explicitly in Fig. 13 that the decay rates for $H \to \mu^+\mu^-$ and $\tau^+\tau^-$ must be very different, a first strong violation of lepton universality, as expected in the mass-dependent couplings of the Higgs boson.
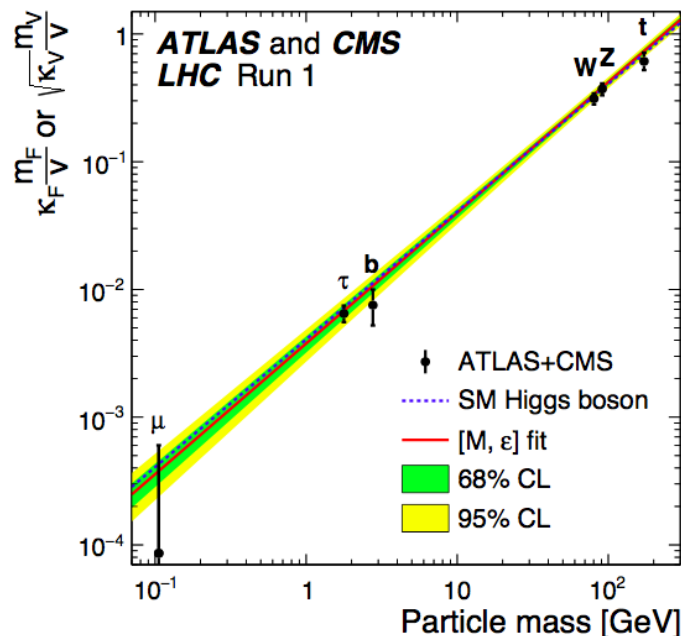
Fig. 13: A fit to a parametrization of the form (35) to Higgs coupling measurements by the ATLAS and CMS Collaborations in various channels. The dotted line connects the Standard Model predictions, the best fit is shown as a red line, and the 68 and 95% CL ranges are shown as green and yellow bands [55].

2.4 Flavour-changing couplings?

Flavour-changing couplings of the Higgs boson are expected to be very suppressed in the Standard Model, though they might be present in extensions with multiple Higgs multiplets. Upper limits on flavour-changing interactions at low energies and dipole moments can be used to constrain the the possible flavour-changing interactions of the $H(125)$ [64]. Examples of relevant tree and loop diagrams involving H are shown in Fig. 14. Upper limits on flavour-changing quark interactions exclude the observability of quark-flavour-violating $H(125)$ decays, but lepton-flavour-violating decays could be relatively large. We found that the branching ratio for either $H \to \tau\mu$ or τe (but not both) could be
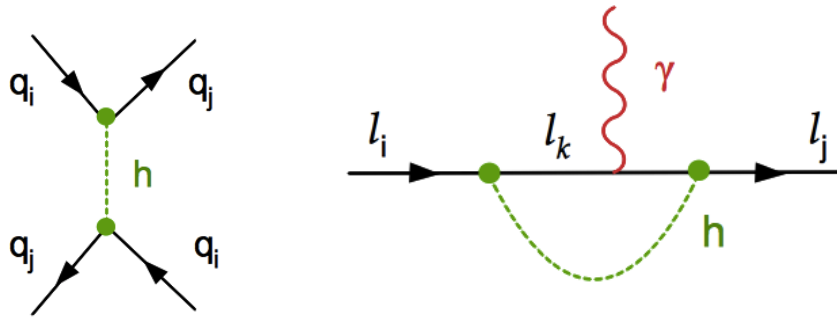
Fig. 14: Left panel: Tree-level H-exchange diagram that may contribute to a generic flavour-changing amplitude. Right panel: One-loop H-exchange diagram that may contribute to anomalous magnetic and electric dipole moments of charged leptons ($i = j$), or to radiative lepton-flavour-violating decays ($i \neq j$) [64].

$\mathcal{O}(10)\%$, comparable to the Standard Model prediction for BR($H \to \tau^+\tau^-$), whereas the branching ratio for $H \to \mu e$ must be $< 2 \times 10^{-5}$. Analyses of LHC Run 1 data yielded results [65, 66] compatible with these upper limits:

$$
\begin{aligned}
\text{CMS}: \text{BR}(H \to \tau\mu) &= 0.84^{+0.39}_{-0.37}\%, \ \text{BR}(H \to \tau e) < 0.69\%, \ \text{BR}(H \to e\mu) < 0.036\%, \\
\text{ATLAS}: \text{BR}(H \to \tau\mu) &= 0.77 \pm 0.62\%.
\end{aligned}
\tag{37}
$$

That said, the CMS result for BR($H \to \tau\mu$), in particular, whetted theoretical appetites for additional data from Run 2 of the LHC. A first preliminary result from CMS does not indicate any deviation from the Standard Model [67], but this is definitely *une affaire à suivre*!

2.5 Loop-induced couplings

As mentioned in the first Lecture, two of the most important Higgs couplings are induced by loop diagrams, namely the ggH vertex responsible for the dominant H production mechanism, which is mainly generated by the top quark in the Standard Model, and the $H\gamma\gamma$ vertex responsible for one of the most distinctive $H(125)$ decays, which is mainly generated by loops of top quarks and $W^\pm$ bosons in the Standard Model, as shown in Fig. 8. Via these vertices, the Run 1 LHC data have already provided important consistency checks on the Standard Model predictions for the H couplings at the quantum level. Fig. 15 displays the combined ATLAS and CMS constraints on the magnitudes of the $H\gamma\gamma$ and ggH couplings relative to their Standard Model values [55]. We see good consistency at the 10 to 20% level, which also provides significant restrictions on possible extensions of the Standard Model such as a fourth generation, supersymmetric particles and heavy vector-like quarks.

2.6 Is it elementary or composite?

Broadly speaking, there are two schools of theoretical thought about this question.

On the one hand, many theorists are attracted by the idea of an elementary Higgs scalar field, as in the original formulation, but are concerned by the problems connected with loop corrections to the Higgs mass. Quantum corrections to the mass parameter μ in the effective potential (5) due to, e.g., the top quark or the Higgs self-coupling, exhibit quadratic divergences. If one cuts the loop integrals off at some momentum scale Λ, one is left with large residual contributions if Λ is identified with some high new physics scale such as that of grand unification or the Planck mass. In the case of a loop of fermions
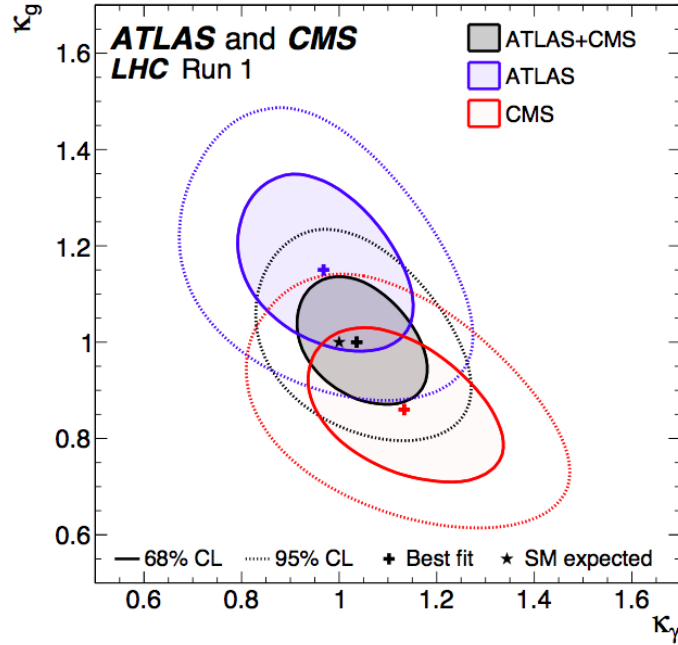
Fig. 15: A fit by the ATLAS and CMS Collaborations to the magnitudes of the $H\gamma\gamma$ and ggH couplings, normalized by factors $(\kappa_\gamma, \kappa_g)$ relative to their Standard Model values [55].
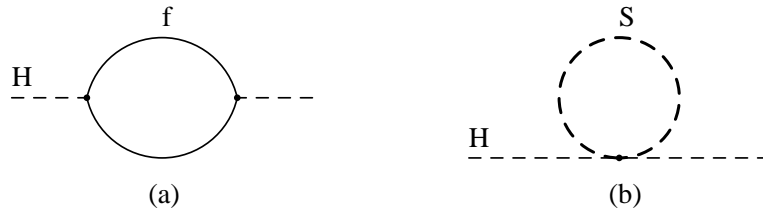
Fig. 16: One-loop quantum corrections to the mass-squared of the Higgs boson due to (a) the loop of a generic fermion f, (b) a generic scalar S.

f such as the top quark, shown in Fig. 16(a), one finds

$$\Delta m_H^2 = -\frac{y_f^2}{8\pi^2}\left[2\Lambda^2 + 6m_f^2 \ln(\Lambda/m_f) + ...\right], \qquad (38)$$

where y_f is the Yukawa coupling and the ... represent non-divergent mass-dependent terms, and in the case of a loop of scalars S, shown in Fig. 16(b), one finds similar divergent contributions:

$$\Delta m_H^2 = \frac{\lambda_S}{16\pi^2}\left[\Lambda^2 - 2m_S^2 \ln(\Lambda/m_S) + ...\right]. \qquad (39)$$

If the Standard Model were to remain valid up to the Planck scale, $M_P \simeq 10^{19}$ GeV, so that $\Lambda = M_P$, each of the quadratic "corrections" would be $\simeq 10^{34}$ times larger than the physical mass-squared of the Higgs, namely (10^4) GeV^2.

The relatively small physical value of the Higgs mass is not protected by any symmetry of the Standard Model, and keeping it small seems to require some unnatural fine-tuning unless there is some

suitable new physics at the TeV scale. The favoured example of such new physics in an elementary Higgs scenario is supersymmetry, which exploits the opposite signs of loop corrections due to fermions and bosons in (38, 39). If these occur in pairs with related couplings:

$$\lambda_S = 2\lambda_f^2 \tag{40}$$

as in supersymmetric models [68], and if the differences between the masses of supersymmetric partners are $\mathcal{O}(1)$ TeV so that the subleading terms in (38, 39) are not large, the quadratic term μ in the Higgs potential (5) is kept naturally small, and hence also the Higgs mass and the electroweak scale. One of the miracles of supersymmetry is that the symmetry between fermions and bosons cancels not only the one-loop quadratic divergences (38, 39), but also all quadratic divergences at higher order in perturbation theory, as well as many logarithmic divergences [69].

On the other hand, many other theorists believe that the Higgs is composite, a bound state of fermions like Cooper pairs in BCS superconductivity and pions in QCD. Such a theory has a natural cut-off at the scale of the strongly-interacting composite dynamics, analogous to Λ_{QCD}. The Standard Model does not contain any candidate for this new strong dynamics, and attention focused initially on some scaled-up version of QCD [70]. However, simple models of this type were incompatible with the precision electroweak data mentioned in the first Lecture, and predicted a heavy strongly-interacting scalar particle unlike the Higgs boson discovered in 2012. Accordingly, attention has shifted to an alternative idea that the Higgs boson is analogous to the pion of QCD, namely that it is a pseudo-Nambu-Goldstone boson of some larger chiral symmetry that is broken down to the Standard Model, much like the pion in QCD [71]. In such a model, the lightness of the Higgs boson is enforced by this approximate chiral symmetry. Generic features of such theories include a coloured top partner fermion that cancels the one-loop Higgs mass corrections due to the top quark, some new scalars and/or gauge bosons with relatively low masses $\lesssim 1$ TeV, and a strongly-interacting ultraviolet completion at a mass scale that is $\mathcal{O}(10)$ TeV.

A convenient way to parametrize the phenomenology of such a theory is to assume that the Higgs sector has an underlying SU(2)×SU(2) structure that is broken down to a custodial SU(2) symmetry so as to retain the successful tree-level relation $\rho \equiv m_W/m_Z \cos\theta_W \simeq 1$. The Goldstone bosons $\pi_a : a = 1, 2, 3$ of this symmetry-breaking pattern that are 'eaten' by the $W^\pm$ and Z to become their longitudinal polarization states are then parametrized by a traceless 2×2 matrix $\Sigma = \exp(i\sigma_a \pi_a/v)$, with the following couplings to the Higgs boson H:

$$\begin{aligned}
\mathcal{L} &= \frac{v^2}{4} \mathrm{Tr} D_\mu \Sigma D^\mu \Sigma \left(1 + 2a\frac{H}{v} + b\frac{H^2}{v^2} + \dots\right) - m_i \bar{\psi}_L^i \Sigma \left(c\frac{H}{v} + \dots\right) + \mathrm{h.c.} \\
&+ \frac{1}{2}\partial_\mu H \partial^\mu H + \frac{1}{2}H^2 + d_3\frac{1}{6}\left(\frac{3m_H^2}{v}\right)H^3 + d_4\frac{1}{24}\left(\frac{3m_H^2}{v}\right)H^4 + \dots,
\end{aligned} \tag{41}$$

where the coefficients $a, b, c, \dots$ are normalized so that they are all unity in the Standard Model. The task of experiments is then to measure these coefficients and see whether they differ from these predictions, as they may in composite Higgs models. For example, in two minimal composite Higgs models $\mathrm{MCHM}_{4,5}$ one has

$$\begin{aligned}
\mathrm{MCHM}_4 &: \quad a = \sqrt{1-\zeta}, \quad c = \sqrt{1-\zeta}, \\
\mathrm{MCHM}_5 &: \quad a = \sqrt{1-\zeta}, \quad c = \frac{1-2\zeta}{\sqrt{1-\zeta}},
\end{aligned} \tag{42}$$

where ζ is a model parameter that is not specified *a priori*.

Fig. 17 shows two experimental analyses of the data, using a different notation: $a \to \kappa_V, c \to \kappa_F$. The left panel compares the constraints from Higgs data alone (yellow and orange ellipses) with the result of a global analysis including also precision electroweak data (blue ellipses) [72]. We see that

these are largely complementary, with the Higgs data constraining $\kappa_F = c$ and the electroweak data constraining $\kappa_V = a$. The Standard Model prediction $\kappa_F = c = 1$, $\kappa_V = a = 1$ is close to the best-fit point and well within the global 68% CL contour. The right panel compares ATLAS and CMS Higgs measurements with the predictions (42) of the MCHM$_{4,5}$ models [73]. We see that the data require $\zeta \lesssim 0.1$, necessitating some tuning of these models so that their predictions resemble those of the Standard Model.
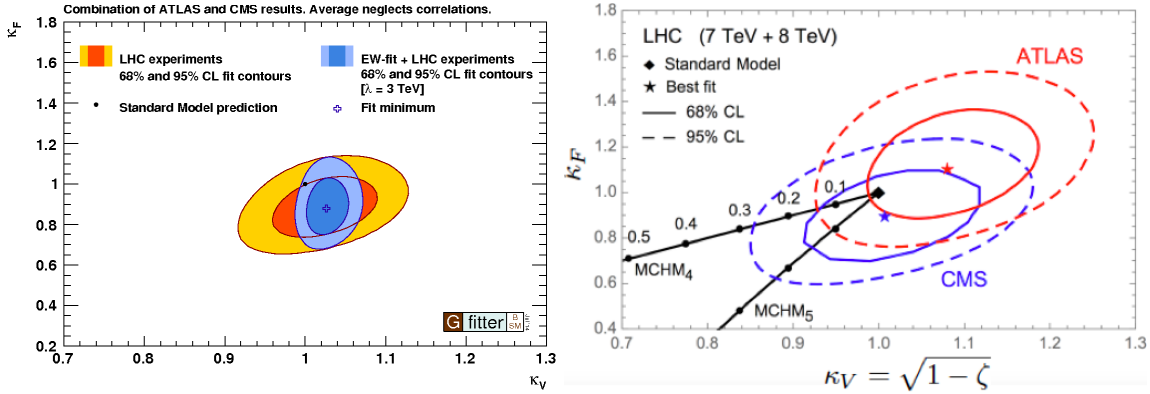

Fig. 17: Left panel: A fit by the Gfitter Group to the LHC H coupling measurements (orange and yellow ellipses) and in combination with precision electroweak data (blue ellipses) [72]. Right panel: Comparison of ATLAS and CMS constraints on H couplings with predictions of the MCHM$_{4,5}$ models [73].

Fig. 18 shows how the different Higgs coupling measurements by ATLAS and CMS combine to give their overall constraints on (κ_V, κ_F) [55]. Most of the measurements are relatively insensitive to the sign of κ_F, the exception being that of the $H\gamma\gamma$ coupling. Its sensitivity is due to the interference between the top and $W^\pm$ loop contributions to the coupling, which interfere destructively for the Standard Model (positive) sign of κ_F and constructively for the non-standard (negative) sign. Largely as a result of this asymmetry, the combined fit decisively favours the Standard Model sign of κ_F. Measuring the cross section for single $t/\bar{t}H$ production could also provide a direct determination of this sign, and could probe the possible existence of a CP-violating $t\bar{t}H$ coupling [74].

The general conclusion of these analyses using the parametrization (41) is that there is no indication of any deviation from the Standard Model predictions for the H couplings of the form that might have arisen in a composite Higgs scenario. Introducing a single global modification factor μ for the H couplings to Standard Model particles, the combined ATLAS and CMS data imply that [55]

$$\mu = 1.09^{+0.11}_{-0.10} = 1.09 \pm 0.07\,(\text{stat.}) \pm 0.04\,(\text{expt}) \pm 0.03\,(\text{thbgrd})^{+0.07}_{-0.06}\,(\text{thsig})\,, \qquad (43)$$

where the last three uncertainties are systematics. Thus, overall the strength of the Higgs couplings agrees with the Standard Model at the $\sim 10\%$ level, though individual couplings have larger uncertainties. Moreover, there is no evidence for any decays of H to unknown particles, in particular invisible decays. The $H(125)$ particle looks very much the way it was predicted in the Standard Model.

For this reason, the Physics Class of the Swedish Academy stated in its citation for the 2013 Nobel Prize [75] that *Today we believe that "Beyond any reasonable doubt, it is a Higgs boson."* [2].

---

[2]This quotation was taken from the preprint version of [63]. They apparently did not notice that this phrase was removed from the published version of [63] at the insistence of the anonymous referee, who considered that "Beyond any reasonable doubt" is not a scientific statement.
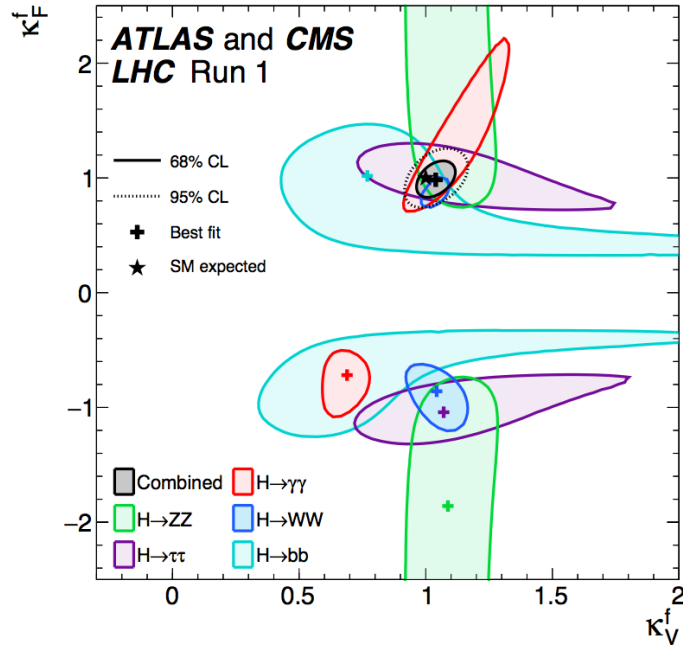
Fig. 18: A fit by the ATLAS and CMS Collaborations to the magnitudes of the HVV and $H\bar{f}f$ couplings, normalized by factors (κ_V, κ_F) relative to their Standard Model values [55].

2.7 The Standard Model effective field theory

At this point a popular approach is to assume that the $H(125)$ particle is exactly Standard Model-like, and use it in a model-independent search for new physics that could manifest itself via higher-dimensional effective interactions between Standard Model fields, in particular those of dimension 6 [76]:

$$\mathcal{L}_{eff} = \sum_n \frac{c_n}{\Lambda^2} \mathcal{O}_n \,, \tag{44}$$

where Λ is some characteristic scale of new physics and the c_n are unknown dimensionless coefficients. These can be constrained by a combination of data on Higgs properties, precision electroweak data, triple-gauge couplings (TGCs), etc.. The beauty of this approach is that it provides an integrated framework for analyzing all these categories of data in a unified and consistent way.

This attractive approach is, however, unwieldy when applied in full generality, because of the large number of possible dimension-6 operators, even if one assumes the SU(2)×U(1) symmetry of the Standard Model. For this reason, one often makes simplifying assumptions, e.g., about the flavour structure of the operators. Furthermore, if one restricts attention to precision electroweak observables, Higgs and TGC measurements, global fits to these data become manageable. Table 3 lists the CP-even dimension-6 operators [77] relevant for these measurements. In each case, we also indicate the categories of observables that provide the greatest sensitivities to the operator coefficients.

The left panel of Fig. 19 shows results from a fit to precision data on leptonic electroweak observables [78]. The lower horizontal axis shows the possible numerical values of these coefficients, and the upper horizontal axis shows the corresponding new physics scales. Here and in subsequent plots, the green bars are for fits to individual operator coefficients assuming the other operators are absent, and the bars of other colours are for global fits marginalizing of all the operators that could contribute. In general, these coloured bars extend further than the green bars. The right panel of Fig. 19 extends this analysis to include hadronic electroweak observables [78]. The vertical dashed lines in the two panels are for the

Table 3: The relevant CP-even dimension-6 operators in the basis [77] that we use. For each operator, we list the categories of observables that provide the greatest sensitivities to the operator.

EWPTs	Higgs Physics	TGCs
$\mathcal{O}_W = \frac{ig}{2}\left(H^\dagger \sigma^a \leftrightarrow D^\mu H\right) D^\nu W_{\mu\nu}^a$		
$\mathcal{O}_B = \frac{ig'}{2}\left(H^\dagger \leftrightarrow D^\mu H\right) \partial^\nu B_{\mu\nu}$		$\mathcal{O}_{3W} = g\frac{\epsilon_{abc}}{3!} W_\mu^{a\,\nu} W_{\nu\rho}^b W^{c\,\rho\mu}$
$\mathcal{O}_T = \frac{1}{2}\left(H^\dagger \leftrightarrow D_\mu H\right)^2$	$\mathcal{O}_{HW} = ig(D^\mu H)^\dagger \sigma^a (D^\nu H) W_{\mu\nu}^a$	
$\mathcal{O}_{LL}^{(3)\,l} = (\bar{L}_L \sigma^a \gamma^\mu L_L)(\bar{L}_L \sigma^a \gamma_\mu L_L)$	$\mathcal{O}_{HB} = ig'(D^\mu H)^\dagger (D^\nu H) B_{\mu\nu}$	
$\mathcal{O}_R^e = (iH^\dagger \leftrightarrow D_\mu H)(\bar{e}_R \gamma^\mu e_R)$	$\mathcal{O}_g = g_s^2 |H|^2 G_{\mu\nu}^A G^{A\mu\nu}$	
$\mathcal{O}_R^u = (iH^\dagger \leftrightarrow D_\mu H)(\bar{u}_R \gamma^\mu u_R)$	$\mathcal{O}_\gamma = g'^2 |H|^2 B_{\mu\nu} B^{\mu\nu}$	
$\mathcal{O}_R^d = (iH^\dagger \leftrightarrow D_\mu H)(\bar{d}_R \gamma^\mu d_R)$	$\mathcal{O}_H = \frac{1}{2}(\partial^\mu |H|^2)^2$	
$\mathcal{O}_L^{(3)\,q} = (iH^\dagger \sigma^a \leftrightarrow D_\mu H)(\bar{Q}_L \sigma^a \gamma^\mu Q_L)$	$\mathcal{O}_f = y_f |H|^2 \bar{F}_L H^{(c)} f_R + \text{h.c.}$	
$\mathcal{O}_L^q = (iH^\dagger \leftrightarrow D_\mu H)(\bar{Q}_L \gamma^\mu Q_L)$	$\mathcal{O}_6 = \lambda |H|^6$	

same new physics scale, and serve to emphasize the point that the constraints on hadronic observables are, in general, weaker than those on leptonic observables and, moreover, some exhibit deviations from the Standard Model predictions that remain to be understood. However, in both cases the new-physics constraints are in the multi-TeV range.
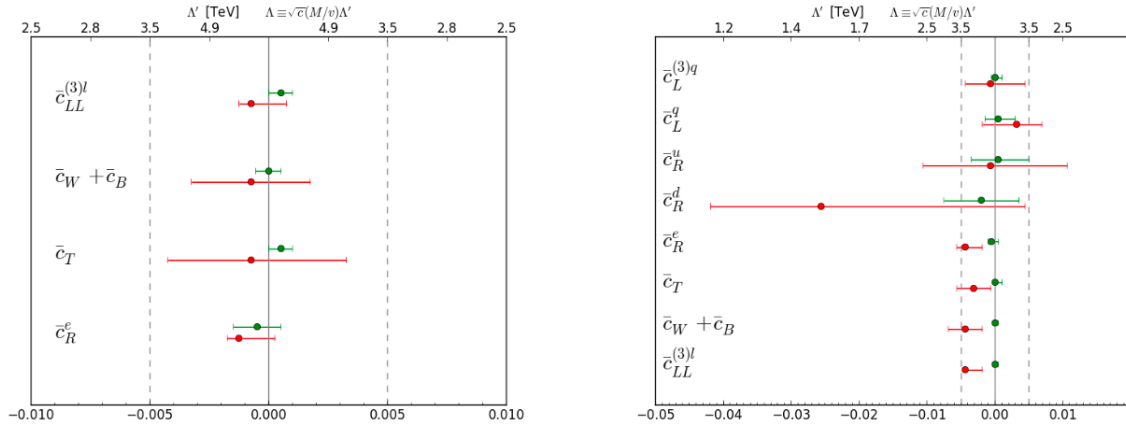
Fig. 19: The 95% CL ranges from an analysis [78] of precision leptonic electroweak observables (left panel) and including also hadronic electroweak observables (right panel). The upper (green) bars denote fits to individual operator coefficients, and the lower (red) bars are for marginalized multi-operator fits. The upper axis should be read with factor $m_W/v \sim 1/3$ for the combination $\bar{c}_W + \bar{c}_B$.

The left panel of Fig. 20 shows results from global fits to data on Higgs production strengths and kinematics (blue bars), to data on TGCs (red bars), and their combination (black bars) [78]. The green bars again show the results of fits to individual operator coefficients, which are generally smaller than the other bars. We note that the constraints on the new-physics scale from Higgs and TGC data shown in the left panel of Fig. 20 are, in general, weaker than from the precision electroweak data: they are typically only a fraction of a TeV. The right panel Fig. 20 emphasizes the complementarity of Higgs and TGC measurements, as reflected in anomalous TGC couplings. The orange and yellow ellipses show the constraints from direct TGC measurements, whereas the green ellipses show the indirect constraints from Higgs measurements, and the blue ellipses show the results of a global fit [79].

The Standard Model effective field theory is the preferred framework for analyzing future LHC data. Fig. 21 shows the results of global fits to LHC Higgs data using only production rates (left panel)
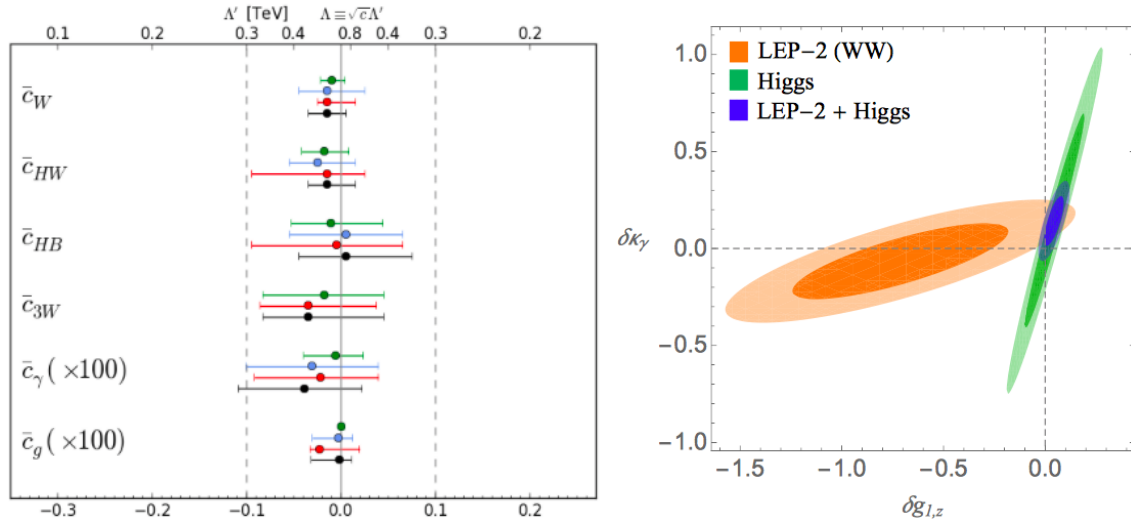
Fig. 20: Left panel: The 95% CL ranges for individual operator fits (green bars), and the marginalised 95% ranges for multi-operator fits. The blue bars combine the LHC signal-strength data with the kinematic distributions for associated $H + V$ production measured by the ATLAS and D0 Collaborations, the red bars includeh the LHC TGC data, and the black bars show results from a global combination with both the associated production and TGC data [78]. Note that the coefficients $\bar{c}_{\gamma,g}$ are shown magnified by factors of 100, so for these coefficients the upper axis should be read with a factor of 10. Right panel: The 68 and 95% CL ranges in the plane of anomalous TGCs $(\delta g_{1,z}, \delta \kappa_\gamma)$ including LEP TGC constraints, LHC Higgs data and their combination [79].

and including production kinematics (right panel) [30]. In each case, the blue bars are obtained from an analysis of present data, the green bars illustrate the prospective sensitivities with 300/fb of data, and the red bars those with 3000/fb of data. The prospective sensitivities are impressive, particularly when the kinematical information is included.

2.8 Beware of historical hubris

Despite the continuing absence of any direct evidence for the new physics beyond the Standard Model at the LHC, one should not become disheartened. History abounds with examples of people who thought they knew it all, but did not. In 1894, just before the discoveries of radioactivity and the electron, Albert Michelson declared that "The more important fundamental laws and facts of physical science have all been discovered" [80]. More recently, prior to the string revolution, Stephen Hawking asked "Is the End in Sight for Theoretical Physics?" [81]. However, my favourite example of a lack of ability to think outside the box is the Spanish Royal Commission that rejected a proposal by Christopher Columbus to sail west before 1492: "So many centuries after the Creation, it is unlikely that anyone could find hitherto unknown lands of any value" [82]. Many of us have seen referees' reports with a similar flavour.

2.9 The Standard Model is not enough

The title of this Subsection is a paraphrase of the title of a James Bond movie [83] and, in deference to him, one may cite 007 reasons for anticipating physics beyond the Standard Model. 001) As discussed in Lecture 1, within the Standard Model the electroweak vacuum is unstable against decay to high H field values. 002) The Standard Model has no candidate for the astrophysical dark matter. 003) The Cabibbo-Kobayashi-Maskawa (CKM) Model does not explain the origin of the matter in the universe. 004) The Standard Model does not have a satisfactory mechanism for generating neutrino masses. 005) The Standard Model does not explain or stabilize the hierarchy of mass scales in physics. 006) The
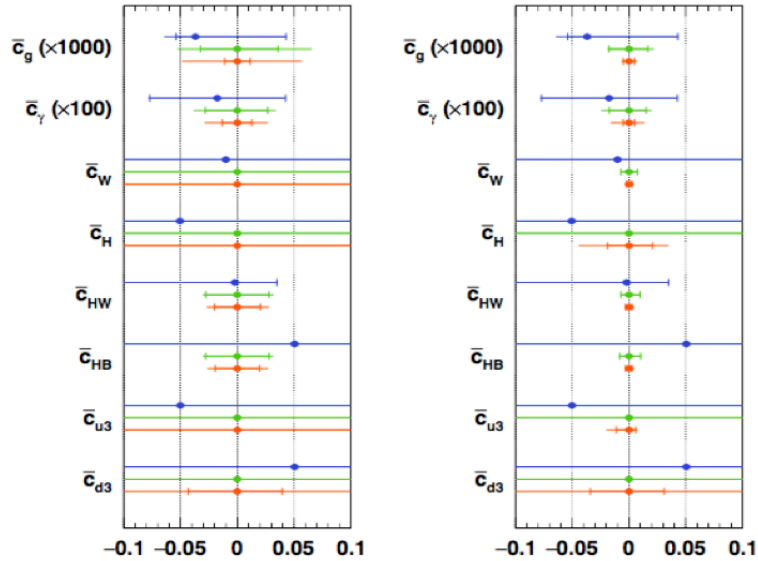
Fig. 21: Results of present and prospective global fits to LHC Higgs data using only production rates (left panel) and including production kinematics (right panel). The blue bars are obtained from an analysis of present data, the green bars illustrate the prospective sensitivities with 300/fb of data, and the red bars those with 3000/fb of data [30].

Standard Model does not have a satisfactory mechanism for cosmological inflation. 007) We need a quantum theory of gravity.

Several of these issues will be addressed by LHC measurements during Run 2, e.g., the top quark mass will be determined more accurately, there will be searches for dark matter particles, there will be searches for CP violation and other flavour physics beyond the CKM model, as well as new particles that could help stabilize the electroweak scale. Personally, I am a fan of supersymmetry as a framework that could solve or at least mitigate many of the problems on James Bond's list, so I focus now on that theory.

2.10 Supersymmetry

Supersymmetry is an extension of the Standard Model that has long been favoured by many theorists [84]. Some are disappointed that it has not yet appeared at the LHC, but then neither has any other proposed extension of the Standard Model such as compositeness or extra dimensions. Rather, I would argue that Run 1 of the LHC has provided three new additional reasons to favour supersymmetry.

One is the apparent instability of the electroweak vacuum within the Standard Model, which can be stabilized by a theory resembling supersymmetry, as discussed in Subsection 1.10. Specifically, in a supersymmetric theory the negative running of the Higgs quartic self-coupling λ due to the top quark loop is exactly cancelled by stop squark loops. Moreover, the negative sign of the quadratic term in the Higgs potential (5) and hence the appearance of the electroweak vacuum can be understood dynamically as a different effect of renormalization by the heavy top quark via the logarithmic terms in (38 39).

A second Run 1 motivation for supersymmetry is the mass of the Higgs boson. Minimal supersymmetric models predicted that it should weigh $\lesssim 130$ GeV [85], as discussed in more detail in the next Subsection, in agreement with the measurement (27). This is because supersymmetry actually predicts the magnitude of the Higgs quartic self-coupling: $\lambda \sim g^2 + g'^2$, where g and g' are the SU(2) and U(1) couplings of the Standard Model.

The third Run-1 motivation for supersymmetry is that simple supersymmetric models also pre-

dicted that the Higgs couplings should be with a few % of the Standard Model values, in perfect consistency with the measurements to date [86]. In fact, in a supersymmetric model it may be very difficult to measure any deviations from the Standard Model predictions for the Higgs couplings [87], as discussed later.

These new reasons for liking supersymmetry are in addition to the many traditional reasons to like it, such as its ability to stabilize the mass hierarchy via the cancellation of the quadratic divergences in loop corrections to the Higgs mass (38 39) [68], the fact that it naturally predicts a cold dark matter particle [88], the fact that it improves the accuracy of the grand unification prediction for $\sin^2 \theta_W$ [89], and its essential rôle in the superstring framework for a theory of quantum gravity.

2.11 Higgs bosons in supersymmetry

Even the minimal supersymmetric extension of the Standard Model (MSSM) requires two complex Higgs doublets, in order to cancel out anomalous triangle diagrams with higgsinos that would otherwise destroy the renomalizability of the theory, and in order to give masses to all the quarks. These two complex Higgs doublets contain 8 degrees of freedom, of which 3 are combined with the massless $W^{\pm}$ and Z fields to give them masses, as discussed in Subsection 1.4. There remain 5 degrees of freedom that manifest themselves as massive Higgs bosons, two neutral scalars h, H, one neutral pseudoscalar A and two charged bosons $H^{\pm}$.

The tree-level Higgs mass-squared matrix has the following form in the MSSM:

$$\mathcal{M}_{\text{tree}}^{2,N=1} = \begin{pmatrix} m_Z^2 \cos^2 \beta + m_A^2 \sin^2 \beta & -(m_A^2 + m_Z^2) \cos \beta \sin \beta \\ -(m_A^2 + m_Z^2) \cos \beta \sin \beta & m_Z^2 \sin^2 \beta + m_A^2 \cos^2 \beta \end{pmatrix} . \tag{45}$$

Diagonalizing (45), we find that the masses of the two scalars at the classical (tree) level can be written as

$$m_{h,H}^2 = \frac{1}{2} \left(m_A^2 + m_Z^2 \mp \sqrt{(m_A^2 + m_Z^2)^2 - 4 m_Z^2 m_A^2 \cos^2 2\beta} \right) , \tag{46}$$

where $\tan \beta$ is the ratio of the vevs of the 2 Higgs doublets. At face value, the formula (46) implies that the lighter neutral scalar Higgs boson h should have a mass $< m_Z$. However, there is an important one-loop correction to m_h due to the stop squarks $\tilde{t}_{1,2}$:

$$\Delta m_h^2 = \frac{3 m_t^4}{4 \pi^2 v^2} \ln \left(\frac{m_{\tilde{t}_1} m_{\tilde{t}_2}}{m_t^2} \right) + \dots , \tag{47}$$

which can increase m_h by $\lesssim 40$ GeV, as seen in Fig. 22. As also seen there, if the other Higgs bosons H, A and $H^{\pm}$ are heavy, they are expected to all be quite degenerate in mass. A curiosity of Fig. 22 is the possibility that the *heavier* neutral scalar H might weigh $\lesssim 130$ GeV, with the h even lighter [90]. It may be difficult to reconcile this possibility with the LHC measurements of the couplings of the $H(125)$, but the possibility of a lighter Higgs boson should not be discounted completely, and further experimental searches in the low-mass range are welcome!

2.12 More supersymmetry, not less?

The Standard Model contains chiral fermions, i.e., the left- and right-handed fermion states live in inequivalent representations of the SU(2)×U(1) gauge group. As such, they can be accommodated only within supermultiplets of simple $N = 1$ supersymmetry. Theories with $N \geq 2$ supersymmetries would require left- and right-handed fermions to transform identically under SU(2)×U(1), so phenomenological supersymmetric models such as the MSSM are usually restricted to $N = 1$. However, left-right symmetric (vector-like) fermions appear in many extensions of the Standard Model, such as models with extra dimensions, string compactifications and some grand unified theories. These extensions of the Standard Model could accommodate $N = 2$ supersymmetry.
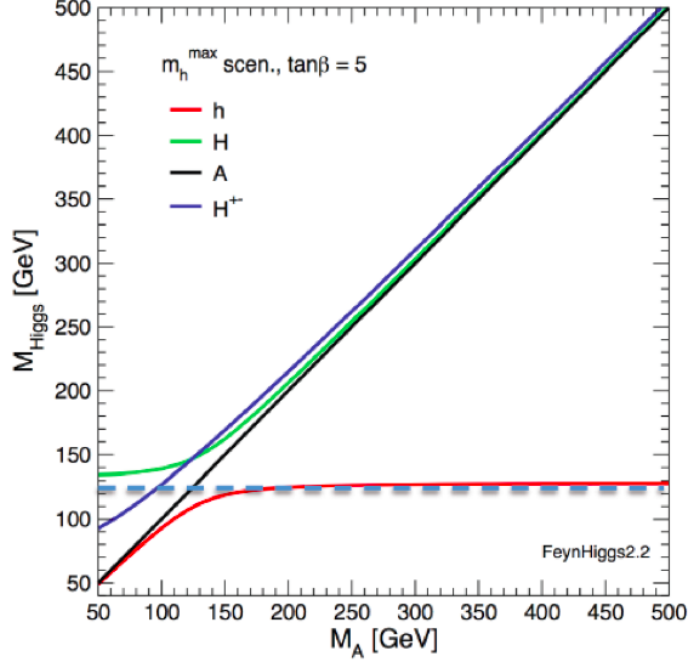
Fig. 22: A representative calculation of MSSM Higgs masses in the m_h^{max} scenario with $\tan\beta = 5$, using the `FeynHiggs 2.2` code [91]. Note a region at larger m_A where the lighter neutral scalar Higgs boson may weigh ~ 125 GeV [85], and a smaller region at small m_A where the heavier neutral scalar Higgs boson may weigh ~ 125 GeV [90].

In the MSSM, although the quarks and leptons are chiral, the Higgs representations form a vector-like pair, and so could in principle also accommodate $N = 2$ supersymmetry [92]. One could consider the possibility that the Higgs sector is just the tip of an $N = 2$ supersymmetric iceberg, which would also include an $N = 2$ gauge sector and possibly vector-like fermion supermultiplets, as occurs in some string compactifications and grand unified theories.

So, what would an $N = 2$ Higgs sector look like?

In this case, differently from (47), the tree-level mass-squared matrix is:

$$\mathcal{M}_{\mathrm{tree}}^{2,N=2} = \begin{pmatrix} m_Z^2 \cos^2\beta + m_A^2 \sin^2\beta & -(m_A^2 - m_Z^2)\cos\beta\sin\beta \\ -(m_A^2 - m_Z^2)\cos\beta\sin\beta & m_Z^2 \sin^2\beta + m_A^2 \cos^2\beta \end{pmatrix} . \tag{48}$$

The crucial difference: is the replacement: $m_A^2 + m_Z^2 \to m_A^2 - m_Z^2$ in the off-diagonal terms between the $N = 1$ and $N = 2$ cases (45) and (48). The corresponding tree-level Higgs masses after diagonalization are shown in Fig. 23. In the $N = 1$ case (left panel) we see level repulsion for $m_A \sim 100$ GeV. However, in the $N = 2$ case (right panel) we see linear level crossing with

$$m_h^{N=2} = m_Z, \quad m_H^{N=2} = m_A \tag{49}$$

at the tree level. Moreover, at the tree level the $N = 2$ Higgs sector is 'aligned', so that the lighter neutral Higgs boson has exactly the same couplings as in the Standard Model [92].

The dominant one-loop corrections ε to (45) and (48) are those due to top quarks and stop squarks, which appear in their [22] entries. Let us assume that they are such as to give the measured Higgs boson mass $m_h = 125$ GeV. In the $N = 1$ case the required loop correction is [93]

$$\varepsilon_{N=1} = \Delta\mathcal{M}_{22}^{2,N=1} = \frac{m_h^2(m_A^2 + m_Z^2 - m_h^2) - m_A^2 m_Z^2 \cos^2 2\beta}{m_Z^2 \cos^2\beta + m_A^2 \sin^2\beta - m_h^2} , \tag{50}$$

Fig. 23: A comparison between the tree-level values of Higgs masses in the MSSM (left panel) and in the $N = 2$ supersymmetric model (right panel) [92].
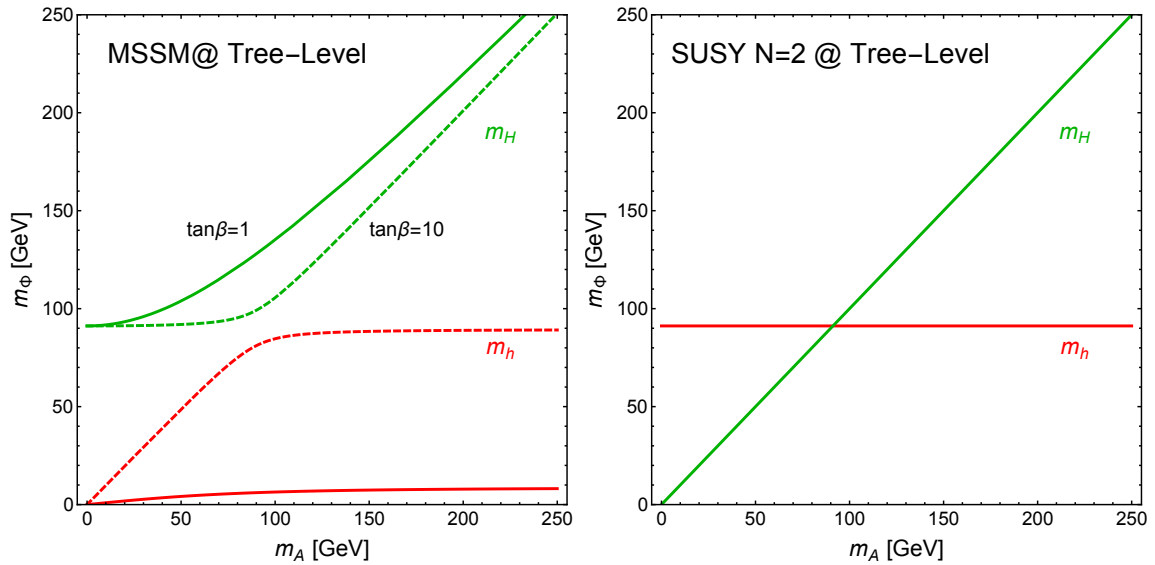
whereas in the $N = 2$ case it is [92]

$$\varepsilon_{N=2} = \Delta\mathcal{M}_{22}^{2,N=2} = \frac{2(m_A^2 - m_h^2)(m_h^2 - m_Z^2)}{\cos 2\beta \left(m_Z^2 - m_A^2\right) + m_A^2 - 2m_h^2 + m_Z^2} \cdot \qquad (51)$$

Fig. 24 compares (left panel) the required value of m_H for $\tan\beta = 1$ in the two cases, (middle panel) the value of $m_H - m_A$ as a function of m_A for $\tan\beta = 3$, and (right panel) the value of $m_H - m_A$ as a function of $\tan\beta$ for $m_A = 300$ GeV [92]. We see that m_H *can be lighter in the $N = 2$ case than when $N = 1$*, and that $m_H - m_A$ is also smaller, in general. Another effect of doubling up on supersymmetry in the Higgs sector is seen in Fig. 25, where we compare the supersymmetry-breaking mass scale M_{SUSY} that is needed in the $N = 1$ and $N = 2$ cases for different values of the squark mass miixing parameter X_t [92]. We see a consistent pattern that *smaller values of M_{SUSY} are required when $N = 2$ than when $N = 1$* for any fixed values of m_A and $\tan\beta$.

On the other hand, the sensitivities of the LHC searches are also different, as seen in the $(m_A, \tan\beta)$ plane in Fig. 26 [92]. The upper part of this plane (shaded grey) is excluded by direct LHC searches for $H, A \to \tau^+\tau^-$, which have similar sensitivities in the $N = 1$ and $N = 2$ cases. The red (green) curves show the ranges of m_A that are excluded indirectly by the LHC. We see that $m_A \gtrsim 200$ GeV is allowed in the $N = 2$ case, whereas $m_A \gtrsim 350$ GeV is required when $N = 1$. The bottom line is that *both supersymmetry and supersymmetric Higgs bosons may be closer in an $N = 2$ supersymmetric model than has been suggested by the $N = 1$ MSSM.*

2.13 What next: A Higgs factory?

Now that a (the?) Higgs boson has been discovered, there is naturally a lot of interest in studying it in detail. The LHC has considerable potential in this respect, with a target of eventually accumulating 3000/fb of data with the HL-LHC that has now been approved by the CERN Council [94]. Ideas for future Higgs factories should take this into account, and should be able to demonstrate how much better they can measure the Higgs boson, as well as look for other possible new physics. Two proposals for linear e^+e^- colliders are on the market: the ILC that aims initially at a centre-of-mass energy of 500 GeV
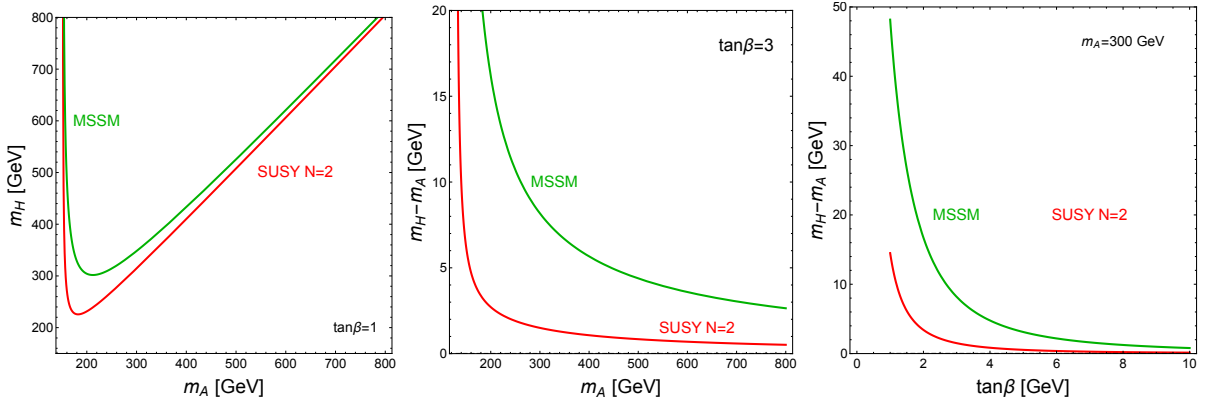
Fig. 24: Left panel: The value of m_H required to obtain $m_h = 125$ GeV via one-loop radiative corrections for $\tan\beta = 1$ in the MSSM and $N = 2$ supersymmetry [92]. Middle panel: The value of $m_H - m_A$ as a function of m_A for $\tan\beta = 3$. Right panel: The value of $m_H - m_A$ as a function of $\tan\beta$ for $m_A = 300$ GeV.
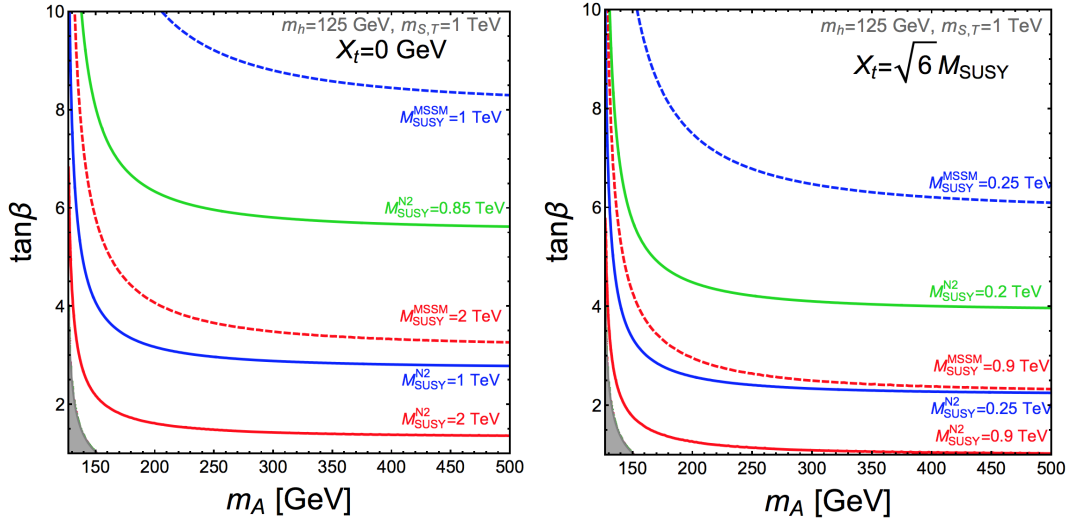
Fig. 25: Contours of the supersymmetry-breaking mass scale M_{SUSY} that are required as functions of m_A and $\tan\beta$ to yield $m_h = 125$ GeV in the MSSM scenario (dotted lines) and the $N = 2$ scenario (full lines) [92]. The left panel is for $X_t = 0$, and the right panel is for the maximal-mixing scenario with $X_t = \sqrt{6}M_{SUSY}$.

with a planned upgrade to 1 TeV [95], and CLIC that aims at centre-of-mass energies between 350 GeV and 3 TeV [96], as seen in Fig. 27. Designs for circular e^+e^- colliders, CEPC in China [97] and FCC-ee near CERN [98], are now also being discussed. As also seen in Fig. 27, these are more limited in centre-of-mass energy, but have the potential for higher luminosities for probing the Higgs boson via the $e^+e^- \to ZH$ process, and for precision electroweak studies at the Z peak and the W^+W^- threshold.

The capabilities of the ILC [95] and FCC-ee [99] for Higgs coupling measurements are shown in the left and right panels of Fig. 28, respectively. The capabilities of the LHC, HL-LHC, ILC and FCC-ee to probe the $H\gamma\gamma, HZZ, HWW$ and Hgg couplings are shown in Fig. 29, and compared with the deviations form the Standard Model that are expected in different supersymmetric models whose parameters were chosen to be consistent with LHC data [87]. As mentioned previously, these typically predict very small deviations from the Standard Model that will be very difficult to distinguish experimentally.
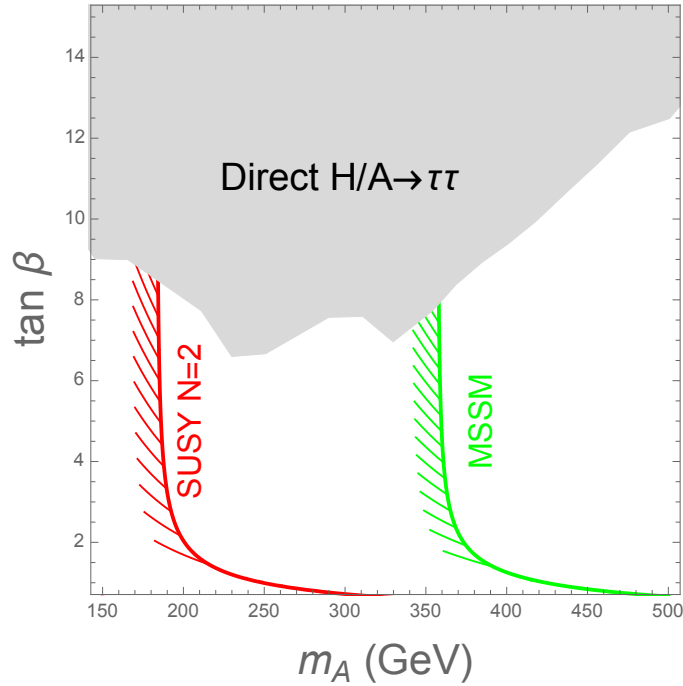
Fig. 26: The direct exclusion from searches for heavy scalars in the $H/A \to \tau\tau$ final state (grey shading), and the indirect bounds from measurements of Higgs couplings to fermions and massive bosons at Run 1 of the LHC in the MSSM (green) and the $N = 2$ model (red) [92].

Moreover, the current theoretical uncertainties in these predictions, indicated by the green bars, are large compared with the prospective experimental accuracies at the FCC-ee, in particular. More theoretical work will be needed!

As discussed earlier, a favoured approach is to use future Higgs, precision electroweak and TGC measurements to constrain the coefficients of possible dimension-6 operators constructed out of Standard Model fields. Fig. 30 compares the LHC constraints (left panel) and the prospective FCC-ee sensitivities (right panel) in global fits to the scale Λ in dimension-6 operator coefficients [100]. Fig. 31 compares the sensitivities of the ILC and FCC-ee in fits combining Higgs and precision electroweak data (left panel), and combining Higgs and TGC data (right panel) [100]. In the left panel, the shadings compare results obtained with and without estimates of the theoretical uncertainties in the precision electroweak observables: we see again the importance of minimizing these. In the right panel, the effects of including TGC measurements at the ILC are also indicated by shading.

By virtue of its higher centre-of-mass energy, the CLIC proposal for an e^+e^- collider has particular advantages in looking for the effects of dimension-6 operators, since the effects of their interferences with Standard Model amplitudes typically increase $\propto E^2$ [101]. The following are some examples of the sensitivities to dimension-6 operator coefficients at 350 GeV and 3 TeV for associated HZ production:

$$
\frac{\Delta\sigma(HZ)}{\sigma(HZ)}\bigg|_{350\,\text{GeV}} = 16\bar{c}_{HW} + 4.7\bar{c}_{HB} + 35\bar{c}_W + 11\bar{c}_B - \bar{c}_H + 5.5\bar{c}_\gamma \,,
$$

$$
\frac{\Delta\sigma(HZ)}{\sigma(HZ)}\bigg|_{3\,\text{TeV}} = 2130\bar{c}_{HW} + 637\bar{c}_{HB} + 2150\bar{c}_W + 193\bar{c}_B - \bar{c}_H + 7.4\bar{c}_\gamma \,, \tag{52}
$$
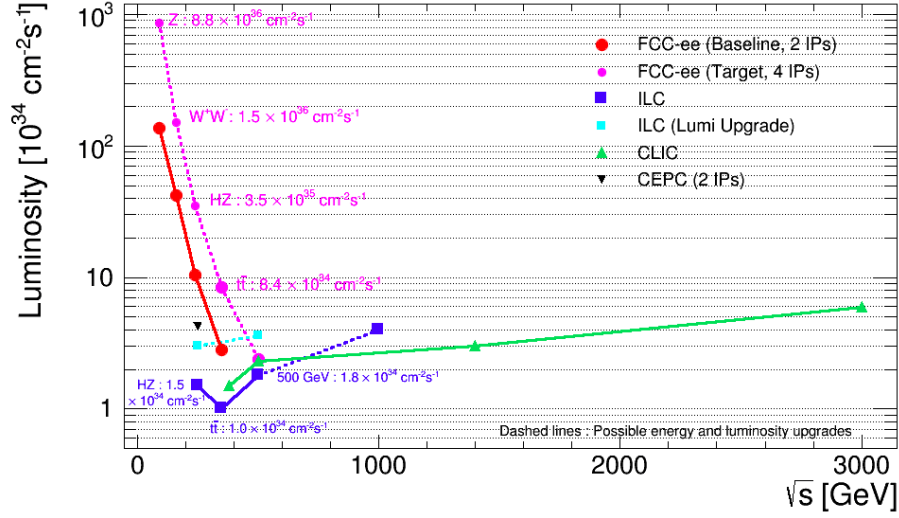
Fig. 27: The design luminosities at various centre-of-mass energies of projects for future high-energy e^+e^- colliders [95–98].
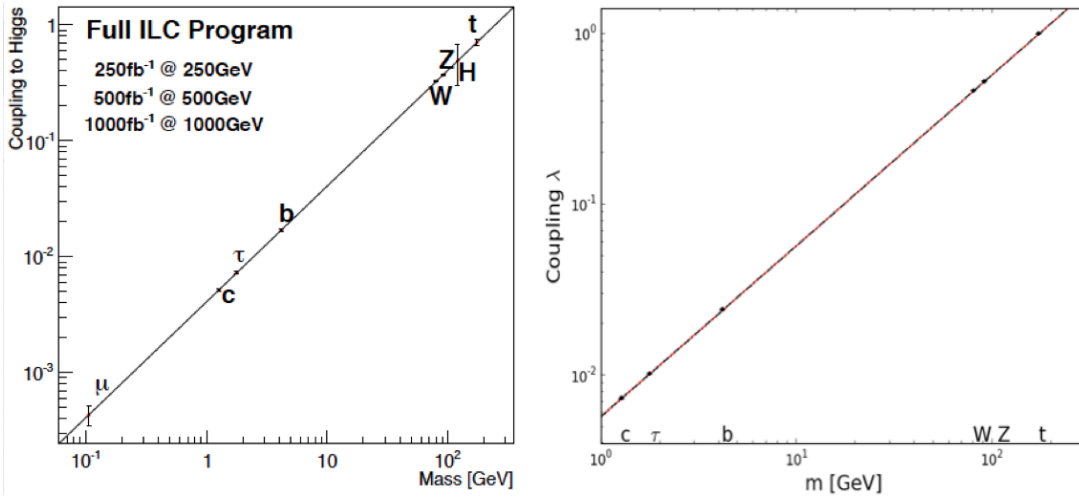
Fig. 28: Left panel: Prospective measurements of Higgs couplings at the ILC [95]. Right panel: Prospective measurements of Higgs couplings at FCC-ee [99].

and for $e^+e^- \to W^+W^-$ production :

$$\left.\frac{\Delta\sigma(W^+W^-)}{\sigma(W^+W^-)}\right|_{350\,\mathrm{GeV}} = 0.63\bar{c}_{HW} + 0.31\bar{c}_{HB} + 4.6\bar{c}_W - 0.43\bar{c}_{3W} \,,$$

$$\left.\frac{\Delta\sigma(W^+W^-)}{\sigma(W^+W^-)}\right|_{3\,\mathrm{TeV}} = 13\bar{c}_{HW} + 7.8\bar{c}_{HB} + 17\bar{c}_W - 4.4\bar{c}_{3W} \,. \qquad (53)$$

The sensitivities to most of the operator coefficients indeed increase substantially with the centre-of-mass energy, for both the associated $H + Z$ and W^+W^- cross-sections, confirming the expected competitive advantage of the high energies attainable with CLIC. Fig. 32 shows the increase in sensitivity of CLIC operating at 3 TeV compared with 350 GeV or 1.4 TeV for a number of dimension-6 operator coeffi-
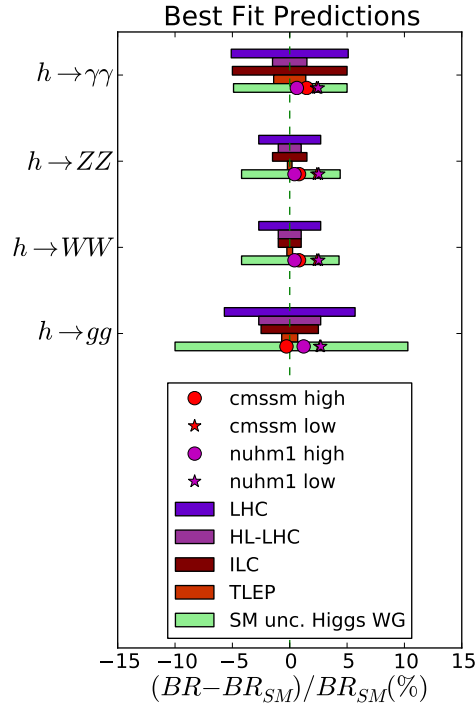
Fig. 29: Comparison between prospective measurements of Higgs branching ratios at future colliders, low- and high-mass CMSSM and NUHM1 predictions (red and purple symbols) and the current uncertainties within the Standard Model (turquoise bars) [87].
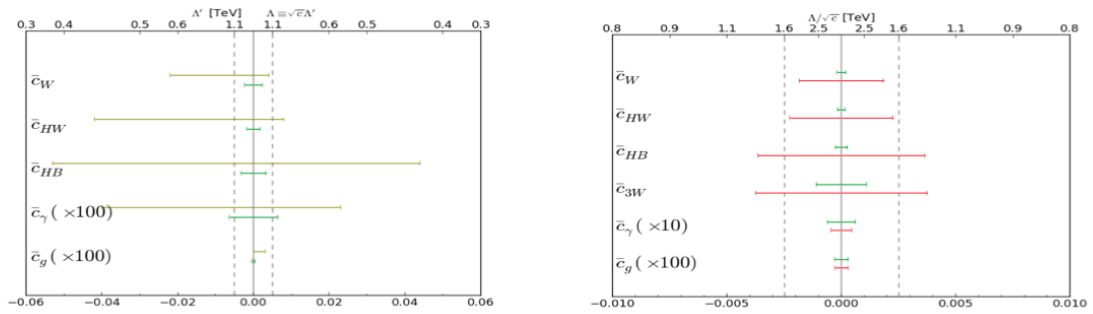
Fig. 30: Left panel: Constraints on dimension-6 operator coefficients from measurements at the LHC. Right panel: Prospective corresponding constraints from measurements at FCC-ee [100].

cients [101]. The green bars are for fits including individual operators, and the red bars are for global fits with the coefficients marginalized.

Studies of the sensitivities to Higgs properties of a 100-TeV pp collider such as FCC-hh are still at an early stage. However, as seen in Fig. 33, the Higgs production cross sections will be much larger than at the LHC, and there will be extensive opportunities for kinematical measurements as well as overall production rates [102]. Moreover, such a machine might provide the first opportunity to measure directly the triple-Higgs coupling with respectable accuracy, since it contributes to the HH cross section that increases by almost two orders of magnitude compared to the LHC, as seen in Fig. 33 (grey line).
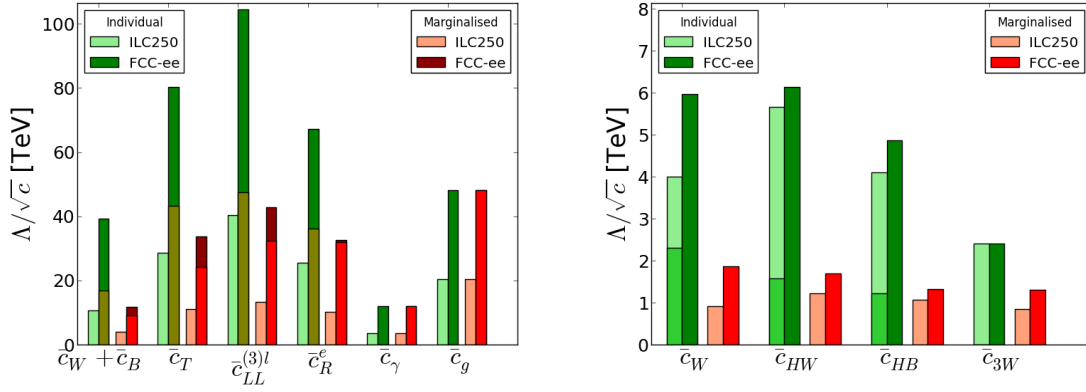
Fig. 31: Summary of the reaches for the dimension-6 operator coefficients, in individual fits (green) and when marginalised in a global fit including all operators (red), from projected ILC250 (lighter shades) and FCC-ee (darker shades) precision measurements [100]. The left plot shows the operators that are most strongly constrained by electroweak precision observables and Higgs physics, and the different shades of dark green and dark red illustrate the effects of theoretical uncertainties at FCC-ee. The right plot is constrained primarily by Higgs physics and TGCs, and the different shades of light green demonstrate the improved sensitivity when TGCs are included in the ILC250 analysis.
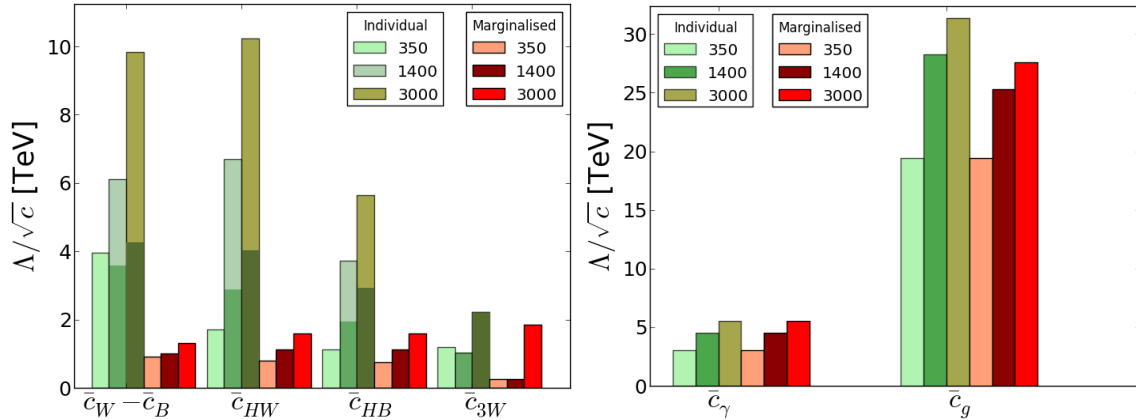
Fig. 32: The estimated sensitivities of CLIC measurements at centre-of-mass energies of 350 GeV, 1.4 TeV and 3.0 TeV to the scales of various (combinations of) dimension-6 operator coefficients [101]. The results of individual (marginalised) fits are shown as green (red) bars. The lighter (darker) green bars in the left panel include (omit) the prospective HZ Higgsstrahlung constraint.

2.14 Final remarks

"Beyond any reasonable doubt", the LHC has discovered a (possibly the) Higgs boson [75]. Whilst being a tremendous success for theoretical physics, it also represents a tremendous challenge. Even in the minimal elementary Higgs model, both the terms in the Higgs potential present problems. Does the quartic term turn negative at high scales, implying vacuum instability? How come the quadratic term is so small compared to plausible fundamental mass scales in physics such as the Planck mass? The LHC may yet discover new physics beyond the Standard Model during Run 2. If it does, the global priority for high-energy physics will surely be to study it. If it does not discover new physics at the TeV scale, it will be natural to focus future accelerator experiments on the Higgs boson. Either way, in my
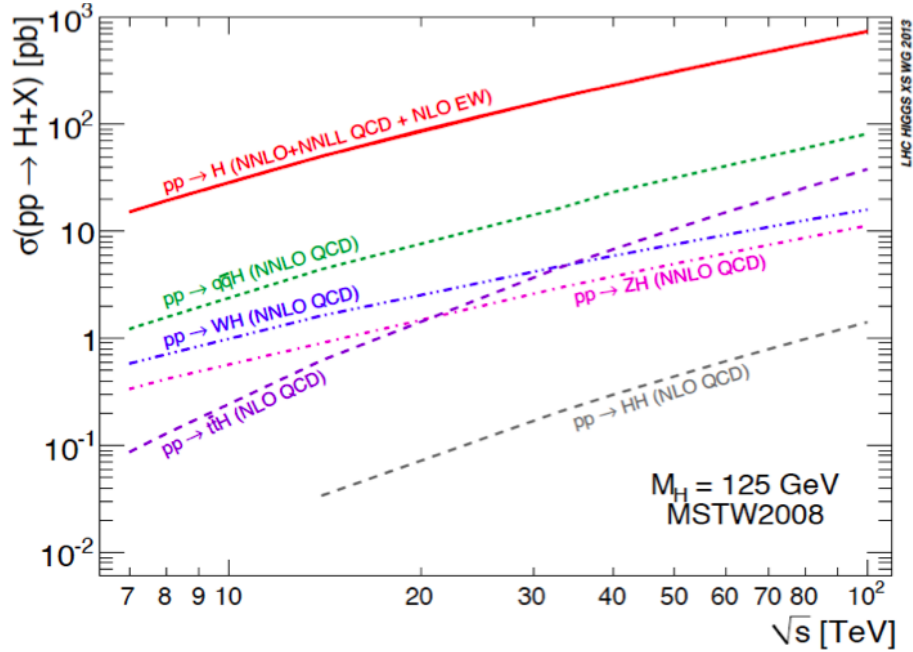
Fig. 33: The most important cross sections for Higgs productions in pp collisions, as functions of the centre-of-mass energy up to 100 TeV [102].

personal opinion future circular colliders may offer the best experimental prospects, being able to probe the 10 TeV scale indirectly via high-precision low-energy experiments, and directly via the production of new heavy particles.

Acknowledgements

References

[1] Y. Nambu, *Phys. Rev. Lett.* **4** (1960) 380.

[2] J. Goldstone, *Nuovo Cim.* **19** (1961) 154.

[3] J. Goldstone, A. Salam and S. Weinberg, *Phys. Rev.* **127** (1962) 965.

[4] P. W. Anderson, *Phys. Rev.* **130** (1963) 439.

[5] Y. Nambu, *Phys. Rev.* **117** (1960) 648.

[6] W. Gilbert, *Phys. Rev. Lett.* **12** (1964) 713.

[7] F. Englert and R. Brout, *Phys. Rev. Lett.* **13** (1964) 321.

[8] P. W. Higgs, *Phys. Lett.* **12** (1964) 132.

[9] P. W. Higgs, *Phys. Rev. Lett.* **13** (1964) 508.

[10] G. S. Guralnik, C. R. Hagen and T. W. B. Kibble, *Phys. Rev. Lett.* **13** (1964) 585.

[11] A. A. Migdal and A. M. Polyakov, *J. Exptl. Theoret. Physics (U.S.S.R.)* **51** (1966) 135.

[12] T. W. B. Kibble, *Phys. Rev.* **155** (1967) 1554.

[13] A. Salam, in the Proceedings of 8th Nobel Symposium, Lerum, Sweden, 19-25 May 1968, pp. 367.

[14] S. Weinberg, *Phys. Rev. Lett.* **19**, (1967) 1264.

[15] G. Aad *et al.* [ATLAS Collaboration], *Phys. Lett. B* **716** (2012) 1 [arXiv:1207.7214 [hep-ex]].

[16] S. Chatrchyan *et al.* [CMS Collaboration], *Phys. Lett. B* **716** (2012) 30 [arXiv:1207.7235 [hep-ex]].

[17] J. R. Ellis, M. K. Gaillard and D. V. Nanopoulos, *Nucl. Phys. B* **106** (1976) 292.

[18] See also P. W. Higgs, *Phys. Rev.* **145** (1966) 1156.

[19] J. Ellis and M. K. Gaillard, *Theoretical remarks*, in L. Camilleri *et al.*, *Physics with very high-energy e^+e^- colliding beams*, CERN report 76-18 (Nov. 1976), pp. 21-94; J. D. Bjorken, *Weak interaction theory and neutral currents,* in the Proceedings of 4th SLAC Summer Institute on Particle Physics: Weak Interactions at High Energies & the Production of New Particles, Stanford, California, 2-10 Aug 1976, SLAC Report 198 (Nov. 1976), pp. 1-84, also available as SLAC-PUB-1866, Jan. 1977; B. L. Ioffe and V. A. Khoze, *Sov. J. Part. Nucl.* **9** (1978) 50 [Fiz. Elem. Chast. Atom. Yadra **9** (1978) 118], also available as LENINGRAD-76-274, Nov 1976; G. Barbiellini, G. Bonneaud, G. Coignet, J. Ellis, J. F. Grivaz, M. K. Gaillard, C. Matteuzzi and B. H. Wiik, *The production and detection of Higgs particles at LEP,* DESY 79/27, ECFA/LEP SSG/9/4, May 1979.

[20] H. Baer et al., New particles, in Physics at LEP, edited by J. Ellis and R. D. Peccei, CERN-1986-002-V-1 (CERN, Geneva, 1986), pp. 297-348, https://doi.org/10.5170/CERN-1986-002-V-1.297;
J. Boucrot et al., Search for neutral Higgs at LEP 200, in Proceedings of the ECFA workshop on LEP 200, Aachen, Germany, 29 Sept.–1 Oct. 1986, edited by A. Böhm and W. Hoogland, CERN-1987-008-V-2 (CERN, Geneva, 1987), p. 312, https://doi.org/10.5170/CERN-1987-008-V-2.312;
P. J. Franzini and P. Taxil, Higgs search, in Workshop on Z Physics at LEP1. Volume 2: Higgs search and new physics, edited by G. Altarelli, R. Kleiss and C. Verzegnassi, CERN-1989-008 (CERN, Geneva, 1989), pp. 59-119, https://doi.org/10.5170/CERN-1989-008-V-2.59;
E. Accommando et al., Higgs physics, in Physics at LEP 2. Volume 1, CERN-1996-001 (CERN, Geneva, 1996), pp. 351-462, https://doi.org/10.5170/CERN-1996-001-V-1.351.

[21] J. R. Ellis, G. Gelmini and H. Kowalski, *New particles and their experimental signatures,* in *Proceedings of the ECFA/CERN Workshop on the Possibility of a Large Hadron Collider*, Lausanne and Geneva, Mar. 21-27, 1984, CERN Report 84-10, ECFA 84/85, Vol. 2, pp. 393-454, also available as DESY 84/071, CERN-TH-3493/84 (1984).

[22] E. Eichten, I. Hinchliffe, K. D. Lane and C. Quigg, *Rev. Mod. Phys.* **56** (1984) 579 Addendum: [*Rev. Mod. Phys.* **58** (1986) 1065]. http://dx.doi.org/10.1103/RevModPhys.56.579, http://dx.doi.org/10.1103/RevModPhys.58.1065.

[23] J. F. Gunion, H. E. Haber, G. L. Kane and S. Dawson, *The Higgs Hunter's Guide,* for an updated version, see *Front. Phys.* **80** (2000) 1.

[24] J. R. Ellis and G. L. Fogli, *Phys. Lett. B* **213** (1988) 526, http://doi.org/10.1016/0370-2693(88)91304-4; *Phys. Lett. B* **231** (1989) 189, http://dx.doi.org/10.1016/0370-2693(89)90138-X.

[25] C. Vayonakis, *Lett. Nuovo Cimento* **17** (1976) 383; M. Veltman, *Acta Phys. Pol.* **B8** (1977) 475; B. W. Lee, C. Quigg and H. B. Thacker, *Phys. Rev.* **D16** (1977) 1519.

[26] J. R. Ellis and G. L. Fogli, *Phys. Lett. B* **249** (1990) 543, J. R. Ellis, G. L. Fogli and E. Lisi, *Phys. Lett. B* **274** (1992) 456 and *Phys. Lett. B* **318** (1993) 148.

[27] R. Barate *et al.* [LEP Working Group for Higgs boson searches and ALEPH and DELPHI and L3 and OPAL Collaborations], *Phys. Lett. B* **565** (2003) 61 [hep-ex/0306033].

[28] Tevatron New Phenomena and Higgs Working Group and CDF and D0 Collaborations, [arXiv:1107.5518 [hep-ex]].

[29] M. Baak, M. Goebel, J. Haller, A. Hoecker, D. Ludwig, K. Moenig, M. Schott and J. Stelzer [Gfitter Group], *Eur. Phys. J. C* **72** (2012) 2003, [arXiv:1107.0975 [hep-ph]].

[30] D. de Florian *et al.* [LHC Higgs Cross Section Working Group], [arXiv:1610.07922 [hep-ph]].

[31] H. M. Georgi, S. L. Glashow, M. E. Machacek and D. V. Nanopoulos, *Phys. Rev. Lett.* **40** (1978) 692, http://dx.doi.org/10.1103/PhysRevLett.40.692.

[32] S. L. Glashow, D. V. Nanopoulos and A. Yildiz, *Phys. Rev. D* **18** (1978) 1724, http://dx.doi.org/10.1103/PhysRevD.18.1724.

[33] R. N. Cahn and S. Dawson, *Phys. Lett.* **136B** (1984) 196 Erratum: [*Phys. Lett.* **138B** (1984) 464], http://dx.doi.org/10.1016/0370-2693(84)91180-8

[34] R. Raitio and W. W. Wada, *Phys. Rev. D* **19** (1979) 941, http://dx.doi.org/10.1103/PhysRevD.19.941; J. N. Ng and P. Zakarauskas, *Phys. Rev. D* **29** (1984) 876, http://dx.doi.org/10.1103/PhysRevD.29.876; Z. Kunszt, *Nucl. Phys. B* **247** (1984) 339, http://dx.doi.org/10.1016/0550-3213(84)90553-4.

[35] F. Maltoni, K. Paul, T. Stelzer and S. Willenbrock, *Phys. Rev. D* **64** (2001) 094023, http://dx.doi.org/10.1103/PhysRevD.64.094023 [hep-ph/0106293].

[36] C. Anastasiou, C. Duhr, F. Dulat, E. Furlan, T. Gehrmann, F. Herzog, A. Lazopoulos and B. Mistlberger, *JHEP* **1605** (2016) 058, http://dx.doi.org/10.1007/JHEP05(2016)058, [arXiv:1602.00695 [hep-ph]].

[37] J. Huston [PDF4LHC Collaboration], *PoS DIS* **2010** (2010) 036.

[38] S. Heinemeyer *et al.* [LHC Higgs Cross Section Working Group], [arXiv:1307.1347 [hep-ph]].

[39] J. Olsen, CMS physics results from Run 2 presented on Dec. 15th, 2015, https://indico.cern.ch/event/442432/; CMS Collaboration, CMS PAS EXO-15-004, https://cds.cern.ch/record/2114808/files/EXO-15-004-pas.pdf;
M. Kado, ATLAS physics results from Run 2 presented on Dec. 15th, 2015, https://indico.cern.ch/event/442432/; ATLAS Collaboration, ATLAS-CONF-2015-081, https://atlas.web.cern.ch/Atlas/GROUPS/PHYSICS/CONFNOTES/ATLAS-CONF-2015-081/.

[40] J. Ellis, S. A. R. Ellis, J. Quevillon, V. Sanz and T. You, *JHEP* **1603** (2016) 176, http://dx.doi.org/10.1007/JHEP03(2016)176, [arXiv:1512.05327 [hep-ph]].

[41] G. Aad *et al.* [ATLAS and CMS Collaborations], *Phys. Rev. Lett.* **114** (2015) 191803, http://dx.doi.org/10.1103/PhysRevLett.114.191803, [arXiv:1503.07589 [hep-ex]].

[42] M. Baak *et al.* [Gfitter Group], *Eur. Phys. J. C* **72** (2012) 2205, http://dx.doi.org/10.1140/epjc/s10052-012-2205-9, [arXiv:1209.2716 [hep-ph]].

[43] G. Degrassi, S. Di Vita, J. Elias-Miro, J. R. Espinosa, G. F. Giudice, G. Isidori and A. Strumia, *JHEP* **1208** (2012) 098, [arXiv:1205.6497 [hep-ph]].

[44] D. Buttazzo, G. Degrassi, P. P. Giardino, G. F. Giudice, F. Sala, A. Salvio and A. Strumia, *JHEP* **1312** (2013) 089, http://dx.doi.org/10.1007/JHEP12(2013)089, [arXiv:1307.3536 [hep-ph]].

[45] A. V. Bednyakov, B. A. Kniehl, A. F. Pikelner and O. L. Veretin, *Phys. Rev. Lett.* **115** (2015) 201802, http://dx.doi.org/10.1103/PhysRevLett.115.201802, [arXiv:1507.08833 [hep-ph]].

[46] ATLAS, CDF, CMS and D0 Collaborations, [arXiv:1403.4427 [hep-ex]].

[47] V. M. Abazov *et al.* [D0 Collaboration], *Phys. Rev. D* **91** (2015) 112003, http://dx.doi.org/10.1103/PhysRevD.91.112003, [arXiv:1501.07912 [hep-ex]].

[48] G. Aad *et al.* [ATLAS Collaboration], *Eur. Phys. J. C* **75** (2015) 330, http://dx.doi.org/10.1140/epjc/s10052-015-3544-0, [arXiv:1503.05427 [hep-ex]].

[49] V. Khachatryan *et al.* [CMS Collaboration], *Phys. Rev. D* **93** (2016) 072004, http://dx.doi.org/10.1103/PhysRevD.93.072004, [arXiv:1509.04044 [hep-ex]].

[50] P. Marquard, A. V. Smirnov, V. A. Smirnov and M. Steinhauser, *Phys. Rev. Lett.* **114** (2015)142002 , http://dx.doi.org/10.1103/PhysRevLett.114.142002, [arXiv:1502.01030 [hep-ph]].

[51] M. Beneke, P. Marquard, P. Nason and M. Steinhauser, [arXiv:1605.03609 [hep-ph]].

[52] M. Fairbairn, P. Grothaus and R. Hogan, JCAP **1406** (2014) 039, http://dx.doi.org/10.1088/1475-7516/2014/06/039, [arXiv:1403.7483 [hep-ph]].

[53] A. Hook, J. Kearney, B. Shakya and K. M. Zurek, *JHEP* **1501** (2015) 061, http://dx.doi.org/10.1007/JHEP01(2015)061, [arXiv:1404.5953 [hep-ph]].

[54] J. R. Ellis and D. Ross, *Phys. Lett. B* **506** (2001) 331, [arXiv:hep-ph/0012067].

[55] G. Aad *et al.* [ATLAS and CMS Collaborations], *JHEP* **1608** (2016) 045,

http://dx.doi.org/10.1007/JHEP08(2016)045, [arXiv:1606.02266 [hep-ex]].

[56] T. Aaltonen *et al.* [CDF and D0 Collaborations], *Phys. Rev. Lett.* **109** (2012) 071804, http://dx.doi.org/10.1103/PhysRevLett.109.071804, [arXiv:1207.6436 [hep-ex]].

[57] ATLAS Collaboration, `http://atlas.cern/updates/physics-briefing/atlas-observes-higgs-boson-run-2-data`;
CMS Collaboration, `http://cms-results.web.cern.ch/cms-results/public-results/preliminary-results/HIG/index.html`.

[58] Peter Higgs, as quoted in The Times newspaper, June 7th, 2013: http://www.thetimes.co.uk/tto/science/article3784820.ece.

[59] J. Ellis and D. S. Hwang, *JHEP* **1209** (2012) 071, [arXiv:1202.6660 [hep-ph]]; J. Ellis, R. Fok, D. S. Hwang, V. Sanz and T. You, *Eur. Phys. J. C* **73** (2013) 2488, [arXiv:1210.5229 [hep-ph]]; S. Bolognesi, Y. Gao, A. V. Gritsan, K. Melnikov, M. Schulze, N. V. Tran and A. Whitbeck, *Phys. Rev. D* **86** (2012) 095031, [arXiv:1208.4018 [hep-ph]].

[60] J. Ellis, D. S. Hwang, V. Sanz and T. You, *JHEP* **1211** (2012) 134, [arXiv:1208.6002 [hep-ph]].

[61] T. Aaltonen *et al.* [CDF and D0 Collaborations], [arXiv:1502.00967 [hep-ex]].

[62] V. Khachatryan *et al.* [CMS Collaboration], [arXiv:1411.3441 [hep-ex]]; see also G. Aad *et al.* [ATLAS Collaboration], *Phys. Lett. B* **726** (2013) 120, [arXiv:1307.1432 [hep-ex]];

[63] J. Ellis and T. You, *JHEP* **1306** (2013) 103, [arXiv:1303.3879 [hep-ph]].

[64] G. Blankenburg, J. Ellis and G. Isidori, *Phys. Lett. B* **712** (2012) 386, [arXiv:1202.5704 [hep-ph]]; R. Harnik, J. Kopp and J. Zupan, *JHEP* **1303** (2013) 026, [arXiv:1209.1397 [hep-ph]].

[65] V. Khachatryan *et al.* [CMS Collaboration], *Phys. Lett. B* **749** (2015) 337, http://dx.doi.org/10.1016/j.physletb.2015.07.053, [arXiv:1502.07400 [hep-ex]].

[66] G. Aad *et al.* [ATLAS Collaboration], *JHEP* **1511** (2015) 211, http://dx.doi.org/10.1007/JHEP11(2015)211, [arXiv:1508.03372 [hep-ex]].

[67] CMS Collaboration, `https://cds.cern.ch/record/2159682/files/HIG-16-005-pas.pdf`.

[68] L. Maiani, *Proc. Summer School on Particle Physics*, Gif-sur-Yvette, 1979 (IN2P3, Paris, 1980) p. 3; G. 't Hooft, in: G. 't Hooft et al., eds., *Recent Developments in Field Theories* (Plenum Press, New York, 1980); E. Witten, *Nucl. Phys.* **B188** (1981) 513; R.K. Kaul, *Phys. Lett.* **109B** (1982) 19.

[69] J. Iliopoulos and B. Zumino, *Nucl. Phys. B* **76** (1974) 310, http://dx.doi.org/10.1016/0550-3213(74)90388-5.

[70] See, for example: S. Weinberg, *Phys. Rev. D* **13** (1976) 974.

[71] See, for example: N. Arkani-Hamed, A. G. Cohen, E. Katz and A. E. Nelson, *JHEP* **0207** (2002) 034, [arXiv:hep-ph/0206021].

[72] M. Baak *et al.* [Gfitter Group], *Eur. Phys. J. C* **74** (2014) 3046, http://dx.doi.org/10.1140/epjc/s10052-014-3046-5, [arXiv:1407.3792 [hep-ph]].

[73] ATLAS and CMS Collaborations, ATLAS-CONF-2015-044, CMS-PAS-HIG-15-002.

[74] J. Ellis, D. S. Hwang, K. Sakurai and M. Takeuchi, *JHEP* **1404** (2014) 004, http://dx.doi.org/10.1007/JHEP04(2014)004, [arXiv:1312.5736 [hep-ph]].

[75] Class for Physics of the Royal Swedish Academy of Sciences, *The BEH-Mechanism, Interactions with Short-Range Forces and Scalar Particles*, `http://www.nobelprize.org/nobel_prizes/physics/laureates/2013/advanced-physicsprize2013.pdf`.

[76] W. Buchmuller and D. Wyler, *Nucl. Phys. B* **268** (1986) 621.

[77] A. Pomarol and F. Riva, *JHEP* **1401** (2014) 151, [arXiv:1308.2803 [hep-ph]].

[78] J. Ellis, V. Sanz and T. You, *JHEP* **1503** (2015) 157, http://dx.doi.org/10.1007/JHEP03(2015)157 [arXiv:1410.7703 [hep-ph]].

[79] A. Falkowski, M. Gonzalez-Alonso, A. Greljo and D. Marzocca, *Phys. Rev. Lett.* **116** (2016)011801, http://dx.doi.org/10.1103/PhysRevLett.116.011801, [arXiv:1508.00581 [hep-ph]].

[80] A. Michelson, https://en.wikiquote.org/wiki/Albert_A._Michelson.

[81] S. W. Hawking, *Is The End In Sight For Theoretical Physics?, Phys. Bull.* **32** (1981) 15.

[82] Spanish Royal Commission, https://en.wikiquote.org/wiki/Talk:Incorrect_predictions.

[83] J. Bond, http://www.imdb.com/title/tt0143145/.

[84] P. Fayet and S. Ferrara, *Phys. Rept.* **32** (1977) 249, http://dx.doi.org/10.1016/0370-1573(77)90066-7; H. E. Haber and G. L. Kane, *Phys. Rept.* **117** (1985) 75, http://dx.doi.org/10.1016/0370-1573(85)90051-1; H. P. Nilles, *Phys. Rept.* **110** (1984) 1, http://dx.doi.org/10.1016/0370-1573(84)90008-5; S. P. Martin, Adv. Ser. Direct. High Energy Phys. **21** (2010) 1 [Adv. Ser. Direct. High Energy Phys. **18** (1998) 1], http://dx.doi.org/10.1142/978981283965_0001, 10.1142/9789814307505_0001 [hep-ph/9709356].

[85] J. R. Ellis, G. Ridolfi and F. Zwirner, *Phys. Lett. B* **257** (1991) 83; H. E. Haber and R. Hempfling, *Phys. Rev. Lett.* **66** (1991) 1815; Y. Okada, M. Yamaguchi and T. Yanagida, *Prog. Theor. Phys.* **85** (1991) 1.

[86] J. R. Ellis, S. Heinemeyer, K. A. Olive and G. Weiglein, *JHEP* **0301** (2003) 006, http://dx.doi.org/10.1088/1126-6708/2003/01/006 [hep-ph/0211206].

[87] O. Buchmueller, M. Citron, J. Ellis, S. Guha, J. Marrouche, K. A. Olive, K. de Vries and J. Zheng, *Eur. Phys. J. C* **75** (2015) 469, Erratum: [*Eur. Phys. J. C* **76** (2016) 190], http://dx.doi.org/10.1140/epjc/s10052-015-3675-3, 10.1140/epjc/s10052-016-4010-3, [arXiv:1505.04702 [hep-ph]].

[88] J. R. Ellis, J. S. Hagelin, D. V. Nanopoulos, K. A. Olive and M. Srednicki, *Nucl. Phys. B* **238** (1984) 453, http://dx.doi.org/10.1016/0550-3213(84)90461-9.

[89] J. Ellis, S. Kelley and D.V. Nanopoulos, Phys. Lett. **B260** (1991) 131; U. Amaldi, W. de Boer and H. Furstenau, Phys. Lett. **B260** (1991) 447; P. Langacker and M. Luo, *Phys. Review* **D44** (1991) 817; C. Giunti, C. W. Kim and U. W. Lee, *Mod. Phys. Lett. A* **6** (1991) 1745.

[90] P. Bechtle, S. Heinemeyer, O. Stal, T. Stefaniak, G. Weiglein and L. Zeune, *Eur. Phys. J. C* **73** (2013) 2354, [arXiv:1211.1955 [hep-ph]].

[91] FeynHiggs Collaboration, http://www.feynhiggs.de.

[92] J. Ellis, J. Quevillon and V. Sanz, *JHEP* **1610** (2016) 086, http://dx.doi.org/10.1007/JHEP10(2016)086, [arXiv:1607.05541 [hep-ph]].

[93] A. Arbey, M. Battaglia, A. Djouadi, F. Mahmoudi and J. Quevillon, *Phys. Lett. B* **708** (2012) 162, http://dx.doi.org/10.1016/j.physletb.2012.01.053, [arXiv:1112.3028 [hep-ph]].

[94] P. Campana, M. Klute and P. Wells, *Ann. Rev. Nucl. Part. Sci.* **66** (2016) 273, http://dx.doi.org/10.1146/annurev-nucl-102115-044812, [arXiv:1603.09549 [hep-ex]].

[95] G. Aarons *et al.* [ILC Collaboration], [arXiv:0709.1893 [hep-ph]]; ILC TDR, H. Baer, T. Barklow, K. Fujii, Y. Gao, A. Hoang, S. Kanemura, J. List and H. E. Logan *et al.*, [arXiv:1306.6352 [hep-ph]]; D. M. Asner *et al.*, [arXiv:1310.0763 [hep-ph]].

[96] CLIC CDR, eds. M. Aicheler, P. Burrows, M. Draper, T. Garvey, P. Lebrun, K. Peach, N. Phinney, H. Schmickler, D. Schulte and N. Toge, CERN-2012-007, http://project-clic-cdr.web.cern.ch/project-CLIC-CDR/; M. J. Boland *et al.* [CLIC and CLICdp Collaborations], http://dx.doi.org/10.5170/CERN-2016-004, [arXiv:1608.07537 [physics.acc-ph]]; H. Abramowicz *et al.*, [arXiv:1608.07538 [hep-ex]].

[97] CEPC-SPPC Study Group, IHEP-CEPC-DR-2015-01, IHEP-TH-2015-01, IHEP-EP-2015-01.

[98] M. Bicer *et al.* [TLEP Design Study Working Group Collaboration], *JHEP* **1401** (2014) 164, [arXiv:1308.6176 [hep-ex]].

[99] J. Ellis and T. You, unpublished.

[100] J. Ellis and T. You, *JHEP* **1603** (2016) 089, http://dx.doi.org/10.1007/JHEP03(2016)089, [arXiv:1510.04561 [hep-ph]].

[101] J. Ellis, P. Roloff, V. Sanz and T. You, [arXiv:1701.04804 [hep-ph]].

[102] R. Contino *et al.*, [arXiv:1606.09408 [hep-ph]].

Basics of QCD for the LHC: $pp \rightarrow H + X$ as a case study[*]

F. Maltoni
Centre for Cosmology, Particle Physics and Phenomenology (CP3)
Université Catholique de Louvain, Louvain-la-Neuve, Belgium

Abstract

Quantum Chromo Dynamics (QCD) provides the theoretical framework for any study of TeV scale physics at LHC. Being familiar with the basic concepts and techniques of QCD is therefore a must for any high-energy physicist. In these notes we consider Higgs production via gluon fusion as an example on how accurate and flexible predictions can be obtained in perturbative QCD. We start by illustrating how to calculate the total cross section at the leading order (yet one loop) in the strong coupling α_S and go through the details of the next-to-leading order calculation eventually highlighting the limitations of fixed-order predictions at the parton level. Finally, we briefly discuss how more exclusive (and practical) predictions can be obtained through matching/merging fixed-order results with parton showers.

Keywords

Lectures; quantum chromodynamics; effective field theory; parton showers; perturbation theory; Monte Carlo.

1 Introduction

Strongly interacting particles can be described in terms of a $SU(3)$ gauge theory field theory involving gluons and quarks:

$$\mathcal{L}_{\text{QCD}} = -\frac{1}{4} G^{\mu\nu,a} G^a_{\mu\nu} + \sum_f \bar{\psi}^f_i \, i \slashed{D}_{ij} \, \psi^f_j \,, \tag{1}$$

where the sum runs over the quark flavors,

$$\begin{aligned} G^a_{\mu\nu} &= \partial_\mu A^a_\nu - \partial_\nu A^a_\mu - g_s f^{abc} A^b_\mu A^c_\nu \,, \\ D_{\mu,ij} &= \partial_\mu \delta_{ij} + i g_s t^a_{ij} A^a_\mu \,, \end{aligned}$$

and t^a_{ij} are the Gell-Mann matrices in the fundamental representation and f^{abc} are the structure functions of SU(3), with

$$[t^a, t^b] = i f^{abc} t^c \,. \tag{2}$$

Notwithstanding its apparent simplicity, QCD is an amazingly rich theory which is able to account for a wide diversity of phenomena, ranging from really strong (non-perturbative) interactions at low scales, below 1 GeV, to rather weak (perturbative) interactions up to scales of the TeV at colliders, from low density to high density states such as those happening in nuclei collisions or inside stars, from low to high temperatures. For proton-proton collisions at the LHC, where one can consider zero temperature and density, QCD is complicated enough that we have no means available (for the moment!) to solve it exactly and we have to resort to a variety of approximate methods, including perturbation theory (when the coupling is small) and lattice calculations (when the coupling is large). Thanks to the work of

---

[*]This article has already been published in the 2013 CERN-Latin-American School of High-Energy Physics, https://doi.org/10.5170/CERN-2015-001.

theoretical and experimental physicists over the last fourty years we are convinced that QCD is a good theory of the strong interactions, of course in the range of energies explored so far and to the level of the theoretical accuracy that can be achieved with current technologies.

There are many excellent references on QCD with applications to collider physics, from books, (e.g., [1]) to review articles, to write-up of lectures given in schools, and in particular some of those given at the CERN schools over the years. My lectures at the school were largely based on the inspiring ones by Michelangelo Mangano [2], Paolo Nason [3] and on the most recent ones by Gavin Salam [4], which I warmly reccommend. In these notes, I'll present a case study, i.e. how QCD can make accurate predictions for Higgs production in gluon fusion at the LHC. The aim is to see the basic concepts at work for a realistic and very important process so to verify their understanding and also to have a closer look at the basic techniques used to perform such calculations. When needed and to avoid repetitions, I will refer to specific sections of Ref. [4] as [QCD: Section number] where the reader will find further information on the basic concepts. Links to simple Mathematica® notebooks with the calculations described below can be found at `http://maltoni.home.cern.ch/`.

2 Higgs cross section at the LHC

The factorisation theorem states that the total cross section for the inclusive production of Higgs at the LHC can be written as [1]

$$\sigma(H + X) = \Sigma_{i,j} \int dx_1 f_i(x_1, \mu_F) \int dx_2 f_j(x_2, \mu_F) \times \hat{\sigma}_{ij \to H+x}(s, m_H, \mu_F, \mu_R), \qquad (3)$$

where the $f_{i/j}(x, \mu_F)$ are the parton distributions functions (long distance term, non-perturbatively calculable) and $\hat{\sigma}$ is the partonic cross section (short distance term, calculable in perturbation theory). $\hat{\sigma}$ can be written as an expansion in α_S:

$$
\begin{aligned}
\hat{\sigma}(ij \to H + x) &= \hat{\sigma}^{(0)}(ij \to H) \\
&+ \hat{\sigma}^{(1)}(ij \to H + \text{up to 1 parton}) \\
&+ \hat{\sigma}^{(2)}(ij \to H + \text{up to 2 partons}) \\
&+ \dots
\end{aligned}
\qquad (4)
$$

where the first term gives the leading order (LO) approximation and it is of order α_S^2, the second next-to-leading (NLO) order (α_S^3) and so on.

It is interesting to know how the Higgs predictions improved and evolved over time. The LO production was considered a long ago [5], the next-to-leading order (NLO) QCD corrections [6–9] were calculated decades ago in the so-called effective field theory (HEFT) approximation (which will be explained in the following) as well in the full SM and found to be very large ($\sigma^{\text{NLO}}/\sigma^{\text{LO}} \sim 2$). This motivated the formidable endeavour of the next-to-next-to-leading order (NNLO) QCD calculations, which have been fully evaluated in HEFT [10–12]. Given that corrections to the HEFT been estimated through a power expansion [13–16] and found to have a negligible impact on total rates, NNLO is the current state of the art for fixed-order predictions.

Before going into the details of the computation of the Higgs cross section, let us remind a few general important points that are relevant for any computation in QCD.

---

[1]Be careful here as for simplicity we adopt the usual pragmatic approach on Higgs production at the LHC and imagine it coming from different channels: gluon-gluon fusion, vector-boson-fusion, vector-boson-associated...and so on. We restrict the discussion to the first one which is the leading mechanism. In fact, various channels overlap if contributions are organized as powers of strong and weak couplings (e.g., $gg \to H$ appears at the same order in α_S and y_t as $gg \to t\bar{t}H$) and in general they mix-up once higher-order QCD and EW corrections are included. The separation into channels is anyway useful from the experimental point of view as they typically lead to different final state signatures.

– At LO the factorisation theorem reduces to the parton model: the parton distribution functions $f_i(x)$ are just the probabilities (and therefore positive-definite) of finding a given parton in the initial state hadrons at a given resolution scale μ_F and $\hat{\sigma}$ gives the probability that such partons with a total energy $s = x_1 x_2 S$ will "fuse" into a Higgs.

– Total cross sections are the first and simplest example of a larger class of observables, called Infrared Safe (IS) quantities [QCD:2.3.2], which can be consistently computed in QCD and then compared to experimental data. Such quantities always need to be (at least to some degree) inclusive on possible extra radiation and in particular resilient under soft and/or collinear radiation. The most known example of IS quantities beyond total cross sections are jets [QCD:5]. The constraint of infrared safety becomes non-trivial already at NLO for Eq. (3).

– Total cross sections always inclusive of any possible extra QCD radiation in the event, hereby denoted by X, even when the calculation is performed at LO. In this case, extra radiation up to the scale μ_F is accounted for by the parton distribution function's (PDF), while hard radiation is consistently neglected being of higher order (α_S). Alternatively, one can prove that the total cross section for producing "just a Higgs", i.e., Higgs + no resolvable radiation at an arbitrary small scale is exactly zero at all orders in perturbation theory.

– A very important point to always keep in mind is that the the "adjectives" LO, NLO, NNLO need to be always referred to a specific observable, i.e. different observables in a given calculation can be predicted at a different order. For example, when talking about a "NNLO calculation for Higgs production in gluon fusion", what is really meant is that the total inclusive cross section is known at NNLO. The same calculation can predict the rate for Higgs+1 jet (inclusive and exclusive) at NLO and Higgs+2 jets only at LO (where exclusive and inclusive is the same).

– Beyond LO, the separation between long-distance and short-distance physics as described by μ_F (and also μ_R) becomes non-trivial. μ_F and μ_R represent arbitrary scales in the calculation, whose dependence is generated by the truncation of the perturbative expansion at a given order. Exploiting the fact that physical results must be independent on such scales one finds renormalisation-group type equations, such as the β function of QCD [QCD:1.2.3] and the so-called DGLAP evolution equations for the PDF's [QCD:3.2].

– The residual dependence of σ on μ_F and μ_R at any given order in perturbation theory is often used to gauge the accuracy of the predictions [QCD:4.4.1]. This is by itself a very crude approximation, while the towers of leading (subleading,...) log's of the scales can be predicted at all orders in perturbation theory, only an explicit computation is able to provide the finite terms at higher orders. In practice, it is common to choose central scales as the typical hard scale in a process and vary them independently between $1/2$ and 2 to identify an uncertainty. However, no solid and unique procedure exists to identify central reference values and variation intervals and to associate a confidence level. However, milder scale dependence of higher-order results compared to lower ones is always used to gauge the improvement on the accuracy of a given prediction.

3 $pp \to H + X$ at leading order

At LO Eq. 3 can be rewritten as

$$\sigma^{\mathrm{LO}}(H + X) = \int_{\tau_0}^1 dx_1 \int_{\tau_0/x_1}^1 dx_2 f_g(x_1, \mu_F) f_g(x_2, \mu_F) \times \hat{\sigma}^{(0)}(gg \to H) , \qquad (5)$$

where $\tau_0 = m_H^2/S$ and $s = x_1 x_2 S$. $\hat{\sigma}$ for a $2 \to 1$ process can be rewritten as

$$\begin{aligned} \hat{\sigma} &= \frac{1}{2s}\overline{|\mathcal{A}|^2}\frac{d^3P}{(2\pi)^3 2E_H}(2\pi)^4\delta^4(p + q - P_H) \\ &= \frac{1}{2s}\overline{|\mathcal{A}|^2}2\pi\delta(s - m_H^2) , \end{aligned} \qquad (6)$$

43

where

$$\tau \equiv x_1 x_2 = \frac{S}{s}, \qquad \tau_0 = \frac{m_H^2}{S}. \tag{7}$$

Performing the change of variables $x_1, x_2 \to \tau, y$ with $x_1 \equiv \sqrt{\tau}e^y$, $x_2 \equiv \sqrt{\tau}e^{-y}$ (verify that the jacobian J is equal to 1) the change of the integration limits and the result becomes

$$\sigma^{\mathrm{LO}}(H+X) = \frac{\pi \overline{|\mathcal{A}|^2}}{m_H^2 S} \int_{\log \sqrt{\tau_0}}^{-\log \sqrt{\tau_0}} dy\, x g(\sqrt{\tau_0}e^y) g(\sqrt{\tau_0}e^{-y}). \tag{8}$$

This expression shows that for the cross section of a $2 \to 1$ process at LO, the contribution from the parton distributions (a quantity known as gluon-gluon luminosity) factorises from the dynamics ($|\mathcal{A}|^2$). The gluon-gluon luminosity depends only on the kinematics in the limits of integration and can be computed once for all for each Higgs mass. The problem is therefore reduced to the computation of the amplitude $\mathcal{A}$.

3.1 My first loop (yet finite!) amplitude: $gg \to H$

Being a color singlet, the Higgs does not couple directly to gluons. However, as no fundamental symmetry forbidding it is present [2] it can via a loop of a colored and massive particle. In the SM such states are the heavy quarks. Let us consider one quark at the time, i.e., the diagram(s) shown in Fig. 1. The first observation to make, even before starting the calculation, is that even though a triangle loop in general can give rise to divergences, both in the ultra-violet (UV) and in the infrared (IR), in this case we expect a finite result. There are several different ways of convincing that this must be the case. A simple one goes as follows. Divergent terms always factorize over lower order amplitudes. The one-loop amplitude is the first non-zero term contributing to $gg \to H$ in the perturbative expansion. Therefore there cannot be any divergence. A finite amplitude, however, does not mean that a consistent regularisation procedure is not needed. The reason is that in intermediate steps of the calculation infinities are found that cancel at the end, yet might leave finite terms. As we will see in $gg \to H$ such finite terms are actually necessary to guarantee the gauge invariance of the result, clearly showing that there is no ambiguity in the procedure. [3]

To evaluate the diagram of Fig. 1 (there are actually two diagrams, the one shown and another one with the gluons exchanged. They give the same contribution so we'll just multiply our final result by two), we employ use dimensional regularisation in $d = 4 - 2\epsilon$ dimensions. [4]

Using the QCD Feynman rules [QCD: Fig. 3] and the Yukawa interaction, the expression for the amplitude corresponding to the diagram of Fig. 1 reads:

$$i\mathcal{A} = -(-ig_s)^2 \mathrm{Tr}(t^a t^b) \left(\frac{-im_Q}{v}\right) \int \frac{d^d\ell}{(2\pi)^d} \frac{t^{\mu\nu}}{\mathrm{Den}} (i)^3 \epsilon_\mu(p)\epsilon_\nu(q) \tag{9}$$

where the overall minus sign is due to the closed fermion loop.[5] The denominator is Den $= (\ell^2 - m_Q^2)[(\ell+p)^2 - m_Q^2][(\ell-q)^2 - m_Q^2]$. Emplyoing the usual Feynman parametrization method to combine

---

[2]In fact, classically, scale invariance would forbid such a coupling. However, scale invariance is broken by renormalisation and therefore it is not a symmetry.

[3]Less obvious is the case of $\gamma\gamma \to H$ where the contribution coming from gauge bosons loop has to be done in different gauges (or via low-energy-theorems) to prove the uniqueness and the correctness of dimensional regularisation procedure. Interestingly enough, people seem to forget this fact quite regularly over the years.

[4]Dimensional regularisation comes in several different flavors and attention has to be paid to the details of the implementation. All formulas quoted in the main body of these lecture notes are in the so-called Conventional Dimensional Regularization (CDR) which is the regularisation procedure where the $\overline{\mathrm{MS}}$ scheme is defined. In practice, NLO calculations nowadays are done in a different scheme which limits the use of the d-dimensional Dirac algebra to the loop computation.

[5]$\epsilon_\mu(p)$ are the transverse gluon polarizations.
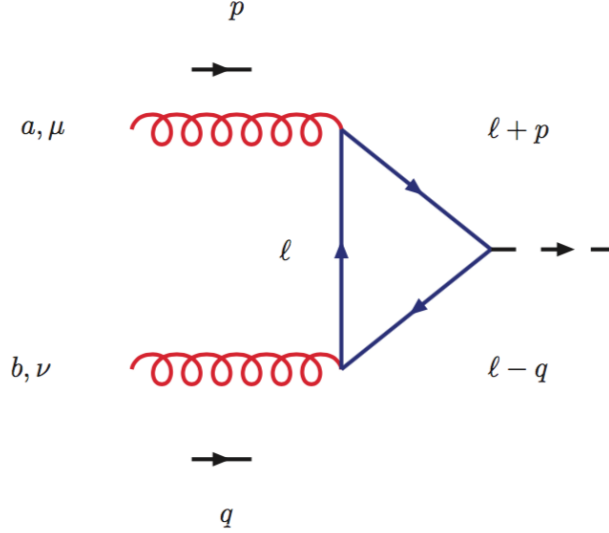
Fig. 1: Representative Feynman diagram for the process $gg \to H$. Another diagram, the one with the gluons exchanged, contributes to the total amplitude.

the denominators of the loop integral into one:

$$\frac{1}{ABC} = 2 \int_0^1 dx \int_0^{1-x} \frac{dy}{[Ax + By + C(1 - x - y)]^3} \tag{10}$$

one obtains

$$\frac{1}{\text{Den}} = 2 \int dx\, dy \frac{1}{[\ell^2 - m_Q^2 + 2\ell \cdot (px - qy)]^3}. \tag{11}$$

The next step is to shift the integration momenta to $\ell' = \ell + px - qy$ so the denominator takes the form

$$\frac{1}{\text{Den}} \to 2 \int dx\, dy \frac{1}{[\ell'^{\,2} - m_Q^2 + m_H^2 xy]^3}. \tag{12}$$

The numerator of the loop integral in the shifted loop momentum becomes

$$
\begin{aligned}
t^{\mu\nu} &= \text{Tr}\left[(\slashed{\ell} + m_Q)\gamma^\mu (\slashed{\ell} + \slashed{p} + m_Q)(\slashed{\ell} - \slashed{q} + m_Q)\gamma^\nu\right] \\
&= 4m_Q\left[g^{\mu\nu}(m_Q^2 - \ell^2 - \frac{m_H^2}{2}) + 4\ell^\mu \ell^\nu + p^\nu q^\mu\right].
\end{aligned}
\tag{13}
$$

where we have used the fact that for transverse gluons, $\epsilon(p) \cdot p = 0$ and so terms proportional to the external momenta, p_μ or q_ν, have been dropped. The above expression shows already several interesting aspects.

The first one is that the trace is proportional to the heavy quark mass. This can be easily understood as an effect of the spin-flip coupling of the Higgs. Gluons or photons do not change the spin of the fermion, as vectors map left (right) spinors into left (right) spinors, while the scalars do couple left (right) spinors with right (left) ones. If the quark circulating in the loop is massless then the trace vanishes due to helicity conservation, independently of the actual Yukawa coupling. This is the reason why even when the Yukawa coupling of the light quark and the Higgs is enhanced (such as in SUSY or 2HDM with large $\tan\beta$), the contribution is anyway suppressed by the kinematical mass.

The second point is that simple power counting shows that the terms proportional to the squared loop momentum ℓ^2 and $\ell^\mu \ell^\nu$ give rise to UV divergences. This means that an intermediate and consistent regularisation prescription is needed for intermediate manipulations and that divergences will have to cancel in the final result.

By shifting momenta in the numerator, dropping terms linear in ℓ' and using the relation

$$\int d^d k \frac{k^\mu k^\nu}{(k^2 - C)^m} = \frac{1}{d} g^{\mu\nu} \int d^d k \frac{k^2}{(k^2 - C)^m} \tag{14}$$

to write the amplitude in the form

$$
\begin{aligned}
i\mathcal{A} = & -\frac{2g_s^2 m_Q^2}{v} \delta^{ab} \int \frac{d^d \ell'}{(2\pi)^d} \int dx dy \Big\{ g^{\mu\nu} \Big[m_Q^2 + \ell'^2 \Big(\frac{4-d}{d} \Big) + m_H^2 (xy - \frac{1}{2}) \Big] \\
& + p^\nu q^\mu (1 - 4xy) \Big\} \frac{2dxdy}{(\ell'^2 - m_Q^2 + m_H^2 xy)^3} \epsilon_\mu(p) \epsilon_\nu(q).
\end{aligned}
\tag{15}
$$

This expression shows that if one computes the integral in $d = 4$, the UV divergent term is absent. For $d = 4 - 2\epsilon$, however, this gives rise to a left-over finite piece, as the scalar integrals are given by

$$
\begin{aligned}
\int \frac{d^d \ell}{(2\pi)^d} \frac{\ell^2}{(\ell^2 - C)^3} &= \frac{i}{32\pi^2} (4\pi)^\epsilon \frac{\Gamma(1+\epsilon)}{\epsilon} (2 - \epsilon) C^{-\epsilon} \\
\int \frac{d^d \ell}{(2\pi)^d} \frac{1}{(\ell^2 - C)^3} &= -\frac{i}{32\pi^2} (4\pi)^\epsilon \Gamma(1+\epsilon) C^{-1-\epsilon}.
\end{aligned}
\tag{16}
$$

So it is manifest that the divergence $1/\epsilon$ cancels against the $(4-d)/d$ term leaving a finite piece, which in fact ensures that the final result is gauge invariant. By combining it with the other terms in the squared parenthesis we obtain

$$\mathcal{A}(gg \to H) = -\frac{\alpha_S m_Q^2}{\pi v} \delta^{ab} \Big(g^{\mu\nu} \frac{m_H^2}{2} - p^\nu q^\mu \Big) \epsilon_\mu(p) \epsilon_\nu(q) \int dx dy \Big(\frac{1 - 4xy}{m_Q^2 - m_H^2 xy} \Big). \tag{17}$$

(Note that we have multiplied by 2 in Eq. (17) to include the diagram where the gluon legs are crossed.) The Feynman integral of Eq. (17) can easily be performed to find an analytic result if desired. Note that the tensor structure could have been predicted from the start by imposing gauge invariance, i.e., $p^\mu \mathcal{A}^{\mu\nu} = q^\nu \mathcal{A}^{\mu\nu} = 0$. By defining $I(a)$ as

$$I(a) \equiv \int_0^1 dx \int_0^{1-x} dy \frac{1 - 4xy}{1 - axy}, \qquad a = \frac{m_H^2}{m_Q^2}, \tag{18}$$

one can factorise a $1/m_Q^2$ out of the integral and cancel the overall m_Q^2 in front of the amplitude (17). In other terms the heavy quark mass dependence is confined in $I(a)$.
For a light quark, $m_Q \ll m_H$,

$$I(a) \xrightarrow{a \to \infty} -\frac{1}{2a} \log^2 a = -\frac{m_Q^2}{2m_H^2} \log^2 \frac{m_Q^2}{m_H^2}, \tag{19}$$

showing that in the Standard Model the charm and bottom quark contributions are strongly suppressed by the square of the quark mass over Higgs mass ratio and come with a minus sign (with respect to the top-quark one).
The opposite limit, $m_H \ll m_Q$,

$$I(a) \xrightarrow{a \to 0} \frac{1}{3}, \tag{20}$$

which is found to be an extremely good approximation even for $m_Q \sim m_H$, is quite surprising at first. In this case the amplitude reads

$$\mathcal{A}(gg \to H) \stackrel{m_Q \gg m_H}{\longrightarrow} -\frac{\alpha_S}{3\pi v}\delta^{ab}\left(g^{\mu\nu}\frac{m_H^2}{2} - p^\nu q^\mu\right)\epsilon_\mu(p)\epsilon_\nu(q). \tag{21}$$

i.e., the amplitude $gg \to H$ becomes *independent* of the mass of the heavy fermion in the loop. This is a special case of a general low energy theorem (which holds in the $p_H \to 0$ limit) that states that if the colored particle mass, independently of the other quantum numbers such as its spin acquires (all of) its mass via the Higgs mechanism, it will contribute to the amplitude $gg \to H$ independently of its mass. In other words $gg \to H$ acts as a counter of heavy colored particles. In a four generation scenario, for instance, the contribution from the t' and b' would lead to a factor of three increase at the amplitude level, i.e. a factor 9 at the cross section level. Note that this is in an apparent contradiction with of our intuition that heavy particles should decouple and not affect the physics at lower energy. The heavy states would not decouple because of our assumption that their (whole) mass is due to electroweak symmetry breaking and the interaction with the Higgs. Another interesting case is that of SUSY, where down-type and up-type quarks can couple differently to the Higgs(es) and other colored states (squarks) are present in the spectrum. At large $\tan\beta$, i.e. when $m_b \tan\beta \simeq m_t$, the Higgs bottom couplings are enhanced by a factor $\tan\beta$, while those of the top suppressed by a $\cot\beta$. However, the scaling with masses is different in the two limits and the contribution from the bottom anyway suppressed by m_Q/m_H. In addition, the the two contributions will have an opposite sign so that will actually interfere destructively in the amplitude squared. What about the squark contributions? Being heavy scalars and therefore coming with an opposite sign shouldn't the stop cancel exactly the contributions from the top and the others squarks give the dominant contribution? In this case, one has to remember that in (possibly) realistic SUSY models the mass of a squark has two sources: one from the coupling to the Higgs vev, which due to SUSY, it is exactly equal to the SM partner coupling and the other from the SUSY soft-breaking terms. For light quarks the latter are by far dominant giving a scaling for $\mathcal{A}$ of the type $m_q/m_{\tilde{q}}$, so highly suppressed and decoupling. A light stop instead, $m_{\tilde{t}} \simeq m_t$ could lead to a possibly strong suppression of $\mathcal{A}$.

3.2 Total cross section at the LHC at LO

The result can be written as:

$$\sigma^{\mathrm{LO}}(pp \to H + X) = \frac{\alpha_S^2(\mu_R)}{64\pi v^2} \mid I\left(\frac{m_H^2}{m_Q^2}\right) \mid^2 \tau_0 \int_{\log\sqrt{\tau_0}}^{-\log\sqrt{\tau_0}} dy g(\sqrt{\tau_0}e^y, \mu_F)g(\sqrt{\tau_0}e^{-y}, \mu_F) \tag{22}$$

Using LO PDF's available in public libraries, such as LHAPDF [17] one can easily compute the gluon-gluon luminosity and therefore the LO Higgs cross section at the LHC14, see Fig. 2. An example is given in a Mathematica® notebook that can be found at the web address mentioned at the end of the Introduction. An interesting exercise is to vary the value of the renormalisation and factorisation scales around the natural central choice $\mu_R = \mu_F = m_H$ to try to estimate the unknown higher-orders terms in the perturbative expansion. It has to be noted that at LO, the cross section depends on μ_R only through $\alpha_S(\mu_R)$ which appears in the short distance coefficient and therefore as an overall factor α_S^2, and depends on μ_F only via the PDF's (both dependences are of logarithmic nature, as the application of the renormalisation group equations easily shows). In other words the dependence on the scales is maximal as there is no explicit dependence on the $\log$ of the scales in the short distance coefficients that can compensate those in the coupling and in the PDF's. At this order, this is consistent as scale changes correspond to a change of at least one order in α_S more and in a LO computation only the first term in the perturbative expansion is present. The result of varying the scales independently $1/2 m_H < \mu_R, \mu_F < 2m_H$ with $1/2 < \mu_F/\mu_R < 2$ in the LO predictions for the LHC is shown in Fig. 9 for different Higgs masses. Result are normalized to the central reference choice $\mu_R = \mu_F = m_H$.
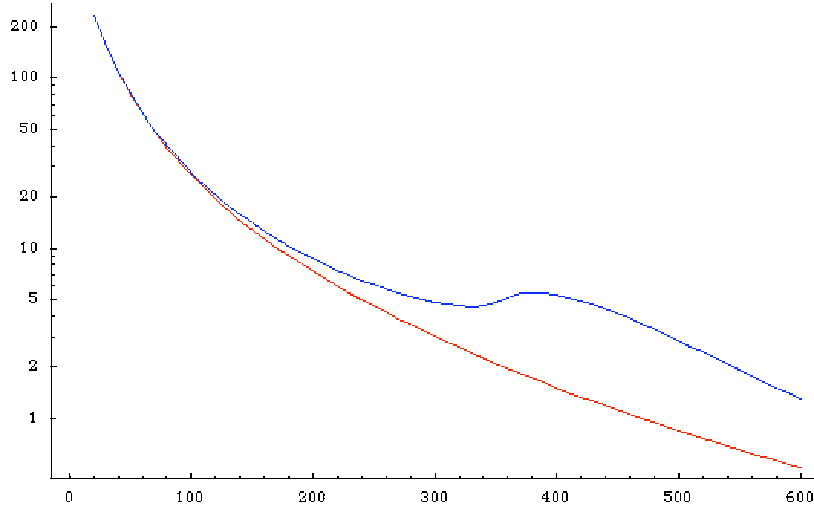
Fig. 2: Example of a plot for the LO cross section for $pp \to H$ at the LHC14 (pb) as a function of the Higgs mass (GeV) obtained with Mathematica® notebook available from the author (link in the text). The red (lower) curve is the large top-mass limit, while the blue (upper) curve is the result withe full top-mass dependence.

4 Higgs Effective field theory

The main result of the simple calculation $gg \to H$ is that gluon fusion is basically independent of the heavy quark mass for a light Higgs boson. The result of Eq. (33) can be easily derived starting from the effective vertex,

$$
\begin{aligned}
\mathcal{L}_{\text{eff}} &= \frac{\alpha_S}{12\pi} G^a_{\mu\nu} G^{a\ \mu\nu} \left(\frac{H}{v} \right) \\
&= \frac{\beta_F}{g_s} G^a_{\mu\nu} G^{a\ \mu\nu} \left(\frac{H}{2v} \right) (1 - \delta),
\end{aligned}
$$

where

$$
\beta_F = \frac{g_s^3 N_F}{24\pi^2} \tag{23}
$$

is the contribution of heavy fermion loops to the $SU(3)$ beta function and $\delta = 2\alpha_S/\pi$.[6] (N_F is the number of heavy fermions with $m \gg m_H$.) The effective Lagrangian of Eq. (23) gives ggH, $gggH$ and $ggggH$ vertices and can be used to compute the radiative corrections of $\mathcal{O}(\alpha_S^3)$ to gluon production. The correction in principle involve 2-loop diagrams. However, using the effective vertices from Eq. (23), the $\mathcal{O}(\alpha_S^3)$ corrections can be found from a 1-loop calculation. To fix the notation we shall use

$$
\mathcal{L}_{\text{eff}} = -\frac{1}{4} A H G^a_{\mu\nu} G^{a,\mu\nu}, \tag{24}
$$

where $G^a_{\mu\nu}$ is the field strength of the SU(3) color gluon field and H is the Higgs-boson field. The effective coupling A is given by

$$
A = \frac{\alpha_S}{3\pi v} \left(1 + \frac{11}{4} \frac{\alpha_S}{\pi} \right), \tag{25}
$$

---

[6]The $(1 - \delta)$ term arises from a subtlety in the use of the low energy theorem. Since the Higgs coupling to the heavy fermions is $M_f(1 + \frac{H}{v})\bar{f}f$, the counterterm for the Higgs Yukawa coupling is fixed in terms of the renormalisation of the fermion mass and wavefunction. The beta function, on the other hand, is evaluated at $q^2 = 0$. The $1 - \delta$ term corrects for this mismatch.

$p_1 \mu a$

$p_2 \nu b$

(a)

$iA\delta^{ab}H^{\mu\nu}(p_1,p_2)$

$p_1 \mu a$

$p_2 \nu b$

(b) $p_3 \sigma c$

$-Agf^{abc}V^{\mu\nu\sigma}(p_1,p_2,p_3)$

$p_1 \mu a$

$p_2 \nu b$ $p_4 \lambda d$

(c) $p_3 \sigma c$

$-iAg^2X^{abcd}_{\mu\nu\sigma\lambda}$
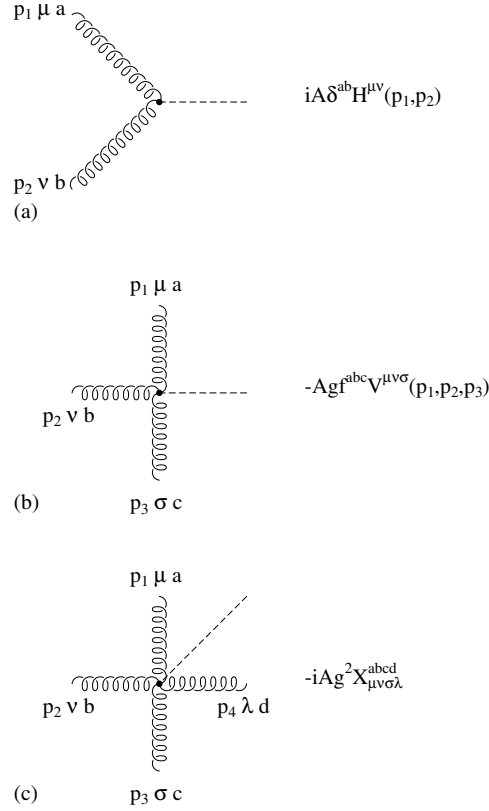
Fig. 3: Feynman rules in the EFT where the top quark is integrated out. Gluon momenta are outgoing.

where v is the vacuum expectation value parameter, $v^2 = (G_F\sqrt{2})^{-1} = (246)^2$ GeV^2 and the α_S correction is included, as discussed above. The effective Lagrangian generates vertices involving the Higgs boson and two, three or four gluons. The associated Feynman rules are displayed in Fig. 3. The two-gluon–Higgs-boson vertex is proportional to the tensor

$$H^{\mu\nu}(p_1,p_2) = g^{\mu\nu}p_1 \cdot p_2 - p_1^{\nu}p_2^{\mu} \,, \tag{26}$$

while the vertices involving three and four gluons and the Higgs boson are exactly proportional to their counterparts from pure QCD

$$V^{\mu\nu\rho}(p_1,p_2,p_3) = (p_1 - p_2)^{\rho}g^{\mu\nu} + (p_2 - p_3)^{\mu}g^{\nu\rho} + (p_3 - p_1)^{\nu}g^{\rho\mu}, \tag{27}$$

and

$$\begin{aligned} X^{\mu\nu\rho\sigma}_{abcd} &= f_{abe}f_{cde}(g^{\mu\rho}g^{\nu\sigma} - g^{\mu\sigma}g^{\nu\rho}) + f_{ace}f_{bde}(g^{\mu\nu}g^{\rho\sigma} - g^{\mu\sigma}g^{\nu\rho}) \\ &+ f_{ade}f_{bce}(g^{\mu\nu}g^{\rho\sigma} - g^{\mu\rho}g^{\nu\sigma}). \end{aligned} \tag{28}$$

5 $gg \rightarrow$ **Higgs @ NLO**

The HEFT is clearly a very powerful approximation as it turns a loop computation into a tree-level one. That means that within the HEFT the calculation of the total cross section for Higgs production at NLO will appear as a usual NLO calculation, i.e., involving only one-loop and tree-level diagrams. This is what we describe in this section.

5.1 The NLO computation in a nutshell

At NLO Eq. 3 can be rewritten as

$$
\begin{aligned}
\sigma^{\mathrm{NLO}}(H + X) &= \int_{\tau_0}^1 dx_1 \int_{\tau_0/x_1}^1 dx_2 f_g(x_1, \mu_F) f_g(x_2, \mu_F) [\hat{\sigma}_B^{(0)}(gg \to H) + \hat{\sigma}_V^{(1)}(gg \to H)] \\
&+ \sum_{ijk} \int_{\tau_0}^1 dx_1 \int_{\tau_0/x_1}^1 dx_2 f_i(x_1, \mu_F) f_j(x_2, \mu_F) \times \hat{\sigma}_R^{(1)}(ij \to H\,k)\,,
\end{aligned}
\tag{29}
$$

where $\hat{\sigma}^{(0)}(gg \to H)$ and $\hat{\sigma}_V^{(1)}(gg \to H)$ denote the Born-level and the virtual cross sections, while $\hat{\sigma}_R^{(1)}(ij \to H\,k)$ is the real-emission cross section:

$$
\begin{aligned}
\hat{\sigma}_{B,V}^{(0,1)}(gg \to H) &= \frac{1}{2s}\overline{|\mathcal{A}_{B,V}|}^2 d\Phi_B\,, \\
\hat{\sigma}_R^{(1)}(ij \to Hk) &= \frac{1}{2s}\overline{|\mathcal{A}_R|}^2 d\Phi_R\,,
\end{aligned}
$$

In general, the virtual term contains ultraviolet (UV), soft and collinear divergences. The UV divergences are absorbed by a universal redefinition of the couplings entering at the Born amplitude, as dictated by the renormalisation of the SM. When integrated over the full real phase space, the real term generates soft and collinear divergences, too, and only when *infrared(IR)-safe* quantities are computed, these divergences cancel to yield a finite result. IR-safe observables $O(\Phi)$ can be best understood by considering the soft or collinear limit in the real phase space, i.e. when the additional parton has low energy or is parallel to another parton. In this limit, an IR-safe observable yields $\lim O(\Phi_R) = O(\Phi_B)$, where the Born-level configuration Φ_B is obtained from Φ_R by eliminating the soft particle (in case of soft singularities) or by merging the collinear particles (in case of collinear singularities).

There several ways to handle the cancellation of the singularities, which fall into two large categories, process-dependent and process-independent methods. In the former, one treats each calculation/process independently and performs manipulations of the integrals over the phase space so to obtain analytic or semi-analytic results.

Process independent methods, on the other hand, are based on a very fundamental result, i.e., that the pattern of the soft and collinear divergences is universal and depends only on the quantum numbers of the initial and final state particles in the Born process. That means that given the Born amplitude, one can predict the divergences that will show up in the virtual contributions and will be then cancelled over integration of the extra radiation in the reals. More importantly, such divergences come in just a handful of different types that can be dealt with once and for all.

Let us now rewrite Eq. (29) in a general and short-hand notation

$$
\sigma^{\mathrm{NLO}} \equiv \int d\Phi_B \left[B(\Phi_B) + V(\Phi_B)\right] O(\Phi_B) + \int d\Phi_R R(\Phi_R)\, O(\Phi_R)
\tag{30}
$$

which will be useful in the following. A NLO cross section is written in terms of matrix elements for the Born and virtual integrated over the Born phase space plus the real matrix elements integrated over the real phase space. Within a subtraction method, the real phase space is parametrized in terms of an underlying Born phase space Φ_B and a radiation phase space $\Phi_{R|B}$. A necessary requirement upon this parametrization is that, in the singular limits, by merging collinear partons, or eliminating the soft parton, the real phase becomes equal to the underlying Born one. Then the expectation value of an IR-safe observable reads

$$
\begin{aligned}
\int d\sigma^{(\mathrm{NLO})} O(\Phi) &= \int d\Phi_B \left[B(\Phi_B) + V(\Phi_B) + \int d\Phi_{R|B} S(\Phi_R)\right] O(\Phi_B) \\
&+ \int d\Phi_R \left[R(\Phi_R)\, O(\Phi_R) - S(\Phi_R) O(\Phi_B)\right]\,.
\end{aligned}
\tag{31}
$$

The third member of the above equation is obtained by adding and subtracting the same quantity from the two terms of the second member. The terms $S(\Phi_{R|B})$ are the subtraction terms, which contain all soft and collinear singularities of the real-emission term. Using the universality of soft and collinear divergences, they are written in a factorised form as

$$S(\Phi_R) = B(\Phi_B) \otimes \tilde{S}(\Phi_{R|B}) \,, \tag{32}$$

where the $\tilde{S}(\Phi_{R|B})$ can be composed from universal, process-independent subtraction kernels with analytically known (divergent) integrals. These integral, when summed and added to the virtual term, yield a finite result. The second term of the last member of Eq. (31) is also finite if O is an IR-safe observable, since by construction S cancels all singularities in R in the soft and collinear regions. The most popular subtraction schemes currently used in public NLO codes are based on the dipole subtraction [18] and the so-called FKS scheme [19]. The case of $gg \to H$ at NLO is particularly simple as the Born amplitude is a $2 \to 1$ process. This means that the integration over phase space of the real corrections is particularly simple and can therefore be done analytically. This has also the pedagogical advantage that shows explicitly where the divergences come from and to "see" the cancellations term by term. We study the process $gg \to H$ at NLO, in the large top-quark mass limit. All results given below are in Conventional Dimensional Regularization (CDR), where matrix elements are calculated in d dimensions, including the Born and real contributions, as well as the integration over phase space [6].

5.2 $gg \to H$: Born in d dimensions

The Born amplitude is calculated via the HEFT feynman rules. The only difference with respect to the previous calculation stems from the fact that now the computation has to be done in $d = 4 - 2\epsilon$-dimensions, with ϵ infinitesimal. The phase space do not bring any extra ϵ term. However, the matrix element changes

$$\left(g^{\mu\nu} \frac{m_H^2}{2} - p^\nu q^\mu \right)^2 = \frac{1}{4}(d-2)m_H^4 \,, \tag{33}$$

as well as the average over the initial state gluon polarizations which in d-dimensions are $d - 2$. This gives

$$
\begin{aligned}
\hat{\sigma}_B &= \frac{\alpha_S^2}{\pi} \frac{m_H^2}{576 v^2 s} \frac{\mu^{2\epsilon}}{(1-\epsilon)} \,\delta(1-z) \\
&\equiv \hat{\sigma}_0 \,\delta(1-z) \,,
\end{aligned}
\tag{34}
$$

where $z \equiv m_H^2/s$ is the inelasticity of the process, i.e. the fraction of the parton parton energy that goes into the Higgs (for the Born $z = 1$). μ is the usual arbitrary scale that needs to be introduced in dimensional regularisation to correct for the different dimensions and keep the action adimensional ($\hbar = c = 1$). Note that a cross section in d dimensions has dimensions $[\sigma] = M^{2-d}$. Also note that we have defined $\hat{\sigma}_0$ as containing an explicit factor z.

5.3 $gg \to H$: virtual corrections

There are several diagrams appearing at one-loop. Diagrams involving bubbles on the external gluon legs (with 3-point gluon-gluon-gluon and gluon-gluon-Higgs verteces) give rise to scaleless integrals that are zero in dimensional regularisation, see Fig. 4, left diagram. The $q\bar{q} \to H$ process, see Fig 4 right, is proportional to the m_q parton mass which are taken massless and therefore null at all orders. As a result, only two diagrams are non-zero, i.e., the vertex correction and the bubble with the four gluon vertex as shown in Fig. 5

$$\hat{\sigma}_{\text{tri}} = \hat{\sigma}_0 \,\delta(1-z) \left[1 + \frac{\alpha_S}{2\pi} C_A \left(\frac{\mu^2}{m_H^2} \right)^\epsilon c_\Gamma \left(-\frac{2}{\epsilon^2} + \frac{10}{3\epsilon} + \frac{179}{36} + \pi^2 \right) \right] \,, \tag{35}$$
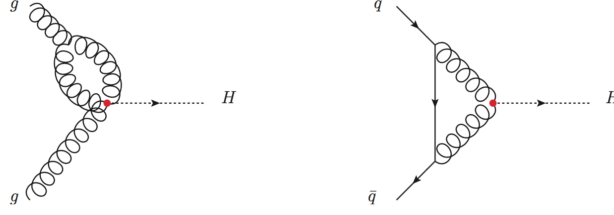
Fig. 4: Example of Feynman diagrams giving null contributions to $ij \to H$ at one-loop in the HEFT. Bubbles on the gluon legs are zero in dimensional regularisation. $q\bar{q} \to H$ is zero at all orders in perturbation theory if $m_q = 0$ due to chiral symmetry.
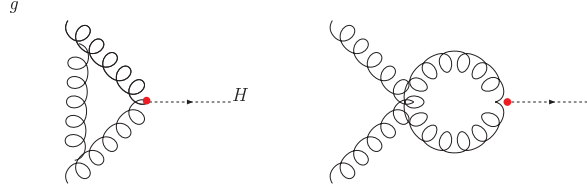
Fig. 5: Feynman diagrams giving non-zero contributionsto $gg \to H$ at one-loop in the HEFT.

$$\hat{\sigma}_{\rm bub} = \hat{\sigma}_0 \, \delta(1-z) \left[1 + \frac{\alpha_S}{2\pi} C_A \left(\frac{\mu^2}{m_H^2}\right)^\epsilon c_\Gamma \left(-\frac{10}{3\epsilon} - \frac{179}{36}\right)\right], \tag{36}$$

where

$$c_\Gamma = (4\pi)^\epsilon \frac{\Gamma(1+\epsilon)\Gamma(1-\epsilon)^2}{\Gamma(1-2\epsilon)}. \tag{37}$$

To obtain the results above, one has to write down the loop amplitudes, perform a few simplifications and the decomposition of the tensor integrals appearing in the amplitudes so to express the results in terms of the following two scalar integrals:

$$\mu^{2\epsilon} \int \frac{{\rm d}^d\ell}{(2\pi)^d} \frac{1}{\ell^2(\ell+p_H)^2} = c_\Gamma \left(\frac{\mu^2}{m_H^2}\right)^\epsilon \left(\frac{1}{\epsilon}+2\right),$$
$$\mu^{2\epsilon} \int \frac{{\rm d}^d\ell}{(2\pi)^d} \frac{1}{\ell^2(\ell+p_1)^2(\ell+p_2)^2} = \frac{c_\Gamma}{2m_H^2} \left(\frac{\mu^2}{m_H^2}\right)^\epsilon \left(\frac{2}{\epsilon^2}-\pi^2\right), \tag{38}$$

with $p_H = p_1 + p_2$. Summing the contributions of the two diagrams above with the α_S correction from Eq. (25), we obtain

$$\hat{\sigma}_V = \hat{\sigma}_0 \, \delta(1-z) \left[1 + \frac{\alpha_S}{2\pi} C_A \left(\frac{\mu^2}{m_H^2}\right)^\epsilon c_\Gamma \left(-\frac{2}{\epsilon^2} + \frac{11}{3} + \pi^2\right)\right], \tag{39}$$

i.e., the total virtual contribution is proportional to the Born amplitude and it contains pole(s) in powers of $1/\epsilon$. The fact that the full virtual amplitude is proportional to the Born is due to the simplicity of a $2 \to 1$ process. However, in general one can prove that the divergent contributions must be proportional to the Born in the case of collinear (and collinear-soft, the double pole) divergences and to the so-called color-connected Born for the soft ones. Given that the Born amplitude is proportional to α_S^2 and we are calculating QCD corrections, we also expect UV divergences, which are proportional to $1/\epsilon$. The fact that apparently we do not see any pole in $1/\epsilon$ in the result above, it simply means that there is an accidental cancellation between simple poles of IR origin and that of UV origin, as we did not keep them
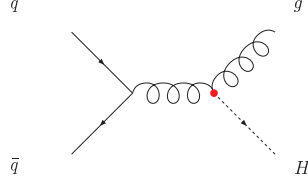
Fig. 6: Feynman diagrams giving $q\bar{q}$ real contributions in the infinite top-quark mass limit. These contributions are finite.

distinct in the calculation. To leave only IR poles in the amplitude to be cancelled with those coming from the real contribution, we therefore proceed here to renormalisation of α_S. This can be attained by the substitution in $\hat{\sigma}_0$, see also [QCD:1.2.3],

$$\alpha_S \to \alpha_S^{\overline{\text{MS}}}(\mu_R) = \alpha_S \left[1 - \frac{\alpha_S}{2\pi} c_\Gamma \left(\frac{\mu^2}{\mu_R^2} \right)^\epsilon \frac{b_0}{\epsilon} \right], \tag{40}$$

where $b_0 = 11/6 \, C_A - 2 n_f T_F / 3$. The UV-renormalized virtual amplitude is

$$\hat{\sigma}_V^{\overline{\text{MS}}}(gg) = \hat{\sigma}_0 \, \delta(1-z) \left[1 + \frac{\alpha_S}{2\pi} C_A \left(\frac{\mu^2}{m_H^2} \right)^\epsilon c_\Gamma \left(-\frac{2}{\epsilon^2} - \frac{2}{\epsilon} \frac{b_0}{C_A} - 2\frac{b_0}{C_A} \log \frac{m_H^2}{\mu_R^2} + \frac{11}{3} + \pi^2 \right) \right]. \tag{41}$$

where now the poles in $1/\epsilon^2$, $1/\epsilon$ are only of IR nature. Another important feature which is manifest in the expression above is the appearance of an explicit $\log$ of the renormalisation scale in the short distance part. As mentioned before, this the improvement expected on the scale dependence of a NLO result: the μ_R dependence of the $\alpha_S^2(\mu_R)$ overall coefficient is exactly cancelled by the explicit log up to order α_S^3.

5.4   Real Contributions

Real corrections imply the calculation of $2 \to 2$ tree-level amplitudes and their integration over phase space in d dimensions. All possible initial and final state partons, gluons, quarks and anti-quarks need to be included,

1. $q\bar{q} \to Hg$ + crossing (i.e., $\bar{q}q \to Hg$),
2. $qg \to Hq$ + crossings (i.e., $\bar{q}g \to H\bar{q}$, $gq \to Hq$, $g\bar{q} \to H\bar{q}$),
3. $gg \to Hg$.

It is easy to predict which divergences to expect from each of the subprocesses above. The reason is that out of the possible (by Lorentz and color invariance) underlying Born amplitudes, i.e., $q\bar{q} \to H$ and $gg \to H$, the only non-zero one is $gg \to H$. Therefore the first processes must give a finite result when integrated over phase space, the second ones can only contain collinear divergences to be absorbed in quark PDF's, while the last is expected to give rise to soft and collinear divergences, part of which will be absorbed in the gluon PDF's and the rest canceled against those coming from the virtual contributions, Eq. (41).

5.4.1 $q\bar{q} \to Hg$

This contribution, shown in Fig. 6 is finite and can be calculated directly in four dimensions. A simple calculation gives

$$\overline{|\mathcal{M}|^2} = \frac{4}{81} \frac{\alpha_S^3}{\pi v^2} \frac{(u^2 + t^2)}{s}, \tag{42}$$
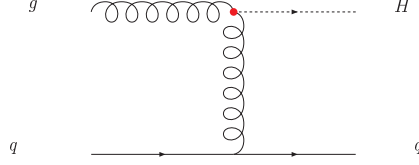
Fig. 7: Feynman diagrams giving qg real contributions in the infinite top-quark mass limit.

to be integrated over the 4-dimensional phase space

$$d\Phi_2 = \frac{1}{8\pi}(1-z)\,dv\,, \tag{43}$$

where $v = 1/2(1 + \cos\theta)$ and $z = m_H^2/s$ as usual. Using

$$t = -s(1-z)(1-v)\,, \tag{44}$$
$$u = -s(1-z)v\,, \tag{45}$$

gives

$$\hat\sigma_R(q\bar q) = \hat\sigma_0 \frac{\alpha_S}{2\pi} \frac{64}{27} \frac{(1-z)^3}{z}\,. \tag{46}$$

5.4.2 $gq \to Hq$

Let us consider now the contribution from the diagrams with an initial quark, i.e., the process $gq \to Hq$. The d-dimensional averaged/summed over initial/final state polarizations and colors amplitude is

$$\overline{|\mathcal{M}|^2} = -\frac{1}{54(1-\epsilon)} \frac{\alpha_S^3}{\pi v^2} \frac{(u^2 + s^2) - \epsilon(u+s)^2}{t}\,. \tag{47}$$

Integrating it over the d-dimensional phase space

$$d\Phi_2 = \frac{1}{8\pi}\left(\frac{4\pi}{s}\right)^\epsilon \frac{1}{\Gamma(1-\epsilon)}\, z^\epsilon (1-z)^{1-2\epsilon}\, v^{-\epsilon}(1-v)^{-\epsilon} dv \tag{48}$$

one gets

$$\hat\sigma_R(gq) = \hat\sigma_0 \frac{\alpha_S}{2\pi} C_F \left(\frac{\mu^2}{m_H^2}\right)^\epsilon c_\Gamma \left[-\frac{1}{\epsilon} p_{gq}(z) + z - \frac{3}{2}\frac{(1-z)^2}{z} + p_{gq}(z) \log\frac{(1-z)^2}{z}\right]\,, \tag{49}$$

where the $p_{gq}(z)$ color-stripped Altarelli-Parisi splitting function is given in the Appendix, Eqs. (67). We perform the factorisation of the collinear divergences adding the counterterm

$$\sigma_{\text{c.t.}}^{\text{coll.}}(gq) = \sigma_0 \frac{\alpha_S}{2\pi} \left[\left(\frac{\mu^2}{\mu_F^2}\right)^\epsilon \frac{c_\Gamma}{\epsilon} P_{gq}(z)\right]\,. \tag{50}$$

We note that in fact in CDR the cross section factorises over the d-dimensional spllitting functions Eqs. (68). However, the collinear counter-term in $\overline{\text{MS}}$ is defined with the 4-dimensional Altarelli-Parisi splitting functions, Eqs. (67), and that is why we have written the result above in terms of $p_{gq}(z)$ leaving out a finite term z (also note that our definition of σ_0, Eq. (34), contains a factor z). This gives

$$\begin{aligned}
\hat\sigma_R^{\overline{\text{MS}}}(gq) &= \hat\sigma_R(gq) + \hat\sigma_{\text{c.t.}}^{\text{coll.}}(gq) \\
&= \sigma_0 \frac{\alpha_S}{2\pi} C_F \left[p_{gq}(z) \log\frac{m_H^2}{\mu_F^2} + p_{gq}(z) \log\frac{(1-z)^2}{z} + z - \frac{3}{2}\frac{(1-z)^2}{z}\right]\,.
\end{aligned} \tag{51}$$
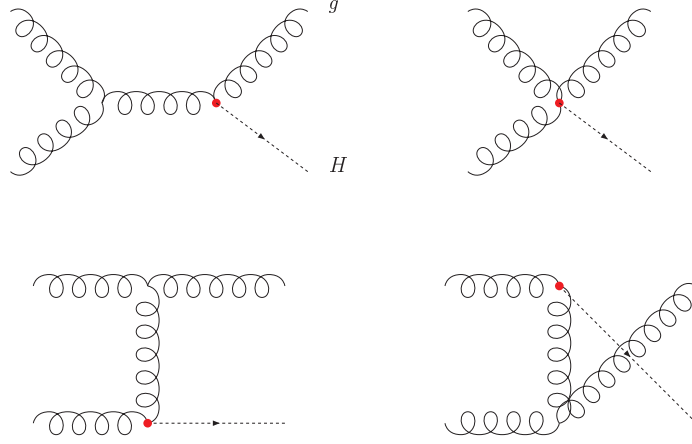
Fig. 8: Feynman diagrams giving gg real contributions in the infinite top-quark mass limit.

5.4.3 $gg \to Hg$

The calculation of the d-dimensional $gg \to Hg$ amplitude involves the four diagrams shown in Fig. 8 and it is not so trivial to do by hand, yet the final result is very compact:

$$\overline{|\mathcal{M}|^2} = \frac{1}{24(1-\epsilon)^2} \frac{\alpha_S^3}{\pi v^2} \frac{(m_H^8 + s^4 + t^4 + u^4)(1-2\epsilon) + \frac{1}{2}\epsilon(m_H^4 + s^2 + t^2 + u^2)^2}{stu} \,. \tag{52}$$

This example is illustrative of the fact that keeping track of the ϵ parts in the amplitude squared makes the calculation significantly more complex for at least two reasons. First the structure of the result itself is more involved. Second, one is forced to work at the squared amplitude level as d dimensional contributions come from the ($d-2$ dimensional) gluon polarizations and therefore cannot exploit the beauty, power and simplicity of helicity amplitude techniques [20, 21]. Computing QCD amplitudes where states have fixed polarizations entails huge simplifications and allows to make predictions for amplitudes with many external partons. For example, tree-level amplitudes in the HEFT involving up to 5 extra partons can be easily obtained automatically using tools such as ALPGEN [22] or MADGRAPH [23]. Fortunately, it turns out that is possible to use a different scheme than CDR and actually perform the computation of the Born and real matrix elements in exactly four dimensions (yet integrate them over the d-dimensional phase space). This involves a different (and a bit tricky) d-dimensional algebra for the loop computations and the introduction of (universal) finite terms for the initial-state counter-terms and UV subtractions, yet with an enormous computational simplification. All public NLO codes for processes at the LHC in practice do use such "maximally four dimensional" d-dimensional regularisation schemes. Integrating the amplitude (52) over the d-dimensional phase space of Eq. (48) gives

$$\begin{aligned}
\hat{\sigma}_R(gg) &= \hat{\sigma}_0 \frac{\alpha_S}{2\pi} C_A \left(\frac{\mu^2}{m_H^2}\right)^\epsilon c_\Gamma \left[\left(\frac{2}{\epsilon^2} + \frac{2}{\epsilon}\frac{b_0}{C_A} - \frac{\pi^2}{3}\right)\delta(1-z) \right. \\
&\quad - \frac{2}{\epsilon}p_{gg}(z) - \frac{11}{3}\frac{(1-z)^3}{z} - 4\frac{(1-z)^2(1+z^2)+z^2}{z(1-z)}\log z \\
&\quad \left. + 4\frac{1+z^4+(1-z)^4}{z}\left(\frac{\log(1-z)}{1-z}\right)_+ \right],
\end{aligned} \tag{53}$$

where the plus prescription is defined as follows:

$$\int_0^1 dx\,[h(x)]_+ f(x) = \int_0^1 dx\,h(x)[f(x) - f(1)]\,. \tag{54}$$

Note that the $\frac{2}{\epsilon}\frac{b_0}{C_A}\delta(1-z)$ in Eq. (53) comes from rexpressing the divergent term $-\frac{4}{\epsilon}\left[\frac{z}{(1-z)_+} + \frac{1-z}{z} + z(1-z)\right]$ in terms of $-\frac{2}{\epsilon}p_{gg}(z)$, see Eq. (67). The factorisation of the collinear divergence is handled by adding the corresponding counterterm

$$\hat{\sigma}_{\mathrm{c.t.}}^{\mathrm{coll.}}(gg) = 2\,\hat{\sigma}_0\,\frac{\alpha_S}{2\pi}\left[\left(\frac{\mu^2}{\mu_F^2}\right)^{\epsilon}\frac{c_\Gamma}{\epsilon}P_{gg}(z)\right]\,, \tag{55}$$

which gives

$$
\begin{aligned}
\hat{\sigma}_R^{\overline{\mathrm{MS}}}(gg) &= \hat{\sigma}_R(gg) + \hat{\sigma}_{\mathrm{c.t.}}^{\mathrm{coll.}}(gg)\\
&= \hat{\sigma}_0\,\frac{\alpha_S}{2\pi}C_A\left(\frac{\mu^2}{m_H^2}\right)^{\epsilon}c_\Gamma\left[\left(\frac{2}{\epsilon^2} + \frac{2}{\epsilon}\frac{b_0}{C_A} - \frac{\pi^2}{3}\right)\delta(1-z)\right.\\
&\quad + 2p_{gg}\log\frac{m_H^2}{\mu_F^2} - \frac{11}{3}\frac{(1-z)^3}{z} - 4\frac{(1-z)^2(1+z^2)+z^2}{z(1-z)}\log z\\
&\quad \left. + 4\frac{1+z^4+(1-z)^4}{z}\left(\frac{\log(1-z)}{1-z}\right)_+\right]\,.
\end{aligned} \tag{56}
$$

We can now recognise that the IR poles match those of the virtual contributions in Eq. (41). Adding up the contributions from real and virtual contributions of the gg channel we obtain (note that our definition of σ_0, Eq. (34), contains a factor z):

$$
\begin{aligned}
\hat{\sigma}^{\overline{\mathrm{MS}}}(gg) &= \hat{\sigma}_R^{\overline{\mathrm{MS}}}(gg) + \hat{\sigma}_V^{\overline{\mathrm{MS}}}(gg)\\
&= \sigma_0\,\frac{\alpha_S}{2\pi}C_A\left[\left(\frac{11}{3} + \frac{2}{3}\pi^2 - 2\frac{b_0}{C_A}\log\frac{m_H^2}{\mu_R^2}\right)\delta(1-z)\right.\\
&\quad -\frac{11}{3}\frac{(1-z)^3}{z} + 2p_{gg}\log\frac{m_H^2}{\mu_F^2} - 4\frac{(1-z+z^2)^2}{z(1-z)}\log z\\
&\quad \left. + 8\frac{(1-z+z^2)^2}{z}\left(\frac{\log(1-z)}{1-z}\right)_+\right]\,.
\end{aligned} \tag{57}
$$

As predicted, the final results for the short distance coefficients is finite (yet scheme dependent) and does contain the necessary log's of the renormalisation and factorisation scales that compensate up to α_S^3 the corresponding dependences in $\alpha_S^2(\mu_R)$ of the Born amplitude and in the PDF's.

5.5 NLO results: discussion

The expressions above can be easily implemented in a numerical code to perform the convolution integrals with PDF's. A few simple numerical optimizations, such as the choice of integration variables, and a bit of attention to the implementation of the $+$ distributions, that's all is needed. The reader can find a sample implementation in a Mathematica® notebook at the web address mentioned at the end of the Introduction. By running the code with different scale choices, one can associate an uncertainty to the NLO predictions as done at LO. The result, shown in Fig. 9, comes as a big surprise! The NLO calculation predicts a rate twice as large and the respective LO and NLO uncertainty bands do not even overlap. That means that our naive estimate of the uncertainties at LO is totally off and therefore unreliable. It seems also to suggest that perturbation expansion is at stake here. As we had mentioned, this motivated the computation of the NNLO corrections, which are also shown in Fig. 9. Fortunately, NNLO
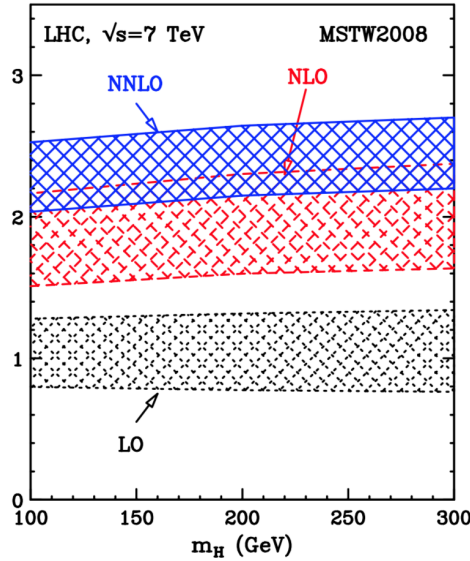
Fig. 9: K-factors for Higgs production from gluon fusion at the LHC. Uncertainty bands are obtained via independent scale variation $1/2\,m_H < \mu_R, \mu_F < 2\,m_H$ with $1/2 < \mu_F/\mu_R < 2$. The LO and NLO bands can be obtained by implementing the formulas obtained in these notes in a code that performs the numerical integration over the PDF's. Cross-checks and NNLO results can be obtained with HNNLO [24]. (Plot courtesy of M. Grazzini).

predictions do overlap with NLO and also display a smaller scale dependence, so that the perturbation picture seems safe starting from NLO on. In fact, this behavior is rather special to $pp \to H + X$ and it is often rephrased by saying that what we call LO (in the perturbative expansion) is not actually the leading one in size and therefore we should not start from that. For instance, in Drell-Yan or VBF this does not happen, and the perturbative expansions (seem to) converge beautifully, see Fig. 10. In any case, the Higgs production reminds us an important fact that we should always keep in mind: scale variation cannot by definition reproduce missing finite terms in the perturbative expansion and as such can only give an indication of what the real uncertainties could be. On the other hand, comparison between predictions from LO and NNLO, their stabilization (or lack thereof) and the use of approximate methods to determine (classes of) higher order terms, all together can provide a rather solid picture on the theoretical uncertainties on a case-by-case basis. We mention, in passing, another important source of uncertainties in making predictions for hadron colliders, i.e., that coming from imperfect knowledge of the PDF's. Uncertainties are related to unknown higher-order terms in the DGLAP evolution equations that determine as well as from the extraction of the initial condition from experimental data, see [QCD:3] and in particular [QCD:3.3.2]. [7]

As far as total cross sections are concerned, the situation is therefore pretty clear. Fixed-order calculations come equipped with self-detecting procedures that can give us information on whether a prediction is reliable or not. If not, it can be systematically improved by including higher-order terms (almost for free nowadays at NLO, yet at a rather high cost at NNLO) and uncertainties can be easily estimated. So it is natural to ask, what about other IR-safe observables?

Let us consider, once again $pp \to H + X$ as an example, and focus on the Higgs momentum (fully inclusive) distribution, which can be parametrized in terms of only two variables[8], the rapidity y_H

---

[7] The latter does in fact imply also the prediction of experimental observables at the same order in perturbation theory and therefore are also intrinsically also affected by scale dependencies. Such effects are not included normally in the estimation of the uncertainties coming from PDF's.

[8] We do not consider the azimuthal angle ϕ, because for symmetry reasons can only lead to a uniform distribution
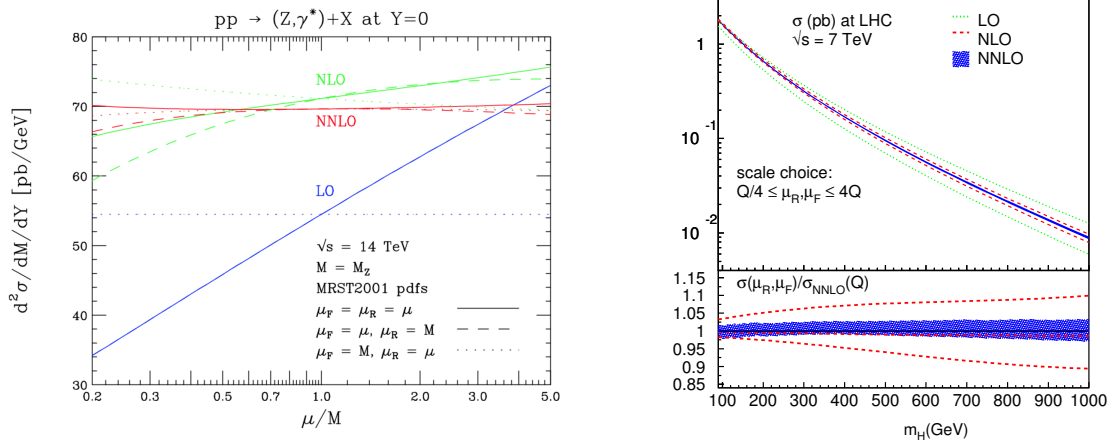
Fig. 10: Examples of improvement in the predictions of processes at LHC in going from LO to NNLO. On the left, scale dependence of the predictions for Z/γ^* production (at $y = 0$) at the LHC14, at fixed order [25]. On the right, Higgs production at the LHC7 via VBF [26] as a function of the Higgs mass. The bands are obtained by independent scale variation in the interval $Q/4 \leq \mu_F, \mu_R \leq 4Q$, Q being the virtuality of the W, Z fusing into the Higgs. In both cases the perturbative expansion behaves extremely well and NNLO predictions overlap with those at LO and NLO and display a much smaller residual uncertainty.

and the transverse momentum p_H^T. At LO (referred to the total cross section), the Higgs can be boosted in the forward or backward directions in the lab system, $y_H = \frac{1}{2} \log \frac{x_1}{x_2}$, yet it has always $p_H^T = 0$, i.e. the distribution in p_H^T is a delta function centered at $p_H^T = 0$. At NLO (again referred to the total cross section), $2 \to 2$ diagrams enter in the calculation and the Higgs can have a non-zero p_H^T. Since at any point in phase space with $p_H^T \neq 0$ this is the first non-zero contribution, the observable p_H^T of the Higgs is only at LO. In other words if we want to know the p_H^T distribution of the Higgs at NLO over all phase space, we need at least a NNLO prediction for the cross section. Another way of thinking about it is to ask oneself what kind of diagrams are present in the calculation for that observable in a given area of the phase space: if there are only tree-level diagrams then the observable is LO. It is important when working with NLO codes to always think about what kind of observables are actually predicted at NLO, what at LO and what not even at LO. Again, a NNLO computation for the total cross section for $pp \to H + X$, gives NNLO information on the Higgs rapidity distribution, NLO for the Higgs p_H^T and $pp \to H + 1$-jet observables, LO for $pp \to H + 2$-jets observables and the structure of the jet in $H + 1$-jet events and no information at all on $pp \to H + 3$-jets observables. In short, a fixed-order computation can only make predictions for a finite number of observables, typically with a rather limited number of resolved partons and a very small number of unresolved ones, i.e. just one for a NLO computation and up to two for a NNLO computation. This is the first main limitation of a fixed-order computation. However, it is not the only one.

Consider again the p_H^T distribution of the Higgs as predicted by a NLO computation for the total cross section, Fig. 11. This curve can be easily obtained using the expressions in four dimensions of Eqs. (42,47,52), performing the integration over the polar angle together with the PDF's via a Monte-Carlo method and plotting it point-by-point during the integration. The p_H^T distribution is divergent in $p_H^T = 0$ as expected from soft and beam-collinear emissions. As we have learnt such divergences are proportional to $\delta(1 - z)$ where z is the fraction of parton-parton energy taken by the Higgs and are cancelled by the virtual contributions, all of which reside in $p_T = 0$. So the cancellation between real and virtual contributions, all of it happens in the first bin of the histogram. How do we interpret such weird distribution? A useful way is to think about the size of the bin of the distribution as our resolution scale: with a rather coarse binning there is no "going-to-infinity" and predictions are rather stable (this of course includes the total cross section which corresponds to using only one bin), while with thin binning,

$m_H = 120$ GeV - LHC@7TeV
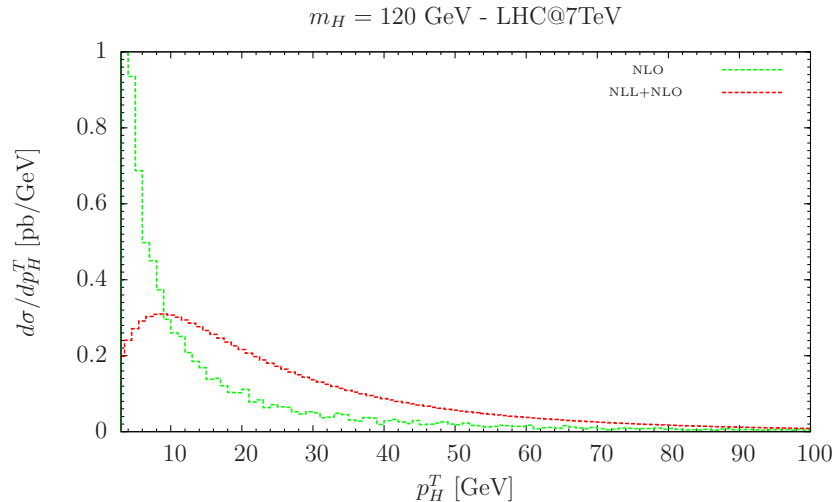
Fig. 11: Higgs p_H^T spectrum for a Higgs of $m_H = 120$ GeV at the LHC7. The labeling NLO and NLL+NLO refer to the total cross section. The curves are normalized to the same value (=total cross section is the same). The green curve is just a LO prediction for the p_H^T of the Higgs. The logarithmic divergence at $p_H^T \to 0$ is cancelled by the negative infinite virtual contributions at $p_H^T = 0$ (not shown!). The resummed prediction (red curve) features a "physical" smooth behavior at small p_H^T. (The resummed prediction is obtained via HqT [27]).

we start to be sensitive to low energy and virtual emissions which become increasingly important and are not included at all in a fixed-order approach. This is the case where resummed predictions come into rescue: one finds that the leading part of soft emissions (real and virtual) is universal, it can be considered at all orders and included by identifying the log's associated to it and exponentiating them. This can be done either at very high accuracy analytically yet fully inclusively or in a numerical and exclusive way at the leading log with a parton shower (which actually resums both soft and collinear enhancements). The result of including these effects analytically is shown in Fig. 11, red curve. In very crude words, the effect of the resummation is to spread the $\delta(p_T)$ of the virtual contributions over a range of a few tens of GeV with the effect of smoothing out the divergence and producing a "physical" distribution.

In summary, fixed-order calculations in perturbative QCD can be performed in a well-defined and quite simple framework, i.e. in the context of the factorization theorem. It is therefore possible to make predictions for inclusive quantities in hadron colliders, which can be systematically improved at the "only" price of an (exponential) increase in the complexity of the calculation. In practice, however, the use of fixed-order predictions is limited by several other important drawbacks. First, only processes with a few resolved partons can be calculated, while in practice we know that hundreds of hadrons can be produced in a single proton-proton interaction of which we are bound to ignore the details. Second, sharp infinities appear in the phase that do cancel between real and virtual contributions if inclusive enough observables are defined, yet lead to unphysical distributions in specific areas of the phase space and/or when the resolved partons become either soft or collinear. Such local positive and negative infinities are unphysical because they appear only due the artificial truncation of the perturbative expansion. Finally, the fact that plus and minus infinities appear locally in phase space also means that fixed order predictions beyond LO cannot be used as probability functions to generate events as distributed in nature. Parton showers, i.e. fully exclusive resummation, and their merging/matching with fixed-order predictions, provide an elegant and powerful way out to all the above limitations.

6   Beyond fixed-order predictions

As we have explicitly verified, fixed-order predictions have important limitations both of principle (areas of phase space and observables, such as jet substructure are poorly described, no hadrons but only partons) and in practice (no event simulation is possible). Fortunately, an alternative approach exists that is based on the fact that the IR structure, soft or collinear, of QCD is universal and contributions can be resummed at all orders. Last but not least, formulas that describe the emission of soft and collinear partons are amenable of a probabilistic interpretation and therefore not only it is possible to perform an explicit resummation but also to associate a full "history" to an hard scattering event, i.e., to associate to every event a full-fledged description of an high-energy event from the two initial protons to the final (possibly hundreds) of hadrons and leptons in the final state. In addition, in the latest years, enormous progress has been achieved in combining the accuracy of fixed-order predictions with the flexibility of parton showers. These methods are briefly presented here together with their applications to Higgs production. The short presentation below is adapted from Ref. [28]. The reader is also referred to [QCD:4.4] for further details, examples and references.

6.1   Parton Showers

Parton Showers (PS) are able to dress a given Born process with all the dominant (i.e. enhanced by collinear logarithms, and to some extent also soft ones) QCD radiation processes at all orders in perturbation theory. In particular, the dominant contributons, i.e. those given by the leading logarithms, coming from both real and virtual emissions are included. The cross section for the first (which is often also the hardest) emission in a shower reads:

$$d\sigma^{\text{1st step}} = d\Phi_B B(\Phi_B) \left[\Delta(p_\perp^{\min}) + d\Phi_{R|B}\Delta(p_{\text{T}}(\Phi_{R|B}))P(\Phi_{R|B}) \right] , \tag{58}$$

where $\Delta(p_{\text{T}})$ denotes the Sudakov form factor

$$\Delta(p_{\text{T}}) = \exp \left[- \int d\Phi_{R|B}P(\Phi_{R|B})\Theta(p_{\text{T}}(\Phi_R) - p_{\text{T}}) \right] . \tag{59}$$

This Sudakov form factor can be understood as a no-emission probability of secondary partons down to a resolution scale of p_{T}. Here $P(\Phi_{R|B})$ is a process-independent universal splitting function that allows to write the PS approximation to the real cross section R^{PS}, typically given schematically by a product of the underlying Born-level term folded with a splitting kernel P

$$R^{\text{PS}}(\Phi) = P(\Phi_{R|B}) \, B(\Phi_B). \tag{60}$$

In this framework, $\Phi_{R|B}$ is often expressed in terms of three showering variables, like the virtuality t in the splitting process, the energy fraction of the splitting z and the azimuth ϕ. A very simple (and widely used) choice for the splitting function, is

$$P(\Phi_{R|B})d\Phi_{R|B} = \frac{\alpha_S(t)}{2\pi} P_{a \to bc}(z) \frac{d\phi}{2\pi} \frac{dt}{t} \, dz \tag{61}$$

where $P(z)$ are Altarelli-Parisi splitting functions on which any QCD amplitude factorises in the collinear limit $b \parallel c$.

The above definition of the Sudakov form factor, guarantees that the square bracket in Eq. (58) integrates to unity, a manifestation of the probabilistic nature of the parton shower. Thus, integrating the shower cross section over the radiation variables yields the total cross section, given at LO by the Born amplitude. The corresponding radiation pattern consists of two parts: one given by the first term in the square bracket, where no further resolvable emission above the parton-shower cut-off $p_\perp^{\min}$ – typically of the order of 1 GeV – emerges, and the other given by the second term in the square bracket describing

the first emission, as determined by the splitting kernel. It is important to stress that the real-emission cross section in a PS generator is only correct in the small angle and/or soft limit, where R^{PS} is a reliable approximation of the complete matrix element.

After the 1st step the process is repeated using the new configuration as the Born one.

While rather crude, the PS approximation is a very powerful one, due mainly to the great flexibility and simplicity in the implementation of $2 \to 1$ and $2 \to 2$ high-Q^2 processes. In addition, once augmented with a hadronisation model the simulation can easily provide a full description of a collision in terms of physical final states, i.e., hadrons, leptons and photons. In the current terminology a generic Monte Carlo generator mainly refers to such tools, the most relevant examples of are PYTHIA 6 and PYTHIA 8 [29, 30], HERWIG [31], HERWIG++ [32], and SHERPA [33]. A very clear and exhaustive presentation of parton shower generators can be found in Ref. [34].

6.2   Matrix-element merging (ME+PS)

In parton showers algorithms QCD radiation is generated in the collinear and soft approximation, using Markov chain techniques based on Sudakov form factors. Hard and widely separated jets are thus poorly described in this approach. On the other hand, tree-level fixed order amplitudes can provide reliable predictions in the hard region, while failing in the collinear and soft limits. To combine both descriptions and avoid double counting or gaps between samples with different multiplicity, an appropriate merging method is required.

Matrix-element merging [35] aims at correcting as many large-angle emissions as possible with the corresponding tree-level accurate prediction, rather than only *small-angle* accurate. This is achieved by generating events up to a given (high) multiplicity using a matrix-element generator, with some internal jet-resolution parameter Q_{cut} on the jet separation, such that practically all emissions above this scale are described by corresponding tree-level matrix elements. Their contributions are corrected for running-coupling effects and by Sudakov form factors. Radiation below Q_{cut} on the other hand is generated by a parton-shower program, which is required to veto radiation with separation larger than Q_{cut}. As far as the hardest emission is concerned, matrix-element merging is as accurate as matrix-element corrections (when these are available) or NLO+PS. Since they lack NLO virtual corrections, however, they do not reach NLO accuracy for inclusive quantities. Nevertheless, they are capable to achieve leading-order accuracy for multiple hard radiation, beyond the hardest only, while NLO+PS programs, relying on the parton shower there are only accurate in the collinear and/or soft limit for these quantities.

Several merging schemes have been proposed, which include the CKKW scheme [35–37] and its improvements [38, 39], the MLM matching [40], and the k_T-MLM variation [41]. The MLM schemes have been implemented in several matrix element codes such as ALPGEN [22], MADGRAPH [23], through interfaces to PYTHIA/HERWIG, while SHERPA [33] and HERWIG++ [32] have adopted the CKKW schemes and rely on their own parton showers. In Ref. [42] a detailed, although somewhat outdated description of each method has been given and a comparative study has been performed.

6.3   NLO+PS in a nutshell

Several proposals have been made for the full inclusion of complete NLO effects in PS generators. At this moment, only two of them have reached a mature enough stage to be used in practice: MC@NLO [43] and POWHEG [44]. Both methods correct – in different ways – the real-emission matrix element to achieve an exact tree-level emission matrix element, even at large angle. As we have seen in the previous subsection, this is what is also achieved with matrix-element corrections in parton showers, at least for the simplest processes listed earlier. This, however, is not sufficient for the NLO accuracy, since the effect of virtual corrections also needs to be included. In both methods, the real-emission cross section is split into a singular and non-singular part, $R = R^s + R^f$. One then computes the total NLO inclusive

cross section, excluding the finite contribution, at fixed underlying Born kinematics, defined as

$$\bar{B}^s = B(\Phi_B) + \left[V(\Phi_B) + \int d\Phi_{R|B} R^s(\Phi_{R|B}) \right] , \qquad (62)$$

and uses the formula

$$d\sigma^{\text{NLO+PS}} = d\Phi_B \bar{B}^s(\Phi_B) \left[\Delta^s(p_\perp^{\min}) + d\Phi_{R|B} \frac{R^s(\Phi_R)}{B(\Phi_B)} \Delta^s(p_T(\Phi)) \right] + d\Phi_R R^f(\Phi_R) \qquad (63)$$

for the generation of the events. In this formula, the term $\bar{B}$ can be understood as a local K-factor reweighting the soft matrix-element correction part of the simulation. Clearly, employing the fact that the term in the first square bracket integrates to unity, as before, the cross section integrates to the full NLO cross section.

In MC@NLO one chooses R^s to be identically equal to the term $B \otimes P$ that the PS generator employs to generate emissions. Within MC@NLO, n-body events are obtained using the $\bar{B}^s$ function, and then fed to the PS, which will generate the hardest emission according to Eq. (62). These are called $\mathcal{S}$ events in the MC@NLO language. An appropriate number of events are also generated according to the R^f cross section, and are directly passed to the PS generator. These are called $\mathcal{H}$ events. In MC@NLO, $R^f = R - R^s$ is not positive definite, and it is thus necessary to generate negative weighted events in this framework. A library of MC@NLO Higgs processes (gluon fusion, vector-boson associated production, and charged Higgs associated with top) is available at Ref. [45], which is interfaced to HERWIG and HERWIG++. A fully automatized approach, AMC@NLO [46] implemented in the MADGRAPH framework, is now available that allows to compute and combine all necessary ingredients (Born, real, virtual matrix elements plus counterterms) at the user's request.

In POWHEG, one chooses $R^s \leq R$, and in many cases even $R^s = R$, so that the finite cross section R^f vanishes. In this case, the hardest emission is generated within POWHEG itself, and the process is passed to the parton shower only after the hardest radiation is generated. Positive weighted events are obtained, since R^f can always be chosen to be positive definite. In all cases the chosen R^s has exactly the same singularity structure as R, so that R^f always yield a finite contribution to the cross section. Implementations of Higgs production processes with the POWHEG method are available in HERWIG++ [47], in the POWHEGBOX [48] (interfaced to both HERWIG and PYTHIA) and recently in SHERPA [49].

6.4 Improved descriptions of Higgs production

Being of primary importance, Higgs kinematic distributions are now quite well predicted and also available via public codes such as ResBos [50] and HqT [27, 51]. Differential p_H^T distributions accurate to LO yet featuring the exact bottom- and top-quarks mass loop dependence (and therefore can be used also for predictions of scalar Higgs in BSM) can be obtained via HIGLU [52] as well as via HPro [53]. However, in experimental analyses, it is also crucial to get as precise predictions as possible for exclusive observables that involve extra jets, such as the jet p_T spectra and the jet rates, at both parton and hadron level. To optimize the search strategies and in particular to curb the very large backgrounds, current analyses both at Tevatron and at the LHC select 0-,1- and 2-jet events and perform independent analyses on each sample. The final systematic uncertainties are effected by both the theoretical and experimental ones of such a jet-bin based separation. In the HEFT, fully exclusive parton- and hadron-level calculations can now be performed by Parton Shower (PS) programs or with NLO QCD codes matched with parton showers: via the MC@NLO and POWHEG methods. Beyond the HEFT, fully exclusive predictions ME+PS and NLO+PS techniques has become available only recently [54, 55]. The reason is that one needs to compromise between the validity of HEFT and the complexity of higher loop calculations.

Fig. 12 shows a comparison of the predictions of the p^T of the Higgs at LHC7 as obtained in HEFT from:
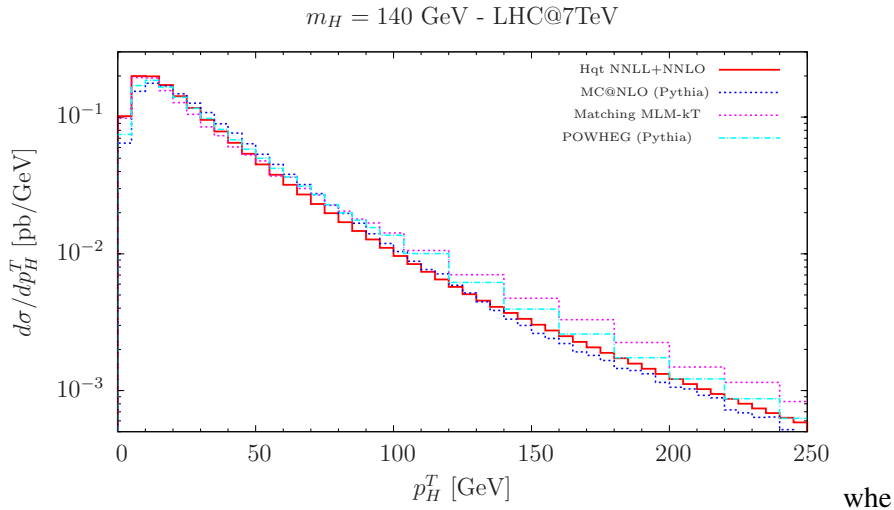
Fig. 12: Higgs p_H^T spectrum for a Higgs of $m_H = 140$ GeV as predicted by a series of improved predictions: NNLL+NNLO resummed (red solid), MC@NLO + Pythia (blue dashes), matrix-element + Pythia merged results (magenta dashes), POWHEG + Pythia (cyan dashes). All predictions display similar features, i.e. a peak between 10-20 GeV and a similar shape at high-p_H^T with differences that lie within their respective uncertainties (not shown).

- a full analytical resummation at NNLL;
- MC@NLO (w/ PYTHIA);
- ME+PS merging (MADGRAPH+PYTHIA);
- POWHEG (w/ PYTHIA).

We first stress (again) that this observable which is at NLO at high-p^T only in the Hqt predictions. The ME+PS approach is built to be LO for all observables, while MC@NLO and POWHEG predictions are based on the NLO calculation for the total cross section, the same performed in these notes. Notwidthstanding we see that given the expected uncertainties which are quite large above all at high-p^T the shapes are in substantial agreement both in the low and high-p^T ranges. In Fig. 13 the p^T distributions for the first and second jets are shown comparing the ME+PS prediction based on the HEFT and one with the full top-mass depedence and PYTHIA. Even in this case the agreeement between the various approaches is extremely good for a light Higgs. For a very heavy Higgs difference in the p_T distributions of the extra jets become visibile at quite a high p^T, a region not very relevant phenomenologically.

7 Conclusions

Progress in the field of QCD predictions for the LHC in the form of MC tools usable by both theorists and experimentalists has made tremendous progress in the last years. It is fair to say that we are now able (or close to be able in some specific very challenging cases) to compute automatically or semi-automatically any interesting cross section for Standard Model and Beyond processes at NLO accuracy and interface it with parton shower programs for event generation. In the LHC era the lowest acceptable accuracy for any serious phenomenological and experimental study is via an NLO event generator. LHC precision physics is now at NNLO in QCD and NLO in EW. Any physicist interested in making discoveries at the LHC needs to be familiar with the ideas, the physics and the reach of the current QCD simulation tools.

To this aim, we have considered $pp \to H + X$ as a case study. We have illustrated how accurate and useful predictions for cross sections and other observables can be obtained in QCD, starting from the calculation of Born amplitude (at one loop) and the corresponding hadronic cross section. We have
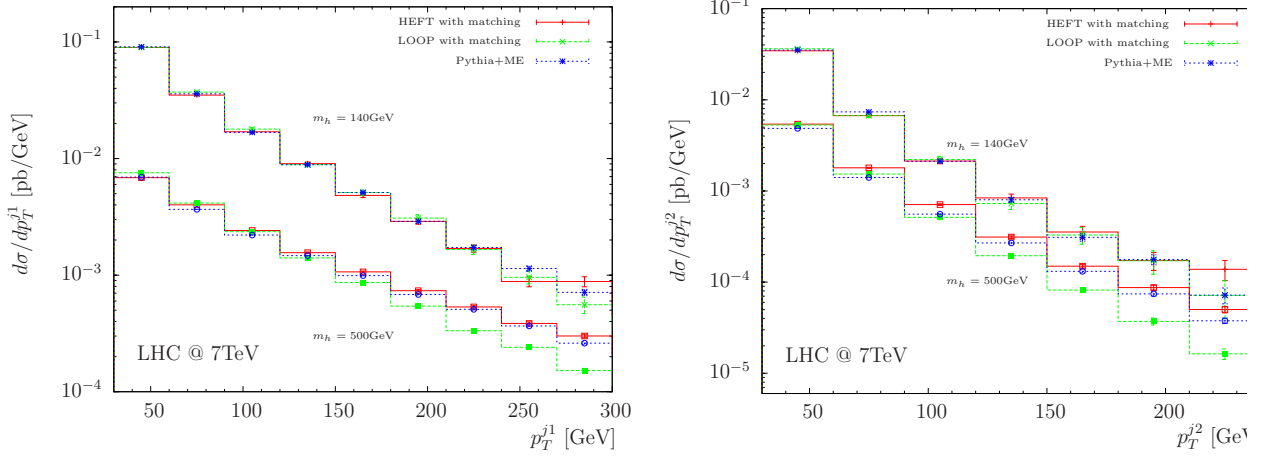
Fig. 13: Jet p_T distributions for associated jets in gluon fusion production of $m_H = 140\,\mathrm{GeV}$ and $m_H = 500\,\mathrm{GeV}$ Higgs bosons at 7 TeV LHC.

then considered Higgs production at NLO in the HEFT and discussed the limitations of fixed-order predictions. Finally, we have briefly discussed how fully exclusive predictions are obtained with modern tools, that allow to reach the accuracy of NLO predictions together with the full exclusivity of a parton shower approach.

Appendix

Splitting functions and collinear counterterms

We define the 4-dimensional splitting functions as in (4.94) of the ESW book:

$$P_{qq}(z) = C_F \, p_{qq}(z) = C_F \left[\frac{1 + z^2}{(1-z)_+} + \frac{3}{2}\delta(1-z) \right] \tag{64}$$

$$P_{qg}(z) = T_R \, p_{qg}(z) = T_R \left[z^2 + (1-z)^2 \right] \tag{65}$$

$$P_{gq}(z) = C_F \, p_{gq}(z) = C_F \left[\frac{1 + (1-z)^2}{z} \right] \tag{66}$$

$$P_{gg}(z) = C_A \, p_{gg}(z) = 2C_A \left[\frac{z}{(1-z)_+} + \frac{1-z}{z} + z(1-z) \right] + b_0 \, \delta(1-z), \tag{67}$$

where $b_0 = 11/6\,C_A - 2n_f T_F/3$. We also define the following quantities as the extension of the splitting functions in d-dimensions:

$$P_{ij}^{\mathrm{d}}(z) = P_{ij}(z) + \epsilon P_{ij}^{\epsilon}(z) \tag{68}$$

where

$$P_{qq}^{\epsilon}(z) = C_F \, p_{qq}^{\epsilon}(z) = -C_F(1-z) \tag{69}$$

$$P_{qg}^{\epsilon}(z) = T_R \, p_{qg}^{\epsilon}(z) = -T_R 2z(1-z) \tag{70}$$

$$P_{gq}^{\epsilon}(z) = C_F \, p_{gq}^{\epsilon}(z) = -C_F z \tag{71}$$

$$P_{gg}^{\epsilon}(z) = 0 \tag{72}$$

factorisation of the collinear divergences is performed through the addition of the following counterterm for each parton in the initial state:

$$\sigma_{\mathrm{c.t.}}^{\mathrm{CDR}} = \sigma_0^{\mathrm{CDR}} \; \frac{\alpha_S}{2\pi} \left[\left(\frac{\mu^2}{\mu_F^2} \right)^{\epsilon} \frac{c_\Gamma}{\epsilon} P_{ij}(z) \right] \tag{73}$$

where σ_0^{SCHEME} is the LO cross section and its value depends on the scheme (see the example for Drell-Yan)]. In CDR, when there is a collinear divergence, the cross section behaves as

$$\sigma_R^{\text{coll}} \sim -\frac{1}{\epsilon} P_{ij}^{\text{d}}(z) \sigma_0^{\text{CDR}} + \text{other terms} . \tag{74}$$

Adding the counterterm (73), leaves a finite part

$$\sigma_R^{\overline{\text{MS}}} \sim -P_{ij}^{\epsilon}(z) \left(\sigma_0^{\text{CDR}}|_{\epsilon \to 0} \right) + \text{other terms} . \tag{75}$$

References

[1] R. K. Ellis, W. J. Stirling, and B. Webber, "QCD and collider physics," *Camb. Monogr. Part. Phys. Nucl. Phys. Cosmol.*, **8** (1996) 1.

[2] M. L. Mangano, "Introduction to QCD," http://cdsweb.cern.ch/record/454171/files/open-2000-255.pdf, no. CERN-OPEN-2000-255, 1999.

[3] P. Nason, in Proceedings of the 1997 European School of High-Energy Physics, Menstrup, Denmark, 25 May–7 June 1997, edited by N. Ellis and M. Neubert, CERN-1998-003 (CERN, Geneva, 1998), pp. 94-149, https://doi.org/10.5170/CERN-1998-003.94.

[4] G. P. Salam, Perturbative QCD for the LHC, Proc. of the ICHEP2010, Paris, France, 22-28 July 2010 [PoS 120 (2011) 556, https://doi.org/10.22323/1.120.0556.

[5] H. Georgi, S. Glashow, M. Machacek, and D. V. Nanopoulos, "Higgs Bosons from Two Gluon Annihilation in Proton Proton Collisions," *Phys. Rev. Lett.* **40** (1978) 692.

[6] S. Dawson, "Radiative corrections to Higgs boson production," *Nucl. Phys.*, **B359** (1991) 283.

[7] A. Djouadi, M. Spira, and P. Zerwas, "Production of Higgs bosons in proton colliders: QCD corrections," *Phys. Lett.*, **B264** (1991) 440.

[8] D. Graudenz, M. Spira, and P. Zerwas, "QCD corrections to Higgs boson production at proton proton colliders," *Phys. Rev. Lett.*, **70** (1993) 1372.

[9] M. Spira, A. Djouadi, D. Graudenz, and P. Zerwas, "Higgs boson production at the LHC," *Nucl. Phys.*, **B453** (1995)17.

[10] R. V. Harlander and W. B. Kilgore, "Next-to-next-to-leading order Higgs production at hadron colliders," *Phys. Rev. Lett.*, **88** (2002) 201801.

[11] C. Anastasiou and K. Melnikov, "Higgs boson production at hadron colliders in NNLO QCD," *Nucl. Phys.*, **B646** (2002) 220.

[12] V. Ravindran, J. Smith, and W. L. van Neerven, "NNLO corrections to the total cross-section for Higgs boson production in hadron hadron collisions," *Nucl. Phys.*, **B665** (2003) 325.

[13] R. V. Harlander, H. Mantler, S. Marzani, and K. J. Ozeren, "Higgs production in gluon fusion at next-to-next-to- leading order QCD for finite top mass," *Eur. Phys. J.*, **C66** (2010) 359.

[14] A. Pak, M. Rogal, and M. Steinhauser, "Finite top quark mass effects in NNLO Higgs boson production at LHC," *JHEP*, **02** (2010) 025.

[15] R. V. Harlander, F. Hofmann, and H. Mantler, "Supersymmetric Higgs production in gluon fusion," *JHEP*, **02** (2011) 055.

[16] A. Pak, M. Rogal, and M. Steinhauser, "Production of scalar and pseudo-scalar Higgs bosons to next-to-next-to-leading order at hadron colliders," *JHEP*, **1109** (2011) 088. * Temporary entry *.

[17] M. R. Whalley, D. Bourilkov, and R. C. Group, "The Les Houches Accord PDFs (LHAPDF) and Lhaglue," 2005.

[18] S. Catani and M. Seymour, "A General algorithm for calculating jet cross-sections in NLO QCD," *Nucl. Phys.*, **B485** (1997) 291.

[19] S. Frixione, Z. Kunszt, and A. Signer, "Three jet cross-sections to next-to-leading order," *Nucl. Phys.*, **B467** (1996) 399.

[20] M. L. Mangano and S. J. Parke, "Multi-Parton Amplitudes in Gauge Theories," *Phys. Rept.*, **200** (1991) 301.

[21] L. J. Dixon, "Calculating scattering amplitudes efficiently," 1996.

[22] M. L. Mangano, M. Moretti, F. Piccinini, R. Pittau, and A. D. Polosa, "ALPGEN, a generator for hard multiparton processes in hadronic collisions," *JHEP*, **0307** (2003) 001.

[23] J. Alwall, M. Herquet, F. Maltoni, O. Mattelaer, and T. Stelzer, "MadGraph 5 : Going Beyond," *JHEP*, **1106** (2011) 128.

[24] S. Catani and M. Grazzini, "An NNLO subtraction formalism in hadron collisions and its application to Higgs boson production at the LHC," *Phys. Rev. Lett.*, **98** (2007) 222002.

[25] C. Anastasiou, L. J. Dixon, K. Melnikov, and F. Petriello, "High precision QCD at hadron colliders: Electroweak gauge boson rapidity distributions at NNLO," *Phys. Rev.*, **D69** (2004) 094008.

[26] P. Bolzoni, F. Maltoni, S.-O. Moch, and M. Zaro, "Vector boson fusion at NNLO in QCD: SM Higgs and beyond," *Phys.Rev.*, **D85** (2012) 035002.

[27] D. de Florian, G. Ferrera, M. Grazzini, and D. Tommasini, "Transverse-momentum resummation: Higgs boson production at the Tevatron and the LHC," *JHEP*, **11** (2011) 064.

[28] S. Dittmaier *et al.*, "Handbook of LHC Higgs Cross Sections: 1. Inclusive Observables," 2011. Long author list - awaiting processing.

[29] T. Sjostrand, S. Mrenna, and P. Z. Skands, "PYTHIA 6.4 Physics and Manual," *JHEP*, **0605** (2006) 026.

[30] T. Sjostrand, S. Mrenna, and P. Z. Skands, "A Brief Introduction to PYTHIA 8.1," *Comput.Phys.Commun.*, **178** (2008) 852.

[31] G. Corcella, I. Knowles, G. Marchesini, S. Moretti, K. Odagiri, *et al.*, "HERWIG 6: An Event generator for hadron emission reactions with interfering gluons (including supersymmetric processes)," *JHEP*, **0101** (2001) 010.

[32] M. Bahr, S. Gieseke, M. Gigg, D. Grellscheid, K. Hamilton, *et al.*, "Herwig++ Physics and Manual," *Eur.Phys.J.*, **C58** (2008) 639. 143 pages, program and additional information available from http://projects.hepforge.org/herwig.

[33] T. Gleisberg, S. Hoeche, F. Krauss, A. Schalicke, S. Schumann, *et al.*, "SHERPA 1. alpha: A Proof of concept version," *JHEP*, vol. 0402, p. 056, 2004.

[34] A. Buckley, J. Butterworth, S. Gieseke, D. Grellscheid, S. Hoche, *et al.*, "General-purpose event generators for LHC physics," *Phys.Rept.*, **504** (2011) 145.

[35] S. Catani, F. Krauss, R. Kuhn, and B. Webber, "QCD matrix elements + parton showers," *JHEP*, **0111** (2001) 063.

[36] F. Krauss, "Matrix elements and parton showers in hadronic interactions," *JHEP*, **0208** (2002) 015.

[37] L. Lonnblad, "Correcting the color dipole cascade model with fixed order matrix elements," *JHEP*, **0205** (2002) 046.

[38] S. Hoeche, F. Krauss, S. Schumann, and F. Siegert, "QCD matrix elements and truncated showers," *JHEP*, **0905** (2009) 053.

[39] K. Hamilton, P. Richardson, and J. Tully, "A Modified CKKW matrix element merging approach to angular-ordered parton showers," *JHEP*, **0911** (2009) 038.

[40] M. L. Mangano, M. Moretti, and R. Pittau, "Multijet matrix elements and shower evolution in hadronic collisions: $Wb\bar{b} + n$ jets as a case study," *Nucl.Phys.*, **B632** (2002) 343.

[41] J. Alwall, S. de Visscher, and F. Maltoni, "QCD radiation in the production of heavy colored particles at the LHC," *JHEP*, **0902** (2009) 017.

[42] J. Alwall, S. Hoche, F. Krauss, N. Lavesson, L. Lonnblad, *et al.*, "Comparative study of various algorithms for the merging of parton showers and matrix elements in hadronic collisions," *Eur.Phys.J.*, **C53** (2008) 473.

[43] S. Frixione and B. R. Webber, "Matching NLO QCD computations and parton shower simulations," *JHEP*, **0206** (2002) 029.

[44] P. Nason, "A New method for combining NLO QCD with shower Monte Carlo algorithms," *JHEP*, **0411** (2004) 040.

[45] S. Frixione, F. Stoeckli, P. Torrielli, B. R. Webber, and C. D. White, "The MCaNLO 4.0 Event Generator," 2010.

[46] R. Frederix, S. Frixione, V. Hirschi, F. Maltoni, R. Pittau, *et al.*, "Scalar and pseudoscalar Higgs production in association with a top-antitop pair," *Phys.Lett.*, **B701** (2011) 427.

[47] K. Hamilton, P. Richardson, and J. Tully, "A Positive-Weight Next-to-Leading Order Monte Carlo Simulation for Higgs Boson Production," *JHEP*, **0904** (2009) 116.

[48] S. Alioli, P. Nason, C. Oleari, and E. Re, "A general framework for implementing NLO calculations in shower Monte Carlo programs: the POWHEG BOX," *JHEP*, **1006** (2010) 043.

[49] S. Hoche, F. Krauss, M. Schonherr, and F. Siegert, "Automating the POWHEG method in Sherpa," *JHEP*, **1104** (2011) 024.

[50] C. Balazs, J. Huston, and I. Puljak, "Higgs production: A Comparison of parton showers and resummation," *Phys. Rev.*, **D63** (2001) 014021.

[51] G. Bozzi, S. Catani, D. de Florian, and M. Grazzini, "Transverse-momentum resummation and the spectrum of the Higgs boson at the LHC," *Nucl. Phys.*, **B737** (2006) 73.

[52] U. Langenegger, M. Spira, A. Starodumov, and P. Trueb, "SM and MSSM Higgs Boson Production: Spectra at large transverse Momentum," *JHEP*, **0606** (2006) 035.

[53] C. Anastasiou, S. Bucherer, and Z. Kunszt, "HPro: A NLO Monte-Carlo for Higgs production via gluon fusion with finite heavy quark masses," *JHEP*, **0910** (2009) 068.

[54] J. Alwall, Q. Li, and F. Maltoni, "Matched predictions for Higgs production via heavy-quark loops in the SM and beyond," *Phys. Rev.*, **D85** (2012) 014031.

[55] E. Bagnaschi, G. Degrassi, P. Slavich, and A. Vicini, "Higgs production via gluon fusion in the POWHEG approach in the SM and in the MSSM," *JHEP*, **02** (2012) 088.

Quarkonium physics: NRQCD factorization formula for $J/\psi \to e^+ e^-$

J.-H. Ee, U-R. Kim, J. Lee, and C. Yu*
Department of Physics, Korea University, Seoul, Korea

Abstract

In this lecture, we briefly review the nonrelativistic QCD (NRQCD) factorization approach to describe the quarkonium production and decay. In the NRQCD factorization formula, the long-distance nature of a heavy quarkonium is factorized into the NRQCD long-distance matrix elements (LDMEs) and a physical measurable is expressed as a linear combination of the LDMEs. If we apply the perturbation theory to enhance the theoretical accuracies in the short-distance contributions there is no way to avoid non-analytic Coulomb divergences in the static limit of the heavy quark and infrared divergences. A systematic procedure to isolate such long-distance contributions out of the correction terms in the short-distance coefficients is called matching. As a heuristic example of finding the NRQCD factorization formula for a specific process, we demonstrate the matching procedure of determining the short-distance coefficients involving the leptonic decay of the S-wave spin-triplet state.

Keywords

NRQCD factorization formula; short-distance coefficient; long-distance NRQCD matrix elements; matching.

1 Introduction

The heavy quarkonium is the bound system of a heavy quark (Q) and a heavy antiquark $(\bar{Q})$, where $Q = c$ or b. If $Q = c$ (b), it is called a charmonium (bottomonium). As we do for a hydrogen atom, we allocate the following quantum numbers for a quarkonium system: In order to describe the radial excitation we use the principal quantum number n. The orbital angular momentum quantum number L $(= 0, 1, 2, \cdots)$ is used to identify the relative motion between Q and $\bar{Q}$. The states with $L = 0, 1, 2$ are also called the S-, P-, D-wave states, respectively. The spin angular momentum quantum number S indicates whether the pair is in the spin-singlet $(S = 0)$ or in the spin-triplet $(S = 1)$ state. The spectroscopic notation $^{2S+1}L_J$ is used to represent a physical quarkonium state, where J is the total angular momentum quantum number. A physical quarkonium system is in a color singlet state. However, we can also think of a $Q\bar{Q}$ pair created or annihilated at short distances in a certain color combination. The notations $^{2S+1}L_J^{[1]}$ and $^{2S+1}L_J^{[8]}$ are used for the color-singlet and -octet states, respectively. A physical quarkonium system of $^{2S+1}L_J^{[1]}$ state is a simultaneous eigenstate of both the parity P and the charge conjugation parity C. If we consider the fact that the spin wave function for a $Q\bar{Q}$ pair is symmetric (antisymmetric) when $S = 0$ $(S = 1)$, then we find that the corresponding symmetry factor in the spin wave function for the exchange of Q and $\bar{Q}$ is $(-1)^{S+1}$. The orbital angular momentum wave function has the parity $(-1)^L$ and the intrinsic parities of Q and $\bar{Q}$ differ. Thus the parity of the $Q\bar{Q}$ bound state is $P = (-1)^{L+1}$. Because the charge conjugation is equivalent to the interchange of the positions and spins for the Q and $\bar{Q}$, $C = (-1)^{S+1}$ and $P = (-1)^{L+S}$. In Table 1 we list the quantum numbers of various quarkonia.

Among various quarkonia, the $^3S_1^{[1]}$ charmonium J/ψ of mass about 3.1 GeV was discovered first in 1974 [1, 2]. This state has a very long life time and, therefore, it has a very narrow width so that it

---

*Based on the lecture given at the 2016 Asia-Europe-Pacific School of HEP in Beijing.

Table 1: Quantum numbers of quarkonia with $n = 1$.

$^{2S+1}L_J^{[1]}$	charmonium	bottomonium	S	L	J^{PC}
$^1S_0^{[1]}$	η_c	η_b	0	0	0^{-+}
$^3S_1^{[1]}$	J/ψ	Υ	1	0	1^{--}
$^1P_1^{[1]}$	h_c	h_b	0	1	1^{+-}
$^3P_{J(=0,1,2)}^{[1]}$	χ_{cJ}	χ_{bJ}	1	1	J^{++}
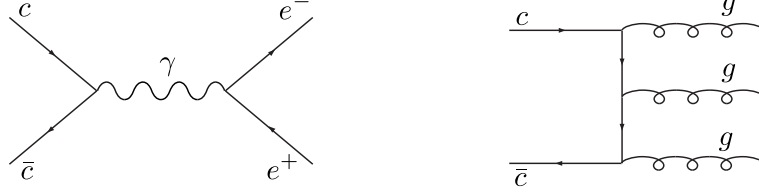
Fig. 1: The Feynman diagrams involving the decay modes $J/\psi \to e^+e^-$ (left) and $J/\psi \to$ light hadrons (right) at LO in α_s, respectively. There are 5 more diagrams for the light-hadronic decay that can be obtained by permutation of three gluons.

Fig. 2: The Feynman diagrams involving the decay modes η_c or $\chi_{c0} \to \gamma\gamma$ (left) and η_c or $\chi_{c0} \to$ light hadrons (right) at LO in α_s, respectively. There is another diagram that can be obtained by exchanging the two final-state particles for each diagram.

can be detected as a sharp resonance in the invariant mass distribution of the lepton pair in the decay mode $J/\psi \to e^+e^-$ or $\mu^+\mu^-$. The annihilation of J/ψ involves the annihilation of a $Q\bar{Q}$ pair because it cannot decay into two charmed mesons ($D\bar{D}$) whose invariant mass is greater than the J/ψ mass. At leading order (LO) in the strong coupling constant α_s the light-hadronic decay mode is dominated by the three-gluon final state of the color-singlet combination whose decay rate is of order α_s^3. This suppression of the hadronic decay mode of the J/ψ makes its width sharper than other quarkonium states such as η_c or χ_{c0} whose leading decay modes are into two gluons. This elementary interpretation is based on the conservation of the charge conjugation parity C as well as the parity P of QCD. Because a physical S-wave spin-triplet $Q\bar{Q}$ bound state has $J^{PC} = 1^{--}$, it may only decay into an odd number of gluons that make a color singlet combination. Thus the color-singlet combination of three gluons appears at LO in α_s so that the dominance of the hadronic decay mode is less severe for the S-wave spin-triplet state in comparison with the cases of the S-wave spin-singlet and the P-wave spin-triplet states whose charge conjugation parities are $+1$. Hence, the leading contributions to the $^1S_0^{[1]}$ or $^3P_J^{[1]}$ hadronic decay rates are color-singlet combination of two gluons that are of order α_s^2. Therefore, the narrow width of $^3S_1^{[1]}$ quarkonium in comparison with other states is well understood in QCD and allows clean signals. In Table 2 we list the total decay rates, branching fractions for the electromagnetic decay modes, and those for the light-hadronic modes for J/ψ, η_c, and χ_{c0}. In Figs. 1 and 2, we list Feynman diagrams for

Table 2: The total decay widths Γ_{tot}, the branching fractions Br_{EM} for the electromagnetic decay modes, and the branching fractions Br_{had} for the light-hadronic decay modes for J/ψ, η_c, and χ_{c0}.

	Γ_{tot}	Br_{EM}	Br_{had}
J/ψ	93 keV	$2 \times 6\%$	88%
η_c	32 MeV	1.6×10^{-4}	~ 1
χ_{c0}	11 MeV	2.2×10^{-4}	~ 1

the electromagnetic and light-hadronic decays of J/ψ and η_c (χ_{c0}), respectively, at LO in α_s.

An S-wave spin-triplet charmonium H is usually detected at colliders through the muon-antimuon or electron-positron pair final states. However, the original hadron H' that results in these final states is not unique. It can be the $^3S_1^{[1]}$ charmonium itself or other hadrons that decay into particles including a $^3S_1^{[1]}$ charmonium. The mother hadron H' is mostly another charmonium resonance or B mesons. If H' is a higher quarkonium resonance, then the main decay mechanism is through the strong or electromagnetic interaction. If H' is a b hadron, then its decay is governed by the weak interaction so that the vertex of $\ell^+\ell^-$ is secondary and it is largely separated from the primary vertex (collision point) at which b hadrons are created. The CDF Collaboration of the Fermilab Tevatron installed the Silicon Vertex Detector (SVX) [3] to achieve the asymptotic impact parameter resolutions of order 10 μm. The SVX enabled one to reconstruct b hadrons effectively so that one can easily separate the signals coming from b hadron decays and isolate the signals from the directly produced charmonium or higher charmonium resonances that we call *prompt* charmonium. Although the SVX is useful to separate the prompt charmonium signal from the charmonium coming from the decay of b hadrons, it is unable to distinguish the signals of the directly produced charmonium from those coming from the feeddowns of higher charmonium resonances. The prompt $\psi(2S)$ is the same as the *direct* $\psi(2S)$ because it does not have any feeddowns from higher resonances. In the case of J/ψ, the prompt signal contains the direct J/ψ, J/ψ coming from the feeddowns $\chi_{cJ} \to J/\psi + \gamma$ and $\psi(2S) \to J/\psi\pi\pi$. Here, the χ_{cJ} is either the direct χ_{cJ} or that coming from $\psi(2S) \to \chi_{cJ} + \gamma$.

The advent of the SVX sped up the progress of the phenomenological studies of prompt J/ψ and $\psi(2S)$. This has eliminated the non-prompt samples whose theoretical prediction has large uncertainties. The enormous surplus of these charmonia measured by the CDF Collaboration at the Fermilab Tevatron in comparison with the prediction based on the conventional phenomenological model so called the color-singlet model (CSM) was successfully explained in Ref. [4] by introduction of the color-octet mechanism [5] of the nonrelativistic QCD (NRQCD) factorization approach [6]. This success of explaining the production rate was followed by a puzzling contradiction that the measurements of the J/ψ polarization at the Tevatron and at the LHC are against the theoretical prediction that the prompt J/ψ produced with large transverse momentum p_T should be transversely polarized [7–13]. In 2014, this puzzle has indeed been resolved by considering the leading-power factorization [14].

In this lecture, we briefly review the NRQCD factorization approach to describe the production and decay of the heavy quarkonium. In Sec. 2 we briefly review the quarkonium theory by considering the basic nature of a quarkonium, an old phenomenological model CSM, the origin of the soft singularities that appear in the perturbative computation of a measurable involving a quarkonium. In the latter part of this section we review the NRQCD factorization approach that provides a systematic procedure to isolate such infrared-sensitive factors out of the short-distance coefficients in the factorization formula. In Sec. 3 we provide a demonstration of matching that determines the short-distance coefficients of the NRQCD factorization formula for a specific process by considering the leptonic decay of the S-wave spin-triplet state and we summarize in Sec. 4.

2 Quarkonium theory

In this section, we briefly review theories regarding heavy quarkonium production and decay. We first summarize the fundamental nature of heavy quarkonia. Next we introduce a phenomenological model so called the color-singlet model that had been resorted until mid 1990's. At the end of this section, we summarize basic ideas of the NRQCD factorization approach which is the most rigorous theoretical approach at present.

2.1 Basic nature of quarkonia

The heavy quarkonium H is a bound state of a heavy quark Q and an antiquark $\bar{Q}$ whose interaction is dominated by the strong interaction. Because the Q and $\bar{Q}$ are heavy, the speed of Q or $\bar{Q}$ in the meson rest frame is assumed to be much smaller than the speed of light. For example, the masses of the spin-triplet states J/ψ and $\psi(2S)$ are about 3.1 GeV and 3.7 GeV, respectively. In the case of bottomonia $\Upsilon(1S)$ and $\Upsilon(2S)$, they are about 9.5 GeV and 10 GeV, respectively. The mass difference between the $1S$ and $2S$ states are about $500-600$ MeV for both $c\bar{c}$ and $b\bar{b}$ states. This mass difference can be scaled by $\sim m_Q v_Q^2$ roughly based on the Virial theorem, where m_Q and v_Q are the mass and the speed of the Q in the meson rest frame, respectively. Thus one can guess that $v_c^2 \sim 0.3$ and $v_b^2 \sim 0.1$. There are typical scales that involve the strong interaction in a quarkonium: The heavy-quark mass $\sim m_Q$ is the hard scale that governs the creation or annihilation of H. The heavy-quark momentum $\sim m_Q v_Q$ in the meson rest frame is the scale that determines the typical size $\sim 1/(m_Q v_Q)$ of the bound state. The life time of the bound state $\sim 1/(m_Q v_Q^2)$ is scaled by the reciprocal of the binding energy $\sim m_Q v_Q^2$. If we can take the approximation that $v_Q \ll 1$, then these scales are well separated as $m_Q \gg m_Q v_Q \gg m_Q v_Q^2$ [6].

The complete production or decay process of a heavy quarkonium H includes all of these interactions over a wide range of scales simultaneously. The annihilation or creation of a $Q\bar{Q}$ pair involving a hard scale of order m_Q or higher can be treated perturbatively because $\alpha_s(m_Q)$ is assumed to be small. The interaction of Q and $\bar{Q}$ that makes the bound state is governed by the strong interaction of scale similar to or less than $m_Q v_Q$ or $m_Q v_Q^2$ are nonperturbative. One can make a guess that the perturbative factor and the nonperturbative factor are separable. The CSM assumes that the two factors are factorized as the product of the short-distance factor that is controlled by the hard scale and the long-distance factor that is responsible for the quarkonium wave function. The NRQCD factorization is a rigorous framework that factorizes the two factors in a systematic double power expansions in $\alpha_s(m_Q)$ and v_Q.

2.2 Color-singlet model

The CSM assumes that the short-distance factor and the long-distance factor are factorized. In addition, it allows only the color-singlet $Q\bar{Q}$ pair with the spectroscopic state identical to the physical quarkonium state in the short-distance contributions [15–27]. According to the CSM, the decay rates for $J/\psi \to e^+e^-$ and $\chi_{c0} \to$ light hadrons are factorized as

$$\Gamma(J/\psi \to e^+e^-) \quad = \quad \hat{\Gamma}\left[c\bar{c}(^3S_1^{[1]}) \to e^+e^-\right] \times |R(0)|^2, \tag{1a}$$

$$\Gamma(\chi_{c0} \to \text{hadrons}) \quad = \quad \hat{\Gamma}\left[c\bar{c}(^3P_0^{[1]}) \to gg\right] \times |R'(0)|^2, \tag{1b}$$

where $\hat{\Gamma}$'s are the corresponding short-distance factors that are assumed not to be sensitive to long-distance interactions. $R(0)$ and $R'(0)$ are radial wave function at the origin and the first-order derivative of the radial wave function at the origin, respectively. The J/ψ decay rate formula is an immediate application of the Van Royen-Weisskopf formula for a meson decay into a lepton pair [28]. However, in the CSM, the infrared (IR) insensitivity of the short-distance coefficient $\hat{\Gamma}$ is not guaranteed at higher orders in α_s. For example, as shown in Fig. 3, the short-distance coefficient for the light-hadronic decay of χ_{c0} contains the three-body decay mode $\chi_{c0} \to gq\bar{q}$, where q is a light quark, at the next-to-leading order (NLO) in α_s. In the end point limit of the phase space that the q and $\bar{q}$ are back to back, the gluon
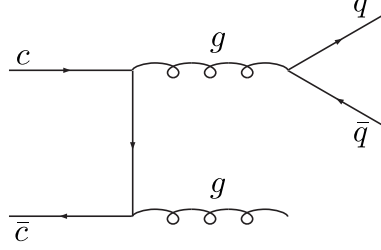
Fig. 3: One of the Feynman diagrams involving $\chi_{c0} \to$ light hadrons at NLO in α_s.

becomes soft. The IR divergence due to the attachment of a soft gluon to c and $\bar{c}$ does not cancel if one cannot ignore the relative momentum between c and $\bar{c}$. This remaining IR divergence of the short-distance coefficient at this order leads to the failure in factorization of the CSM [5]. Such a failure of factorization in the CSM appears also in the S-wave case from order v_Q^4 [29, 30] even at LO in α_s. The order-α_s correction to the short-distance process for $J/\psi \to e^+ e^-$ also brings in the IR sensitivity to all orders in v_Q as shown in Ref. [31].

2.3 Infrared divergence

The cancellation of the IR divergence when we attach a soft gluon to the $Q\bar{Q}$ pair is exact as long as the two momenta for the Q and $\bar{Q}$ are identical to each other. However, such cancellation does not hold once the two momenta are different. We demonstrate this phenomenon in a schematic way. Consider the amplitude for the production of a $Q\bar{Q}$ pair

$$i\mathcal{M}_0 = \bar{u}(p_1)\mathcal{A}v(p_2), \tag{2}$$

where $\mathcal{A}$ is the amputated amplitude that excludes the external lines for the $Q\bar{Q}$ pair, p_1 and p_2 are the momenta for the on-shell Q and $\bar{Q}$, respectively, with $p_1^2 = p_2^2 = m^2$. They can be expressed as linear combinations of the momentum $P = p_1 + p_2$ for the $Q\bar{Q}$ pair and half their relative momentum $q = (p_1 - p_2)/2$ as

$$p_1 = \frac{1}{2}P + q, \tag{3a}$$

$$p_2 = \frac{1}{2}P - q. \tag{3b}$$

Analogously one can apply a similar method to the annihilation decay process.

If we attach a gluon with momentum k to the external line of the heavy quark Q, then the amplitude becomes

$$
\begin{aligned}
i\mathcal{M}_1 &= g_s\mu^\epsilon \bar{u}(p_1)[-i\slashed{\epsilon}^*]\frac{i(\slashed{p}_1 + \slashed{k} + m)}{(p_1 + k)^2 - m^2}T^a\mathcal{A}v(p_2) \\
&= g_s\mu^\epsilon \bar{u}(p_1)\frac{\slashed{\epsilon}^*(\slashed{p}_1 + \slashed{k} + m)}{(p_1 + k)^2 - m^2}T^a\mathcal{A}v(p_2) \\
&= g_s\mu^\epsilon \bar{u}(p_1)\frac{2\epsilon^* \cdot (p_1 + k) - (\slashed{p}_1 + \slashed{k} - m)\slashed{\epsilon}^*}{2p_1 \cdot k}T^a\mathcal{A}v(p_2),
\end{aligned}
\tag{4}
$$

where ϵ^* and a are the polarization vector and color index of the gluon, T^a is the generator of the fundamental representation of color SU(N_c) with $N_c = 3$, $g_s = \sqrt{4\pi\alpha_s}$, μ is the renormalization scale, and we use dimensional regularization in $d = 4 - 2\epsilon$ space-time dimensions. By making use of the equation of motion for the external quark,

$$\bar{u}(p_1)(\slashed{p}_1 - m) = 0, \tag{5}$$

and the transverse condition for the external gluon

$$\epsilon^* \cdot k = 0, \tag{6}$$

we find that

$$i\mathcal{M}_1 = g_s \mu^\epsilon \bar{u}(p_1) \frac{2\epsilon^* \cdot p_1 - \slashed{k}\slashed{\epsilon}^*}{2p_1 \cdot k} T^a \mathcal{A} v(p_2). \tag{7}$$

Taking the leading contribution as $k \to 0$ to collect the IR sensitive part, we find that

$$i\mathcal{M}_1^{\mathrm{IR}} = g_s \mu^\epsilon \frac{p_1 \cdot \epsilon^*}{p_1 \cdot k} \bar{u}(p_1) T^a \Gamma v(p_2). \tag{8}$$

If we attach a gluon with momentum k to the external line of the heavy antiquark $\bar{Q}$, then

$$
\begin{aligned}
i\mathcal{M}_2 &= \bar{u}(p_1) \mathcal{A} T^a \frac{i(-\slashed{p}_2 - \slashed{k} + m)}{(-p_2 - k)^2 - m^2} [-i\slashed{\epsilon}^*] v(p_2) \\
&= g_s \mu^\epsilon \bar{u}(p_1) \mathcal{A} T^a \frac{\slashed{\epsilon}^*(-\slashed{p}_2 - \slashed{k} + m)}{(p_2 + k)^2 - m^2} v(p_2) \\
&= g_s \mu^\epsilon \bar{u}(p_1) \mathcal{A} T^a \frac{-2\epsilon^* \cdot (p_2 + k) + (\slashed{p}_2 + \slashed{k} + m)\slashed{\epsilon}^*}{2p_2 \cdot k} v(p_2).
\end{aligned} \tag{9}
$$

By making use of the equation of motion for the external antiquark,

$$(\slashed{p}_2 + m)v(p_2) = 0, \tag{10}$$

and the transverse condition

$$\epsilon^* \cdot k = 0, \tag{11}$$

we find that

$$i\mathcal{M}_2 = g_s \mu^\epsilon \bar{u}(p_1) \mathcal{A} T^a \frac{-2\epsilon^* \cdot (p_2 + k) + \slashed{k}\slashed{\epsilon}^*}{2p_2 \cdot k} v(p_2). \tag{12}$$

Taking the leading contribution as $k \to 0$ to collect the IR sensitive part, we find that

$$i\mathcal{M}_2 = -g_s \mu^\epsilon \frac{p_2 \cdot \epsilon^*}{p_2 \cdot k} \bar{u}(p_1) \mathcal{A} T^a v(p_2). \tag{13}$$

In summary, the approximation for the final-state quark and antiquark amplitude emitting a soft gluon with momentum k and the polarization vector ϵ^* can be expressed as

$$i(\mathcal{M}_1 + \mathcal{M}_2) = i\mathcal{M}_0|_{\mathcal{A} \to \mathcal{A}'}, \tag{14}$$

where

$$\mathcal{A}' = g_s \mu^\epsilon \left[T^a \frac{p_1 \cdot \epsilon^*}{p_1 \cdot k} \mathcal{A} - \mathcal{A} T^a \frac{p_2 \cdot \epsilon^*}{p_2 \cdot k} \right]. \tag{15}$$

We consider the simplest case like the amputated amplitude for $\gamma^* \to Q\bar{Q}$ that is free of color structure. In such a case, the soft-gluon attachment leads to the replacement $\mathcal{A} \to \mathcal{A}' = C_{\mathrm{soft}} \mathcal{A}$, where

$$
\begin{aligned}
C_{\mathrm{soft}} &= g_s \mu^\epsilon T^a \left[\frac{p_1 \cdot \epsilon^*}{p_1 \cdot k} - \frac{p_2 \cdot \epsilon^*}{p_2 \cdot k} \right] \\
&= g_s \mu^\epsilon T^a \left[\frac{(\frac{1}{2}P + q) \cdot \epsilon^*}{(\frac{1}{2}P + q) \cdot k} - \frac{(\frac{1}{2}P - q) \cdot \epsilon^*}{(\frac{1}{2}P - q) \cdot k} \right].
\end{aligned} \tag{16}
$$

It is manifest that the factor C_{soft} vanishes in the limit $q \to 0$. Thus the soft-gluon attachment is free of IR divergence as long as we consider the S-wave case with vanishing relative momentum $q = 0$. In

case of the P-wave contribution, the cancellation does not hold and the attachment of a soft gluon leads to the IR divergence. Even in the S-wave case, the relativistic correction of order v_Q^2 at the amplitude level brings in the IR divergence. Therefore, in the cross section or the decay rate, the S-wave process acquires the IR divergence from relative order v_Q^4 or higher. Note that the soft gluon does not change the spin state of the $Q\bar{Q}$ pair while it carries the orbital angular momentum resulting in the transition with $\Delta L = \pm 1$. Because the gluon carries color, the color state of the $Q\bar{Q}$ state changes. This is a chromoelectric dipole transition. As a result, the perturbative corrections to the short-distance coefficient for the amplitude of the color-singlet $Q\bar{Q}$ pair acquires the sensitivity to the long-distance contribution. Without introducing a systematic separation of this long-distance contribution of QCD corrections, the factorization is not achieved in the CSM.

2.4 NRQCD factorization approach

We have observed that the perturbative QCD correction to the short-distance coefficient involving the annihilation decay or production of a color-singlet $Q\bar{Q}$ pair with the spectroscopic state $^{2S+1}L_J^{[1]}$ introduces IR sensitive contributions if one does not neglect v_Q. The divergent contribution involves the $Q\bar{Q}$ pair with the spectroscopic state $^{2S+1}L'^{[8]}_{J'}$, where $L' - L = \pm 1$ and S is invariant. Actually this contribution can be understood as the QCD correction to the state $^{2S+1}L'^{[8]}_{J'}$ through the long-distance QCD interactions. Based on this, the Fock-state expansion can be made to express a physical quarkonium state such as χ_{c0} as $|\chi_{c0}\rangle = |c\bar{c}(^3P_0^{[1]})\rangle + |c\bar{c}(^3S_1^{[8]}) + g_{\text{soft}}\rangle + \cdots$, while the CSM only allows $|\chi_{c0}\rangle = |c\bar{c}(^3P_0^{[1]})\rangle$. The higher-order Fock state components are scaled with powers of v_Q that involves the strength of the corresponding long-distance interactions. The NRQCD factorization approach is a systematic theoretical formalism to treat these long-distance transition of a $Q\bar{Q}$ state to another as a power series of v_Q that are assumed to be small like $v_c^2 \sim 0.3$ and $v_b^2 \sim 0.1$. By making use of this formalism, the separation of the long-distance contribution out of the perturbative corrections to the short-distance coefficient is carried out. If such a separation is proved to be valid to all orders in α_s, then we call it the factorization theorem. A rigorous proof of the factorization theorem has been made for the electromagnetic annihilation decay and the annihilation decay into light hadrons [6] as a generalization of the work on the P-wave quarkonium decay [5]. The rigorousness of the proof is similar to that for the Drell-Yan process [32]. Since the introduction of the factorization conjecture for the inclusive quarkonium production in Ref. [6], a bunch of phenomenological studies and the corresponding experimental verifications have been carried out. We refer the readers to a recent review paper [33] for more details. The rigorous construction of the factorization theorem for the inclusive quarkonium production is still under way. Such efforts can be found, for example, in Refs. [34–37].

2.4.1 NRQCD Lagrangian

In order to describe the long-distance QCD interactions of the $Q\bar{Q}$ pair, it is convenient to reformulate the full QCD in terms of an effective theory called the NRQCD. The NRQCD Lagrangian is therefore equivalent to the full QCD except that in NRQCD the annihilation and/or decay of the $Q\bar{Q}$ pair is forbidden because they are of the scale above the ultraviolet (UV) cutoff $\sim m_Q$ of this effective theory. Thus the full QCD Lagrangian can be expressed as the sum of the Lagrangian $\mathcal{L}_{\text{light}}$ for the light degrees of freedom and that ($\mathcal{L}_{\text{heavy}}$) for the heavy quark as

$$\mathcal{L}_{\text{QCD}} = \mathcal{L}_{\text{light}} + \mathcal{L}_{\text{heavy}} + \delta\mathcal{L}. \tag{17}$$

$\mathcal{L}_{\text{light}}$ is identical to that for the full QCD as

$$\mathcal{L}_{\text{light}} = -\frac{1}{2}\text{tr}\, G_{\mu\nu}G^{\mu\nu} + \sum_q \bar{\Psi}_q(i\slashed{D} - m_q)\Psi_q, \tag{18}$$

where $G_{\mu\nu} = G_a^{\mu\nu}T^a$ and $G_a^{\mu\nu}$ is the field strength tensor of the gluon with color index a, Ψ_q is the Dirac spinor field for the light quark q, m_q is the mass of the light quark q, $D^\mu = (D_t, -\mathbf{D}) = \partial^\mu + ig_s A^\mu$ is the gauge-covariant derivative, and $A^\mu = (\phi, \mathbf{A}) = A_a^\mu T^a$ is the SU(3) color matrix valued gauge field. $\mathcal{L}_{\text{heavy}}$ is the contribution to the heavy quark and antiquark at LO in v_Q:

$$\mathcal{L}_{\text{heavy}} = \psi^\dagger \left(iD_t + \frac{\mathbf{D}^2}{2m_Q} \right) \psi + \chi^\dagger \left(iD_t - \frac{\mathbf{D}^2}{2m_Q} \right) \chi, \tag{19}$$

where ψ (χ) is the Pauli spinor field that annihilates (creates) a heavy quark (antiquark). The leading contribution $\mathcal{L}_{\text{heavy}}$ and the relativistic corrections $\delta\mathcal{L}_{\text{bilinear}}$ can be obtained by block-diagonalizing the full QCD Lagrangian for the heavy quark by making use of the Foldy-Wouthuysen-Tani transformation [38] except that we have subtracted the mass terms. Explicit expressions for the bilinear contributions can be found in Eq. (25) of Ref. [5]. The remaining contribution $\delta\mathcal{L}$ is expressed as

$$\delta\mathcal{L} = \delta\mathcal{L}_{\text{bilinear}} + \delta\mathcal{L}_{\text{four-fermion}}. \tag{20}$$

Here, $\delta\mathcal{L}_{\text{bilinear}}$ is bilinear in either the quark field or the antiquark field that can be read off from the block-diagonalized expression of the full-QCD Lagrangian for the heavy quark. A convenient set of Feynman rules for the NRQCD perturbation theory involving the bilinear contribution can be found in Table I of Ref. [39]. The annihilation decay of a $Q\bar{Q}$ pair cannot be reproduced in terms of $\mathcal{L}_{\text{heavy}}$ and $\delta\mathcal{L}_{\text{bilinear}}$. Such contribution can only be reproduced by the four-fermion terms,

$$\delta\mathcal{L}_{\text{four-fermion}} = \sum_n \frac{f_n(\Lambda)}{m_Q^{d_n-4}} \mathcal{O}_n(\Lambda), \tag{21}$$

where $f_n(\Lambda)$ is the short-distance coefficient that is insensitive to the long-distance interactions, $\mathcal{O}_n(\Lambda)$ is a higher dimensional operator, and d_n is the dimension of the operator $\mathcal{O}_n(\Lambda)$. Because the scale involving the creation or annihilation of a $Q\bar{Q}$ pair is above the UV cutoff Λ, such a relativistic effects can only be reproduced by adding four-fermion operators like $\psi^\dagger \chi \chi^\dagger \psi$. In the following section, we list definitions of four-quark operators and summarize a way to determine the short-distance coefficient by matching NRQCD Lagrangian on to the full QCD counterpart.

2.4.2 NRQCD operators

We list frequently used four-fermion NRQCD operators $\mathcal{O}_n(\Lambda)$ that appear in $\delta\mathcal{L}_{\text{four-fermion}}$. The dimension-6 operators of $\mathcal{O}_n(\Lambda)$ that involve light-hadronic decays are given by

$$\mathcal{O}(^1S_0^{[1]}) = \psi^\dagger \chi \chi^\dagger \psi, \tag{22a}$$

$$\mathcal{O}(^3S_1^{[1]}) = \psi^\dagger \boldsymbol{\sigma} \chi \cdot \chi^\dagger \boldsymbol{\sigma} \psi, \tag{22b}$$

$$\mathcal{O}(^1S_0^{[8]}) = \psi^\dagger T^a \chi \chi^\dagger T^a \psi, \tag{22c}$$

$$\mathcal{O}(^3S_1^{[8]}) = \psi^\dagger \boldsymbol{\sigma} T^a \chi \cdot \chi^\dagger \boldsymbol{\sigma} T^a \psi. \tag{22d}$$

The color-singlet dimension-8 operators that involve light-hadronic decays are given by

$$\mathcal{O}(^1P_1^{[1]}) = \psi^\dagger \left(-\frac{i}{2}\overleftrightarrow{\mathbf{D}} \right) \chi \cdot \chi^\dagger \left(-\frac{i}{2}\overleftrightarrow{\mathbf{D}} \right) \psi, \tag{23a}$$

$$\mathcal{O}(^3P_0^{[1]}) = \psi^\dagger \left(-\frac{i}{2}\overleftrightarrow{\mathbf{D}} \cdot \boldsymbol{\sigma} \right) \chi \chi^\dagger \left(-\frac{i}{2}\overleftrightarrow{\mathbf{D}} \cdot \boldsymbol{\sigma} \right) \psi, \tag{23b}$$

$$\mathcal{O}(^3P_1^{[1]}) = \psi^\dagger \left(-\frac{i}{2}\overleftrightarrow{\mathbf{D}} \times \boldsymbol{\sigma} \right) \chi \cdot \chi^\dagger \left(-\frac{i}{2}\overleftrightarrow{\mathbf{D}} \times \boldsymbol{\sigma} \right) \psi, \tag{23c}$$

$$\mathcal{O}(^3P_2^{[1]}) = \psi^\dagger \left(-\frac{i}{2}\overleftrightarrow{\mathbf{D}}^{(i}\sigma^{j)} \right) \chi \chi^\dagger \left(-\frac{i}{2}\overleftrightarrow{\mathbf{D}}^{(i}\sigma^{j)} \right) \psi, \tag{23d}$$

$$\mathcal{O}_2(^1S_0^{[1]}) = \frac{1}{2}\left[\psi^\dagger\chi\cdot\chi^\dagger\left(-\frac{i}{2}\overleftrightarrow{\boldsymbol{D}}\right)^2\psi + \text{h.c.}\right], \tag{23e}$$

$$\mathcal{O}_2(^3S_1^{[1]}) = \frac{1}{2}\left[\psi^\dagger\boldsymbol{\sigma}\chi\cdot\chi^\dagger\boldsymbol{\sigma}\left(-\frac{i}{2}\overleftrightarrow{\boldsymbol{D}}\right)^2\psi + \text{h.c.}\right], \tag{23f}$$

$$\mathcal{O}_2(^3S_1^{[1]},{}^3D_1^{[1]}) = \frac{1}{2}\left[\psi^\dagger\chi\chi^\dagger\left(-\frac{i}{2}\right)^2\overleftrightarrow{D}{}^{(i}\overleftrightarrow{D}{}^{j)}\psi + \text{h.c.}\right], \tag{23g}$$

where $\mathcal{O}_2(^{2S+1}L_J^{[1]})$ represents the relativistic corrections of relative order v_Q^2 to the LO operator $\mathcal{O}(^{2S+1}L_J^{[1]})$, and $A^{(i}B^{j)} = \frac{1}{2}\left(A^iB^j + A^jB^i\right) - \frac{1}{3}\delta^{ij}A^kB^k$ is the traceless symmetric component of the Cartesian tensor A^iB^j. The corresponding color-octet operators can be obtained in a similar manner as those for the dimension-6 case that are listed in Eq. (22).

The four-quark operators involving the electromagnetic annihilation decay of a $Q\bar{Q}$ pair is very similar to those for the light-hadronic decay except that the virtual state is the QCD vacuum. This replacement can be achieved by inserting the projection operator $|0\rangle\langle0|$ that projects out the QCD vacuum. In addition, the color-octet operators are omitted because they have vanishing contribution to the vacuum-to-quarkonium matrix element. For example, the dimension-6 operators for electromagnetic annihilation decay of a $Q\bar{Q}$ pair are given by

$$\mathcal{O}^{\text{EM}}(^1S_0^{[1]}) = \psi^\dagger\chi|0\rangle\langle0|\chi^\dagger\psi, \tag{24a}$$

$$\mathcal{O}^{\text{EM}}(^3S_1^{[1]}) = \psi^\dagger\boldsymbol{\sigma}\chi|0\rangle\cdot\langle0|\chi^\dagger\boldsymbol{\sigma}\psi. \tag{24b}$$

2.4.3 NRQCD factorization formula

By making use of the effective Lagrangian $\delta L_{\text{four-fermion}}$ and the optical theorem, one can evaluate the inclusive decay rate of H as [6]

$$\begin{aligned}\Gamma(H \to X) &= 2\text{Im}\langle H|\delta\mathcal{L}_{\text{four-fermion}}|H\rangle \\ &= \sum_n \frac{2\text{Im}f_n(\Lambda)}{M^{d_n-4}}\langle H|\mathcal{O}_n(\Lambda)|H\rangle,\end{aligned} \tag{25}$$

where $|H\rangle$ is an eigenstate of the NRQCD Hamiltonian with the standard nonrelativistic normalization $\langle H(\boldsymbol{P}')|H(\boldsymbol{P})\rangle = (2\pi)^3\delta^{(3)}(\boldsymbol{P}' - \boldsymbol{P})$. In Appendix A of Ref. [6], one can find a systematic way to read off the short-distance coefficients $f_n(\Lambda)$ and $f_n^{\text{EM}}(\Lambda)$ by evaluating the $Q\bar{Q} \to Q\bar{Q}$ scattering amplitude in full QCD, taking the imaginary part, and comparing this expression with the linear combination of the corresponding perturbative NRQCD matrix elements $\langle Q\bar{Q}|\mathcal{O}_n(\Lambda)|Q\bar{Q}\rangle$ and $\langle Q\bar{Q}|\mathcal{O}_n^{\text{EM}}(\Lambda)|Q\bar{Q}\rangle$, respectively. Because the NRQCD matrix elements for H and $Q\bar{Q}$ have a common structure in the short-distance limit, the corresponding short-distance coefficients must be equal. This step is called the perturbative matching. The NRQCD long-distance matrix element (LDME) $\langle H|\mathcal{O}_n(\Lambda)|H\rangle$ cannot be computed perturbatively. Instead, some of them can be computed on the lattice [40–42] or they must be determined phenomenologically against experimental data involving the LDME. The numerical accuracy of the NRQCD factorization formula can be improved by extending the perturbative corrections to the short-distance coefficients and by considering as many NRQCD LDMEs that are suppressed in powers of v_Q as possible. In practice, it is impossible to extend the series in v_Q to all orders because it brings in too many LDMEs in comparison with the number of independent measurables. There is no way but to terminate the series at a certain order as long as the terminated factorization formula has uncertainties within desirable accuracies. The velocity scaling rules of NRQCD [6,43], that are derived in the Coulomb gauge on which the NRQCD LDMEs are formulated, can be used to determine the relative importance of the NRQCD LDMEs.

2.4.4 Matching

The short-distance coefficients $f_n(\Lambda)$ in Eq. (25) are insensitive to the long-distance nature of the quarkonium state and can be computed perturbatively. In order to determine the coefficients for the light-hadronic decays, we can consider the full-QCD amplitude $\mathcal{A}(Q\bar{Q} \to Q\bar{Q})$ for the scattering process $Q\bar{Q} \to Q\bar{Q}$ whose intermediate state consists of only light degrees of freedom. This full-QCD expression can be expanded as a linear combination of perturbative NRQCD matrix elements $\langle Q\bar{Q}|\mathcal{O}_n(\Lambda)|Q\bar{Q}\rangle$ as

$$\mathcal{A}(Q\bar{Q} \to Q\bar{Q}) = \sum_n \frac{f_n(\Lambda)}{M^{d_n-4}}\langle Q\bar{Q}|\mathcal{O}_n(\Lambda)|Q\bar{Q}\rangle, \tag{26}$$

which is given in Ref. [6]. Thus the determination of $f_n(\Lambda)$ is straightforward by reading off the coefficient of $\langle Q\bar{Q}|\mathcal{O}_n(\Lambda)|Q\bar{Q}\rangle$ in this expansion. This process is called the matching. Substituting the coefficients $f_n(\Lambda)$ into the NRQCD factorization formula in Eq. (25), one can predict the light-hadronic decay rate as long as the nonperturbative NRQCD LDMEs $\langle H|\mathcal{O}_n(\Lambda)|H\rangle$ are known.

The determination of the short-distance coefficients for the NRQCD factorization formula for the electromagnetic decay is quite similar to that for the light-hadronic decay. However, in the electromagnetic decay, the intermediate state for the scattering amplitude $Q\bar{Q} \to Q\bar{Q}$ must not include any colored particles.

3   Application to $J/\psi \to e^+e^-$

While the coefficients at LO in α_s are intrinsically free of IR divergence, higher-order corrections acquire soft singularities. The NRQCD factorization approach provides a systematic procedure to isolate such a long-distance contribution. This long-distance contribution will be identified as the α_s corrections to the NRQCD LDMEs and eventually we can obtain the short-distance coefficients that are insensitive to the long-distance interactions. We provide only a schematic description and further details can be found in Refs. [31, 44–46]. In this section, we demonstrate how to carry out the matching procedure to determine the short-distance coefficients of the NRQCD factorization formula by considering the relativistic corrections to $J/\psi \to e^+e^-$ at NLO in α_s. The relativistic corrections are to be computed to all orders in v_c keeping the $^3S_1^{[1]}$ contribution only.

The NRQCD factorization formula for $J/\psi \to e^+e^-$ at LO in v_c and at order α_s is given in Ref. [6] that can be read off from the result in Ref. [47]:

$$\Gamma[J/\psi \to e^+e^-] = \frac{8\pi e_c^2\alpha^2}{3M_{J/\Psi}^2}\left(1 - 4C_F\frac{\alpha_s}{\pi}\right)\langle J/\psi|\mathcal{O}^{\text{EM}}(^3S_1^{[1]})|J/\psi\rangle, \tag{27}$$

where e_c is the fractional electric charge of the charm quark, α is the electromagnetic fine structure constant, $C_F = (N_c^2 - 1)/(2N_c) = 4/3$, and the J/ψ mass can be set $M_{J/\psi} = 2m_c$ at order v_c^0. The order-α_s^2 and -α_s^3 corrections are also available in Ref. [48] and [49], respectively. The perturbative matching introduced in the previous section involves the analysis of the scattering amplitude $Q\bar{Q} \to Q\bar{Q}$. In case of the electromagnetic decay that omits QCD states in the final state, it is convenient to carry out perturbative matching at the amplitude level.

In quite a few processes involving charmonium production and decay, the corresponding predictions at LO in α_s and at LO in v_c have poor accuracies in comparison with the empirical data. It is partly due to the fact that both α_s and v_c for a charmonium process are not sufficiently small. For example, the prediction of the cross section for the exclusive process $e^+e^- \to J/\psi + \eta_c$ at B factories is smaller than the empirical values [50] by about an order of magnitude at LO in both α_s and v_c [51, 52]. A reasonable agreement between theory and experiment for this process was reached only after including the order-α_s corrections and the relativistic corrections resummed to all orders in v_c [53–55]. As is stated in Refs. [45], the NRQCD LDMEs involving relativistic corrections has intrinsic power UV divergence

that must be subtracted in dimensional regularization, that is the most commonly used in phenomenology. This leads to large numerical uncertainties in determining the LDMEs even in the signs when we compute the LDMEs on the lattice which employs a hard cutoff regulator [45, 56]. The generalized Gremm-Kapustin relation [45, 57] can be used to resum relativistic corrections to a color-singlet contribution resulting in a significant improvement of the numerical accuracies in the theoretical predictions. We regularize the UV and IR singularities using dimensional regularization in $d = 4 - 2\epsilon$ space-time dimensions.

3.1   1-loop matching

The amplitude for $J/\psi \to e^+ e^-$ can be factorized into the leptonic current, which is free of colored particles, and the hadronic part $\mathcal{A}_H^\mu$ [31],

$$-iee_c\, i\mathcal{A}_H^\mu = \langle 0|\mathcal{J}_{\mathrm{EM}}^\mu|H\rangle, \tag{28}$$

where $-e$ is the electric charge, H is the spin-triplet S-wave charmonium (J/ψ), and $\mathcal{J}_{\mathrm{EM}}^\mu$ is the heavy-quark electromagnetic current

$$\mathcal{J}_{\mathrm{EM}}^\mu = (-iee_c)\bar\psi\gamma^\mu\psi. \tag{29}$$

The conservation of the electromagnetic current restricts that $i\mathcal{A}_H^0 = 0$ in the quarkonium rest frame. In that frame, the spatial component must be a linear combination of the NRQCD matrix elements as

$$i\mathcal{A}_H^i = \sqrt{2m_H}\sum_n c_n\langle 0|\mathcal{O}_n^i|H\rangle, \tag{30}$$

where c_n are short-distance coefficients, $\mathcal{O}_n^i$ are the NRQCD operators, and m_H is the quarkonium mass. The overall factor $\sqrt{2m_H}$ is introduced because the quarkonium state $|H\rangle$ on the right side is normalized nonrelativistically while the full expression is normalized relativistically. We can think of the corresponding amplitude for the free $Q\bar{Q}$ pair, where $Q = c$. The short-distance nature of the process for the $Q\bar{Q}$ pair must be identical to that of the H. Therefore, $Q\bar{Q}$ must be in a state $Q\bar{Q}(^3S_1^{[1]})$. Thus the two processes have a common set of short-distance coefficients c_n. Then the coefficients c_n can be determined from the following matching formula:

$$i\mathcal{A}_{Q\bar{Q}}^i = \sum_n c_n\langle 0|\mathcal{O}_n^i|Q\bar{Q}\rangle, \tag{31}$$

where $\mathcal{A}_{Q\bar{Q}}^i$ is the amplitude for the on-shell $Q\bar{Q}$ pair that has the same short-distance process as $\mathcal{A}_H^i$ and $|Q\bar{Q}\rangle$ is the on-shell $Q\bar{Q}$ pair state. At LO in α_s, the short-distance coefficients are free of UV and IR divergences. If we consider the perturbation of the amplitude corrected to order α_s, then the matching formula is modified as

$$i\mathcal{A}_{Q\bar{Q}}^{i(0)} = \sum_n c_n^{(0)}\langle 0|\mathcal{O}_n^i|Q\bar{Q}\rangle^{(0)}, \tag{32}$$

$$i\mathcal{A}_{Q\bar{Q}}^{i(0)} + i\mathcal{A}_{Q\bar{Q}}^{i(1)} = \sum_n (c_n^{(0)} + c_n^{(1)})\langle 0|\mathcal{O}_n^i|Q\bar{Q}\rangle^{(0)} + \sum_n c_n^{(0)}\langle 0|\mathcal{O}_n^i|Q\bar{Q}\rangle^{(1)}, \tag{33}$$

where the superscript (i) stands for the order in α_s. As the first step, we can read off the coefficients $c_n^{(0)}$ from the expression for $i\mathcal{A}_{Q\bar{Q}}^{i(0)}$. Note that the NRQCD LDME $\langle 0|\mathcal{O}_n^i|Q\bar{Q}\rangle^{(i)}$ can be computed perturbatively although the LDME $\langle 0|\mathcal{O}_n^i|H\rangle$ for a quarkonium state is nonperturbative. As the next step, we subtract Eq. (32) from Eq. (33).

$$i\mathcal{A}_{Q\bar{Q}}^{i(1)} = \sum_n c_n^{(1)}\langle 0|\mathcal{O}_n^i|Q\bar{Q}\rangle^{(0)} + \sum_n c_n^{(0)}\langle 0|\mathcal{O}_n^i|Q\bar{Q}\rangle^{(1)}. \tag{34}$$

The first term is the order-α_s correction to the short-distance coefficient multiplied by the NRQCD ME at LO. The second term is the LO short-distance coefficient multiplied by the NRQCD ME at NLO. The IR divergent contribution of the short-distance coefficient, for example in the CSM, at NLO in α_s is to be identified as the second term in this expression. In this manner, the separation of long-distance contribution from the short-distance factor is being carried out order by order systematically.

In order to find the relativistic corrections, it is convenient to define the following perturbative NRQCD LDMEs for the $Q\bar{Q}$ pair:

$$
\begin{aligned}
\langle 0|\mathcal{O}_{1n}^i|Q\bar{Q}\rangle^{(0)} &= \langle 0|\chi^\dagger \left(-\frac{i}{2}\overleftrightarrow{\nabla}\right)^{2n}\sigma^i\psi|Q\bar{Q}\rangle^{(0)} \\
&= \boldsymbol{q}^{2n}\eta^\dagger\sigma^i\xi,
\end{aligned}
\tag{35a}
$$

$$
\begin{aligned}
\langle 0|\mathcal{O}_{2n}^i|Q\bar{Q}\rangle^{(0)} &= \langle 0|\chi^\dagger \left(-\frac{i}{2}\overleftrightarrow{\nabla}\right)^{2n-2}\left(-\frac{i}{2}\overleftrightarrow{\nabla}^i\right)\left(-\frac{i}{2}\overleftrightarrow{\nabla}\cdot\boldsymbol{\sigma}\right)\psi|Q\bar{Q}\rangle^{(0)} \\
&= \boldsymbol{q}^{2n-2}q^i\eta^\dagger\boldsymbol{q}\cdot\boldsymbol{\sigma}\xi,
\end{aligned}
\tag{35b}
$$

where ξ and η are Pauli spinors for the Q and $\bar{Q}$, respectively, $q = (p_1 - p_2)/2$, p_1 and p_2 are the momenta for Q and $\bar{Q}$, respectively, and $\boldsymbol{q}$ is the spatial component of q in the $Q\bar{Q}$ rest frame.

Then the one-loop matching formula reduces into

$$
i\mathcal{A}_{Q\bar{Q}}^{i(1)} = \sum_n c_{1n}^{(1)}\langle 0|\mathcal{O}_{1n}^i|Q\bar{Q}\rangle^{(0)} + \sum_n c_{2n}^{(1)}\langle 0|\mathcal{O}_{2n}^i|Q\bar{Q}\rangle^{(0)} + i\mathcal{A}_{Q\bar{Q}}^{\mathrm{NRQCD},i},
\tag{36}
$$

where $i\mathcal{A}_{Q\bar{Q}}^{\mathrm{NRQCD},i}$ represents the contribution that is a product of the short-distance coefficient at LO in α_s and the perturbative NRQCD MEs at NLO in α_s. For further information on the matching procedure, refer to Ref. [31].

3.2 computation of $\mathcal{A}_{Q\bar{Q}}^\mu$

To any order in α_s, the $Q\bar{Q}$ amplitude corresponding to the hadronic current $\mathcal{A}_H^\mu$ is of the form [31]

$$
i\mathcal{A}_{Q\bar{Q}}^\mu = \bar{v}(p_2)\left[Z_Q(1+\Lambda)\gamma^\mu + Bq^\mu\right]u(p_1),
\tag{37}
$$

where Z_Q is the heavy-quark wave function renormalization factor, Λ is the multiplicative factor for the vertex correction, and B is the multiplicative correction factor coming from the magnetic moment contribution that appears from order α_s corrections to the vertex. At LO in α_s, $Z_Q = 1$ and $\Lambda = 0$ and $B = 0$. The B term contributes to the S-wave spin-triplet contribution only from the corrections of order α_s with relativistic corrections. One can find the values for Z_Q and Λ at order α_s keeping only the leading contributions in powers in v_c, for example, in Refs. [31] and [58] and as

$$
Z_Q = 1 + \frac{\alpha_s C_F}{4\pi}\left(-\frac{1}{\epsilon_{\mathrm{UV}}} - \frac{2}{\epsilon_{\mathrm{IR}}} - 3\log\frac{4\pi\mu^2 e^{-\gamma_{\mathrm{E}}}}{m_c^2} - 4\right),
\tag{38a}
$$

$$
\Lambda = \frac{\alpha_s C_F}{4\pi}\left\{\frac{1}{\epsilon_{\mathrm{UV}}} + \frac{2}{\epsilon_{\mathrm{IR}}} + 3\log\frac{4\pi\mu^2 e^{-\gamma_{\mathrm{E}}}}{m_c^2} - 4 + \frac{1}{v_c}\left(\pi^2 - \frac{i\pi}{\epsilon_{\mathrm{IR}}} - i\pi\log\frac{\pi\mu^2 e^{-\gamma_{\mathrm{E}}}}{\boldsymbol{q}^2}\right)\right\},
\tag{38b}
$$

where μ is the dimensional regularization scale, γ_{E} is the Euler-Marscheroni constant, and the subscript of $1/\epsilon$ indicates the origin of divergence.

If we keep the leading contributions in v_c only at this order, then the contribution proportianal to q^μ in the current in Eq. (37) does not appear because the corresponding NRQCD ME is to be neglected. Then, it is sufficient to know

$$
Z_Q(1+\Lambda) = 1 + \frac{\alpha_s C_F}{4\pi}\left\{-8 + \frac{1}{v_c}\left[\pi^2 - \frac{i\pi}{\epsilon_{\mathrm{IR}}} - i\pi\log\frac{\pi\mu^2 e^{-\gamma_{\mathrm{E}}}}{\boldsymbol{q}^2}\right]\right\} + O(\alpha_s^2).
\tag{39}
$$

The result shows that the IR divergence survives while the UV divergence cancels. In addition, there is a non-analytic contribution as $v_c \to 0$ which is originated from the Coulomb interaction.

According to Ref. [31], the correction factors contributing to the S-wave spin-triplet state resummed to all orders in v_c are given by

$$
\begin{aligned}
Z_Q(1+\Lambda) &= 1 + \frac{\alpha_s C_F}{4\pi} \Bigg\{ 2[(1+\delta^2)L(\delta) - 1]\left(\frac{1}{\epsilon_{\text{IR}}} + \log\frac{4\pi\mu^2 e^{-\gamma_{\text{E}}}}{m_c^2}\right) + 6\delta^2 L(\delta) \\
&\quad -4(1+\delta^2)K(\delta) - 4 + (1+\delta^2)\left[\frac{\pi^2}{\delta} - \frac{i\pi}{\delta}\left(\frac{1}{\epsilon_{\text{IR}}} + \log\frac{\pi\mu^2 e^{-\gamma_{\text{E}}}}{\boldsymbol{q}^2} + \frac{3\delta^2}{1+\delta^2}\right)\right] \Bigg\},
\end{aligned}
\tag{40}
$$

$$
B = \frac{\alpha_s C_F}{4\pi}\frac{1-\delta^2}{m_c}\left[2L(\delta) - \frac{i\pi}{\delta}\right],
\tag{41}
$$

where

$$
\delta = \frac{v_c}{\sqrt{1+v_c^2}},
\tag{42a}
$$

$$
L(\delta) = \frac{1}{2\delta}\log\frac{1+\delta}{1-\delta},
\tag{42b}
$$

$$
K(\delta) = \frac{1}{4\delta}\left[\text{Li}_2\left(\frac{2\delta}{1+\delta}\right) - \text{Li}_2\left(-\frac{2\delta}{1+\delta}\right)\right],
\tag{42c}
$$

and Li_2 is the Spence function:

$$
\text{Li}_2(x) = \int_x^0 dt\,\frac{\log(1-t)}{t}.
\tag{42d}
$$

We use the nonrelativistic normalization for the spinors to find that

$$
\bar{v}(p_2)\gamma^i u(p_1) = \eta^\dagger \sigma^i \xi - \frac{q^i \eta^\dagger \boldsymbol{q}\cdot\boldsymbol{\sigma}\xi}{E(E+m_c)},
\tag{43a}
$$

$$
\bar{v}(p_2)q^i u(p_1) = -\frac{q^i \eta^\dagger \boldsymbol{q}\cdot\boldsymbol{\sigma}\xi}{E},
\tag{43b}
$$

where $E = \sqrt{m_c^2 + \boldsymbol{q}^2}$ that is the energy of the quark or antiquark in the $Q\bar{Q}$ rest frame. Substituting Eq. (43) into Eq. (37) and expanding in powers of v_c, we obtain

$$
\begin{aligned}
i\mathcal{A}_{Q\bar{Q}}^i &= \eta^\dagger \sigma^i \xi\Bigg[1 + \frac{\alpha_s C_F}{4\pi}\Bigg\{\frac{8v_c^2}{3}\left(\frac{1}{\epsilon_{\text{IR}}} + \log\frac{4\pi\mu^2 e^{-\gamma_{\text{E}}}}{m_c^2}\right) - 8 + \frac{2v_c^2}{9} \\
&\quad + \left(1+\frac{3v_c^2}{2}\right)\left[\frac{\pi^2}{v_c} - \frac{i\pi}{v_c}\left(\frac{1}{\epsilon_{\text{IR}}} + \log\frac{\pi\mu^2 e^{-\gamma_{\text{E}}}}{\boldsymbol{q}^2}\right)\right] - 3i\pi v_c\Bigg] \\
&\quad - \frac{q^i \eta^\dagger \boldsymbol{q}\cdot\boldsymbol{\sigma}\xi}{2m_c^2}\Bigg\{1 + \frac{\alpha_s C_F}{4\pi}\left[-4 + \frac{\pi^2}{v_c} - \frac{i\pi}{v_c}\left(\frac{1}{\epsilon_{\text{IR}}} + \log\frac{\pi\mu^2 e^{-\gamma_{\text{E}}}}{\boldsymbol{q}^2} + 2\right)\right]\Bigg\}\Bigg\} + O(v_c^3).
\end{aligned}
\tag{44}
$$

In comparison with the case in Eq. (39), there are a lot of terms that carries IR divergences and non-analytic Coulomb contributions. Note that the term proportional to $q^i \eta^\dagger \boldsymbol{q}\cdot\boldsymbol{\sigma}\xi$ contributes to both the S-wave spin-triplet state and D-wave state.

3.3 computation of $\mathcal{A}_{Q\bar{Q}}^{\text{NRQCD},\mu}$

Next we compute the amplitude $i\mathcal{A}_{Q\bar{Q}}^{\text{NRQCD},\mu}$ by making use of the NRQCD perturbation theory rather than the full QCD. Again, the amplitude must be of the form

$$
i\mathcal{A}_{Q\bar{Q}}^{\text{NRQCD},\mu} = \bar{v}(p_2)\left[Z_Q^{\text{NRQCD}}(1+\Lambda^{\text{NRQCD}})\gamma^\mu + B^{\text{NRQCD}}q^\mu\right]u(p_1).
\tag{45}
$$

If we follow the standard approach that is described in Ref. [5], it is practically impossible to carry out the NRQCD perturbation because there are infinite number of Feynman rules that involve the relativistic corrections to all orders in v_c. Fortunately, the authors of Ref. [31] have devised a very convenient way to achieve this goal without applying the infinite number of Feynman rules. Instead, they have introduced an equivalent way in which they evaluate the loop integral to remove the UV power divergent scaleless integrals. Here, we quote the results of Ref. [31]:

$$
\begin{aligned}
Z_Q^{\mathrm{NRQCD}}(1 + \Lambda^{\mathrm{NRQCD}}) &= 1 + \frac{\alpha_s C_F}{4\pi}\Bigg\{ 2[(1+\delta^2)L(\delta) - 1]\left(\frac{1}{\epsilon_{\mathrm{IR}}} - \frac{1}{\epsilon_{\mathrm{UV}}}\right) \\
&\quad + (1+\delta^2)\left[\frac{\pi^2}{\delta} - \frac{i\pi}{\delta}\left(\frac{1}{\epsilon_{\mathrm{IR}}} + \log\frac{\pi\mu^2 e^{-\gamma_{\mathrm{E}}}}{\boldsymbol{q}^2} + \frac{3\delta^2}{1+\delta^2}\right)\right]\Bigg\}, \quad (46\mathrm{a})
\end{aligned}
$$

$$
B^{\mathrm{NRQCD}} = \frac{\alpha_s C_F}{4\pi}\frac{1-\delta^2}{m_c}\left[-\frac{i\pi}{\delta}\right]. \quad (46\mathrm{b})
$$

If we apply Eqs. (43) and (46) into Eq. (45) and expand in powers of v_c, then we find that

$$
\begin{aligned}
i\mathcal{A}_{Q\bar{Q}}^{\mathrm{NRQCD},i} &= \eta^\dagger \sigma^i \xi\Bigg\{1 + \frac{\alpha_s C_F}{4\pi}\Bigg\{\frac{8v_c^2}{3}\left(\frac{1}{\epsilon_{\mathrm{IR}}} - \frac{1}{\epsilon_{\mathrm{UV}}}\right) + \\
&\quad \left(1 + \frac{3v_c^2}{2}\right)\left[\frac{\pi^2}{v_c} - \frac{i\pi}{v_c}\left(\frac{1}{\epsilon_{\mathrm{IR}}} + \log\frac{\pi\mu^2 e^{-\gamma_{\mathrm{E}}}}{\boldsymbol{q}^2}\right)\right] - 3i\pi v_c\Bigg\} \\
&\quad - \frac{q^i \eta^\dagger \boldsymbol{q}\cdot\boldsymbol{\sigma}\xi}{2m_c^2}\Bigg\{1 + \frac{\alpha_s C_F}{4\pi}\left[\frac{\pi^2}{v_c} - \frac{i\pi}{v_c}\left(\frac{1}{\epsilon_{\mathrm{IR}}} + \log\frac{\pi\mu^2 e^{-\gamma_{\mathrm{E}}}}{\boldsymbol{q}^2} + 2\right)\right]\Bigg\}\Bigg\} + O(v_c^3). \quad (47)
\end{aligned}
$$

3.4 determination of short-distance coefficients

Now we are ready to apply the matching condition in Eq. (36) to determine the short-distance coefficients. In this step, the IR divergent contribution and the non-analytic Coulomb divergent terms in Eqs. (44) and (47) cancel. The remaining UV divergence is to be removed by renormalizing the NRQCD operator in the modified minimal subtraction ($\overline{\mathrm{MS}}$) scheme as

$$
\chi^\dagger \sigma^i \psi = \left[\chi^\dagger \sigma^i \psi\right]_{\overline{\mathrm{MS}}} - \frac{(4\pi e^{-\gamma_{\mathrm{E}}})^\epsilon}{\epsilon_{\mathrm{UV}}}\frac{2\alpha_s C_F}{3\pi m_c^2}\chi^\dagger\left(-\frac{i}{2}\overset{\leftrightarrow}{\boldsymbol{\nabla}}\right)^2 \sigma^i \psi, \quad (48)
$$

where the subscript $\overline{\mathrm{MS}}$ indicates that the corresponding operator is renormalized in the $\overline{\mathrm{MS}}$ scheme. The resultant short-distance coefficients are free of long-distance sensitivities:

$$
c_{10}^{(1)} = \frac{\alpha_s C_F}{4\pi}(-8), \quad (49\mathrm{a})
$$

$$
c_{11}^{(1)} = \frac{\alpha_s C_F}{4\pi}\frac{1}{m_c^2}\left(\frac{2}{9} + \frac{8}{3}\log\frac{\mu_{\mathrm{NRQCD}}^2}{m_c^2}\right), \quad (49\mathrm{b})
$$

$$
c_{21}^{(1)} = \frac{\alpha_s C_F}{4\pi}\frac{2}{m_c^2}, \quad (49\mathrm{c})
$$

$$
(49\mathrm{d})
$$

where μ_{NRQCD} is the NRQCD factorization scale. At LO in α_s through order v_c^2, the short-distance coefficients are given by [29, 31, 59]

$$
c_{1n}^{(0)} = \delta_{n0}, \quad (50\mathrm{a})
$$

$$
c_{21}^{(0)} = -\frac{1}{2m_c^2}. \quad (50\mathrm{b})
$$

In order to apply this factorization formula for an S-wave spin-triplet state like J/ψ, we need to project out the S-wave contribution out of $i\mathcal{A}^i_{Q\bar{Q}}$. Thus we decompose the operator $\mathcal{O}^i_{2n}$ into

$$\mathcal{O}^i_{2n} = \frac{\mathcal{O}^i_{1n}}{d-1} + \mathcal{O}^i_{Dn}, \tag{51}$$

where the D-wave operator $\mathcal{O}^i_{Dn}$ is defined by

$$\mathcal{O}^i_{Dn} = \chi^\dagger \left(-\frac{i}{2}\overleftrightarrow{\nabla}\right)^{2n-2} \left[\left(-\frac{i}{2}\overleftrightarrow{\nabla}^i\right)\left(-\frac{i}{2}\overleftrightarrow{\nabla}\cdot\boldsymbol{\sigma}\right) - \frac{1}{d-1}\left(-\frac{i}{2}\overleftrightarrow{\nabla}\right)^2 \sigma^i\right]\psi. \tag{52}$$

The S-wave component in $i\mathcal{A}^i_{Q\bar{Q}}$ through order $\alpha_s v^2$ is

$$
\begin{aligned}
i\mathcal{A}^i_{Q\bar{Q}}\Big|_{S-\text{wave}} &= (c^{(0)}_{10} + c^{(1)}_{10})\langle 0|\mathcal{O}^i_{10}|Q\bar{Q}\rangle + \left(c^{(1)}_{11} + \frac{c^{(0)}_{21} + c^{(1)}_{21}}{d-1}\right)\langle 0|\mathcal{O}^i_{11}|Q\bar{Q}\rangle \\
&= \left(1 - \frac{8\alpha_s C_F}{4\pi}\right)\langle 0|\chi^\dagger \sigma^i \psi|Q\bar{Q}\rangle + \left[\frac{\alpha_s C_F}{4\pi}\left(\frac{2}{9} + \frac{8}{3}\log\frac{\mu^2_{\text{NRQCD}}}{m^2_c}\right)\right. \\
&\quad \left. + \frac{1}{d-1}\left(-\frac{1}{2} + \frac{2\alpha_s C_F}{4\pi}\right)\right] \frac{\langle 0|\chi^\dagger\left(-\frac{i}{2}\overleftrightarrow{\nabla}\right)^2 \sigma^i \psi|Q\bar{Q}\rangle}{m^2_c} \\
&= \left(1 - \frac{8\alpha_s C_F}{4\pi}\right)\langle 0|\chi^\dagger \sigma^i \psi|Q\bar{Q}\rangle \\
&\quad + \left[-\frac{1}{6} + \frac{\alpha_s C_F}{4\pi}\left(\frac{8}{9} + \frac{8}{3}\log\frac{\mu^2_{\text{NRQCD}}}{m^2_c}\right)\right] \frac{\langle 0|\chi^\dagger\left(-\frac{i}{2}\overleftrightarrow{\nabla}\right)^2 \sigma^i \psi|Q\bar{Q}\rangle}{m^2_c}. \tag{53}
\end{aligned}
$$

Our final results for the NRQCD factorization formula for the hadronic current that contributes to the leptonic decay of the S-wave spin-triplet state is

$$
\begin{aligned}
i\mathcal{A}^i_{H}\Big|_{S-\text{wave}} &= \sqrt{2m_H}\left(1 - \frac{8\alpha_s C_F}{4\pi}\right)\langle 0|\chi^\dagger \sigma^i \psi|H\rangle \\
&\quad + \sqrt{2m_H}\left[-\frac{1}{6} + \frac{\alpha_s C_F}{4\pi}\left(\frac{8}{9} + \frac{8}{3}\log\frac{\mu^2_{\text{NRQCD}}}{m^2_c}\right)\right] \frac{\langle 0|\chi^\dagger\left(-\frac{i}{2}\overleftrightarrow{\nabla}\right)^2 \sigma^i \psi|H\rangle}{m^2_c}. \tag{54}
\end{aligned}
$$

4 Summary

In this lecture, we have briefly reviewed the NRQCD factorization approach to describe the quarkonium production and decay. In the NRQCD factorization formula, the long-distance nature of heavy quarkonium is factorized into the NRQCD long-distance matrix elements (LDMEs) and a physical measurable is expressed as a linear combination of LDMEs. We have reviewed that the infrared sensitivity emerges if we apply the perturbation theory to enhance the theoretical accuracies in the short-distance contributions. This infrared divergence always appears as long as one does not neglect v_Q and there exists the non-analytic Coulomb singularities as $v_Q \to 0$. The color-singlet model breaks down because this theory is not equipped with a systematic procedure to cure this problem. In the NRQCD factorization approach, the corresponding short-distance factors are free of infrared sensitivities. In order to improve the numerical accuracies of such a measurable, one can compute corrections in powers of α_s and v_Q. One can truncate the series in v_Q by considering the velocity scaling rules that estimate the relative numerical importance of a long-distance process in powers of v_Q.

A systematic procedure to isolate such a long-distance interactions out of the correction terms in the short-distance coefficients is called matching. The matching procedure makes use of the fact that the short-distance coefficients for the NRQCD factorization formula for a quarkonium must be identical to those for the on-shell $Q\bar{Q}$ counterparts. While one cannot compute the NRQCD LDMEs for a quarkonium, one can compute the NRQCD LDMEs for an on-shell $Q\bar{Q}$ pair under the NRQCD perturbation theory. By comparing the $Q\bar{Q}$ amplitude computed in the full QCD with that computed in the NRQCD perturbation theory, one can isolate the infrared sensitive contributions and absorb them into the NRQCD LDMEs. The resultant short-distance factors are free of infrared divergences. A standard renormalization procedure can be applied to absorb the remaining UV divergences. As a heuristic example of finding the NRQCD factorization formula for a specific process, we have demonstrated the matching procedure of determining the short-distance coefficients involving the leptonic decay of the S-wave spin-triplet state.

In the latter part of the lecture, we have reviewed the NRQCD factorization approach for J/ψ hadroproduction and polarization. Due to the page limit of the proceedings contribution, we were not able to describe these subjects in the text. We refer the readers to Ref. [60] for details.

Acknowledgements

References

[1] J. J. Aubert *et al.* [E598 Collaboration], *Phys. Rev. Lett.* **33** (1974) 1404.

[2] J. E. Augustin *et al.* [SLAC-SP-017 Collaboration], *Phys. Rev. Lett.* **33**(1974) 1406 [Adv. Exp. Phys. **5**,141 (1976)].

[3] D. E. Amidei *et al.* [CDF Collaboration], *Nucl. Instrum. Meth. A* **350** (1994) 73.

[4] E. Braaten and S. Fleming, *Phys. Rev. Lett.* **74** (1995) 3327.

[5] G. T. Bodwin, E. Braaten and G. P. Lepage, *Phys. Rev. D* **46** (1992) R1914.

[6] G. T. Bodwin, E. Braaten and G. P. Lepage, *Phys. Rev. D* **51** (1995) 1125, Erratum: [Phys. Rev. D **55**, 5853 (1997)].

[7] E. Braaten, B. A. Kniehl and J. Lee, *Phys. Rev. D* **62** (2000) 094005.

[8] M. Butenschoen and B. A. Kniehl, *Phys. Rev. Lett.* **106** (2011) 022003.

[9] Y.-Q. Ma, K. Wang, and K.-T. Chao, *Phys. Rev. D* **84** (2011) 114001.

[10] Y.-Q. Ma, K. Wang, and K.-T. Chao, *Phys. Rev. Lett.* **106** (2011) 042002.

[11] B. Gong, L.-P. Wan, J.-X. Wang, and H.-F. Zhang, *Phys. Rev. Lett.* **110** (2013) 042002.

[12] K.-T. Chao, Y.-Q. Ma, H.-S. Shao, K. Wang, and Y.-J. Zhang, *Phys. Rev. Lett.* **108** (2012) 242004.

[13] M. Butenschoen and B. A. Kniehl, *Phys. Rev. Lett.* **108**(2012) 172002.

[14] G. T. Bodwin, H. S. Chung, U-R. Kim and J. Lee, *Phys. Rev. Lett.* **113** (2014) 022001.

[15] M. B. Einhorn and S. D. Ellis, *Phys. Rev. D* **12** (1975) 2007.

[16] S. D. Ellis, M. B. Einhorn, and C. Quigg, *Phys. Rev. Lett.* **36** (1976) 1263.

[17] C. E. Carlson and R. Suaya, *Phys. Rev. D* **14** (1976) 3115.

[18] J. H. Kühn, *Phys. Lett. B* **89** (1980) 385.

[19] T. A. DeGrand and D. Toussaint, *Phys. Lett. B* **89** (1980) 256.

[20] J. H. Kühn, S. Nussinov, and R. Rückl, *Z. Phys. C* **5** (1980) 117.

[21] M. B. Wise, *Phys. Lett. B* **89** (1980) 229.

[22] C. H. Chang, *Nucl. Phys. B* **172** (1980) 425.

[23] R. Baier and R. Rückl, *Nucl. Phys. B* **201** (1982) 1.

[24] R. Baier and R. Rückl, *Phys. Lett. B* **102**(1981) 364.

[25] R. Baier and R. Rückl, *Z. Phys. C* **19** (1983) 251.

[26] E. L. Berger and D. L. Jones, *Phys. Rev. D* **23** (1981) 1521.

[27] W. Y. Keung, Print-81-0161 (BNL) *Presented at Z0 Physics Workshop, Ithaca, N.Y., Feb 6-8, 1981.*

[28] R. Van Royen and V. F. Weisskopf, *Nuovo Cim. A* **50**(1967) 617, Erratum: [Nuovo Cim. A **51** (1967) 583].

[29] G. T. Bodwin and A. Petrelli, *Phys. Rev. D* **66** (2002) 094011, Erratum: [*Phys. Rev. D* **87** (2013) 039902].

[30] G. T. Bodwin, U-R. Kim and J. Lee, *JHEP* **1211** (2012) 020.

[31] G. T. Bodwin, H. S. Chung, J. Lee and C. Yu, *Phys. Rev. D* **79** (2009) 014007.

[32] G. T. Bodwin, *Phys. Rev. D* **31** (1985) 2616, Erratum: [*Phys. Rev. D* **34** (1986) 3932].

[33] G. T. Bodwin, E. Braaten, E. Eichten, S. L. Olsen, T. K. Pedlar and J. Russ, [arXiv:1307.7425 [hep-ph]].

[34] G. T. Bodwin, X. Garcia i Tormo and J. Lee, *Phys. Rev. Lett.* **101** (2008) 102002.

[35] G. T. Bodwin, X. Garcia i Tormo and J. Lee, *Phys. Rev. D* **81** (2010) 114005.

[36] G. T. Bodwin, X. Garcia i Tormo and J. Lee, *Phys. Rev. D* **81** (2010) 114014.

[37] G. T. Bodwin, H. S. Chung and J. Lee, *Phys. Rev. D* **90** (2014) 074028.

[38] L. L. Foldy and S. A. Wouthuysen, *Phys. Rev.* **78** (1950) 29; S. Tani, Prog. Theor. Phys. 6 (1951) 267.

[39] G. T. Bodwin and Y. Q. Chen, *Phys. Rev. D* **60** (1999) 054008.

[40] G. T. Bodwin, D. K. Sinclair and S. Kim, *Phys. Rev. Lett.* **77** (1996) 2376.

[41] G. T. Bodwin, D. K. Sinclair and S. Kim, *Phys. Rev. D* **65**(2002) 054504.

[42] G. T. Bodwin, J. Lee and D. K. Sinclair, *Phys. Rev. D* **72**(2005) 014009.

[43] G. P. Lepage, L. Magnea, C. Nakhleh, U. Magnea and K. Hornbostel, *Phys. Rev. D* **46**(1992) 4052.

[44] E. Braaten and Y. Q. Chen, *Phys. Rev. D* **54** (1996) 3216.

[45] G. T. Bodwin, D. Kang and J. Lee, *Phys. Rev. D* **74**(2006) 014014.

[46] G. T. Bodwin, H. S. Chung, D. Kang, J. Lee and C. Yu, *Phys. Rev. D* **77** (2008) 094017.

[47] R. Barbieri, R. Gatto, R. Kogerler and Z. Kunszt, *Phys. Lett.* **57B** (1975) 455; W. Celmaster, *Phys. Rev. D* **19** (1979) 1517.

[48] M. Beneke, A. Signer and V. A. Smirnov, *Phys. Rev. Lett.* **80** (1998) 2535.

[49] M. Beneke, Y. Kiyo, P. Marquard, A. Penin, J. Piclum, D. Seidel and M. Steinhauser, *Phys. Rev. Lett.* **112**(2014) 151801.

[50] K. Abe *et al.* [Belle Collaboration], *Phys. Rev. Lett.* **89** (2002) 142001.

[51] E. Braaten and J. Lee, *Phys. Rev. D* **67** (2003) 054007, Erratum: [*Phys. Rev. D* **72** (2005) 099901].

[52] K. Y. Liu, Z. G. He and K. T. Chao, *Phys. Lett. B* **557** (2003) 45.

[53] Z. G. He, Y. Fan and K. T. Chao, *Phys. Rev. D* **75** (2007) 074011.

[54] H. R. Dong, F. Feng and Y. Jia, *Phys. Rev. D* **85**(2012) 114018.

[55] G. T. Bodwin, J. Lee and C. Yu, *Phys. Rev. D* **77**(2008) 094018.

[56] G. T. Bodwin, D. Kang and J. Lee, *Phys. Rev. D* **74**(2006) 114028.

[57] M. Gremm and A. Kapustin, *Phys. Lett. B* **407**(1997) 323.

[58] E. Braaten and S. Fleming, *Phys. Rev. D* **52**(1995) 181.

[59] N. Brambilla, E. Mereghetti and A. Vairo, *JHEP* **0608** (2006) 039, Erratum: [JHEP **1104**(2011) 058].

[60] G. T. Bodwin, K. T. Chao, H. S. Chung, U-R. Kim, J. Lee and Y. Q. Ma, *Phys. Rev. D* **93** (2016) 034041.

Physics beyond the Standard Model (Mostly Supersymmetry)

S. K. Vempati

Centre for High Energy Physics, Indian Institute of Science, Bangalore, India.
Institut de Physique Théorique, CEA/Saclay, Gif-sur-Yvette, France

Abstract

We motivate various reasons for going beyond Standard Model. A detailed introduction of Supersymmetry is presented and the Supersymmetric Standard Model is introduced. The present status of supersymmetry is reviewed. A brief introduction to extra dimensions is presented. These are notes for lectures presented at AEPSHEP 2016, Beijing, China.

Keywords

Standard Model; Hierarchy Problem; Supersymmetric Standard Model; Phenomenology.

1 Prerequisites

In the course of these lectures, I will summarise the various reasons we need to extend the Standard Model of Particle Physics. This includes theoretical issues like hierarchy problem and phenomenological issues like dark matter, neutrino masses etc. Of all the models which have been proposed to be extensions of the Standard Model, we focus on supersymmetry. To discuss how supersymmetry solves the hierarchy problem, we will use a simple toy model of SUSY QED. In this model, we show that scalar masses are protected by supersymmetry. We then discuss the construction of the Minimal Supersymmetric Standard Model (MSSM) including soft supersymmetry breaking and electroweak symmetry breaking. The physical mass spectrum of the supersymmetric particles is presented.

In the second part, I discuss the phenomenological status of the MSSM, reviewing all the probes of supersymmetric particles in various direct and indirect experiments. I review the status in flavour violating rare decays, dark matter and of course the LHC results. I then discuss the implications of various results on various supersymmetry breaking models, like minimal Supergravity/Constrained Minimal Supersymmetric Standard Model (mSUGRA/cMSSM) and Gauge Mediation. I finally close with with a small discussion on extra-dimensional models. An is provided on the Standard Model, which is to make these lecture notes self-consistent. We will refer to some of the equations in the appendix while discussing MSSM.

A small list of textbooks and review articles on BSM physics is given below: (a) P. Ramond, Journeys Beyond Standard Model [1], (b)R. N. Mohapatra, Unification and Supersymmetry [2], (c) G. G. Ross, Grand Unified Theories [3], (d) T. T. Yanagida, Physics of Neutrino Physics and Applications to Astrophysics [4] (e) C. Csaki and F. Tanedo, Beyond Standard Model, [5], which contains a modern review of most of the ideas of extensions of physics beyond Standard Model. I also recommend a concise and a pedagogical review by (f) Gautam Bhattacharyya [6].

2 Why BSM ?

The Standard Model provides a coherent successful explanation of electroweak and strong interactions in terms of a (non-abelian) gauged quantum field theory. A lightning review of the structure of the Standard Model lagrangian is presented in Appendix A. The Standard Model has been well tested at various colliders starting from the CERN SPS where the W and Z bosons have been discovered. All the particles in the SM fermion spectrum have been discovered with the top quark discovered in 1995 and the tau neutrino in 2000. Precision measurements conducted at CERN LEP experiment confirm that the quantum

Table 1: A summary of some of the main reasons why we consider Standard Model to be incomplete.

Phenomenological	*Theoretical*
neutrino masses	hierarchy problem
dark matter	Grand Unification, Quantum Gravity
leptogenesis/baryogenesis	Strong CP

perturbative theory of the SM works very well and matches with the experiment. Measurements of the rare decays at various B-factories like Babar and Belle studied the flavour mixing and CP violation of the quark sector confirming the Cabibbo-Kobayashi-Masakawa (CKM) mixing of the Standard Model. In addition, other measurements include the renormalisation group running of α_s, qauntum chromodynamic (QCD) corrections to electroweak and strong production cross-sections, electric and magnetic dipole moments etc,. The crowning glory being the recent discovery of the Higgs boson which confirms the symmetry breaking mechanism of the Standard Model. While this success of the Standard Model is amazing, there are still several theoretical and phenomenological issues with the Standard Model which give us strong hints that the Standard Model is not the complete picture of the Nature. In the following we list some of the reasons why we need to go beyond the Standard Model.

2.1 Hierarchy Problem

Quantum field theories with a fundamental scalar have a technical problem called hierarchy problem. We will illustrate this problem by comparing two well known theories, namely, QED (Quantum Electrodynamics) and Yukawa theory [7, 8].

Consider QED, the lagrangian is given by

$$\mathcal{L}_{\text{QED}} = \bar{\Psi}\left(i\not{D} - m_e\right)\Psi - \frac{1}{4}F_{\mu\nu}F^{\mu\nu} \tag{1}$$

Here the electron mass is protected by a symmetry. In the limit $m_e \to 0$, there is an enhanced symmetry in the theory, which is the chiral symmetry of the electron. Using cut-off regularisation, we find at 1-loop the correction to the electron mass to be

$$\Delta m_e \sim e^2 m_e \ln \Lambda \tag{2}$$

This correction is proportional to electron mass itself, and thus, in the limit $m_e \to 0$, $\Delta m_e \to 0$. This holds true at all orders in perturbation theory, with the chiral symmetry protecting the left handed and right handed states separately. Theories such as these are called 'natural' theories based on G. 't Hooft principle of naturalness [9]. u In these theories, there is an enhanced symmetry in the limit when a parameter of the theory is set to zero.

Consider now a Yukawa theory with the following lagrangian:

$$\mathcal{L} = \frac{1}{2}(\partial^\mu\phi)(\partial_\mu\phi) - \frac{1}{2}m_S^2\phi^2 + \psi(i\not{\partial} - m_F)\psi + y\bar{\psi}\psi\phi \tag{3}$$

In this case, the mass of the scalar particle is not protected by any symmetry. In the limit $m_S \to 0$ there is no enhanced symmetry in the theory. Furthermore, the corrections to the scalar mass at 1-loop are not proportional to scalar mass itself. Thus even if we set the tree level scalar mass term to zero, it can be generated at higher order in perturbation theory. The correction from the fermion Yukawa coupling to the scalar mass at 1-loop (using dimensional regularisation) is given by

$$\delta m_S^2 = -y^2 m_F^2 \ln\left(\frac{m_F^2}{\mu^2}\right), \tag{4}$$

where μ is the parameter which sets the renormalisation scale. The fermion corrections to the scalar mass do not decouple in the limit $m_F \to \infty$ but instead drive mass to infinity. Theories such as these are technically unnatural theories. We now consider the case of the Standard Model.

In the Standard Model, the Higgs boson is introduced as a fundamental scale, making it a technically unnatural theory. The mass of the Higgs boson is not protected by any symmetry. In the limit $m_H^2 \to 0$ there is no enhanced symmetry in the Standard Model. There are several ways in which this unnaturalness manifests itself in the Standard Model which forms the crux of the *hierarchy problem*.

(a) Within a framework of Grand Unification

Consider a Grand Unified theory (GUT) which is spontaneously broken at the GUT scale. All the particles which are so far protected by the GUT symmetry, like the GUT gauge bosons are no longer protected by it. They attain masses at the GUT scale $\sim \mathcal{O}(g_{GUT}^2 M_{GUT}^2)$. However, the particles which are protected by the residual symmetry of the theory do not attain masses. The Standard Model gauge bosons remain massless as they are protected by the Standard Model gauge symmetry, which remains unbroken at the GUT scale. The SM fermions remain massless as they are protected by the chiral symmetries. The Higgs boson, however as we have discussed does not posses any symmetry which protects it's mass. Thus when the GUT symmetry is broken, one would expect that the SM Higgs boson also attains mass of the order of GUT scale [10]. To avoid this, one can fine tune the parameters of the GUT scalar potential so that the SM Higgs can be light ≈ 125 GeV. However, such a fine tuned mass may not be stable under radiative corrections as discussed earlier. This gets related to the doublet triplet splitting problem in GUT models like SU(5) [11].

(b) SM as an effective theory

Irrespective of the existence of a Grand Unified Theory at the high scale, the Standard Model is by no means a complete theory of the Universe. This is because gravitational interactions are not incorporated in the Standard Model. The gravitational interactions become important (quantum mechanically) at a scale around $M_{Pl} \sim 10^{19}$ GeV. The Standard Model can be viewed as an effective lagrangian of the full theory describing all the interactions including quantum gravity. Assuming Standard Model is valid all the way up to the Planck scale and remains perturbative, one can derive the one loop effective lagrangian of the SM [68]. Again since the Higgs mass is not protected by any symmetry, it gets corrected by the highest momentum cut-off of the effective theory which is the M_{Pl}.

$$
\begin{aligned}
\delta m_h^2 &\approx \frac{1}{16\pi^2}\Lambda^2 \approx \frac{1}{16\pi^2}M_{Pl}^2, \\
(m_h^2)_{phys} &\approx (m_h^2)_{bare} + \delta m_h^2
\end{aligned}
\tag{5}
$$

where δm_h^2 represents the radiative correction to the Higgs mass and $(m_h^2)_{bare}$ and $(m_h^2)_{phys}$ represent the bare and the physical Higgs masses. It would mean that to generate the Higgs mass of the right order $(m_h^2)_{phys} \sim (125 \text{ GeV})^2$, one needs fine tuning of one part in $\mathcal{O}(10^{38})$ between the bare mass term and radiative corrections, which is highly unnatural [12]. In the next section, we will discuss ways to make the Standard Model natural.

In the rest of this section, we will summarise the other theoretical and phenomenological reasons to go beyond the Standard Model.

2.1.1 Evolution of Standard Model gauge couplings

Most Grand Unified theories are described in terms of a single (also simple) gauge group for all three interactions, namely, strong and electroweak interactions, and also a single coupling constant. Examples are SU(5) guage group and SO(10) gauge group. They predict that all gauge couplings of the Standard Model unify at the GUT scale. Using the renormalisation group equations for the gauge couplings of the Standard Model, we can run these couplings from the weak scale, where they are well known, all the way up to GUT scale. With the particle content of the Standard Model, as we can see from Fig.(1), the gauge couplings do not exactly unify at the high scale. This figure assumes an SU(5) GUT at the
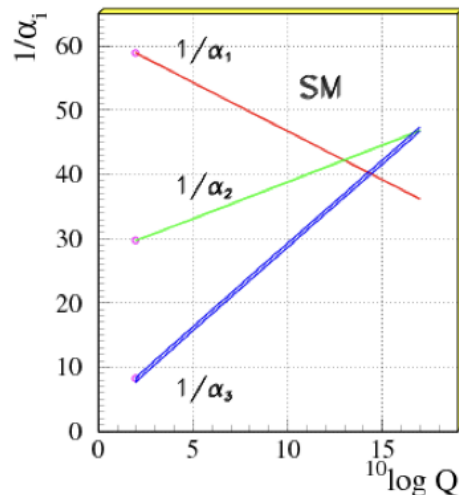
Fig. 1: Evolution of gauge couplings in the Standard Model. It can be clearly seen that they do not unify at high scale.

high scale. The non-unification can be seen as an indication for existence of new particles at the weak scale, which in turn modify the renormalisation group equations such that the gauge couplings unify at the GUT scale.

2.1.2 Dark Matter

There is strong phenomenological evidence for the existence of dark matter at all length scales in Nature. The (virial velocity) rotational curves of (spherical) galaxies, collision of bullet cluster, structure formation and measurement of cosmological energy density of the universe all point out to the existence of dark matter. More details on this can be found in lectures by Moroi san [13]. The Standard Model does not have a particle which can be the dark matter. The dark particle should be chargeless, (most probably) colourless and long lived (stable). Quarks (in addtion to be being coloured) and charged leptons are charged. The gauge and Higgs bosons are short lived. Neutrinos are too light (and thus fast) to form large scale structure which requires significant amount of cold dark matter. One possibility is that the dark matter is made up of a stand-alone particle independent of the Standard Model. A more interesting possibility would be to consider that dark matter is a part of the physics beyond standard model and could have weak interactions (Weakly Interacting Massive Particle). Frameworks like supersymmetry and extra-dimensions typically have such a particle, which thus could be produced at a collider.

2.1.3 Baryon Asymmetry

The standard big bang cosmology predicts equal amount of matter and anti-matter to be present at the beginning of the Universe. However, as the Universe evolved only matter remained and most of the anti-matter disappeared. An asymmetry of the order of one part in 10^{10} between matter and anti-matter at the big bang epoch is sufficient to generate the almost complete matter domination that we see in the present epoch. Three well known mechanism exist for generation of baryon asymmetry (a) Electroweak baryogenesis (b) GUT baryogenesis and (c) leptogenesis. All the above three mechanisms require Standard Model to be extended. Of the three, leptogenesis can be successfully incorporated with the most minimal extension while solving the neutrino mass problem also. More details can be found in [13].

2.1.4 Neutrino Masses

Starting from 1998, it has been increasingly established that neutrinos have masses. The corresponding mixing angles are Currently, the two mass squared differences and the three mixing angles have been well measured. Questions about whether they are Dirac or Majorana, CP-violation in the leptonic sector are still to be answered. However, the present information is sufficient to argue that discovery of neutrino masses signals existence of physics beyond Standard Model. The new physics could be in terms of new particles or new symmetries or both. More aspects of this physics are discussed in Kajitha san's lectures [14].

2.1.5 Strong CP problem

One of the questions which is not discussed in the present set of lectures is called the Strong CP problem. The strong interactions conserve CP to a high degree even though a CP violating term $\langle\theta\rangle_{QCD}G^{\mu\nu}\tilde{G}_{\mu\nu}$, where $\tilde{G}_{\mu\nu}$ is the dual field strength tensor of the Gluon Fields, is allowed by the QCD SU(3) gauge group in the lagrangian. The question is why the coefficient $\langle\theta\rangle_{QCD}$ is very small and is close to zero. One of the popular solutions to the strong CP problem require to introduce additional new particles called axions in to the Standard Model. This topic has been discussed in detail in your cosmology lectures by Moroi san [13].

In addition to the above, there are other issues like the flavour problem in the SM, which we will not elaborate here.

2.2 Nature and energy scale New Physics

After considering the various reasons for going beyond the Standard Model, let us discuss the possible nature of new physics and the energy scale of the new physics from various indications we have discussed so far. We will consider the following indications for new physics: (i) Neutrino Masses: There is a wide range of scales available from keV to 10^15 GeV where new physics can manifest itself to explain neutrino masses. If neutrinos are Majorana like, various kinds of seesaw mechanisms are available to explain the neutrino masses and their mixing patterns within this energy range. If they are Dirac, the right handed neutrinos are introduced at the neutrino mass scale with an extra symmetry (lepton number) protecting them. (ii) Dark Matter: Here too there is a wide range in the mass spin, and interactions of the dark matter particle available to satisfy the relic density of the universe as well as the direct and indirect experimental constraints. However, if the dark matter has weak interactions, then a particle of mass ~ 100 GeV satisfies the relic density constraint. This is the so-called WIMP miracle. (iii). Baryogensis can be explained by leptogenesis via right handed neutrinos with masses between a TeV and the GUT scale. (iv). Solutions to hierarchy problem however predict masses close to a TeV.

Let us now concentrate on solutions to the hierarchy problem as the motivation for new physics. Since the New Physics is closely related to the nature of the Higgs boson and the hierarchy problem, there can be two broad classes of solutions to be considered: (a) The Standard Model is valid only up to the scale of quantum gravity as we discussed above. However, the cut-off scale of new physics or quantum gravity, is low, *i.e*, it is no longer $\Lambda \sim M_{Pl}$ but, $\Lambda \sim (1\text{TeV})$. This is possible in theories with extra space time dimensions where the fundamental Planck constant in α extra dimensional theory is related to the four dimensional M_{Pl} by $M_{Pl}^2 = M_\star^{2+n} R^n$. By choosing sufficiently large extra dimensions, the fundamental Planck scale can be brought close to TeV scale in a theory with n extra dimensions. If the gravity in the extra dimensions is assumed to be strongly interacting, then the radius of the extra dimensions could be much smaller.

Another possibility is that Higgs is not a elementary particle at all, but is a composite of some other tiny fundamental particles. In such a case, the Standard Model is valid only up to a scale where the compositeness of the Higgs comes in to play. A well known example of this type is the pion in ordinary QCD. The pion, a pseudo-scalar particle can be treated as an elementary particle up to energies close to

a (maximum) GeV, but beyond that energy scale, the composite nature of the pion should be considered. The quarks become elementary particles from that energy scale. (b) There is a symmetry which protects the Higgs mass. Models of the type Supersymmetry, Little Higgs, Twin Higgs come in to this category. Of these, supersymmetry is interesting as a symmetry of quantum field theory. When softly broken, it preserves most of it's nice features and remains perturbative and calculable. In the following sections, we will introduce supersymmetry and construct the Minimal Supersymmetric Standard Model (MSSM). We then study the phenomenology of this model and discuss the present status of this model. A small supplement to a introduction to extra-dimensions will be provided in the appendix B.

Supersymmetries were first introduced in the context of string theories by Ramond. In quantum field theories, this symmetry is realised through fermionic generators, thus escaping the no-go theorems of Coleman and Mandula [15]. The simplest Lagrangian realising this symmetry in four dimensions was built by Wess and Zumino which contains a spin $\frac{1}{2}$ fermion and a scalar. Supersymmetry relates a particle with another particle varied by a spin 1/2. For example, spin 0 and spin 1/2 form a supersymmetric pair, similarly, spin 1/2 and spin 1 form a supersymmetric pair. Supersymmetry ensures that the within a pair, both the particles have the same mass and same couplings.

In particle physics, supersymmetry plays an important role in protecting the Higgs mass. To understand how it protects the Higgs mass, let us repeat the hierarchy problem once again. The Higgs mass enters as a bare mass parameter in the Standard Model lagrangian, eq.(A.10). Contributions from the self energy diagrams of the Higgs are quadratically divergent pushing the Higgs mass up to cut-off scale. In the absence of any new physics at the intermediate energies, the cut-off scale is typically M_{GUT} or M_{planck}. As we have seen, cancellation of these divergences with the bare mass parameter would require fine-tuning of order one part in 10^{-38} rendering the theory 'unnatural'. On the other hand, if one has additional contributions, say, for example, for the diagram with the Higgs self coupling, there is an additional contribution from a fermionic loop, with the fermion carrying the same mass as the scalar, the contribution from this additional diagram would now cancel the quadratically divergent part of the SM diagram, with the total contribution now being only logarithmically divergent. If this mechanism needs to work for all the diagrams, not just for the Higgs self-coupling and for all orders in perturbation theory, it would require a symmetry which would relate a fermion and a boson with same mass. Supersymmetry is such a symmetry.

3 Supersymmetry and Superfields

Supersymmetry is based on graded Lie algebra, which means it's generators are anti-commuting Grassman operators. For $N = 1$ supersymmetry we have

$$\{Q_\alpha, Q^\dagger_{\dot\beta}\} = 2\sigma^\mu_{\alpha\dot\beta} P_\mu \tag{6}$$

The supersymmetry generators change the spin of an field by 1/2 unit. For example a scalar (spin =0) is transformed to spin 1/2 field.

$$|\text{fermion} >= Q^\dagger|\text{scalar} > . \tag{7}$$

Furthermore, since

$$[Q, P^\mu] = [Q^\dagger, P^\mu] = 0 \tag{8}$$

it can be shown that, the particle and it's super-partner have the same mass. Furthermore, as long as supersymmetry is conserved, the particle and it's superpartner also share the same couplings.

We now move to study the simplest irreducible representations of $N = 1$ SUSY algebra. Two of the simplest supermultiplets will be of use are the chiral supermultiplet and the Vector supermultiplet. The supermultiplets can be expressed in terms of superfields which can be thought of as 'upgraded' versions of quantum fields. Superfields are functions (fields) written over a 'superspace' made of ordinary

space (x_μ) and two fermionic 'directions' $(\theta, \bar{\theta})$; they are made up of quantum fields whose spins differ by 1/2. To build interaction lagrangians one normally resorts to this formalism, originally given by Salam and Strathdee [16], as superfields simplify addition and multiplication of the representations. It should be noted however that the component fields may always be recovered from superfields by a power series expansion in grassman variable, θ.

Given that supersymmetry transforms a fermion into a boson and vice-versa, supermultiplets or superfields are multiplets which collect fermion-boson pairs which transform in to each other. We will deal with two kinds of superfields - vector superfields and chiral superfields. A chiral superfield has particle content in the off-shell formalism, contains a weyl fermion, a scalar and and an auxiliary scalar field generally denoted by F. A vector superfield contains a spin 1 boson, a spin 1/2 fermion and an auxiliary scalar field called D.

A chiral superfield has an expansion :

$$\Phi = \phi + \sqrt{2}\theta\psi + \theta\theta F, \tag{9}$$

where ϕ is the scalar component, ψ, the two component spin 1/2 fermion and F the auxiliary field.

The second possible function of the superfields is the analytic or holomorphic function of the superfields called the superpotential, W. This would mean that W is purely a function of complex fields $(z_1 z_2 z_3)$ or its conjugates $(z_1^\star z_2^\star z_3^\star)$. This function essentially gives the interaction part of the lagrangian which is independent of the gauge couplings, like the Yukawa couplings. If renormalisability is demanded, the dimension of the superpotential is restricted to be less than or equal to three, $[W] \leq 3$ *i.e,* only products of three or less number of chiral superfields are allowed.

The $\theta\theta$ components of the product of three chiral superfields is given as [17]

$$\Phi_i \Phi_j \Phi_k|_{\theta\theta} = -\psi_i\psi_j\phi_k - \psi_j\psi_k\phi_i - \psi_k\psi_i\phi_j + F_i\phi_j\phi_k + F_j\phi_k\phi_i + F_k\phi_i\phi_j, \tag{10}$$

where as earlier, ψ_i represents the fermionic, ϕ_i the scalar and F_i the auxiliary component of the chiral superfield Φ_i. Similarly for the product of two superfields on has :

$$\Phi_i \Phi_j|_{\theta\theta} = -\psi_i\psi_j + F_i\phi_j + F_j\phi_i \tag{11}$$

A vector superfield in (Wess-Zumino gauge) has an expansion :

$$V = -\theta\sigma^\mu\bar{\theta}A_\mu + i\theta\theta\bar{\theta}\bar{\lambda} - i\bar{\theta}\bar{\theta}\theta\lambda + \frac{1}{2}\theta\theta\bar{\theta}\bar{\theta}D \tag{12}$$

Remember that in supersymmetric theories, the gauge symmetry is imposed by the transformations on matter superfields as :

$$\Phi' = e^{i\Lambda_l t_l}\Phi \tag{13}$$

where Λ_l is an arbitrary chiral superfield and t_l represent the generators of the gauge group which are l in number and the index l is summed over[1].

The gauge invariance is restored in the kinetic part by introducing a (real) vector superfield, V such that the combination

$$\Phi^\dagger e^{gV}\Phi \tag{14}$$

remains gauge invariant. For this to happen, the vector superfield V itselves transforms under the gauge symmetry as

$$\delta V = i(\Lambda - \Lambda^\dagger) \tag{15}$$

---

[1]To be more specific, t_l is just a number for the abelian groups. For non-abelian groups, t_l is a matrix and so is Λ_l, with $\Lambda_{ij} = t_{ij}^l \Lambda_l$ Note that V is also becomes a matrix in this case.

The supersymmetric invariant kinetic part of the lagrangian is given by:

$$\mathcal{L}_{kin} = \int d\theta^2 d\bar{\theta}^2 \Phi^\dagger e^{gV} \Phi = \Phi^\dagger e^{gV} \Phi|_{\theta\theta\bar{\theta}\bar{\theta}} \tag{16}$$

Remember that the function e^{gV} truncates at $\frac{1}{2}g^2V^2$ in the Wess-Zumino gauge. In fact, in this gauge, this function can be determined by noting:

$$\exp V_{WZ} = 1 - \theta\sigma^\mu\bar{\theta}A_\mu + i\theta\theta\bar{\theta}\bar{\lambda} - i\bar{\theta}\bar{\theta}\theta\lambda + \frac{1}{2}\,\theta\theta\bar{\theta}\bar{\theta}\,(D - \frac{1}{2}A^\mu A_\mu), \tag{17}$$

for an abelian Vector superfield. Here as usual λ denotes the gaugino field while A_μ represents the gauge field. D represents the auxiliary field of the Vector multiplet. The extension to the non-abelian case is straight forward.

Finally, for every vector superfield (or a set of superfields) we have an associated field strength superfield $\mathcal{W}^\alpha$, which gives the kinetic terms for the gauginos and the field strength tensors for the gauge fields. Given that it is a chiral superfield, the component expansion is given by taking the $\theta\theta$ component of 'square' of that superfield. In the Wess-Zumino gauge, $\mathcal{W}_\alpha = -\frac{1}{4}\bar{\mathcal{D}}\bar{\mathcal{D}}\mathcal{D}_\alpha V_{WZ}$ [17] ($\mathcal{D}$ is the differential operator on superfields) and the lagrangian has the form :

$$\mathcal{L} \supset \frac{1}{4}\left(\mathcal{W}^\alpha\mathcal{W}_\alpha|_{\theta\theta} + \mathcal{W}_{\dot{\alpha}}\mathcal{W}^{\dot{\alpha}}|_{\bar{\theta}\bar{\theta}}\right) = \frac{1}{2}D^2 - \frac{1}{4}F_{\mu\nu}F^{\mu\nu} - i\lambda\sigma^\mu\partial_\mu\bar{\lambda} \tag{18}$$

D represents the auxiliary component of the vector superfields. The extension to non-abelian vector superfields in straight forward.

3.1 How supersymmetry works

We now demonstrate with a simple example of supersymmetric QED as how in supersymmetric theories, the mass of the scalar particle is protected. The QED lagragian is $U(1)$ invariant, which is given by

$$\mathcal{L}_{\text{QED}} = \frac{-1}{4}F_{\mu\nu}F^{\mu\nu} + \bar{\Psi}\left(i\partial^\mu\gamma_\mu - m_e\right)\Psi + ie\bar{\Psi}\gamma_\mu\Psi A_\mu, \tag{19}$$

where Ψ stands for the Dirac fermion field, the electron, A_μ is the photon field. We would like to construct the supersymmetric version of the lagrangian. For each 'left handed' or chiral field, we now replace it with a chiral superfield. Thus the two chiral components of the Dirac field, $\Psi = \Psi_L + \Psi_R$, where $\Psi_{L,R} = (1 \pm \gamma_5)/2\ \Psi$. In the supersymmetric version, each of the chiral components will be replaced by a corresponding chiral superfield. Thus we will have $\Psi_{L,R} \to \Phi_{L,R}$. As we have seen each chiral superfield contains, a fermion along with a spin zero partner. The $\Phi_{L,R}$ contain $\{e_{L,R}, \tilde{e}_{L,R}\}$ a left(right) electron along with it's spin zero partner, left (right) handed selectron. Note that the left/right subscripts on the scalar does not indicate the chiral structure of the scalar particles, but just to distinguish them from their chiral fermion partners - one complex scalars for each chiral fermion. The photon field is replaced by a vector superfield, V, introduced above, which contains the photon field A_μ and it's spin half fermonic partner, the photino, λ or $\tilde{A}$. We denote it by $V = \{A_\mu, \tilde{A}\}$. To construct the supersymmetric QED lagrangian, we will need to construct the superpotential , the Kahler potential and the field strength superpotential as discussed above.

The superpotential is just given by $W = m_e\Phi_L\Phi_R$. To get the lagrangian in terms of the component fields, one needs to expand the superfields in the superspace and do the two-component grassman integration, which corresponds to identifying the co-efficient of the $\theta\theta$ component. The Kähler potential is given by

$$K = \Phi_L^\dagger e^{gV}\Phi_L + \Phi_R^\dagger e^{gV}\Phi_R \tag{20}$$

The K and W functions are $U(1)$ gauge invariant. To get the lagragian in terms of the component fields, we have to integrate K over the superspace, which leaves us with the coefficient of $\theta^2\bar{\theta}^2$ term. The third

function is the field strength superpotential, which leads to the kinetic terms for the photon field and photino fields. The product of two field strength superpotentials $\mathcal{W}_\alpha \mathcal{W}^\alpha$ is integrated over superspace and the coefficient of $\theta\theta$ gives the component lagrangian. Before writing down the full lagrangian, we should remember that the auxiliary fields F and D should be removed by using their (non-dynamical) equations of motion, which leads to the following definitions in terms of scalar fields:

$$F = \frac{\partial W}{\phi_i} \quad ; \quad D = g q_i \phi^\star \phi \tag{21}$$

where ϕ runs over all the scalar fields in the theory, g is the coupling constant and q_i are the charges of the field. Putting everything together we have the following lagrangian for supersymmetric QED:

$$
\begin{aligned}
\mathcal{L}_{SQED} =& -\frac{1}{4} F_{\mu\nu} F^{\mu\nu} + i\bar\lambda \bar\sigma^\mu \partial_\mu \lambda + (\mathcal{D}_\mu \tilde e_L)^\dagger (\mathcal{D}^\mu \tilde e_L) + (\mathcal{D}_\mu \tilde e_R)^\dagger (\mathcal{D}_\mu \tilde e_R) \\
&+ i\bar e_L \sigma^\mu \mathcal{D}_\mu e_L + i\bar e_L \bar\sigma^\mu \mathcal{D}_\mu e_L + \left(\sqrt{2} e e_L \lambda \tilde e_L^\dagger + H.c\right) + \left(\sqrt{2} e e_R \lambda \tilde e_R^\dagger + H.c\right) \\
&+ m_e(e_L e_R + \bar e_R \bar e_L) - m_e^2(|\tilde e_L|^2 - |\tilde e_R|^2) - \frac{e^2}{2}(\tilde e_L^2 - \tilde e_R^2)^2
\end{aligned} \tag{22}
$$

The last two terms are the F^2 and D^2 terms respectively. $\mathcal{D}_\mu = \partial_\mu + ieA_\mu$, e being the electromagnetic coupling. The charges are normalised to be +1 for Φ_L and -1 for Φ_R. We can easily read of the various Feynman rules of supersymmetric QED from the above lagrangian, Eq.(22). The vertices are presented in Fig. 2. A couple of points are important to note here: (a) There s no covariant derivative for the photino. It does not interact with the gauge bosons. (b) The scalar quartic couplings are given by the gauge couplings. This is to ensure that the couplings of fermions and the scalars remain the same keeping supersymmetry intact.

The slectron, which has the same mass as the electron, does not receive large mass corrections as it is protected by supersymmetry. All the mass corrections are proportional the mass of the electron itself, protected by the so called non-renormalisable theorems of supersymmetry. The one loop corrections to the selectron mass are given by diagrams of the type shown in Fig. 3. The boson loops cancel with the fermionic loops, note that both of them have the same coupling and mass structure but with opposite sign as a consequence of supersymmetry. This cancellation holds at all orders in perturbation theory. This is how the mass of any scalar in any supersymmetry theory is predicted. We now use this theory as a stepping block to construct the full MSSM. We do so by constantly connecting with the SM lagrangian, it's particle content and gauge group, summarised in Appendix A.

4 Particle Spectrum of the MSSM

What we aim to build over the course of next few lectures is a supersymmetric version of the Standard Model, which means the lagrangian we construct should not only be gauge invariant under the Standard Model gauge group G_{SM} but also now be supersymmetric invariant. Such a model is called Minimal Supersymmetric Standard Model with the word 'Minimal' referring to minimal choice of the particle spectrum required to make it work. Furthermore, we would also like the MSSM to be renormalisable and anomaly free, just like the Standard Model is.

The minimal supersymmetric extension of the Standard Model is built by replacing every standard model matter field by a chiral superfield and every vector field by a vector superfield. Thus the existing particle spectrum of the Standard Model is doubled. The particle spectrum of the MSSM and their transformation properties under G_{SM} is given by,

$$Q_i \equiv \begin{pmatrix} u_{L_i} & \tilde u_{L_i} \\ d_{L_i} & \tilde d_{L_i} \end{pmatrix} \sim \left(3, 2, \frac{1}{6}\right) \qquad U_i^c \equiv \begin{pmatrix} u_i^c & \tilde u_i^c \end{pmatrix} \sim \left(\bar 3, 1, -\frac{2}{3}\right)$$

$$D_i \equiv \begin{pmatrix} d_i^c & \tilde d_i^c \end{pmatrix} \sim \left(\bar 3, 1, \frac{1}{3}\right)$$
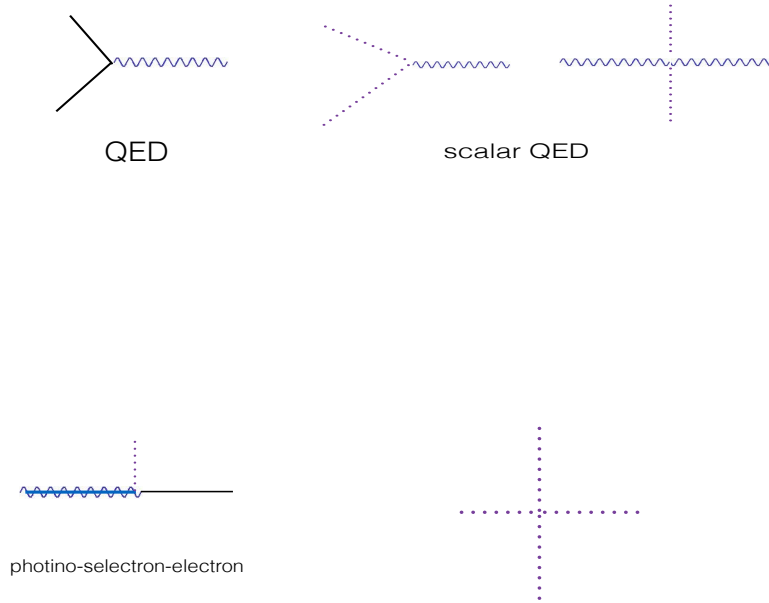
Fig. 2: Feynman Diagrams in Supersymmetric Quantum Electrodynamics contain vertices from QED, Scalar QED and further new diagrams like the last two ones.
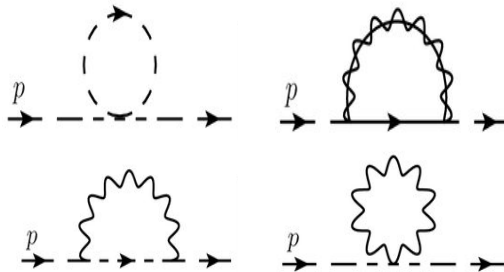
Fig. 3: Typical 1-loop corrections to the left and right selectron masses in supersymmetric QED.

$$L_i \equiv \left(\begin{array}{cc} \nu_{L_i} & \tilde{\nu}_{L_i} \\ e_{L_i} & \tilde{e}_{L_i} \end{array} \right) \sim \left(1, \ 2, \ -\frac{1}{2} \right) \qquad E_i \equiv \left(\begin{array}{cc} e_i^c & \tilde{e}_i^c \end{array} \right) \sim (1, \ 1, \ 1)$$

(23)

The scalar partners of the quarks and the leptons are typically named as 's'quarks and 's'leptons. Together they are called sfermions. For example, the scalar partner of the top quark is known as the 'stop'. In the above, these are represented by a 'tilde' on their SM counterparts. As in the earlier case, the index i stands for the generation index.

There are two distinct features in the spectrum of MSSM : (a) Note that we have used the conjugates of the right handed particles, instead of the right handed particles themselves. There is no additional conjugation on the superfield itselves, the c in the superscript just to remind ourselves that this chiral su-

perfield is made up of conjugates of SM quantum fields. In eq.(8), $u^c = u_R^\dagger$ and $\tilde{u}^c = \tilde{u}_R^\star$. This way of writing down the particle spectrum is highly useful for reasons to be mentioned later in this section. Secondly (b) At least two Higgs superfields are required to complete the spectrum - one giving masses to the up-type quarks and the other giving masses to the down type quarks and charged leptons. As mentioned earlier, this is the minimal number of Higgs particles required for the model to be consistent from a quantum field theory point of view[2]. These two Higgs superfields have the following transformation properties under G_{SM}:

$$
\begin{aligned}
H_1 &\equiv \left(\begin{array}{cc} H_1^0 & \tilde{H}_1^0 \\ H_1^- & \tilde{H}_1^- \end{array} \right) \sim \left(1,\ 2,\ -\frac{1}{2} \right) \\
H_2 &\equiv \left(\begin{array}{cc} H_2^+ & \tilde{H}_2^+ \\ H_2^0 & \tilde{H}_2^0 \end{array} \right) \sim \left(1,\ 2,\ \frac{1}{2} \right)
\end{aligned}
\tag{24}
$$

The Higgsinos are represented by a ˜ on them. This completes the matter spectrum of the MSSM. Then there are the gauge bosons and their super particles.

In the MSSM, corresponding to three gauge groups of the SM and for each of their corresponding gauge bosons, we need to add a vector superfield which transforms as the adjoint under the gauge group action. Each vector superfield contains the gauge boson and its corresponding super partner called gaugino. Thus in MSSM we have the following vector superfields and their corresponding transformation properties under the gauge group, completing the particle spectrum of the MSSM:

$$
\begin{aligned}
V_s^A &: \left(\begin{array}{cc} G^{\mu A} & \tilde{G}^A \end{array} \right) \sim (8,1,0) \\
V_W^I &: \left(\begin{array}{cc} W^{\mu I} & \tilde{W}^I \end{array} \right) \sim (1,3,0) \\
V_Y &: \left(\begin{array}{cc} B^{\mu} & \tilde{B} \end{array} \right) \sim (1,1,0)
\end{aligned}
\tag{25}
$$

The G's (G and $\tilde{G}$) represent the gluonic fields and their superpartners called gluinos, the index A runs from 1 to 8. The W's are the $SU(2)$ gauge bosons and their superpartners 'Winos', the index I taking values from 1 to 3 and finally Bs represents the $U(1)$ gauge boson and its superpartner 'Bino'. Together all the superpartners of the gauge bosons are called 'gauginos'. This completes the particle spectrum of the MSSM.

5 The superpotential and R-parity

The supersymmetric invariant lagrangian is constructed from functions of superfields. In general there are three functions which are: (a) The Kähler potential, K, which is a real function of the superfields (b) The superpotential W, which is a holomorphic (analytic) function of the superfields, and (c) the gauge kinetic function $f_{\alpha\beta}$ which appears in supersymmetric gauge theories. This is the coefficient of the product of field strength superfields, $\mathcal{W}_\alpha \mathcal{W}^\beta$. The field strength superfield is derived from the vector superfields contained in the model. $f_{\alpha\beta}$ determines the normalisation for the gauge kinetic terms. In MSSM, $f_{\alpha\beta} = \delta_{\alpha\beta}$. The lagrangian of the MSSM is thus given in terms of G_{SM} gauge invariant functions K, W and add the field strength superfield $\mathcal{W}$, for each of the vector superfields in the spectrum.

The gauge invariant Kähler potential has already been discussed in the eqs.(16). For the MSSM case, the Kähler potential will contain all the three vector superfields corresponding to the G_{SM} given in the eq.(25). Thus we have :

$$
\mathcal{L}_{kin} = \int d\theta^2 d\bar{\theta}^2 \sum_{\text{SU(3),SU(2),U(1)}} \Phi_\beta^\dagger\, e^{gV}\, \Phi_\beta
\tag{26}
$$

---

[2]The Higgs field has a fermionic partner, higgsino which contributes to the anomalies of the SM. At least two such fields with opposite hyper-charges ($U(1)_Y$) should exist to cancel the anomalies of the Standard Model.

where the index β runs over all the matter fields $\Phi_\beta = \{Q_i, U_i^c, D_i^c, L_i, e_i^c, H_1, H_2\}$[3] in appropriate representations. Corresponding to each of the gauge groups in G_{SM}, all the matter fields which transform non-trivially under this gauge group[4] are individually taken and the grassman ($d\theta^2 d\bar{\theta}^2$) integral is evaluated with the corresponding vector superfields in the exponential

After expanding and evaluating the integral, we get the lagrangian which is supersymmetric invariant in terms of the ordinary quantum fields - the SM particles and the superparticles. This part of the lagrangian would give us the kinetic terms for the SM fermions, kinetic terms for the sfermions and their interactions with the gauge bosons and in addition also the interactions of the type: fermion-sfermion-gaugino which are structurally like the Yukawa interactions ($ff\phi$), but carry gauge couplings. Similarly, for the Higgs fields, this part of the lagrangian gives the kinetic terms for the Higgs fields and their fermionic superpartners Higgsinos and the interaction of the gauge bosons with the Higgs fields and Higgs-Higgsino-gaugino vertices.

Imposing the restriction of renormalisability the most general G_{SM} gauge invariant form of the W for the matter spectrum of MSSM (8,24) is given as

$$W = W_1 + W_2, \tag{27}$$

where

$$W_1 = h_{ij}^u Q_i U_j^c H_2 + h_{ij}^d Q_i D_j^c H_1 + h_{ij}^e L_i E_j^c H_1 + \mu H_1 H_2 \tag{28}$$

$$W_2 = \epsilon_i L_i H_2 + \lambda_{ijk} L_i L_j E_k^c + \lambda'_{ijk} L_i Q_j D_k^c + \lambda''_{ijk} U_i^c D_j^c D_k^c. \tag{29}$$

Here we have arranged the entire superpotential in to two parts, W_1 and W_2 with a purpose. Though both these parts are gauge invariant, W_2 also violates the global lepton number and baryon quantum numbers. The simultaneous presence of both these set of operators can lead to rapid proton decay and thus can make the MSSM phenomenologically invalid. For these reasons, one typically imposes an additional symmetry called R-parity in MSSM which removes all the dangerous operators in W_2. We will deal with R-parity in greater detail in the next section. For the present, let us just set W_2 to be zero due to a symmetry called R-parity and just call W_1 as W. The lagrangian can be derived from the superpotential containing (mostly) gauge invariant product of the three superfields by taking the $\theta\theta$ component, which can be represented in the integral form as

$$\mathcal{L}_{yuk} = \int d\theta^2 \ W(\Phi) + \int d\bar{\theta}^2 \ \bar{W}(\bar{\Phi}) \tag{30}$$

This part gives the standard Yukawa couplings for the fermions with the Higgs, in addition also give the fermion-sfermion-higgsino couplings and scalar terms. For example, the coupling $h_{ij}^u \ Q_i u_j^c H_2$ in the superpotential has the following expansion in terms of the component fields :

$$
\begin{aligned}
\mathcal{L}_{yuk} \supset{}& h_{ij}^u \ Q_i u_j^c H_2 \ |_{\theta\theta} \\
\supset{}& h_{ij}^u \ (\ u_i u_j^c H_2^0 - d_i u_j^c H_2^+ \ ) \ |_{\theta\theta} \\
\supset{}& h_{ij}^u (\psi_{u_i}\psi_{u_j^c}\phi_{H_2^0} + \phi_{\tilde{u}_i}\psi_{u_j^c}\psi_{\tilde{H}_2^0} + \psi_{u_i}\phi_{\tilde{u}_j^c}\psi_{\tilde{H}_2^0} - \psi_{d_i}\psi_{u_j^c}\phi_{H_2^+} - \phi_{\tilde{d}_i}\psi_{u_j^c}\psi_{\tilde{H}_2^+} - \psi_{d_i}\phi_{\tilde{u}_j^c}\psi_{\tilde{H}_2^+}) \\
\equiv{}& h_{ij}^u \ (\ u_i u_j^c H_2^0 + \ \tilde{u}_i u_j^c \tilde{H}_2^0 + u_i \tilde{u}_j^c \tilde{H}_2^0 - d_i u_j^c H_2^+ \ - \ \tilde{d}_i u_j^c \tilde{H}_2^+ \ - \ d_i \tilde{u}_j^c \tilde{H}_2^+ \ ), \tag{32}
\end{aligned}
$$

where in the last equation, we have used the same notation for the chiral superfield as well as for its lowest component namely the scalar component. Note that we have not written the F-terms which give rise to the scalar terms in the potential. Similarly, there is the μ term which gives 'Majorana' type mass term for the Higgsino fields.

---

[3]The indices i, j, k always stand for the three generations through out this notes, taking values between 1 and 3.

[4]As given in the list of representations in eqs. (8,24)

In the MSSM, we have to add the corresponding field strength $\mathcal{W}$ superfields for electroweak vector superfields, W and B as well as for the gluonic G vector superfields of eqs.(25).

So far we have kept the auxiliary fields (D and F) of various chiral and vector superfields in the component form of our lagrangian. However, given that these fields are unphysical, they have to be removed from the lagrangian to go "on-shell". To eliminate the D and F fields, we have to use the equations of motions of these fields which have simple solutions for the F and D as :

$$F_i = \frac{\partial W}{\partial \phi_i} \quad ; \quad D_A = -g_A \; \phi_i^\star \, T_{ij}^A \; \phi_j, \tag{33}$$

where ϕ_i represents all the scalar fields present in MSSM. The index A runs over all the gauge groups in the model. For example, for $U(1)_Y$, $T_{ij}^A = (Y^2/2)\delta_{ij}$. The F and D terms together form the scalar potential of the MSSM[5] which is given as

$$V = \sum_i |F_i|^2 + \frac{1}{2} D^A D_A \tag{34}$$

Putting together, we see that the lagrangian of the MSSM with SUSY unbroken is of the form :

$$\mathcal{L}_{MSSM}^{(0)} = \int \left(d\theta^2 \, W(\Phi) + H.c \right) + \int d\theta^2 \, d\bar{\theta}^2 \, \Phi_i^\dagger \, e^{gV} \, \Phi_i + \int \left(d\theta^2 \, \mathcal{W}^\alpha \mathcal{W}_\alpha + H.c \right). \tag{35}$$

where all the functions appearing in (35) have been discussed in eqs.(26,28) and (18).

5.1 R-parity

In the previous section, we have seen that there are terms in the superpotential, eq.(29) which are invariant under the Standard Model gauge group G_{SM} but however violate baryon (B) and individual lepton numbers ($L_{e,\mu,\tau}$). At the first sight, it is bit surprising : the matter *superfields* carry the same quantum numbers under the G_{SM} just like the ordinary matter fields do in the Standard Model and B and $L_{e,\mu,\tau}$ violating terms are not present in the Standard Model. The reason can be traced to the fact that in the MSSM, where matter sector is represented in terms of superfields, there is no distinction between the fermions and the bosons of the model. In the Standard Model, the Higgs field is a boson and the leptons and quarks are fermions and they are different representations of the Lorentz group. This distinction is lost in the MSSM, the Higgs superfield, H_1 and the lepton superfields L_i have the same quantum numbers under G_{SM} and given that they are both (chiral) superfields, there is no way of distinguishing them. For this reason, the second part of the superpotential W_2 makes an appearance in supersymmetric version of the Standard Model. In fact, the first three terms of eq.(29) can be achieved by replacing $H_1 \to L_i$ in the terms containing H_1 of W_1.

The first three terms of the second part of the superpotential W_2 (eq.(29)), are lepton number violating whereas the last term is baryon number violating. The simultaneous presence of both these interactions can lead to proton decay, for example, through a squark exchange. An example of such an process in given in Figure 1. Experimentally the proton is quite stable. In fact its life time is pretty large $\gtrsim \mathcal{O}(10^{33})$ years [18]. Thus products of these couplings (λ'' and one of (λ', ϵ, λ) which can lead to proton decay are severely constrained to be of the order of $(O)(10^{-20})$[6]. Thus to make the MSSM phenomenologically viable one should expect these couplings in W_2 to take such extremely small values.

A more natural way of dealing with such small numbers for these couplings would be to set them to be zero. This can be arrived at by imposing a discrete symmetry on the lagrangian called R-parity.

---

[5]Later we will see that there are also additional terms which contribute to the scalar potential which come from the supersymmetry breaking sector.

[6]The magnitude of these constraints depends also on the scale of supersymmetry breaking, which we will come to discuss only in the next section. For a list of constraints on R-violating couplings, please see G. Bhattacharyya [19].

R-parity has been originally introduced as a discrete R-symmetry [7] by Ferrar and Fayet [20] and then later realised to be of the following form by Ferrar and Weinberg [21] acting on the component fields:

$$R_p = (-1)^{3(B-L)+2s}, \qquad (36)$$

where B and L represent the Baryon and Lepton number respectively and s represents the spin of the particle. Under R-parity the transformation properties of various superfields can be summarised as:

$$
\begin{aligned}
\{V_s^A, V_w^I, V_y\} &\rightarrow \{V_s^A, V_w^I, V_y\} \\
\theta &\rightarrow -\theta^\star \\
\{Q_i, U_i^c, D_i^c, L_i, E_i^c\} &\rightarrow -\{Q_i, U_i^c, D_i^c, L_i, E_i^c\} \\
\{H_1, H_2\} &\rightarrow \{H_1, H_2\}
\end{aligned}
\qquad (37)
$$

Imposing these constraints on the superfields will now set all the couplings in W_2 to zero.

Imposing R-parity has an advantage that it provides a natural candidate for dark matter. This can be seen by observing that R-parity distinguishes a particle from its superpartner. This ensures that every interaction vertex has at least two supersymmetric partners when R-parity is conserved. The lightest supersymmetric particle (LSP) cannot decay in to a pair of SM particles and remains stable. R-parity can also be thought of as a remnant symmetry theories with an additional $U(1)$ symmetry, which is natural in a large class of supersymmetric Grand Unified theories. Finally, one curious fact about R-parity : it should be noted that R-parity constraints baryon and lepton number violating couplings of dimension four or rather only at the renormalisable level. If one allows for non-renormalisable operators in the MSSM, *i.e* that is terms of dimension more than three in the superpotential, they can induce dim 6 operators which violate baryon and lepton numbers at the lagrangian level and are still allowed by R-parity. Such operators are typically suppressed by high mass scale $\sim M_{Pl}$ or M_{GUT} and thus are less dangerous. In the present set of lectures, we will always impose R-parity in the MSSM so that the proton does not decay, though there are alternatives to R-parity which can also make proton stable.

6   Supersymmetry breaking

So far, we have seen that the Supersymmetric Standard Model lagrangian can also be organised in a similar way like the Standard Model lagrangian though one uses functions of superfields now to get the lagrangian rather than the ordinary fields. In the present section we will cover the last part (term) of the total MSSM lagrangian

$$\mathcal{L}_{\text{MSSM}} = \mathcal{L}_{\text{gauge/kinetic}}\left(K(\Phi, V)\right) + \mathcal{L}_{\text{yukawa}}\left(W(\Phi)\right) + \mathcal{L}_{\text{scalar}}\left(F^2, D^2\right) + \mathcal{L}_{\text{SSB}} \qquad (38)$$

which we have left out so far and that concerns supersymmetry breaking (SSB). Note that the first three terms are essentially from $\mathcal{L}_{\text{MSSM}}^{(0)}$ of eq.(35). In Nature, we do not observe supersymmetry. Supersymmetry breaking has to be incorporated in the MSSM to make it realistic. In a general lagrangian, supersymmetry can be broken spontaneously if the auxiliary fields F or D appearing in the definitions of the chiral and vector superfields respectively attain a vacuum expectation value (*vev*). If the F fields get a *vev*, it is called F-breaking whereas if the D fields get a *vev*, it is called D-breaking.

Incorporation of spontaneous SUSY breaking in MSSM would mean that at least one (or more) of the F-components corresponding to one (or more) of the MSSM chiral (matter) superfields would attain a vacuum expectation value. However, this approach fails as this leads to phenomenologically unacceptable prediction that at least one of the super-partner should be lighter (in mass) than the ordinary particle. This is not valid phenomenologically as such a light super partner (of SM particle) has been ruled out experimentally. One has to think of a different approach for incorporating supersymmetry breaking in to the MSSM [23].

---

[7]R-symmetries are symmetries under which the θ parameter transform non-trivially.
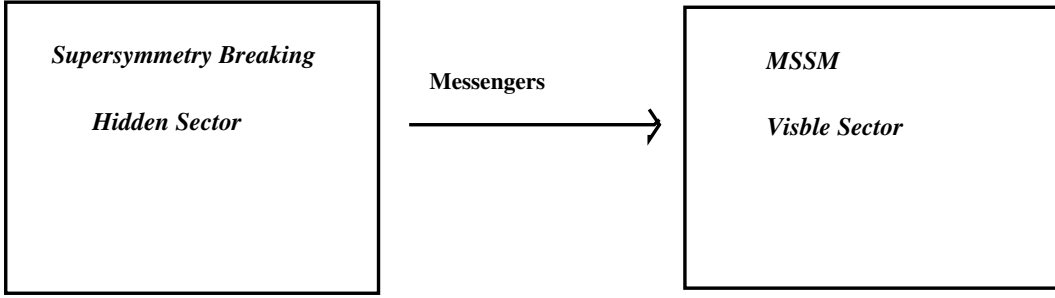
Fig. 4: A schematic diagram showing SUSY breaking using Hidden sector models

One of the most popular and successful approaches has been to assume another sector of the theory consisting of superfields which are not charged under the Standard Model gauge group. Such a sector of the theory is called 'Hidden Sector' as they cannot been "seen" like the Standard Model particles and remain hidden. Supersymmetry can be broken spontaneously in this sector. This information is communicated to the visible sector or MSSM through a messenger sector. The messenger sector can be made up of gravitational interactions or ordinary gauge interactions. The communication of supersymmetry breaking leads to supersymmetry breaking terms in MSSM. Thus, supersymmetry is not broken spontaneously within the MSSM, but *explicitly* by adding supersymmetry breaking terms in the lagrangian.

However, not all supersymmetric terms can be added. We need to add only those terms which do not re-introduce quadratic divergences back into the theory[8]. It should be noted that in most models of spontaneous supersymmetry breaking, only such terms are generated. These terms which are called "soft" supersymmetry breaking terms can be classified as follows:

 - a) Mass terms for the gauginos which are a part of the various vector superfields of the MSSM.
 - b) Mass terms for the scalar particles, $m^2_{\phi_{ij}} \phi^\star_i \phi_j$ with $\phi_{i,j}$ representing the scalar partners of chiral superfields of the MSSM.
 - c) Trilinear scalar interactions, $A_{ijk} \phi_i \phi_j \phi_k$ corresponding to the cubic terms in the superpotential.
 - d) Bilinear scalar interactions, $B_{ij} \phi_i \phi_j$ corresponding to the bilinear terms in the superpotential.

Note that all the above terms are dimensionful. Adding these terms would make the MSSM non-supersymmetric and thus realistic. The total MSSM lagrangian is thus equal to

$$\mathcal{L}_{total} = \mathcal{L}^{(0)}_{MSSM} + \mathcal{L}_{SSB} \tag{39}$$

with $\mathcal{L}^{(0)}_{MSSM}$ given in eq.(35). Sometimes in literature we have $\mathcal{L}_{SSB} = \mathcal{L}_{soft}$. Let us now see the complete list of all the soft SUSY breaking terms one can incorporate in the MSSM:

 1. *Gaugino Mass terms*: Corresponding to the three vector superfields (for gauge groups $U(1)$, $SU(2)$ and $SU(3)$) we have $\tilde{B}, \tilde{W}$ and $\tilde{G}$) we have three gaugino mass terms which are given as $M_1 \tilde{B}\tilde{B}$, $M_2 \tilde{W}_I \tilde{W}_I$ and $M_3 \tilde{G}_A \tilde{G}_A$, where $I(A)$ runs over all the $SU(2)(SU(3))$ group generators.
 2. *Scalar Mass terms*: For every scalar in each chiral (matter) superfield , we can add a mass term of the form $m^2 \phi^\star_i \phi_j$. Note that the generation indices i, j *need* not be the same. Thus the mass terms can violate flavour. Further, given that SUSY is broken prior to $SU(2) \times U(1)$ breaking , all these mass terms for the scalar fields should be written in terms of their 'unbroken' $SU(2) \times$

---

[8]Interaction terms and other couplings which do not lead to quadratically divergent (in cut-off Λ) terms in the theory once loop corrections are taken in to consideration. It essentially means we only add dimensional full couplings which are supersymmetry breaking.

$U(1)$ representations. Thus the scalar mass terms are : $m^2_{Q_{ij}} \tilde{Q}^\dagger_i \tilde{Q}_j$, $m^2_{u_{ij}} \tilde{u^c}^\star_i \tilde{u^c}_j$, $m^2_{d_{ij}} \tilde{d^c}^\star_i \tilde{d^c}_j$, $m^2_{L_{ij}} \tilde{L}^\dagger_i \tilde{L}_j$, $m^2_{e_{ij}} \tilde{e^c}^\star_i \tilde{e^c}_j$, $m^2_{H_1} H^\dagger_1 H_1$ and $m^2_{H_2} H^\dagger_2 H_2$.

3. *Trilinear Scalar Couplings*: As mentioned again, there are only three types of trilinear scalar couplings one can write which are G_{SM} gauge invariant. In fact, their form exactly follows from the Yukawa couplings. These are : $A^u_{ij} \tilde{Q}_i \tilde{u}^c_j H_2$, $A^d_{ij} \tilde{Q}_i \tilde{d}^c_j H_1$ and $A^e_{ij} \tilde{L}_i \tilde{e}^c_j H_1$.

4. *Bilinear Scalar Couplings*: Finally, there is only one bilinear scalar coupling (other than the mass terms) which is gauge invariant. The form of this term also follows from the superpotential. It is given as : $B H_1 H_2$.

Adding all these terms completes the lagrangian for the MSSM. However, the particles are still not in their 'physical' basis as $SU(2) \times U(1)$ breaking is not yet incorporated. Once incorporated the physical states of the MSSM and their couplings could be derived.

7 $SU(2) \times U(1)$ breaking

As a starting point, it is important to realize that the MSSM is a two Higgs doublet model *i.e*, SM with two Higgs doublets instead of one, with a different set of couplings [24]. Just as in Standard Model, spontaneous breaking of $SU(2)_L \times U(1)_Y \rightarrow U(1)_{EM}$ can be incorporated here too. Doing this leads to constraints relating various parameters of the model. To see this, consider the neutral Higgs part of the total scalar potential including the soft terms. It is given as

$$
\begin{aligned}
V_{scalar} &= (m^2_{H_1} + \mu^2)|H^0_1|^2 + (m^2_{H_2} + \mu^2)|H^0_2|^2 - (B_\mu \mu H^0_1 H^0_2 + H.c) \\
&+ \frac{1}{8}(g^2 + g'^2)(H^{0^2}_2 - H^{0^2}_1)^2 + \ldots,
\end{aligned} \tag{40}
$$

where H^0_1, H^0_2 stand for the neutral Higgs scalars and we have parameterised the bilinear soft term $B \equiv B_\mu \mu$. Firstly, we should require that the potential should be bounded from below. This gives the condition (in field configurations where the D-term goes to zero, *i.e*, the second line in eq.(40)):

$$
2B_\mu < 2|\mu|^2 + m^2_{H_2} + m^2_{H_1} \tag{41}
$$

Secondly, the existence of a minima for the above potential would require at least one of the Higgs mass squared to be negative giving the condition, (determinant of the 2×2 neutral Higgs mass squared matrix should be negative)

$$
B^2_\mu > (|\mu|^2 + m^2_{H_2})(|\mu|^2 + m^2_{H_1}) \tag{42}
$$

In addition to ensuring the existence of a minima, one would also require that the minima should be able to reproduce the standard model relations i.e, correct gauge boson masses. We insist that both the neutral Higgs attain vacuum expectation values :

$$
< H^0_1 >= \frac{v_1}{\sqrt{2}} \quad ; \quad < H^0_2 >= \frac{v_2}{\sqrt{2}} \tag{43}
$$

and furthermore we define

$$
v^2_1 + v^2_2 = v^2 = 246^2 \text{ GeV}^2,
$$

where v represents the vev of the Standard Model (SM) Higgs field. However, these *vev*s should correspond to the minima of the MSSM potential. The minima are derived by requiring $\partial V/\partial H^0_1 = 0$ and $\partial V/H^0_2 = 0$ at the minimum, where the form of V is given in eq.(40). These derivative conditions lead to relations between the various parameters of the model at the minimum of the potential. We have,

using the Higgs vev (43) and the formulae for[9] $M_Z^2 = \frac{1}{4}(g^2 + g'^2)v^2$, the minimisation conditions can rewritten as

$$\frac{1}{2}M_Z^2 = \frac{m_{H_1}^2 - \tan^2\beta\, m_{H_2}^2}{\tan^2\beta - 1} - \mu^2$$

$$\mathrm{Sin}2\beta = \frac{2B_\mu\,\mu}{m_{H_2}^2 + m_{H_1}^2 + 2\mu^2}, \tag{44}$$

where we have used the definition $\tan\beta = v_2/v_1$ as the ratio of the vacuum expectation values of H_2^0 and H_1^0 respectively. Note that the parameters $m_{H_1}^2$, $m_{H_2}^2$, B_μ are all supersymmetry breaking 'soft' terms. μ is the coupling which comes in the superpotential giving the supersymmetry conserving masses to the Higgs scalars. These are related to the Standard Model parameters M_Z and a ratio of *vev*s, parameterised by an angle $\tan\beta$. Thus these conditions relate SUSY breaking soft parameters with the SUSY conserving ones and the Standard Model parameters. For any model of supersymmetry to make contact with reality, the above two conditions (44)need to be satisfied.

The above minimisation conditions are given for the 'tree level' potential only. 1-loop corrections a 'la Coleman-Weinberg can significantly modify these minima. We will discuss a part of them in later sections when we discuss the Higgs spectrum. Finally we should mention that, in a more concrete approach, one should consider the entire scalar potential including all the scalars in the theory, not just confining ourselves to the neutral Higgs scalars. For such a potential one should further demand that there are no deeper minima which are color and charge breaking (which effectively means none of the colored and charged scalar fields get vacuum expectation values). These conditions lead to additional constraints on parameters of the MSSM [25].

8 Mass spectrum

We have seen in the earlier section, supersymmetry breaking terms introduce mass-splittings between ordinary particles and their super-partners. Given that particles have zero masses in the limit of exact G_{SM}, only superpartners are given soft mass terms. After the $SU(2) \times U(1)$ breaking, ordinary particles as well as superparticles attain mass terms. For the supersymmetric partners, these mass terms are either additional contributions or mixing terms between the various super-particles. Thus, just like in the case of ordinary SM fermions, where one has to diagonalise the fermion mass matrices to write the lagrangian in the 'on-shell' format or the physical basis, a similar diagonalisation has to be done for the supersymmetric particles and their mass matrices.

8.1 The Neutralino Sector

To begin with lets start with the gauge sector. The superpartners of the neutral gauge bosons (neutral gauginos) and the fermionic partners of the neutral higgs bosons (neutral higgsinos) mix to form Neutralinos. The neutralino mass matrix in the basis

$$\mathcal{L} \supset \frac{1}{2}\,\Psi_N \mathcal{M}_N \Psi_N^T + H.c$$

where $\Psi_N = \{\tilde{B},\ \tilde{W}^0, \tilde{H}_1^0, \tilde{H}_2^0\}$ is given as :

$$\mathcal{M}_N = \begin{pmatrix} M_1 & 0 & -M_Z c\beta\, s\theta_W & M_Z s\beta\, s\theta_W \\ 0 & M_2 & M_Z c\beta\, c\theta_W & M_Z s\beta\, c\theta_W \\ -M_Z c\beta\, s\theta_W & M_Z c\beta\, c\theta_W & 0 & -\mu \\ M_Z s\beta\, s\theta_W & -M_Z s\beta\, c\theta_W & -\mu & 0 \end{pmatrix}, \tag{45}$$

---

[9]In this lecture note, we will be using $g_2 = g = g_W$ for the SU(2) coupling, whereas $g' = g_1$ for the $U(1)_Y$ coupling and $g_s = g_3$ for the SU(3) strong coupling.

with $c\beta(s\beta)$ and $c\theta_W(s\theta_W)$ standing for $\cos\beta(\sin\beta)$ and $\cos\theta_W(\sin\theta_W)$ respectively. As mentioned earlier, M_1 and M_2 are the soft parameters, whereas μ is the superpotential parameter, thus SUSY conserving. The angle β is typically taken as a input parameter, $tan\beta = v_2/v_1$ whereas θ_W is the Weinberg angle given by the inverse tangent of the ratio of the gauge couplings as in the SM. Note that the neutralino mass matrix being a Majorana mass matrix is complex symmetric in nature. Hence it is diagonalised by a unitary matrix N,

$$N^* \cdot M_{\tilde{N}} \cdot N^\dagger = \text{Diag.}(m_{\chi_1^0}, m_{\chi_2^0}, m_{\chi_3^0}, m_{\chi_4^0}) \tag{46}$$

The states are rotated by $\chi_i^0 = N^\star\Psi$ to go the physical basis.

8.2 The Chargino Sector

In a similar manner to the neutralino sector, all the fermionic partners of the charged gauge bosons and of the charged Higgs bosons mix after electroweak symmetry breaking. However, they combine in a such a way that a Wino-Higgsino Weyl fermion pair forms a Dirac fermion called the chargino. This mass matrix is given as

$$\mathcal{L} \supset -\frac{1}{2} \begin{pmatrix} \tilde{W}^- & \tilde{H}_1^- \end{pmatrix} \begin{pmatrix} M_2 & \sqrt{2}M_W \sin\beta \\ \sqrt{2}M_W \cos\beta & \mu \end{pmatrix} \begin{pmatrix} \tilde{W}^+ \\ \tilde{H}_2^+ \end{pmatrix}, \tag{47}$$

Given the non-symmetric (non-hermitian) matrix nature of this matrix, it is diagonalised by a bi-unitary transformation, $U^* \cdot M_C \cdot V^\dagger = \text{Diag.}(m_{\chi_1^+}, m_{\chi_2^+})$. The chargino eigenstates are typically represented by $\chi^\pm$ with mass eigenvalues $m_{\chi^\pm}$. The explicit forms for U and V can be found by the eigenvectors of $M_C M_C^\dagger$ and $M_C^\dagger M_C$ respectively [26].

8.3 The Sfermion Sector

Next let us come to the sfermion sector. Remember that we have added different scalar fields for the right and left handed fermions in the Standard Model. After electroweak symmetry breaking, the sfermions corresponding to the left fermion and the right fermion mix with each other. Furthermore while writing down the mass matrix for the sfermions, we should remember that these terms could break the flavour *i.e*, we can have mass terms which mix different generation. Thus, in general the sfermion mass matrix is a 6×6 mass matrix given as :

$$\xi^\dagger M_{\tilde{f}}^2 \xi \; ; \quad \xi = \{\tilde{f}_{L_i}, \tilde{f}_{R_i}\}$$

From the total scalar potential, the mass matrix for these sfermions can be derived using standard definition given as

$$m_{ij}^2 = \begin{pmatrix} \frac{\partial^2 V}{\partial\phi_i \partial\phi_j^\star} & \frac{\partial^2 V}{\partial\phi_i \partial\phi_j} \\ \frac{\partial^2 V}{\partial\phi_i^\star \partial\phi_j^\star} & \frac{\partial^2 V}{\partial\phi_i^\star \partial\phi_j} \end{pmatrix} \tag{48}$$

Using this for sfermions, we have :

$$M_{\tilde{f}}^2 = \begin{pmatrix} m_{\tilde{f}_{\text{LL}}}^2 & m_{\tilde{f}_{\text{LR}}}^2 \\ m_{\tilde{f}_{\text{LR}}}^{2\dagger} & m_{\tilde{f}_{\text{RR}}}^2 \end{pmatrix}, \tag{49}$$

where each of the above entries represents 3×3 matrices in the generation space. More specifically, they have the form (as usual, i, j are generation indices):

$$m_{\tilde{f}_{L_i L_j}}^2 = M_{\tilde{f}_{L_i L_j}}^2 + m_f^2 \delta_{ij} + M_Z^2 \cos 2\beta (T_3 + \sin^2\theta_W Q_{\text{em}})\delta_{ij}$$

$$m_{\tilde{f}_{L_i R_j}}^2 = \left(\left(Y_f^A \cdot^{v_2}_{v_1} - m_f \mu^{\tan\beta}_{\cot\beta} \right) \text{ for } f =^{e,d}_u \right) \delta_{ij}$$

$$m^2_{\tilde{f}\text{RR}} = M^2_{\tilde{f}_{R_{ij}}} + \left(m^2_f + M^2_Z \cos 2\beta \sin^2 \theta_W Q_{\text{em}} \right) \delta_{ij} \tag{50}$$

In the above, $M^2_{\tilde{f}_L}$ represents the soft mass term for the corresponding fermion (L for left, R for right), T_3 is the eigenvalue of the diagonal generator of $SU(2)$, m_f is the mass of the fermion with Y and Q_{em} representing the hypercharge and electromagnetic charge (in units of the charge of the electron) respectively. The sfermion mass matrices are hermitian and are thus diagonalised by a unitary rotation, $R_{\tilde{f}} R^\dagger_{\tilde{f}} = 1$:

$$R_{\tilde{f}} \cdot M_{\tilde{f}} \cdot R^\dagger_{\tilde{f}} = \text{Diag.}(m_{\tilde{f}_1}, m_{\tilde{f}_2}, \ldots, m_{\tilde{f}_6}) \tag{51}$$

8.4 The Higgs sector

Now let us turn our attention to the Higgs fields. We will use again use the standard formula of eq.(48), to derive the Higgs mass matrices. The eight Higgs degrees of freedom form a 8×8 Higgs mass matrix which breaks down diagonally in to three 2×2 mass matrices[10].

The mass matrices are divided in to charged sector, CP odd neutral and CP even neutral. This helps us in identifying the goldstone modes and the physical spectrum in an simple manner. Before writing down the mass matrices, let us first define the following parameters :

$$m^2_1 = m^2_{H_1} + \mu^2, \quad m^2_2 = m^2_{H_2} + \mu^2, \quad m^2_3 = B_\mu \mu.$$

In terms of these parameters, the various mass matrices and the corresponding physical states obtained after diagonalising the mass matrices are given below:

Charged Higgs and Goldstone Modes:

$$\begin{pmatrix} H^+_1 & H^+_2 \end{pmatrix} \begin{pmatrix} m^2_1 + \frac{1}{8}(g^2_1 + g^2_2)(v^2_1 - v^2_2) + \frac{1}{4}g^2_2 v^2_2 & m^2_3 + \frac{1}{4}g^2_2 v_1 v_2 \\ m^2_3 + \frac{1}{4}g^2_2 v_1 v_2 & m^2_2 - \frac{1}{8}(g^2_1 + g^2_2)(v^2_1 - v^2_2) + \frac{1}{4}g^2_2 v^2_2 \end{pmatrix} \begin{pmatrix} H^-_1 \\ H^-_2 \end{pmatrix} \tag{52}$$

Using the minimisation conditions (44), this matrix becomes,

$$\begin{pmatrix} H^+_1 & H^+_2 \end{pmatrix} \left(\frac{m^2_3}{v_1 v_2} + \frac{1}{4}g^2_2 \right) \begin{pmatrix} v^2_2 & v_1 v_2 \\ v_1 v_2 & v^2_1 \end{pmatrix} \begin{pmatrix} H^-_1 \\ H^-_2 \end{pmatrix} \tag{53}$$

which has determinant zero leading to the two eigenvalues as :

$$\begin{aligned} m^2_{G^\pm} &= 0 \\ m^2_{H^\pm} &= \left(\frac{m^2_3}{v_1 v_2} + \frac{1}{4}g^2_2 \right)(v^2_1 + v^2_2), \tag{54} \\ &= \frac{2m^2_3}{sin2\beta} + M^2_W \tag{55} \end{aligned}$$

where $G^\pm$ represents the Goldstone mode. The physical states are obtained just by rotating the original states in terms of the H_1, H_2 fields by an mixing angle. The mixing angle in the present case (in the unitary gauge) is just $\tan\beta$:

$$\begin{pmatrix} H^\pm \\ G^\pm \end{pmatrix} = \begin{pmatrix} sin\beta & cos\beta \\ -cos\beta & sin\beta \end{pmatrix} \begin{pmatrix} H^\pm \\ G^\pm \end{pmatrix} \tag{56}$$

CP odd Higgs and Goldstone Modes:

---

[10]The discussion in this section closely follows from the discussion presented in Ref. [27]

Let us now turn our attention to the CP-odd Higgs sector. The mass matrices can be written in a similar manner but this time for imaginary components of the neutral Higgs.

$$
\begin{pmatrix} ImH_1^0 & ImH_2^0 \end{pmatrix} \begin{pmatrix} m_1^2 + \frac{1}{8}(g_1^2 + g_2^2)(v_1^2 - v_2^2) & m_3^2 \\ m_3^2 & m_2^2 - \frac{1}{8}(g_1^2 + g_2^2)(v_1^2 - v_2^2) \end{pmatrix} \begin{pmatrix} ImH_1^0 \\ ImH_2^0 \end{pmatrix} \quad (57)
$$

As before, again using the minimisation conditions, this matrix becomes,

$$
\begin{pmatrix} ImH_1^0 & ImH_2^0 \end{pmatrix} m_3^2 \begin{pmatrix} v_2/v_1 & 1 \\ 1 & v_1/v_2 \end{pmatrix} \begin{pmatrix} ImH_1^0 \\ ImH_2^0 \end{pmatrix} \quad (58)
$$

which has determinant zero leading to the two eigenvalues as :

$$
\begin{aligned}
m_{G^0}^2 &= 0 \\
m_{A^0}^2 &= \left(\frac{m_3^2}{v_1 v_2} \right)(v_1^2 + v_2^2) = \frac{2m_3^2}{sin2\beta}
\end{aligned} \quad (59)
$$

Similar to the charged sector, the mixing angle between these two states in the unitary gauge is again just $tan\beta$.

$$
\frac{1}{\sqrt{2}} \begin{pmatrix} A^0 \\ G^0 \end{pmatrix} = \begin{pmatrix} sin\beta & cos\beta \\ -cos\beta & sin\beta \end{pmatrix} \begin{pmatrix} ImH_1^0 \\ ImH_2^0 \end{pmatrix} \quad (60)
$$

CP even Higgs:
Finally, let us come to the real part of the neutral Higgs sector. The mass matrix in this case is given by the following.

$$
\begin{pmatrix} ReH_1^0 & ReH_2^0 \end{pmatrix} \frac{1}{2} \begin{pmatrix} 2m_1^2 + \frac{1}{4}(g_1^2 + g_2^2)(3v_1^2 - v_2^2) & -2m_3^2 - \frac{1}{4}v_1 v_2(g_1^2 + g_2^2) \\ -2m_3^2 - \frac{1}{4}v_1 v_2(g_1^2 + g_2^2) & 2m_2^2 + \frac{1}{4}(g_1^2 + g_2^2)(3v_2^2 - v_1^2) \end{pmatrix} \begin{pmatrix} ReH_1^0 \\ ReH_2^0 \end{pmatrix}
$$
$$\quad (61)$$

Note that in the present case, there is no Goldstone mode. As before, we will use the minimisation conditions and further using the definition of m_A^2 from eq.(59), we have :

$$
\begin{pmatrix} ReH_1^0 & ReH_2^0 \end{pmatrix} \begin{pmatrix} m_A^2 sin^2\beta + M_z^2 cos\beta & -(m_A^2 + m_Z^2)sin\beta cos\beta \\ -(m_A^2 + m_Z^2)sin\beta cos\beta & m_A^2 cos^2\beta + M_z^2 sin\beta \end{pmatrix} \begin{pmatrix} ReH_1^0 \\ ReH_2^0 \end{pmatrix} \quad (62)
$$

The matrix has two eigenvalues which are given by the two signs of the following equation:

$$
m_{H,h}^2 = \frac{1}{2} \left[m_A^2 + m_Z^2 \pm \{(m_A^2 + m_Z^2)^2 - 4m_Z^2 m_A^2 cos^2 2\beta\}^{1/2} \right] \quad (63)
$$

The heavier eigenvalue m_H^2, is obtained by taken the positive sign, whereas the lighter eigenvalue m_h^2 is obtained by taking the negative sign respectively. The mixing angle between these two states can be read out from the mass matrix of the above[11] as :

$$
tan\,2\alpha = \frac{m_A^2 + m_Z^2}{m_A^2 - m_Z^2}\,tan\,2\beta \quad (64)
$$

Tree Level Catastrophe:
So far we have seen that out of the eight Higgs degrees of freedom, three of them form the Goldstone modes after incorporating $SU(2) \times U(1)$ breaking and there are five *physical* Higgs bosons fields in the MSSM spectrum. These are the charged Higgs ($H^\pm$) a CP-odd Higgs (A) and two CP-even Higgs bosons

---

[11]The mixing angle for a 2×2 symmetric matrix, C_{ij} is given by

$$
tan2\theta = 2C_{12}/(C_{22} - C_{11}).
$$

(h, H). From the mass spectrum analysis above, we have seen that the mass eigenvalues of these Higgs bosons are related to each other. In fact, putting together all the eigenvalue equations, we summarise the relations between them as follows :

$$
\begin{aligned}
m_{H^\pm}^2 &= m_A^2 + m_W^2 > \max(M_W^2, m_A^2) \\
m_h^2 + m_H^2 &= m_A^2 + m_Z^2 \\
m_H &> max(m_A, m_Z) \\
m_h &< min(m_A, M_Z)|cos2\beta| < min(m_A, m_Z)
\end{aligned}
\tag{65}
$$

Let us concentrate on the last relation of the above eq.(65). The condition on the lightest CP even Higgs mass, m_h, tell us that it should be equal to m_Z in the limit $\tan\beta$ is saturated to be maximum, such that $\cos2\beta \rightarrow 1$ and $m_A \rightarrow \infty$. If these limits are not saturated, it is evident that the light higgs mass is less that m_Z. This is one of main predictions of MSSM which could make it easily falsifiable from the current generation of experiments like LEP, Tevatron and the upcoming LHC. Given that present day experiments have not found a Higgs less that Z-boson mass, it is tempting to conclude that the MSSM is not realised in Nature. However caution should be exercised before taking such a route as our results are valid only at the tree level. In fact, in a series of papers in the early nineties [28], it has been shown that large one-loop corrections to the Higgs mass can easily circumvent this limit.

The light Higgs Spectrum at 1-loop

As mentioned previously, radiative corrections can significantly modify the mass relations which we have presented in the previous section. As is evident, these corrections can be very important for the light Higgs boson mass. Along with the 1-loop corrections previously, in the recent years dominant parts of two-loop corrections have also been available [29] with a more complete version recently given [30]. In the following we will present the one-loop corrections to the light Higgs mass and try to understand the implications for the condition eq.(65). Writing down the 1-loop corrections to the CP-even part of the Higgs mass matrix as :

$$
M_{Re}^2 = M_{Re}^2(0) + \delta M_{Re}^2,
\tag{66}
$$

where $M_{Re}^2(0)$ represents the tree level mass matrix given by eq.(62) and δM_{Re}^2 represents its one-loop correction. The dominant one-loop correction comes from the top quark and stop squark loops which can be written in the following form:

$$
\delta M_{Re}^2 = \begin{pmatrix} \Delta_{11} & \Delta_{12} \\ \Delta_{12} & \Delta_{22} \end{pmatrix},
\tag{67}
$$

where

$$
\begin{aligned}
\Delta_{11} &= \frac{3G_F m_t^4}{2\sqrt{2}\pi^2 sin^2\beta} \left[\frac{\mu(A_t + \mu cot\beta)}{m_{\tilde{t}_1}^2 - m_{\tilde{t}_2}^2} \right]^2 \left(2 - \frac{m_{\tilde{t}_1}^2 + m_{\tilde{t}_2}^2}{m_{\tilde{t}_1}^2 - m_{\tilde{t}_2}^2} ln\frac{m_{\tilde{t}_1}^2}{m_{\tilde{t}_2}^2} \right) \\
\Delta_{12} &= \frac{3G_F m_t^4}{2\sqrt{2}\pi^2 sin^2\beta} \left[\frac{\mu(A_t + \mu cot\beta)}{m_{\tilde{t}_1}^2 - m_{\tilde{t}_2}^2} \right] ln\frac{m_{\tilde{t}_1}^2}{m_{\tilde{t}_2}^2} + \frac{A_t}{\mu}\Delta_{11} \\
\Delta_{22} &= \frac{3G_F m_t^4}{\sqrt{2}\pi^2 sin^2\beta} \left[ln\frac{m_{\tilde{t}_1}^2 m_{\tilde{t}_2}^2}{m_t^2} + \frac{A_t(A_t + \mu cot\beta)}{m_{\tilde{t}_1}^2 - m_{\tilde{t}_2}^2} ln\frac{m_{\tilde{t}_1}^2}{m_{\tilde{t}_2}^2} \right] + \frac{A_t}{\mu}\Delta_{11}
\end{aligned}
\tag{68}
$$

In the above G_F represents Fermi Decay constant, m_t, the top mass, $m_{\tilde{t}_1}^2$, $m_{\tilde{t}_1}^2$ are the eigenvalues of the stop mass matrix and A_t is the trilinear scalar coupling (corresponding to the top Yukawa coupling) in the stop mass matrix. μ and the angle β have their usual meanings. Taking in to account these corrections, the condition (65) takes the form:

$$
m_h^2 < m_Z^2 cos^2 2\beta + \Delta_{11} cos^2\beta + \Delta_{12} sin2\beta + \Delta_{22} sin^2\beta
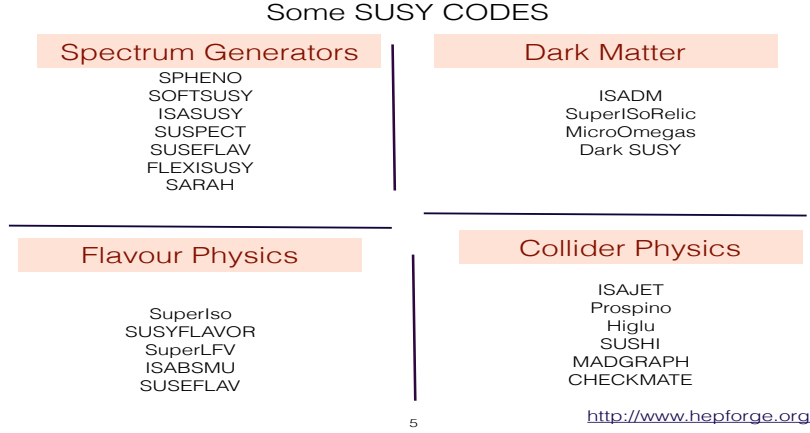\tag{69}
$$

Some SUSY CODES

Spectrum Generators
SPHENO
SOFTSUSY
ISASUSY
SUSPECT
SUSEFLAV
FLEXISUSY
SARAH

Dark Matter
ISADM
SuperISoRelic
MicroOmegas
Dark SUSY

Flavour Physics
SuperIso
SUSYFLAVOR
SuperLFV
ISABSMU
SUSEFLAV

Collider Physics
ISAJET
Prospino
Higlu
SUSHI
MADGRAPH
CHECKMATE

http://www.hepforge.org

5

Fig. 5: Some of the computer codes relevant for studying supersymmetric phenomenology.

Given that m_t is quite large, almost twice the m_Z mass, for suitable values of the stop masses, it is clear that the tree level upper limit on the light Higgs mass is now evaded. However, a reasonable upper limit can still be got by assuming reasonable values for the stop mass. For example assuming stop masses to be around 1 TeV and maximal mixing the stop sector, one attains an upper bound on the light Higgs mass as:

$$m_h \stackrel{<}{\sim} 135 \text{ GeV}. \tag{70}$$

8.5 Feynman Rules

In this section, we have written down all the mass matrices of the superpartners, their eigenvalues and finally the eigenvectors which are required to transform the superpartners in to their physical basis. The feynman rules corresponding to the various vertices have to be written down in this basis. Thus various soft supersymmetry breaking and supersymmetry conserving parameters entering these mass matrices would now determine these couplings as well as the masses, which in turn determine the strength of various physical processes like crosssections and decay rates. A complete list of the Feynman rules in the mass basis can be found in various references like Physics Reports like Haber & Kane [26] and D Chung et. al [32] and also in textbooks like Sparticles [27] and Baer & Tata [31]. A complete set of Feynman rules is out of reach of this set of lectures. Here I will just present two examples to illustrate the points I have been making here.

Due to the mixing between the fermionic partners of the gauge bosons and the fermionic partners of the Higgs bosons, the gauge and the yukawa vertices get mixed in MSSM. We will present here the vertices of fermion-sfermion-chargino and fermion-sfermion-neutralino where this is evident.

(i) Fermion-Sfermion-Chargino :

This is the first vertex on the left of the figure. The explicit structure of this vertex is given by:

$$\tilde{C}_{iAX} = C_{iAX}^R P_R + C_{iAX}^L P_L \tag{71}$$

where $P_L(P_R)$ are the project operators[12] and C^R and C^L are given by

$$c_{iAX}^R = -g_2(U)_{A1} R_{Xi}^\nu \tag{72}$$

$$C_{iAX}^L = g_2 \frac{m_{l_i}}{\sqrt{2} m_W \cos\beta} (V)_{A2} R_{Xi}^\nu \tag{73}$$

In the above U and V are the diagonalising matrices of chargino mass matrix M_C, R^ν is the diagonalising matrix of the sneutrino mass matrix, $M_{\tilde{\nu}}^2$. And the indices A and X runs over the dimensions of the

---

[12]$P_L = (1 - \gamma_5)/2$ and $P_R = (1 + \gamma_5)/2$.

respective matrices ($A = 1, 2$ for Charginos, $X = 1, 2, 3$ for sneutrinos), whereas i as usual runs over the generations, m_{l_i} is the mass of the i th lepton and rest of the parameters carry the standard definitions.
(ii) Fermion-Sfermion-Neutralino :
In a similar manner, the fermion-sfermion-neutralino vertex is given by:

$$\tilde{D}_{iAX} = D^R_{iAX} P_R + D^L_{iAX} P_L \tag{74}$$

where D^L and D^R have the following forms:

$$D^R_{iAX} = -\frac{g_2}{\sqrt{2}} \left\{ \left[-N_{A2} - N_{A1} tan\theta_W \right] R^l_{Xi} + \frac{m_{l_i}}{m_W cos\beta} N_{A3} R^l_{X,i+3} \right\} \tag{75}$$

$$D^L_{iAX} = -\frac{g_2}{\sqrt{2}} \left\{ \frac{m_{l_i}}{m_W cos\beta} N_{A3} R^l_{Xi} + 2N_{A1} tan\theta_W R^l_{X,i+3} \right\} \tag{76}$$

In the above N is diagonalising matrices of neutralino mass matrix M_N, R^l is the diagonalising matrix of the slepton mass matrix, $M^2_{\tilde{l}}$. And the indices A and X runs over the dimensions of the respective matrices ($A = 1, .., 4$ for neutralinos, $X = 1, .., 6$ for sleptons), whereas i as usual runs over the generations.

9   Phenomenology of Supersymmetric Models

We now have all the ingredients to discuss the phenomenology of supersymmetric theories. Before doing that, let us summarise some main features of supersymmetric theories:

- Supersymmetric theories are calculable. Compared to other extensions of SM, this is one of the most important positive characteristics of supersymmetric theories.
- The three gauge couplings unify in MSSM leading to a successful incorporation of it in a Grand Unified theory.
- As discussed before, the Higgs mass remains stable under radiative corrections.
- The MSSM with R-parity also provides a natural dark matter candidate in terms of the lightest supersymmetric particle (LSP). In most models, the LSP is the lightest neutralino providing a good WIMP candidate.

The spectrum of the supersymmetric particles discussed so far in sections 8 is defined at the tree level, except for the Higgs mass. In actual phenomenological calculations, radiative corrections to the all mass matrices and couplings are computed. The MSSM parameters are masses are typically defined at 1-loop level and the SM parameters defined at two loop level. Most of these calculations are tedious, long and are done by computer programs called spectrum generators. These programs not only compute the masses at high precision, but also compute that the electroweak symmetry breaking conditions, direct and indirect constraints on supersymmetric spectrum, supersymmetric contributions to rare processes like $b \rightarrow s\gamma$ etc are also computed. Some of these spectrum generators are SOFTSUSY, SPHENO,suspect, etc. We have constructed our own spectrum generator SUSEFLAV. While these have been the traditional spectrum generators, recently, there have been more flexible programs available which have much larger applicability like Flexisusy, SARAH etc. The reference [33] provides more detailed discussions in this regard. A small summary of available programs is available in Fig 5.

The phenomenology of supersymmetry can divided in to three small sub-areas through which we probe supersymmetry : (a) LHC searches (b) Flavour and other precision measurements like electric and magnetic dipole moments (c) Astrophysical/cosmological probes like dark matter, matter-anti-matter relic density etc. These three 'roads' are schematically depicted in Fig 6. We now review the present status of each of these sectors. An additional sector which has huge impact on various models of supersymmetry breaking is the Higgs sector which will be summarised in the next section. For a recent review on the present status of supersymmetric models, please see, N. Craig's review [34].
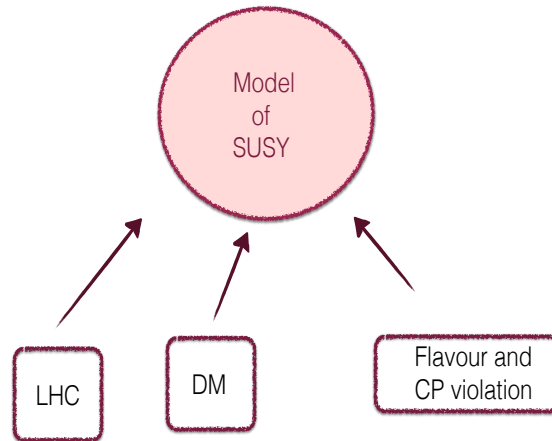
Fig. 6: A schematic representation of the three directions through which we probe supersymmetry
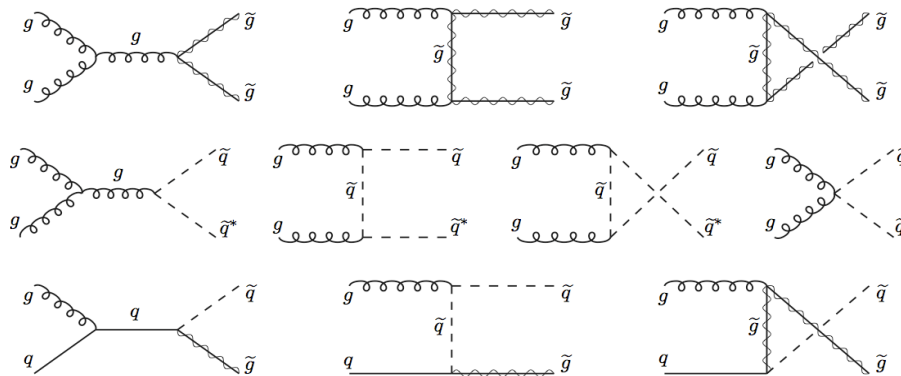

Fig. 7: A list of Feynman diagrams contributing to the production of gluinos and first two generation squarks is presented above. From Ref. [59]

9.1 LHC limits

At the LHC, the dominant processes are strong processes, which lead to the production of strongly interacting supersymmetric particles, such as gluinos and squarks. The main production channels are through qq, qg, and gg initial states as depicted in Fig 7. These production cross-sections are large about 1pb first two generations of squarks and gluinos if their masses are around a TeV. The cross-sections however fall off rapidly with increasing masses as shown in Fig. 8. As can be seen in the figure, the production cross-sections for stops are about an order of magnitude smaller for 100 GeV stops, but fall even more rapidly reaching ~ 10 fb for 1 TeV stops. The backgrounds are very large, typically by several orders of magnitude as shown in Fig. 8. Inspite of these difficulties, the LHC experiments, ATLAS and CMS looking for supersymmetry have already put strong constraints on the masses of the superpartners.

As expected the strongest constraints are on the coloured supersymmetric partners such as gluinos and first two generation squarks. Gluinos are ruled out between 0.8-2.1 TeV depending on the lightest neutralino mass. Similarly the first two generation squarks are ruled out up to 1-2.0 TeV. The third generation top partners, the stops are ruled out between 200-700 GeV. The limits on weakly interacting particles such as charginos and neutralinos are steadily improving and reaching to 1 TeV in some extreme limits. It should be noted that most of these limits are within simplified models of supersymmetry and
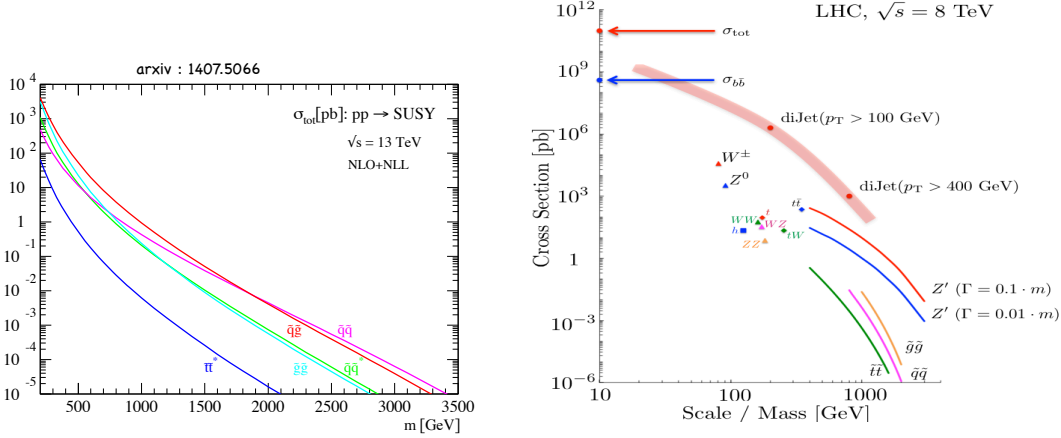
Fig. 8: A summary of production crosssection magnitudes (left) and backgrounds (right) is presented in the above figures.

therefore could lead to large variations in various other models.

A summary of these limits are presented in Fig. 9.

9.2 Flavour Constraints

Flavour physics is already covered in this school [37]. Here, I focus on the discussion relavant for MSSM. The supersymmetric soft terms introduced in the Sec. 6 contain flavour violating soft terms.

$$
\begin{aligned}
\mathcal{L}_{soft} \;=\;& m_{Q_{ii}}^2 \tilde{Q}_i^\dagger \tilde{Q}_i + m_{u_{ii}}^2 \tilde{u}^{c\,\star}_i \tilde{u}^c_i + m_{d_{ii}}^2 \tilde{d}^{c\,\star}_i \tilde{d}^c_i + m_{L_{ii}}^2 \tilde{L}_i^\dagger \tilde{L}_i + m_{e_{ij}}^2 \tilde{e}^{c\,\star}_i \tilde{e}^c_i \\
&+ \left(\Delta_{i\neq j}^{u,d}\right)_{LL} \tilde{Q}_i^\dagger \tilde{Q}_j + \left(\Delta_{i\neq j}^{u}\right)_{RR} \tilde{u}^{c\,\star}_i \tilde{u}^c_j + \left(\Delta_{i\neq j}^{d}\right)_{RR} \tilde{d}^{c\,\star}_i \tilde{d}^c_j \\
&+ \left(\Delta_{i\neq j}^{l}\right)_{LL} \tilde{L}_i^\dagger \tilde{L}_j + \left(\Delta_{i\neq j}^{l}\right)_{LR} \tilde{e}^{c\,\star}_i \tilde{e}^c_j + \dots
\end{aligned}
\tag{77}
$$

As mentioned previously, the soft mass terms m_{ij}^2 and the trilinear scalar couplings A_{ijk} can violate flavour. This gives us new flavour violating structures beyond the standard CKM structure of the quark sector which can also be incorporated in the MSSM. Furthermore, all these couplings can also be complex and thus could serve as new sources of CP violation in addition to the CKM phase present in the Standard Model. Given that all these terms arbitrary and could be of any magnitude close to weak scale, these terms can contribute dominantly compared to the SM amplitudes to various flavour violating processes at the weak scale, like flavour violating decays like $b \to s + \gamma$ or flavour oscillations like $K^0 \leftrightarrow \bar{K}^0$ etc and even flavour violating decays which do not have any Standard Model counterparts like $\mu \to e + \gamma$ etc. A sample Feynman diagrams are listed in Fig. 10. The CP violating phases can also contribute to electric dipole moments (EDM)s which are precisely measured at experiments.

To analyse the phenomenological impact of these processes on these terms, an useful and powerful tool is the so called Mass Insertion (MI) approximation. In this approximation, we use flavour diagonal gaugino vertices and the flavour changing is encoded in non-diagonal sfermion propagators. These propagators are then expanded assuming that the flavour changing parts are much smaller than the flavour diagonal ones. In this way we can isolate the relevant elements of the sfermion mass matrix for a given flavour changing process and it is not necessary to analyse the full 6×6 sfermion mass matrix. Using this method, the experimental limits lead to upper bounds on the parameters (or combinations of) $\delta_{ij}^f \equiv \Delta_{ij}^f / m_{\tilde{f}}^2$, known as mass insertions; where Δ_{ij}^f is the flavour-violating off-diagonal entry appearing in the $f = (u, d, l)$ sfermion mass matrices and $m_{\tilde{f}}^2$ is the average sfermion mass. In addition, the
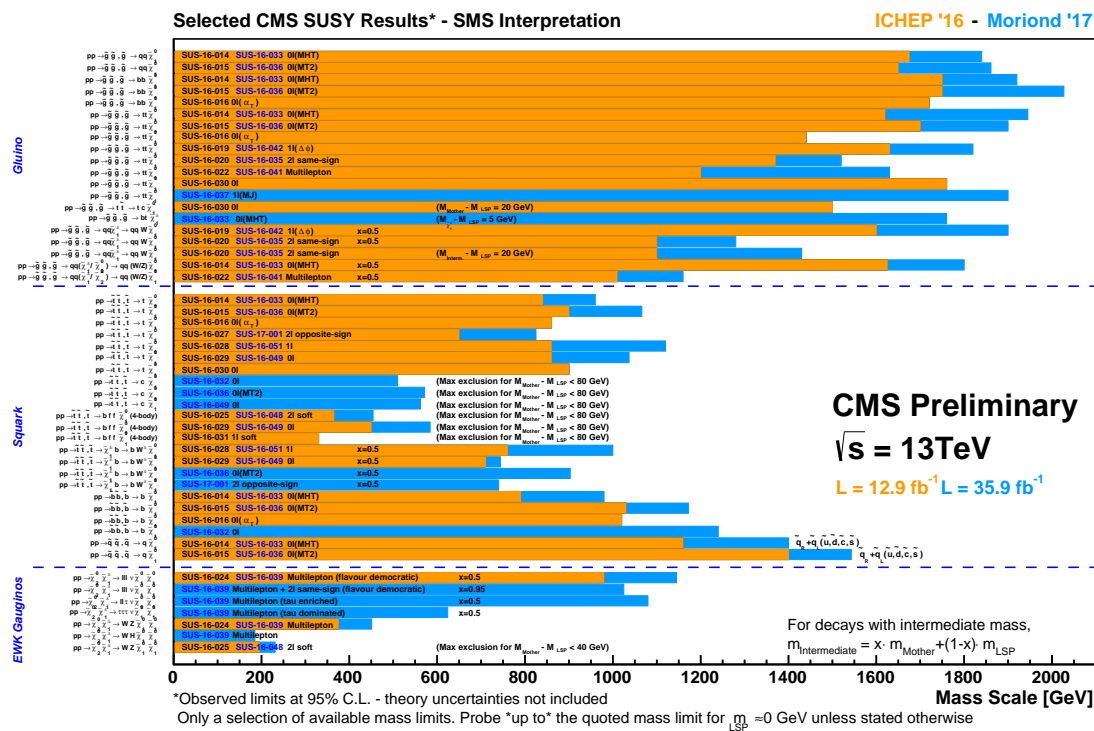
Fig. 9: A summary of current limits are presented from the CMS [35] experiment. Similar results are also presented by the ATLAS experiment. [36]
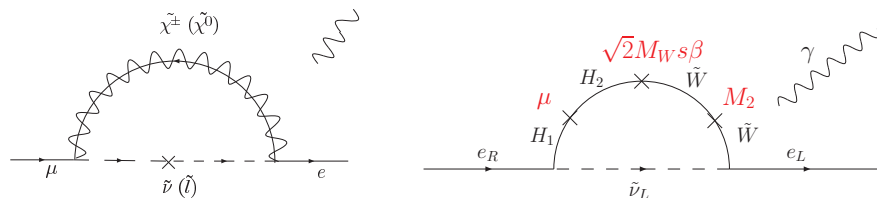

Fig. 10: Feynman Diagram contributing to the rare decay $\mu \to e + \gamma$ in mass eigenstate basis (left) and in mass insertion basis or flavour basis (right).

.

mass-insertions are further sub-divided into LL/LR/RL/RR types, labeled by the chirality of the corresponding SM fermions. The latest set of results on the hadronic sector can be found in [38] and in the leptonic sector in [39]. The limits on various δ's coming from various flavour violating processes have been computed and tabulate in the literature and can be found for instance in Ref. [40, 41] (For a more recent statistical approach, see also [42]).

These limits show that the flavour violating terms should be typically at least a couple of orders of magnitude suppressed compared to the flavour conserving soft terms. The flavour problem could also be alleviated by considering decoupling soft masses or alignment mechanisms (see [40] and references there in). While this is true for the first two generations of soft terms, the recent results from B-factories have started constraining flavour violating terms involving the third generation too.

ij AB	LL	LR	RL	RR
12	1.4×10^{-2}	9.0×10^{-5}	9.0×10^{-5}	9.0×10^{-3}
13	9.0×10^{-2}	1.7×10^{-2}	1.7×10^{-2}	7.0×10^{-2}
23	1.6×10^{-1}	4.5×10^{-3}	6.0×10^{-3}	2.2×10^{-1}

Fig. 11: Bounds on $(\delta)_{ij}^d$) from Flavour data in the hadronic sector from the paper [41]. The parameter space chosen is such that the third generation squark masses are close to 500 GeV and the weakly interacting gauginos are around 200 GeV. These bounds scale inversely with the squark mass and thus can be scaled for the present limits on them.

An important point is that if we set all the flavour violating off-diagonal entries to zero through some mechanism or by choosing an appropriate supersymmetry breaking mechanism (as we will see in the next section), contribution from supersymmetric sector to flavour violation will not be completely zero. This is because CKM (Cabibbo-Kobayashi-Masakawa) matrix will induce non-trivial flavour violating interactions between the SM fermion and it's supersymmetric partner. One of the strongest constraints in this case comes from BR$(b \to s + \gamma)$ which has been measured very precisely by the experimental collaborations (with an error of about 5% at the one sigma level). The present numbers are as follows [43]

$$
\begin{aligned}
BR(b \to s + \gamma)^{exp} &= (3.43 \pm 0.21 \pm 0.07) \times 10^{-4} \\
BR(b \to s + \gamma)^{SM} &= (3.36 \pm 0.23) \times 10^{-4}
\end{aligned}
\tag{78}
$$

Given the closeness of the Standard Model expectation to the experimental number, any new physics should either be very heavy such that it's contributions to this rare process are suppressed or should contain cancellations within its contributions such that the total SM+ New physics contribution is close to the experimental value. Both these scenarios are possible within the MSSM. If supersymmetric partners are heavy $\gtrsim$ a few TeV, then their contributions to $b \to s + \gamma$ are highly suppressed. On the other hand, it is possible that the dominant contributions from charged Higgs and the chargino diagrams cancel with each other (they come with opposite sign) for a large region of the parameter space. The general class of new physics models which do not introduce any new flavour violation other than the one originating from the CKM matrix in the Standard Model come under the umbrella of "Minimal Flavour Violation" [44].

9.3 Dark Matter

While supersymmetry offers many dark matter candidates like axino, saxion, gravitino etc, one of the most popular candidate is the lightest neutralino. For reviews, please see [45]. The neutralinos are as we have seen linear combinations of neutral gauginos and higgsinos. The composition of the lightest neutralino determines it's annihilation cross-section, which in turn determines its mass required to satisfy the relic density of the universe. The relic density has been measured very well by the satellite based experiments of the cosmic microwave background radiation (CMB), notably by WMAP and the Planck satellites. The present day relic density is given to be [46]

$$
\Omega_{\text{CDM}} h^2 = 0.01199 \pm 0.0022
\tag{79}
$$

Note that the lightest neutralino from the neutralino mass matrix of eq.(45) has the form

$$
M_{\chi_1^0} = N_{\tilde{B}1} \tilde{B}^0 + N_{\tilde{W}1} \tilde{W}^0 + N_{\tilde{H}_u1} \tilde{H}_u^0 + N_{\tilde{H}_d1} \tilde{H}_d^0
\tag{80}
$$

We now look at various possible compositions of the LSP to satisfy this relic density.

f (a) *Pure Bino:* If the neutralino is a pure Bino, the annihilation cross-section is given by [47]

$$\langle \sigma_\chi v \rangle = \frac{3g^4 \tan \theta_W^4 r(1+r^2)}{2\pi m_{\tilde{e}_R}^2 x(1+r)^4} \tag{81}$$

where $x = \frac{M_1}{T}$ the mass of the bino over the temperature and $r =$. θ_W is the weak mixing angle, or the Weinberg angle. The relic density in this case is given by

$$\Omega_{\tilde{B}} h^2 = 1.3 \times 10^{-2} \left(\frac{m_{\tilde{e}_R}}{100 \text{ GeV}} \right)^2 \frac{(1+r)^4}{r^2(1+r)^2} \left(1 + 0.07 \log \frac{\sqrt{r} \ 100 \text{ GeV}}{m_{\tilde{e}_R}} \right) \tag{82}$$

The above relic density is typically large for reasonable range of parameters. One thus invokes typically co-annihilating partners which are very close in the mass with the bino, there by increasing the cross-section and there by bringing down the relic density to acceptable levels.

(b) *Pure Wino:* In this case the cross-section of the dark matter particle goes as g, the weak coupling and is given by

$$\langle \sigma_\chi v \rangle = \left(\frac{3g^4}{16\pi M_2^2} \right) \tag{83}$$

where M_2 stands for the Wino mass. The relic density is approximately given by

$$\Omega_{\tilde{W}} h^2 \sim 0.13 \left(\frac{M_2}{2.5 \text{ TeV}} \right)^2 \tag{84}$$

This requires heavy Neutralino of the order of 2.5 TeV.

(c) *Pure Higgsino:* In this case the cross-section of the dark matter particle is given by

$$\langle \sigma_\chi v \rangle = \frac{3g^4}{512\pi\mu^2} \left(21 + 3 \tan \theta_W^2 + 11 \tan \theta_W^4 \right) \tag{85}$$

The relic density in this case is given by

$$\Omega_{\tilde{H}} h^2 \sim 0.10 \left(\frac{\mu}{1 \text{ TeV}} \right)^2 \tag{86}$$

A neutralino of 1 TeV would be required to satisfy the relic density. In summary a pure bino neutralino can be light but would require co-annihilating partners (or other mechanisms) to have the correct relic density, whereas both a pure Higgsino or a pure Wino would have to close to a TeV or larger. Admixtures of various components can however give the right relic density.

In addition to the relic density constraint, the WIMP dark matter is tested at the various direct detection experiments summarised in your cosmology lectures [13]. They also receive constraints from various indirect dark matter detection experiments like FERMI, AMS 02 etc. Here we present the updated constraints for various supersymmetric models from Ref. [48]. From the figures, one can see that supersymmetric neutralino dark matter is strongly constrained from the LUX results. Regions with co-annihilations are still largely allowed.

9.4 Higgs Mass Constraint

This part of the lectures might have been discussed already in the school [49]. As we have seen in the MSSM, the lightest neutral Higgs mass is a calculable quantity. It an be considered as a prediction of a supersymmetric model as it is dependent dominantly on a very few parameters such as $\tan \beta$, stop masses, and the stop mixing paramter $X_t \equiv A_t + \mu \cot \beta$. Thus the measured Higgs can be provide a strong constraint on supersymmetric models. In fact, this constraint is as strong as the constraint from
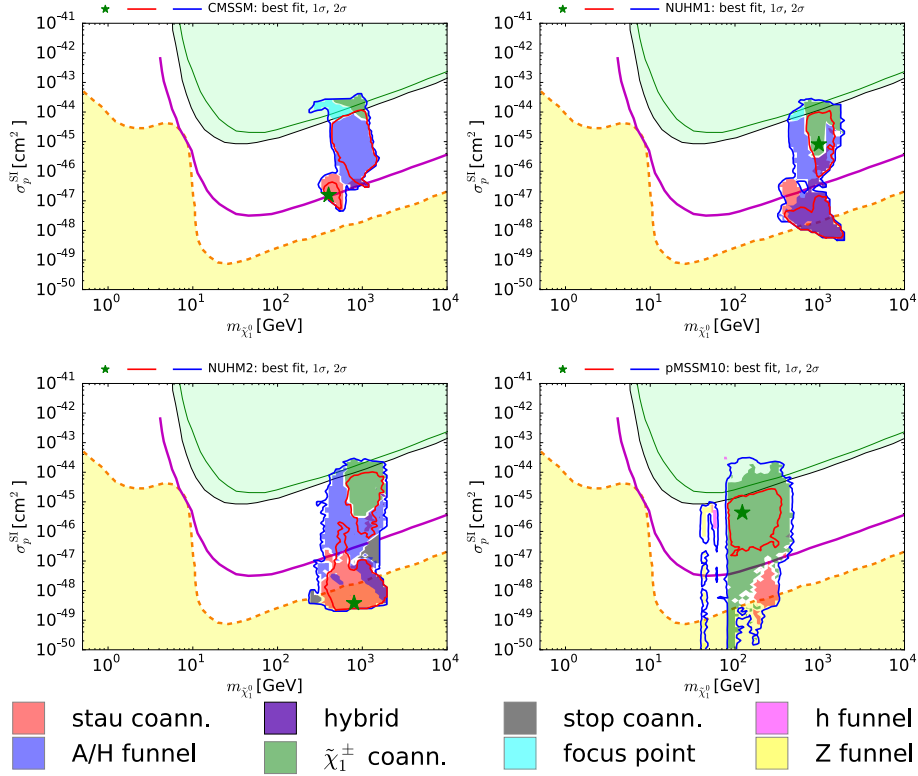
Fig. 12: Status of supersymmetric dark matter searches [48]: exclusion limits in the CMSSM (upper left), the NUHM1 (upper right), the NUHM2 (lower left) and the pMSSM10 (lower right). The red and blue solid lines are the $\Delta\chi^2 = 2.30$ and 5.99 contours, and the solid purple lines show the projected 95% exclusion sensitivity of the LUX-Zepelin (LZ) experiment. The green and black lines show the current sensitivities of the XENON100 and LUX experiments, respectively, and the dashed orange line shows the astrophysical neutrino 'floor', below which astrophysical neutrino backgrounds dominate (yellow region).

non-discovery of supersymmetry particles at the LHC, summarised in section 9.1 if not stronger. The calculation of the Higgs mass is done currently at three loop level. While the 1-loop corrections are large, two loop corrections can also be significant giving corrections to the order of 10-12 GeV in regions of parameter space. While recently full three loop calculations are being done, the efforts are towards bringing down the theoretical error in the Higgs mass computation to be around 1 GeV. For a recent review on the computation of the Higgs mass in MSSM, including various schemes, please see Patrick Draper's review [50].

To see implications of the Higgs mass measurement on supersymmetric stop parameter space, please see fig (13). We can see from the figure that for zero stop mixing $X_t \sim 0$, the stops should be above 3 TeV or heavier to give the correct Higgs mass. On the other hand, in the limit of maximal stop mixing $X_t \sim \sqrt{6}m_{susy}$, where $m_{susy} = \sqrt{m_{\tilde{t}_1}m_{\tilde{t}_2}}$, stop can be as light as a couple hundred GeV. This 'no-go' theorem should be considered from the point of view of discoverability at LHC. While stops up to 1-1.5 TeV can be discovered by the time full run of LHC is completed, it is not possible produce stops of the order of 3-4 TeV at the LHC. Since typically stops are the lightest colored particles in most supersymmetric models, this has strong implications on discoverability of various supersymmetric models.

Due to the requirement that the X_t should be large to generate the right higgs mass, another important constraint comes to play. This is from the scalar potential of the MSSM. Remember that X_t is
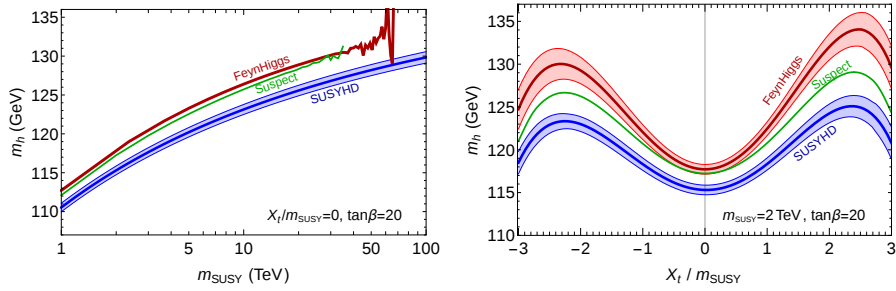
Fig. 13: A comparison [51] of the various computations of the Higgs mass in MSSM: the EFT computation (lower blue band) is compared to two existing codes; FeynHiggs and Suspect. A degenerate SUSY spectrum was used with mass $m_{\rm SUSY}$ in the $\overline{\rm DR}$-scheme with $\tan\beta = 20$. The plot on the left shows $m_{\rm h}$ vs $m_{\rm SUSY}$ for vanishing stop mixing. The plot on the right shows $m_{\rm h}$ vs $X_t/m_{\rm SUSY}$ for $m_{\rm SUSY} = 2$ TeV. On the left plot the instability of the non-EFT codes at large $m_{\rm SUSY}$ is visible.
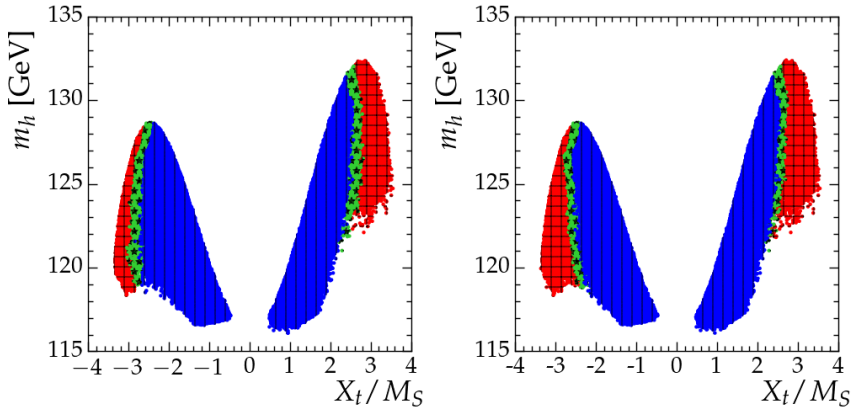

Fig. 14: Stable (blue, vertical lines), meta-stable (green, stars) and unstable (red, checkered) vacuum in the $m_{\rm h}$ vs X_t/M_S plane, from three-field analysis (left) and four-field analysis (right) [52].

a trilinear term of stops and the Higgs, and thus, there is a danger that the stops get a vacuum expectation value for large values of it. If stop fields get a vaccum expectation value, they break the charge and colour symmetries of the Standard Model which is unwanted and unphysical. Thus these regions of the parameter space should be avoided. In Fig. (14), we show the present constraints from charge and colour breaking minima and in the parameter space of X_t and higgs mass from the Ref. [52]. As can be seen, a significant portion of the Higgs mass region is invalid or unphysical due to constraints from charge and colour breaking minima.

10 'Standard' Models of Supersymmetry breaking

So far we have included supersymmetry breaking within the MSSM through a set of explicit supersymmetry breaking soft terms however, at a more fundamental we would like to understand the origins of these soft terms as coming from a theory where supersymmetry is spontaneously broken. In a previous section, we have mentioned that supersymmetry needs to be broken spontaneously in a hidden sector and then communicated to the visible sector through a messenger sector. In the below we will

consider two main models for the messenger sector (a) the gravitational interactions and (b) the gauge interactions. But before we proceed to list problems with the general form soft supersymmetry breaking terms as discussed in the previous section. This is essential to understand what kind of constructions of supersymmetric breaking models are likely to be realised in Nature and thus are consistent with phenomenology.

The way we have parameterised supersymmetry breaking in the MSSM, using a set of gauge invariant soft terms, at the first sight, seems to be the most natural thing to do in the absence of a complete theory of supersymmetry breaking. However, this approach is itselves laden with problems as we realise once we start confronting this model with phenomenology. The two main problems can be listed as below:

(i). Large number of parameters

Compared to the SM, in MSSM, we have a set of more than 50 new particles; writing down all possible gauge invariant and supersymmetry breaking soft terms, limits the number of possible terms to about 105. All these terms are completely arbitrary, there is no theoretical input on their magnitudes, relative strengths, in short there is no theoretical guiding principle about these terms. Given that these are large in number, they can significantly effect the phenomenology. In fact, the MSSM in its softly broken form seems to have lost predictive power except to say that there are some new particles within a broad range in mass(energy) scale. The main culprit being the large dimensional parameter space ~ 105 dimensional space which determines the couplings of the supersymmetric particles and their the masses. If there is a model of supersymmetry breaking which can act as a guiding principle and reduce the number of free parameters of the MSSM, it would only make MSSM more predictive.

(ii). Large Flavour and CP violations. We have seen in the previous section that generic supersymmetry breaking leads to large flavour and CP violating soft terms. The limits are very strong on these terms. In light of this stringent constraint, it is more plausible to think that the fundamental supersymmetry breaking mechanism some how suppresses these flavour violating entries. Similarly, this mechanism should also reduce the number of parameters such that the MSSM could be easily be confronted with phenomenology and make it more predictive. We will consider two such models of supersymmetry breaking below which will use two different kinds of messenger sectors.

10.1 Minimal Supergravity

In the minimal supergravity framework, gravitational interactions play the role of messenger sector. Supersymmetry is broken spontaneously in the hidden sector. This information is communicated to the MSSM sector through gravitational sector leading to the soft terms. Since gravitational interactions play an important role only at very high energies, $M_p \sim O(10^{19})$ GeV, the breaking information is passed on to the visible sector only at those scales. The strength of the soft terms is characterised roughly by, $m_{\tilde{f}}^2 \approx M_S^2/M_{planck}$, where M_S is the scale of supersymmetry breaking. These masses can be comparable to weak scale for $M_S \sim 10^{10}$ GeV. This M_S^2 can correspond to the F-term vev of the Hidden sector. The above mechanism of supersymmetry breaking is called supergravity (SUGRA) mediated supersymmetry breaking.

A particular class of supergravity mediated supersymmetry breaking models are those which go under the name of "minimal" supergravity. This model has special features that it reduces to total number of free parameters determining the entire soft spectrum to five. Furthermore, it also removes the dangerous flavour violating soft terms in the MSSM. The classic features of this model are the following boundary conditions to the soft terms at the high scale $\sim M_{Planck}$:

- All the gaugino mass terms are equal at the high scale.
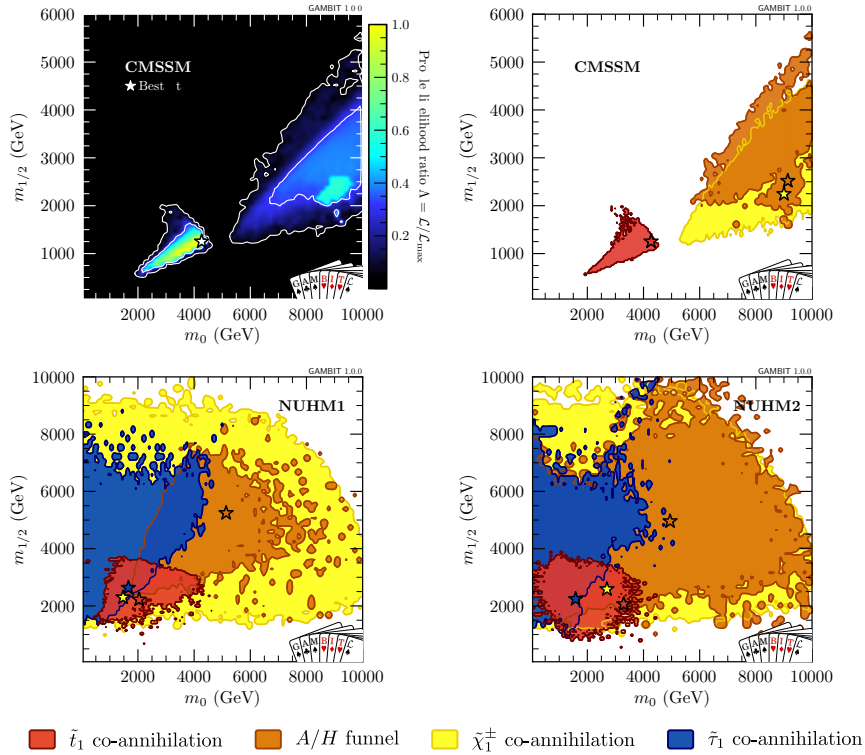
$$M_1 = M_2 = M_3 = M_{1/2}$$

Fig. 15: Status of the CMSSM (top) and NUHM1 and NUHM2 (bottom) models according to GAMBIT [53]. Top left: the profile likelihood ratio (top left) in the $m_0 - m_{1/2}$ plane of the CMSSM. The white lines depict the 68% and 95% CL contours while the white star indicates the best fit. Top right and bottom plots: colouring of the 95% CL regions to indicate which mechanisms contribute to keeping the neutralino relic density below the observed value. Note that the colouring is not exclusive, i.e. overlapping colours indicate that multiple mechanisms may contribute in the given region.

    – All the scalar mass terms at the high scale are equal.

$$m_{\phi_{ij}}^2 = m_0^2 \delta_{ij}$$

    – All the trilinear scalar interactions are equal at the high scale.

$$A_{ijk} = A h_{ijk}$$

    – All bilinear scalar interactions are equal at the high scale.

$$B_{ij} = B$$

Using these boundary conditions, one evolves the soft terms to the weak scale using renormalisation group equations. It is possible to construct supergravity models which can give rise to such kind of strong universality in soft terms close to Planck scale. This would require the Kahler potential of the theory to be of the canonical form. As mentioned earlier, the advantage of this model is that it drastically reduces the number of parameters of the theory to about five, m_0, M (or equivalently M_2), ratio of the *vevs* of the two Higgs, $\tan\beta$, A, B. Thus, these models are also known as 'Constrained' MSSM in literature. The supersymmetric mass spectrum of these models has been extensively studied in literature. The Lightest Supersymmetric Particle (LSP) is mostly a neutralino in this case.

    The present status of the CMSSM is summarised in a detailed analysis by the GAMBIT collaboration [53]. As can be seen from Fig.15, the most of the valid regions point to a very heavy supersymmetric spectrum way outside the reach of the LHC.
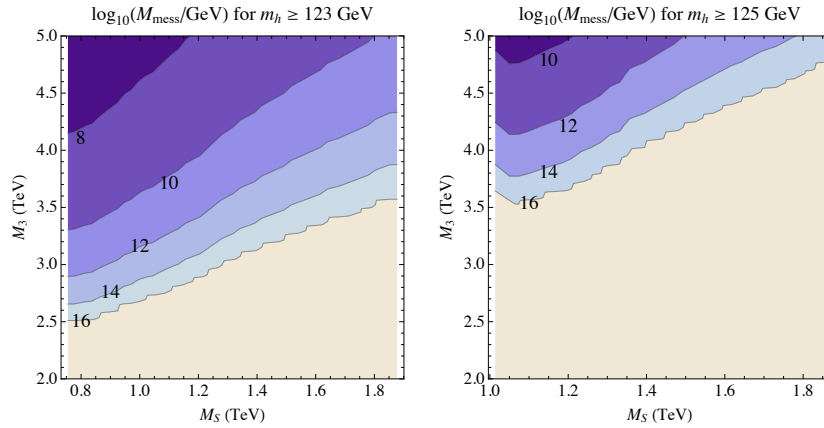
Fig. 16: Implications of the Higgs discovery on minimal GMSB models [54]: the coloured regions indicate the messenger scale required to produce a sufficiently large $|A_t|$ for $m_h = 123$ GeV (left) and $m_h = 125$ GeV (right) through renormalization group evolution.

10.2 Gauge Mediated Supersymmetry breaking

In a more generic case, the Kahler potential need not have the required canonical form. In particular, most low energy effective supergravities from string theories do not posses such a Kahler potential. In such a case, large FCNC's and again large number of parameters are expected from supergravity theories. An alternative mechanism has been proposed which tries to avoid these problems in a natural way. The key idea is to use gauge interactions instead of gravity to mediate the supersymmetry breaking from the hidden (also called secluded sector sometimes) to the visible MSSM sector. In this case supersymmetry breaking can be communicated at much lower energies ~ 100 TeV.

A typical model would contain a susy breaking sector called 'messenger sector' which contains a set of superfields transforming under a gauge group which 'contains' G_{SM}. Supersymmetry is broken spontaneously in this sector and this breaking information is passed on to the ordinary sector through gauge bosons and their fermionic partners in loops. The end-effect of this mechanism also is to add the soft terms in to the lagrangian. But now these soft terms are flavour diagonal as they are generated by gauge interactions. The soft terms at the messenger scale also have simple expressions in terms of the susy breaking parameters. In addition, in minimal models of gauge mediated supersymmetry breaking, only one parameter can essentially determine the entire soft spectrum.

In a similar manner as in the above, the low energy susy spectrum is determined by the RG scaling of the soft parameters. But now the high scale is around 100 TeV instead of M_{GUT} as in the previous case. The mass spectrum of these models has been studied in many papers. The lightest supersymmetric particle in this case is mostly the gravitino in contrast to the mSUGRA case.

The discovery of the Higgs boson with a mass range ~ 126 GeV has put strong constraints on the (minimal) GMSB models. In Fig. 16, we present the analysis of Ref. [54] which shows that it is not possible to generate the correct higgs mass in GMSB models unless the stop and the gluino spectrum is made very heavy, much out of the reach of LHC. Several models have been proposed since then to generate Higgs mass while keeping the stops light $\sim 1-2$TeV. The popular among them involve adding Yukawa interactions between the messengers and the MSSM fields in addition to the gauge interactions. A survey of these kind of models is presented in Ref. [55].

Another popular supersymmetry breaking mechanism is called Anomaly mediated supersymmetry breaking [66], which are not covered in this set of lectures.
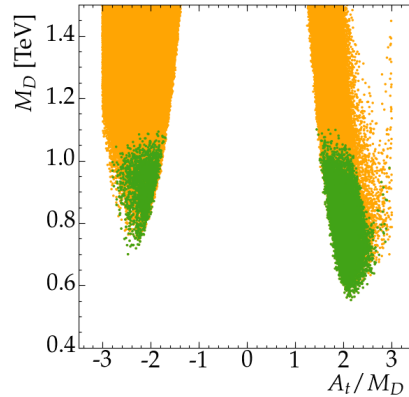
Fig. 17: Parameter space allowed for degenerate/compressed MSSM scenarios [56]. The green (orange) regions in the $A_t - M_D$ plane are consistent with the experimental value of $(g-2)_\mu$ at 2σ (3σ).

10.2.1 Radiative Electroweak symmetry breaking

In both gravity mediated as well as gauge mediated supersymmetry breaking models, we have seen that RG running effects have to included to study the soft terms at the weak scale. Typically, the soft masses which appear at those scales are positive at the high scale. But radiative corrections can significantly modify the low scale values of these parameters; in particular, making one of the Higgs mass squared to be negative at the weak scale leading to spontaneous breaking of electroweak symmetry. This mechanism is called radiative electroweak symmetry breaking.

10.3 Escaping The LHC limits

The LHC has not seen any signals of supersymmetric particles. This has put strong constraints on various supersymmetric models as we have seen. In fact, in most models, this would push all the supersymmetric particles to be very heavy $\sim$ with masses around several TeV. However, it could be that the supersymmetry particles are present within masses close to TeV, and they somehow escaped detection at the LHC. Several ideas were presented : stealth supersymmetry, compressed/degenerate supersymmetry, R-parity violation etc.

In the following we will not go in to the details of all the possible scenarios discussed above but make a few comments on the compressed/degenerate supersymmetry models. In these models, all the supersymmetric particles are almost degenerate in mass. Thus the decay chains of supersymmetric particles produced at LHC will end up leading to very soft (very low energy) final state particles that will not trigger the detectors at the LHC. Thus the only constraints would be from the Higgs mass, $b \rightarrow s + \gamma$ and other indirect constraints. In Fig.17 we show the parameter space remaining after taking in to consideration all these constraints. As you can see, the mass spectrum of MSSM can still be low to give the correct contribution to muon $g - 2$. The degenerate MSSM scenarios are tested by the mono-jet, mono-photon searches at the LHC. The current limits can be found at [35].

11 Remarks

The present set of lectures are only a set of elementary introduction to the MSSM. More detailed accounts can be found in various references which we have listed at various places in the text. In preparing for these set of lectures, I have greatly benefitted from various review articles and text books. I have already listed some of them at various places in the text. Some parts of it are taken from [57, 58]. Martin's review [59] is perhaps the most comprehensive and popular references. It is also constantly updated. Another review which I strongly recommend is by Matteo Bertollini [60]. Some other excellent reviews are [61] and [62].

A concise introduction can also be found in [63]. For more formal aspects of supersymmetry including a good introduction to supergravity please have a look at [64] and [65]. Happy Susying.

Acknowledgements

We would like to thank the Organisers for giving me this wonderful opportunity to teach in the Asia–Europe–Pacific School of High Energy Physics. The questions by the students and the discussion leaders also made the school a wonderful learning place. I also thank the visit to Physics Department of the Technical University of Munich, supported by DFG cluster of excellence EXC 153 "Origin and Structure of the Universe". I also thank the hospitality of IPHT, CEA, Saclay and CNRS, during the final stages of this work. Without these visits, these lectures would not have been possible. He also acknowledges support from Department of Science & Technology, Govt. of India, Grant No : EMR/2016/001097, 'Nature of New Physics Beyond Standard Model'.

Appendices

A   A lightning recap of the Standard Model

The present recap is only for completeness sake and is not considered a detailed introduction to quantum field theories and electroweak standard model can be found in lectures by Prof. Kitano [67].

The Standard Model (SM) is a spontaneously broken Yang-Mills quantum field theory describing the strong and electroweak interactions. The theoretical assumption on which the Standard Model rests on is the principle of local gauge invariance with the gauge group given by

$$G_{SM} \equiv SU(3)_c \times SU(2)_L \times U(1)_Y, \tag{A.1}$$

where the subscript c stands for color, L stands for the 'left-handed' chiral group whereas Y is the hypercharge. The particle spectrum and their transformation properties under these gauge groups are given as,

$$Q_i \equiv \begin{pmatrix} u_{Li} \\ d_{Li} \end{pmatrix} \sim \left(3,\, 2,\, \frac{1}{6}\right) \qquad U_i \equiv u_{Ri} \sim \left(\bar{3},\, 1,\, \frac{2}{3}\right)$$

$$D_i \equiv d_{Ri} \sim \left(\bar{3},\, 1,\, -\frac{1}{3}\right)$$

$$L_i \equiv \begin{pmatrix} \nu_{Li} \\ e_{Li} \end{pmatrix} \sim \left(1,\, 2,\, -\frac{1}{2}\right) \qquad E_i \equiv e_{Ri} \sim (1,\, 1,\, -1)$$

In the above i stands for the generation index, which runs over the there generations $i = 1, 2, 3$. Q_i represents the left handed quark doublets containing both the up and down quarks of each generation. Similarly, L_i represents left handed lepton doublet, U_i, D_i, E_i represent right handed up-quark, down-quark and charged lepton singlets respectively. The numbers in the parenthesis represent the transformation properties of the particles under G_{SM} in the order given in eq.(A.1). For example, the quark doublet Q transforms a triplet (3) under $SU(3)$ of strong interactions, a doublet (2) under weak interactions gauge group and carry a hypercharge $(Y/2)$ of 1/6 [13]. In addition to the fermion spectra represented above, there is also a fundamental scalar called Higgs whose transformation properties are given as

$$H \equiv \begin{pmatrix} H^+ \\ H^0 \end{pmatrix} \sim (1,\, 2,\, 1/2)\,. \tag{A.2}$$

However, the requirement of local gauge invariance will not be fulfilled unless one includes the gauge boson fields also. Including them, the total lagrangian with the above particle spectrum and gauge group can be represented as,

---

[13]Note that the hypercharges are fixed by the Gellman-Nishijima relation $Y/2 = Q - T_3$, where Q stands for the charge of the particle and T_3 is the eigenvalue of the third generation of the particle under $SU(2)$.

$$\mathcal{L}_{SM} = \mathcal{L}_F + \mathcal{L}_{YM} + \mathcal{L}_{yuk} + \mathcal{L}_S. \tag{A.3}$$

The fermion part $\mathcal{L}_F$ gives the kinetic terms for the fermions as well as their interactions with the gauge bosons. It is given as,

$$\mathcal{L}_F = i\bar{\Psi}\gamma^\mu \mathcal{D}_\mu \Psi, \tag{A.4}$$

where Ψ represents all the fermions in the model,

$$\Psi = (Q_i\ U_i,\ D_i,\ L_i,\ E_i) \tag{A.5}$$

where $\mathcal{D}_\mu$ represents the covariant derivative of the field given as,

$$\mathcal{D}_\mu = \partial\mu - ig_s G_\mu^A \lambda^A - i\frac{g}{2}W_\mu^I \tau^I - ig' B_\mu Y \tag{A.6}$$

Here $A = 1, .., 8$ with G_μ^A representing the $SU(3)_c$ gauge bosons, $I = 1, 2, 3$ with W_μ^I representing the $SU(2)_L$ gauge bosons. The $U(1)_Y$ gauge field is represented by B_μ. The kinetic terms for the gauge fields and their self interactions are given by,

$$\mathcal{L}_{YM} = -\frac{1}{4}G^{\mu\nu A}G_{\mu\nu}^A - \frac{1}{4}W^{\mu\nu I}W_{\mu\nu}^I - \frac{1}{4}B^{\mu\nu}B_{\mu\nu} \tag{A.7}$$

with

$$
\begin{aligned}
G_{\mu\nu}^A &= \partial_\mu G_\nu^A - \partial_\nu G_\mu^A + g_s\, f_{ABC}G_\mu^B G_\nu^C \\
F_{\mu\nu}^I &= \partial_\mu W_\nu^I - \partial_\nu W_\mu^I + g\, f_{IJK}W_\mu^J W_\nu^K \\
B_{\mu\nu} &= \partial_\mu B_\nu - \partial_\nu B_\mu,
\end{aligned}
\tag{A.8}
$$

where $f_{ABC(IJK)}$ represent the structure constants of the $SU(3)(SU(2))$ group.

In addition to the gauge bosons, the fermions also interact with the Higgs boson, through the dimensionless Yukawa couplings given by

$$\mathcal{L}_{yuk} = h_{ij}^u \bar{Q}_i U_j \tilde{H} + h_{ij}^d \bar{Q}_i D_j H + h_{ij}^e \bar{L}_i E_j H + H.c \tag{A.9}$$

where $\tilde{H} = i\sigma^2 H^\star$. These couplings are responsible for the fermions to attain masses once the gauge symmetry is broken from $G_{SM} \rightarrow SU(3)_c \times U(1)_{em}$. This itselves is achieved by the scalar part of the lagrangian which undergoes spontaneous symmetry breakdown. The scalar part of the lagrangian is given by,

$$\mathcal{L}_S = (\mathcal{D}_\mu H)^\dagger \mathcal{D}_\mu H - V(H), \tag{A.10}$$

where

$$V(H) = \mu^2 H^\dagger H + \lambda \left(H^\dagger H\right)^2 \tag{A.11}$$

For $\mu^2 < 0$, the Higgs field attains a vacuum expectation value (*vev*) at the minimum of the potential. The resulting goldstone bosons are 'eaten away' by the gauge bosons making them massive through the so-called Higgs mechanism. Only one degree of the Higgs field remains physical, the only scalar particle of the SM - the Higgs boson. The fermions also attain their masses through their Yukawa couplings, once the Higgs field attains a *vev*. The only exception is the neutrinos which do not attain any mass due to the absence of right handed neutrinos in the particle spectrum and thus the corresponding Yukawa couplings. Finally, the Standard Model is renormalisable and anomaly free. We would also insist that the Supersymmetric version of the Standard Model keeps these features of the Standard Model intact.

B   Extra Dimensions and the hierarchy problem

Extra-dimensions with a flat geometry are simplest realizations of models with additional space dimensions. The extra-dimensions are in general compactified on an $n - torus$ thus forming a compact manifold M_n. Thus the total space-time is a $R^{(4)} \times \mathcal{M}_n$ manifold, where $R^{(4)}$ corresponds to the usual $3 + 1$ space-time. In earlier realizations of such theories the SM spectrum was confined on the $3 + 1$ manifold while only gravity was allowed to extend into the bulk. In addition to 1 massless 4D graviton, 1 massless gauge field and 1 massless scalar, we get a tower of massive gravitons called Kaluza-Klein modes.

We now consider examples where specific realizations of extra-dimensional scenarios can be useful in solving the hierarchy problem. They include (a) ADD model (b) RS model.

B.1   ADD model

The proposal to use extra-dimensional brane-world scenarios to solve the hierarchy problem was first put forward by Arkani-Hamed, Dimopoulos and Dvali [69]. The model assumes a setup with n extra spatial dimensions compactified on a $n - sphere$ with equal radius a. The metric for the $4 + n$ dimensional space-time is given as

$$ds^2 = \eta_{\mu\nu}dx^\mu dx^\nu - na^2\phi^2 \tag{B.1}$$

where $0 \leq \phi \leq 2\pi$. While the SM spectrum is assumed to be confined on the 3-brane, only gravity is allowed to propagate in all the $4 + n$ dimensions. The $4 + n$ dimensional gravity action is given as

$$S_{4+n} = M_\star^{2+n} \int d^{4+n}\sqrt{g^{4+n}}R^{4+n} \tag{B.2}$$

where $M_\star$ is the $4 + n$ dimensional fundamental Planck scale. Integrating Eq.(B.2) over the n compact extra dimension yields

$$
\begin{aligned}
S_{4+n} &= M_\star^{2+n}(2\pi a)^n \int d^4x \sqrt{-g^4}R^4 \\
S_{4+n} &= M_\star^{2+n}(2\pi a)^n S_4
\end{aligned}
\tag{B.3}
$$

where the effective 4 dimensional Planck scale is then $M_{pl}^2 = M_\star^{2+n}(2\pi a)^n$ and S_4 effective 4D gravity action.

Putting $M_\star \sim 1$ TeV, we find the condition on the compactification radius a as

$$a \sim \times 10^{\frac{30}{n}-17}\text{cm} \tag{B.4}$$

Putting $n = 1$, above gives a value of a which is $\sim 10^{13}cm$. This would signal deviations from Newtonian gravity at the astronomical scale and hence is ruled out. For $n \geq 2$ we get $a \leq 10^{-2}$ cm thus leading to possible modifications of Newtonian gravity at the sub-millimeter scale. Thus the ADD model links the two fundamental scales of nature by means of a large volume factor related to the size of the bulk. Hence such models are referred to as large extra-dimensional models.

B.2   Randall Sundrum model of warped extra dimension

The ADD model reduced the higher fundamental "Planck" scale to around the TeV scale from which the effective 4D scale of 10^{15} TeV resulted owing to the large volume of the extra-dimensions. This explanation of the hierarchy problem between the electroweak scale and the Planck scale in the ADD model resulted in its reintroduction between the compactification scale (10^{-2} cm) and the electroweak scale (10^{-17} cm). As a result an alternate extra-dimensional mechanism to generate the hierarchy was put forward by Randall and Sundrum [70]. The model consisted of a single extra-dimension compactified on $S1/Z_2$ orbifold. Thus the domain of the extra-dimensional coordinate is $[0, \pi R]$ where R is the

compactification radius. A 3-brane[14] is introduced at each of the orbifold fixed point. The brane at $y = 0$ is referred to as the *hidden* brane while the brane at $y = \pi R$ is referred to as the *visible* brane. Introduction of a large bulk cosmological constant Λ "warps" the bulk. Brane localized sources are added to balance the effects of Λ thereby inducing a vanishing effective 4D cosmological constant. An ansatz for the line element with a warped geometry is given as

$$ds^2 = G_{MN}dx^M dx^N = e^{-2\sigma(y)}\eta_{\mu\nu}dx^\mu dx^\nu - dy^2 \tag{B.5}$$

where $\eta_{\mu\nu}$ is the Minkowski metric. Unlike the ADD case, the presence of the exponential factor e^{-kry} renders this metric to be non-factorizable. The metric induced at each of the orbifold fixed points are given as

$$g_{\mu\nu}^{vis} = G_{\mu\nu}(x^\mu, y = \pi R) \qquad g_{\mu\nu}^{hid} = G_{\mu\nu}(x^\mu, y = 0) \tag{B.6}$$

Thus action for the theory in the absence of any matter is as follows:

$$S = S_{Gravity} + S_{vis} + S_{hid} \tag{B.7}$$

where

$$
\begin{aligned}
S_{Gravity} &= \int d^4x d\phi \sqrt{-G}[2M^3 R + \Lambda] \\
S_{vis} &= \int d^4x \sqrt{-g_s}[-V_{vis}] \\
S_{hid} &= \int d^4x \sqrt{-g_p}[-V_{hid}]
\end{aligned}
$$
$$\tag{B.8}$$

where Λ is the bulk cosmological constant. V_{vis} and V_{hid} are the brane localized potential at the corresponding branes and M is higher dimensional Planck scale. The Einstein's equations corresponding to the action in Eq.(B.8)

$$\frac{\sigma'^2}{R^2} = \frac{-\Lambda}{24M^3} \tag{B.9}$$

$$\sigma'' = \frac{V_{hid}R\delta(\phi)}{12M^3} + \frac{V_{vis}R\delta(\phi - \pi)}{12M^3} \tag{B.10}$$

Solving for σ we get

$$\sigma = R|\phi|\sqrt{\frac{-\Lambda}{24M^3}} \tag{B.11}$$

This solution is valid only for $\Lambda < 0$ implying that the space between the two $3 - branes$ is an *Anti De-Sitter* space. Differentiating σ in Eq.(B.11) twice we get

$$\sigma'' = 2R\sqrt{\frac{-\Lambda}{24M^3}}[\delta(\phi) - \delta(\phi - \pi)] \tag{B.12}$$

Thus comparing above equation with the second line in Eq.(B.10) we get $V_{hid} = -V_{vis} = 24M^3 k, \Lambda = -24M^3 k^2$ where $k = \frac{-\Lambda}{24M^3}$ being the reduced Planck scale. Thus, we see that we have two opposite tension branes. The hidden brane has positive tension and the visible brane tension is the negative of the former.

---

[14]3-brane here means a 4 dimensional spacetime.

The higher dimensional fundamental Planck scale M is related to the effective 4-D Planck scale M_{Pl} by the following relation

$$M_{Pl}^2 = \frac{M^3}{k}\left[1 - e^{-2kR\pi}\right] \tag{B.13}$$

This implies a weak dependence of M_{Pl} on the compactification radius R.

The resolution to the hierarchy problem can be seen by considering the Higgs field to be localized on the visible brane. The action in this case is given as

$$S = \int d^4x\sqrt{-g_{vis}}\left[g_{vis}^{\mu\nu}(\partial_\mu H)^\dagger \partial_\nu H - m^2 H^\dagger H + \lambda(H^\dagger H)^2\right] \tag{B.14}$$

where $\sqrt{-g_{vis}} = e^{-4kR\pi}$ and $g_{vis}^{\mu\nu} = e^{2kR\pi}\eta^{\mu\nu}$. Redefining the Higgs field as $H \to e^{kR\pi}H$ the action in Eq.(B.14) reduces to

$$S = \int d^4x\left[\eta_{vis}^{\mu\nu}(\partial_\mu H)^\dagger \partial_\nu H - (e^{-kR\pi}m)^2 H^\dagger H + \lambda(H^\dagger H)^2\right] \tag{B.15}$$

We see that the effective Higgs mass is now defined as

$$m_{eff} = e^{-kR\pi}m \tag{B.16}$$

Choosing $kR \sim \mathcal{O}(10)$ electroweak scale Higgs mass can be achieved by exponential warping of scales thus solving the Hierarchy problem. The radius R in the RS setup was considered a free parameter and was appropriately adjusted to resolve the hierarchy problem. Metric fluctuations along the radial direction corresponds to the existence of a massless radion. The radius R is determined by the vev of the radion and is not included in the dynamics of the original RS setup. A proposal in this direction to was put forward by Goldberger and Wise [71]. A massive bulk scalar field with brane localized potentials is introduced. The role of the scalar field is to generate a potential for the radion. It can be shown that the radion attains a mass at the minimum of the potential thus generating an R at which the hierarchy problem is solved for reasonable choices of parameters in the radion potential. The radius of the AdS space is very small *i.e.* $R \sim \frac{1}{k}$ and hence such models are referred to as small extra-dimensional models. The observed weakness of gravity in this scenario can be very elegantly explained by the localization of the zero mode gravitons towards the UV resulting in small overlap with IR brane where the SM fields are localized.

References

[1] P. Ramond, *Journeys Beyond The Standard Model*, (Reading, Mass., Perseus Books, 1999).

[2] R. N. Mohapatra, *Unification and Supersymmetry. The Frontiers of quark - lepton physics*, (Springer, Berlin, 1986), p.309.
R. N. Mohapatra, [arXiv:hep-ph/9911272].

[3] G. G. Ross, *Grand Unified Theories* (Reading USA, Benjamin-Cummings, 1984), Frontiers In Physics (Book 60), p. 49.

[4] M. Fukugita and T. Yanagida, *Physics of neutrinos and applications to astrophysics*, (Springer, Berlin, 2003), p. 593.

[5] C. Csáki and P. Tanedo, 2013 European School of High-Energy Physics, Paradfurdo, Hungary, 5 - 18 Jun 2013, edited by M. Mulders and G. Perez, CERN-2015-004 (CERN, Geneva, 2015), pp.169-268, http://dx.doi.org/10.5170/CERN-2015-004.169, [arXiv:1602.04228 [hep-ph]].

[6] G. Bhattacharyya, *Rept. Prog. Phys.*, **74** (2011) 026201, http://dx.doi.org/10.1088/0034-4885/74/2/026201, [arXiv:0910.5095 [hep-ph]].

[7] Romesh Kaul, *Phys. Lett.*, **109B** (1982) 19-24.

[8] Hitoshi Murayama, hep-ph/0002232.

[9] Gerard 't Hooft, *NATO Sci. Ser. B*, **59** (1980) 135-157.

[10] Eldad Gildener, Steven Weinberg (Harvard U.), *Phys. Rev.*, **D13** (1976) 3333.

[11] A. J. Buras, J. R. Ellis, M. K. Gaillard and D. V. Nanopoulos, *Nucl. Phys. B*, **135** (1978) 66. http://dx.doi.org/10.1016/0550-3213(78)90214-6

[12] L. Susskind, *Phys. Rev. D*, **20** (1979) 2619.

[13] T. Moroi, Lectures at this school.

[14] T. Kajitha, Lectures at this school.

[15] For a more thorough historical introduction, see, S. Weinberg, *The quantum theory of fields. Vol. 3: Supersymmetry* (Cambridge, UK, 2000), p. 419.

[16] A. Salam and J. A. Strathdee, *Phys. Rev. D*, **11** (1975) 1521.
A. Salam and J. A. Strathdee, *Fortsch. Phys.*, **26** (1978) 57.

[17] J. Wess and J. Bagger, *Supersymmetry and supergravity* (Princeton, USA, 1992), p. 259.

[18] See for example, the direct experimental limit from Super-K: Y. Hayato *et al.* [Super-Kamiokande Collaboration], *Phys. Rev. Lett.*, **83** (1999) 1529, [arXiv:hep-ex/9904020].

[19] G. Bhattacharyya, [arXiv:hep-ph/9709395].

[20] G. R. Farrar and P. Fayet, *Phys. Lett. B*, **76** (1978) 575.

[21] G. R. Farrar and S. Weinberg, *Phys. Rev. D*, **27** (1983) 2732.

[22] M. C. Bento, L. J. Hall and G. G. Ross, *Nucl. Phys. B*, **292** (1987) 400.

[23] For a detailed introduction to the topic of supersymmetry breaking see for example Markus Luty's TASI Lectures on SUSY breaking : M. A. Luty, [arXiv:hep-th/0509029]. See Also, Y. Shirman, [arXiv:0907.0039 [hep-ph]].

[24] J. F. Gunion, H. E. Haber, G. L. Kane and S. Dawson, "The Higgs Hunter'S Guide," ; See also, A. Djouadi, *Phys. Rept.*, **459** (2008) 1, [arXiv:hep-ph/0503173].

[25] J. A. Casas and S. Dimopoulos, *Phys. Lett. B*, **387** (1996) 107, [arXiv:hep-ph/9606237].

[26] H. E. Haber and G. L. Kane, *Phys. Rept.*, **117** (1985) 75.

[27] M. Drees, R. Godbole and P. Roy, *Theory and phenomenology of sparticles: An account of four-dimensional N=1 supersymmetry in high energy physics* (Hackensack, USA, 2004), p. 555.

[28] H. E. Haber and R. Hempfling, *Phys. Rev. Lett.*, **66** (1991) 1815. J. R. Ellis, G. Ridolfi and F. Zwirner, *Phys. Lett. B*, **257** (1991) 83.

[29] J. R. Espinosa and R. J. Zhang, *Nucl. Phys. B*, **586** (2000) 3, [arXiv:hep-ph/0003246]; A. Brignole, G. Degrassi, P. Slavich and F. Zwirner, *Nucl. Phys. B*, **631** (2002)195, [arXiv:hep-ph/0112177].

[30] S. P. Martin, *Phys. Rev. D*, **75** (2007) 055005, [arXiv:hep-ph/0701051]. S. P. Martin, *Phys. Rev. D*, **71** (2005) 016012, [arXiv:hep-ph/0405022].

[31] H. Baer and X. Tata, *Weak scale supersymmetry: From superfields to scattering events* (Cambridge, UK, 2006), p. 537.

[32] D. J. H. Chung, L. L. Everett, G. L. Kane, S. F. King, J. D. Lykken and L. T. Wang, *Phys. Rept.*, **407** (2005) 1, [arXiv:hep-ph/0312378].

[33] A. Vicente, [arXiv:1507.06349 [hep-ph]].

[34] N. Craig, [arXiv:1309.0528 [hep-ph]].

[35] https://twiki.cern.ch/twiki/bin/view/CMSPublic/PhysicsResultsSUS

[36] https://twiki.cern.ch/twiki/bin/view/AtlasPublic/SupersymmetryPublicResults

[37] Ahmed Ali, Lectures at this school.

[38] http://www.utfibit.org/UTfit/Constraints

[39] L. Calibbi and G. Signorelli, [arXiv:1709.00294 [hep-ph]].

[40] A. Masiero, S. K. Vempati and O. Vives, [arXiv:0711.2903 [hep-ph]].

[41] M. Ciuchini, A. Masiero, P. Paradisi, L. Silvestrini, S. K. Vempati and O. Vives, *Nucl. Phys. B*, **783** (2007) 112, http://dx.doi.org/10.1016/j.nuclphysb.2007.05.032, [hep-ph/0702144 [HEP-PH]].

[42] K. De Causmaecker, B. Fuks, B. Herrmann, F. Mahmoudi, B. O'Leary, W. Porod, S. Sekmen and N. Strobbe, *JHEP*, **1511** (2015) 125, http://dx.doi.org/10.1007/JHEP11(2015)125, [arXiv:1509.05414 [hep-ph]].

[43] M. Misiak *et al.*, *Phys. Rev. Lett.*, **114** (2015) 221801, http://dx.doi.org/10.1103/PhysRevLett.114.221801, [arXiv:1503.01789 [hep-ph]].

[44] G. D'Ambrosio, G. F. Giudice, G. Isidori and A. Strumia, *Nucl. Phys. B*, **645** (2002) 155, http://dx.doi.org/10.1016/S0550-3213(02)00836-2, [hep-ph/0207036].

[45] G. Jungman, M. Kamionkowski and K. Griest, *Phys. Rept.*, **267** (1996) 195, [arXiv:hep-ph/9506380]; K. Griest and M. Kamionkowski, *Phys. Rept.*, **333** (2000) 167. J. Ellis and K. A. Olive, , in *Particle dark matter*, Ed. G. Bertone (Cambridge University Press, UK, 2010), pp. 142-163, [arXiv:1001.3651 [astro-ph.CO]].

[46] P. A. R. Ade *et al.* [Planck Collaboration], *Astron. Astrophys.*, **594** (2016) A13, http://dx.doi.org/10.1051/0004-6361/201525830, [arXiv:1502.01589 [astro-ph.CO]].

[47] N. Arkani-Hamed, A. Delgado and G. F. Giudice, *Nucl. Phys. B*, **741** (2006) 108, http://dx.doi.org/10.1016/j.nuclphysb.2006.02.010, [hep-ph/0601041].

[48] E. A. Bagnaschi *et al.*, *Eur. Phys. J. C*, **75** (2015) 500, http://dx.doi.org/10.1140/epjc/s10052-015-3718-9, [arXiv:1508.01173 [hep-ph]].

[49] J. Ellis, [arXiv:1702.05436 [hep-ph]].

[50] P. Draper and H. Rzehak, *Phys. Rept.*, **619** (2016) 1, http://dx.doi.org/10.1016/j.physrep.2016.01.001, [arXiv:1601.01890 [hep-ph]].

[51] J. Pardo Vega and G. Villadoro, *JHEP*, **1507** (2015) 159, http://dx.doi.org/10.1007/JHEP07(2015)159, [arXiv:1504.05200 [hep-ph]].

[52] D. Chowdhury, R. M. Godbole, K. A. Mohan and S. K. Vempati, *JHEP*, **1402** (2014) 110, http://dx.doi.org/10.1007/JHEP02(2014)110, [arXiv:1310.1932 [hep-ph]].

[53] P. Athron *et al.* [GAMBIT Collaboration], *Eur. Phys. J. C*, **77** (2017) 824, http://dx.doi.org/10.1140/epjc/s10052-017-5167-0, [arXiv:1705.07935 [hep-ph]].

[54] P. Draper, P. Meade, M. Reece and D. Shih, *Phys. Rev. D*, **85** (2012) 095007, http://dx.doi.org/10.1103/PhysRevD.85.095007, [arXiv:1112.3068 [hep-ph]].

[55] P. Byakti and T. S. Ray, *JHEP*, **1305** (2013) 055, http://dx.doi.org/10.1007/JHEP05(2013)055, [arXiv:1301.7605 [hep-ph]]; J. A. Evans and D. Shih, *JHEP*, **1308** (2013) 093, http://dx.doi.org/10.1007/JHEP08(2013)093, [arXiv:1303.0228 [hep-ph]]; P. Byakti, C. K. Khosa, V. S. Mummidi and S. K. Vempati, *JHEP*, **1703** (2017) 028, http://dx.doi.org/10.1007/JHEP03(2017)028, [arXiv:1607.03447 [hep-ph]].

[56] D. Chowdhury, K. M. Patel, X. Tata and S. K. Vempati, *Phys. Rev. D*, **95** (2017) 075025, http://dx.doi.org/10.1103/PhysRevD.95.075025, [arXiv:1612.06471 [hep-ph]].

[57] S. K. Vempati, [arXiv:1201.0334 [hep-ph]].

[58] Abhishek. M Iyer, Ph.D thesis, Indian Institute of Science, 2015.

[59] S. P. Martin, [arXiv:hep-ph/9709356].

[60] Lectures on Supersymmetry by Matteo Bertolini, http://people.sissa.it/ bertmat/teaching.htm

[61] M. E. Peskin, [arXiv:0801.1928 [hep-ph]].

[62] J. A. Bagger, [arXiv:hep-ph/9604232].

[63] C. Csaki, *Mod. Phys. Lett. A* **11** (1996) 599, [arXiv:hep-ph/9606414].

[64] A. Van Proeyen, "Superconformal Tensor Calculus In N=1 And N=2 Supergravity," in Proc. of

Karpacz Winter School, Karpacz, Poland, Feb 14-26, 1983.

[65] P. C. West, *Introduction to supersymmetry and supergravity* (World Scientific, Singapore, 1990), p. 425.

[66] L. Randall and R. Sundrum, *Nucl. Phys. B*, **557** (1999) 79, [arXiv:hep-th/9810155]; G. F. Giudice, M. A. Luty, H. Murayama and R. Rattazzi, *JHEP*, **9812** (1998) 027, [arXiv:hep-ph/9810442].

[67] R. Kitano, Lectures at this school.

[68] *See for example*, A. Dobado, A. Gomez-Nicola, A. L. Maroto and J. R. Pelaez, *Effective lagrangians for the standard model* (Springer-Verlag, USA, 1997), Texts and Monographs in Physics.

[69] N. Arkani-Hamed, S. Dimopoulos and G. R. Dvali, *Phys. Lett. B*, **429** (1998) 263, http://dx.doi.org/10.1016/S0370-2693(98)00466-3, [hep-ph/9803315].

[70] L. Randall and R. Sundrum, *Phys. Rev. Lett.*, **83** (1999) 3370, http://dx.doi.org/10.1103/PhysRevLett.83.3370, [hep-ph/9905221].

[71] W. D. Goldberger and M. B. Wise, *Phys. Rev. Lett.*, **83** (1999) 4922, http://dx.doi.org/10.1103/PhysRevLett.83.4922, [hep-ph/9907447].

Local Organizing Committee

Lijun Guo (IHEP)
Jiangxi Lan (UCAS)
Xiaorui Lyu (UCAS)
Yeliu Mo (IHEP)
Congfeng Qiao (UCAS)
Shanjun Ren (IHEP)
Xiaoyan Shen (IHEP)
Nan Song (IHEP)
Changzheng Yuan (IHEP, Co-chair)
Yangheng Zheng (UCAS, Co-chair)
Shilin Zhu (PKU)

International Organizing Committee

Ashfaq Ahmad (NCP)
Elisabetta Barberio (Melbourne)
Marc Besancon (CEA/Irfu)
Subhasis Chattopadhyay (VECC)
Nick Ellis (CERN, Chair)
Kazunori Hanagaki (KEK)
Yee Bob Hsiung (National Taiwan University)
Kiyotomo Kawagoe (Kyushu)
Pyungwon Ko (KIAS)
Martijn Mulders (CERN)
Sreerup Raychaudhuri (TIFR)
Lydia Roos (IN2P3/LPNHE)
Thomas Schoerner-Sadenius (DESY)
Boris Shwartz (BINP)
Changzheng Yuan (IHEP)
Shi-Lin Zhu (Peking University)

International Advisory Committee

Ursula Bassler (IN2P3/CNRS)
Alexander Bondar (BINP)
Rohini Godbole (IISc)
Hafeez Hoorani (NCP)
Tomio Kobayashi (KEK, Chair)
Joachim Mnich (DESY)
Martin Sevior (University of Melbourne)
Xiaoyan Shen (IHEP)
Dongchul Son (KNU)
Henry Tsz-king Wong (Academia Sinica)
Rüdiger Voss (CERN)

Lecturers

Ahmed Ali (DESY)
Simon Eidelman (BINP and NSU)
John Ellis (King's College London and CERN)
Fabiola Gianotti (CERN)
Ingrid-Maria Gregor (DESY)
Takaaki Kajita (University of Tokyo)
Ryuichiro Kitano (KEK)
Youngjoon Kwon (Yonsei University)
Jungil Lee (Korea University)
Fabio Maltoni (UCL)
Takeo Moroi (University of Tokyo)
Tsuyoshi Nakaya (Kyoto University)
Sudhir Vempati (IISc)
Yifang Wang (IHEP)
Nu Xu (CCNU and LBNL)
Masanori Yamauchi (KEK)

Discussion Leaders

Qing-Hong Cao (Peking University)
Sebastien Descotes-Genon (LPT Orsay, CNRS/U. Paris-Sud)
Kentarou Mawatari (LPSC Grenoble)
Hua-Sheng Shao (CERN, ILP and LPTHE)
Cen Zhang (BNL)

Students

Govinda ADHIKARI

Muhammad AHMAD

Yermek ALDABERGENOV

Liupan AN

Abeeha BATOOL

Lydia BERESFORD

Muzamil Ahmad BHAT

Jing CHEN

Kai-bao CHEN

Ye CHEN

Huajie CHENG

Arthur CHOMONT

Shuddha Shankar DASGUPTA

Adam DENDEK

Karola DETTE

Alexander Sascha ERMAKOV

Yinqiang GONG

Hiromitsu GOTO

Kirill GREVTSOV

Dooyeon GYUN

Qamar ul HASSAN

Anton HAWTHORNE-GONZALVEZ

Jochen Jens HEINRICH

Satoshi HIGASHINO

Guoyuan HUANG

Priya Sajid HUSSAIN

Shahin IQBAL

Miao JIANG

James KAHN

Rebin KARAPARAMBIL RAJAN

Daniel KERSZBERG

Jae Sung KIM

On KIM

Thorwald KLAPDOR-KLEINGROTHAUS

Alexandr KOROBOV

Brian LE

Rémy LE BRETON

Peirong LI

Anthony LIONTI

Jun Hao LIU

Kunfeng LYU

Yosuke MAEDA

Fahmi MAULIDA

Laurie MCCLYMONT

AKM Moinul Haque MEAZE

Maren Tabea MEINHARD

Giulio MEZZADRI

Pradiphat MUANGHA

Naoki NAGAKURA

Elizaveta NAZAROVA

Henrik OPPEN

Hitoshi OSHIMA

Santosh PARAJULI

Seokhee PARK

Ann-Kathrin PERREVOORT

Resmi P K

Hongrong QI

Sergii RASPOPOV

Dharmesh RATHAUD

Suvankar ROY CHOWDHURY

Samrangy SADHU

Yuta SANO

Tanmay SARKAR

Andrey SERYAKOV

Sarmad Masood SHAHEEN

Vivek SHARMA

Shohei SHIRABE

Benjamin SOWDEN

Naoyuki SUMI

Khuram TARIQ

Savannah THAIS

Muhammad USMAN

Leonora VESTERBACKA OLSSON

Eiasha WAHEED

Binlong WANG

Xing WANG

Muhammad WAQAS

Jinyun WU

Wenjie WU

Yan jia XIAO

Ke-Pan XIE

Xi'an XIONG

Kazuki YAJIMA

Kimiko YAMASHITA

Beomki YEO

Inseok YOON

Ruobing ZHANG

Ya ZHANG

Yang ZHANG

Yu ZHANG

Jing-yu ZHU

Posters

Poster title	Presenter
Status of COSINE-100 Experiment	ADHIKARI, G.
SUSY breaking after inflation with inflaton in a massive vector supermultiplet	ALDABERGENOV, Y.
Measurement of the branching fraction ratio Br($B_c \to \psi(2S) \pi$)/Br($B_c \to$ J/$\psi\pi$)	AN, L.
Search for Light Dijet Resonances	BERESFORD, L.
Search for the Pair Production of First Generation Scalar Leptoquarks at 13 TeV	BHAT, M.
Study of J/$\psi \to \mu^+\mu$ and $\psi(2S) \to \mu^+\mu^-$ production with the 2015 pp data at 5.02 TeV with the ATLAS detector	CHEN, J.
Fragmentation functions and azimuthal/spin asymmetries in $e^+e^- \to V\pi X$ at high energies	CHEN, K.
Measurements of $t\bar{t}$ differential cross-sections in the all-hadronic channel with the ATLAS detector using highly boosted top quarks in pp collisions at $\sqrt{s}$=13 TeV	CHEN, Y.
Scale Invariant QCD-like Hidden Sector	GOTO, H.
Search for high-mass diphoton resonances with the ATLAS detector	GREVTSOV, K.
Study of Neutrino Oscillation Parameters at the INO-ICAL Detector	KARAPARAMBIL RAJAN, R.
Deriving the electron spectrum with H.E.S.S. using a template analysis approach	KERSZBERG, D.
Precision Spin Tracking Study with Geometric Algebra	KIM, O.
Studies of MicroMegas Chambers for the New Small Wheel using Cosmic Muons	KLAPDOR-KLEINGROTHAUS, T.
Optical Bench Design and Fitter to Measure Distortions in LSST's Candidate Sensors	LE BRETON, R.
Searches for Magnetic Monopoles at ATLAS and MoEDAL	LIONTI, A.
Commissioning of the Belle II Time-Of-Propagation (TOP) counter	MAEDA, Y.

Poster title	Presenter
Radiation hardness of the read-out chip for layer 1 of the Phase I upgrade barrel pixel detector of CMS	MEINHARD, M.
A new CGEM Inner Tracker for the BES III experiment	MEZZADRI, G.
Variation in Cosmic Ray Count Rate at Doi Inthanon with Atmospheric Water Vapor	MUANGHA, P.
Measurement of β decay asymmetry at J-PARC	NAGAKURA, N.
Flow fluctuations at the LHC energy within HYDJET++	NAZAROVA, E.
Supersymmetry and dark matter	OPPEN, H.
J-PARC T60 – Study of neutrino-nucleus interactions with nuclear emulsion at J-PARC	OSHIMA, H.
Search for Higgs boson pair production in the bbWW final state at 13 TeV with the ATLAS detector	PARAJULI, S.
The Mu3e Experiment – Searching for Lepton Flavour Violation	PERREVOORT, A.
Techniques for the search for scalar diphoton resonances with the ATLAS detector at LHC	RASPOPOV, S.
Application of flash-based field-programmable gate arrays in high energy physics	SANO, Y.
Study of Event Shape Variables at 13 TeV	SARKAR, T.
Search for $t\bar{t}H(H \to b\bar{b})$ at ATLAS	SOWDEN, B.
Neutron Lifetime Measurement at J-PARC	SUMI, N.
Dark matter constraints on simplified models with s-channel spin-2 mediators	YAMASHITA, K.
Ratchet Baryogenesis with an Analogy to the Forced Pendulum	YAMASHITA, K.
COMET for the Observation of Charged Lepton Flavor Violation of the Muon	YEO, B.